Investigating the functional morphology, locomotor diversification, and paleoecology of Mesozoic mammals

Meng Chen

A dissertation

submitted in partial fulfillment of the

requirements for the degree of

Doctor of Philosophy

University of Washington

2015

Reading Committee:

Gregory P. Wilson, Chair

Christian A. Sidor

Caroline A. E. Strömberg

Program Authorized to Offer Degree:

Biology

University of Washington

Abstract

Investigating the functional morphology, locomotor diversification, and paleoecology of Mesozoic mammals

Meng Chen

Chair of the Supervisory Committee:

Gregory P. Wilson

Departments of Biology

The first two-thirds of mammalian history occurred in the Mesozoic Era (252–66 Ma). Mesozoic mammals have been long thought of as generalized, nocturnal, terrestrial taxa that were constrained by selective and ecological pressures imposed by contemporary terrestrial vertebrates. However, this notion has been challenged by discoveries of the last two decades. A number of relatively complete Mesozoic mammal skeletons have distinctive morphologies that suggest their evolution of ecological diversity comparable to extant mammals. To test this hypothesis, I used qualitative and quantitative approaches to infer functional morphology, locomotor diversity, and ecological structure of Mesozoic mammals at the species, clade, and community scale, respectively. The first study uses functional morphology and comparative anatomy to

infer locomotion and posture in a recently recovered Early Cretaceous eutriconodontan mammal, *Yanoconodon allini*. The second study uses multivariate morphometrics of the appendicular skeleton in a broad sample of extant, small-bodied mammals as a basis to infer locomotor modes in ten Mesozoic mammal species. The results are combined with previous interpretations of other Mesozoic mammals to assemble temporal patterns of locomotor diversification of mammalian clades through the Mesozoic. The third study compares ecological structure and occupation, as measured by body size, diet, and locomotion, from a broad sample of extant, small-bodied mammalian communities to the inferred paleoecological structure of two Early Cretaceous mammalian communities. Results indicate that the ancient mammalian communities significantly differed from the modern mammalian communities, perhaps due to sampling artifacts of the fossil record, non-analog paleoenvironments of the Early Cretaceous communities, and/or evolutionary ecological transitions that only occurred after the extinction of non-avian dinosaurs. Together, these studies provide a more comprehensive and more quantitative approach to the study of Mesozoic mammals at both the species- and community levels.

TABLE OF CONTENTS

ACKNOWNLEDGEMENTS

This dissertation is a result six-year adventure that transformed me from a Mesozoic mammal paleontologist to a paleoecologist at the University of Washington (UW). During this adventure, I will never get to this point without much help and encouragement along the way. For the people that I've met and that shared their love, support, and kindness, I thank you with all my heart.

I would like to sincerely thank my advisor Gregory P. Wilson for his enormous patience and help during my doctoral dissertation research. I remember every time I look for help he always dropped whatever he was doing to help me sort out my questions. Nothing gets any better than that. He showed me an excellent example of how to develop research ideas, conduct science, and synthesize scientific outcomes. Most importantly, he taught me how to broaden my research interests. It has been wonderful for last six years working with him. Particularly, the fieldwork was the especially fun time that I enjoyed with him. I'm honored to have been his student. I am considering him as one of my best friends in my life.

My other committee members, Caroline A. E. Strömberg, Christian A. Sidor, and Patricia A. Kramer, helped develop ideas, and provided editorial comments and encouragement during the conducting of the project and writing of the dissertation. I thank them for their tremendous effort to help me complete this dissertation and develop my future academic research. Zhe-Xi Luo generously provided the invaluable access to well-preserved Mesozoic mammal specimens for my dissertation project. Without his kindly help, the dissertation research will never come close to the finishing line. He also provided a great amount of intellectual input for the dissertation project. Ann K. Behremeyer, Jeff Bradley, Alexandria Brannick, Ian

Breckheimer, Lauren B. Buckley, Jonathan Calede, Pei-Ji Chen, Stephen G. B. Chester, Thomas Daniel, Lauren DeBey, Dave DeMar, Jr., David M. Grossnickle, Kyndall Hidebrantdt, April Isch, Bao-Yu Jiang, Jim Kenagy, Janneke Hille Ris Lambers, Gang Li, Jia-Run Liu, Ling-De Liu, Darrin Lunde, Kathleen Lyons, Thomas Martin, Qing-Jing Meng, P. David Polly, Joshua Samuels, Yi-Kun Shi, Stephanie Smith, Eileen Westwig, Qun Yang, and Xiang-Ning Yang either provided access to specimens for the dissertation, commented on early drafts of chapters of the dissertation, or offered helpful suggestion for the dissertation project.

My dissertation project was supported by Hall International Student Fellowship, WRF-Hall Fellowship, Tunnicliffe Writing Fellowship, Burke Museum Vertebrate Paleontology Fellowship, Wilson Lab at University of Washington, and Luo Lab at University of Chicago.

My academic experience at UW has been most enriched by conducting fieldworks in Montana. Specially thank Lauren DeBey for teaching me enormous new knowledge of American life that I have never experienced before I entered the United States soil during my first two years at UW. You were the best teacher. Thank Dave DeMar, Jr., Shelly L. Donohue, Steven Lautzenheiser, Abby Vander Linden, Scott Swan, Mark Vorhoff, and Rachel Wallace for teaching me “Survival Skills in the Wild America”. It is unforgettable experience to me. I would like to thank Dave DeMar, Jr., Stephanie Smith, Jacob Cooper, Hannah Jordt, Katrina van Raay for being exemplary office mates. I was lucky to have you all.

I am lucky to have a great family that supports and encourages me during the PhD adventure. Thank Mom and Dad for preparing me for such a long and tough adventure that I’ve never thought I would take. Lastly, thank my wife Hanyu for her encouragement. Your love and advice have inspired me in many ways. I love you and look forward to continuing our future adventures together.

CHAPTER 1:

INTRODUCTION

Mesozoic mammals originated in the Late Triassic (approximately 220 Ma; Kielan-Jaworowska et al., 2004) at about the same time as dinosaurs (Brusatte et al., 2010). Through the Mesozoic Era, mammals became relatively taxonomically rich (more than 320 species) and were distributed in both northern and southern landmasses (Lillegraven et al., 1979; Kielan-Jaworowska et al., 2004). Mammals also underwent critical morphological transformations during this interval that shaped their evolution and ecology and likely those of modern mammals (e.g., Kielan- Jaworowska et al., 2004). Previous studies of these transformations have mostly focused on the skull and dentition (e.g., tri-ossicular middle ear [Allin and Hopson, 1992; Rowe, 1996], tribosphenic molar [Luo et al., 2001a,b], and encephalization [Jerison, 1973; Rowe et al., 2011]). Inferences about the evolution of functional morphology, ecological diversification, and the ecological roles of mammals in Mesozoic terrestrial ecosystems have historically been hampered by a fossil record of mostly dental specimens, some cranial material, and very few postcranial skeletons (e.g., Kielan-Jaworowska et al., 2004).

In the last three decades, discoveries of relatively complete fossil skeletons of Mesozoic mammals have facilitated the study of the evolution and ecology of these mammals (Kielan-Jaworowska et al., 2004; Luo, 2007; Bi et al., 2014; Krause et al., 2014; Luo et al., 2015). Now there is little doubt that Mesozoic mammals evolved an array of ecomorphologies, functionally comparable to those of extant mammals (e.g., Wilson et al., 2013; Chen and Wilson, 2015), which enabled them to occupy diverse regions of ecospace in Mesozoic terrestrial ecosystems (Luo, 2007). However, no study has tested this hypothesis by quantifying how ecologically diverse Mesozoic mammals were through time, across clades, and within communities.

This dissertation attempts to test the aforementioned hypothesis. I used functional morphological, morphometric, and community paleoecological approaches to quantitatively and qualitatively investigate locomotor mode and posture, locomotor diversification, and ecological structure at the species-, clade-, and community levels, respectively, through the Mesozoic.

In *Chapter Two*, I use the Early Cretaceous mammal, *Yanoconodon allini,* as a case study to investigate locomotion and posture in Mesozoic mammals. Previous studies of *Yanoconodon allini* focused on the evolutionary and developmental transition to a tri-ossicular middle ear and the homoplasy in the thoraco-lumbar transition (Luo et al., 2007). In this study, I focus on postcranial skeleton and use a comparative anatomy approach to evaluate the function of each element in order to infer possible locomotor mode and posture used by *Yanoconodon allini*.

In *Chapter Three*, I develop a new multivariate morphometric approach to infer locomotor modes in Mesozoic mammals. The study was motivated by an increasing number of Mesozoic mammal specimens that have been recovered worldwide with relatively complete postcranial skeletons, providing a unique opportunity for investigating locomotor diversification of Mesozoic mammals in a comprehensive way. Previous studies on these new fossils have focused on a single taxon, a limited region of the skeleton, or have been largely qualitative. To build upon these studies, I first developed morphometric models using modern analogs. I applied multivariate analyses to a large dataset of osteological indices derived from appendicular skeletal measurements of a taxonomically diverse sample of extant, small-bodied mammals representing diverse locomotor modes. I found that the eight locomotor modes could be reliably distinguished

from one another in these analyses and that they form a morphofunctional continuum reflecting similarity in biomechanical demands. The resulting models were then used to infer locomotor mode in ten fossil mammals from different clades and different times in the Mesozoic. Combined with previous locomotor inferences of 19 additional taxa, I compiled temporal patterns of locomotor diversification across and within Mesozoic mammal clades.

In *Chapter Four*, I extend the quantitative approach to investigate the ecological structure of Mesozoic mammal communities. I first compiled ecological trait data (body size, diet, locomotion) of 28 extant, small-bodied mammal communities from four climate regions (arid, tropical, temperate, cold) across the world. In plotting these data in ecospace and analyzing the disparity (magnitude of differences among species within the same community) and diversity (number of ecological combinations) of these ecospace occupations, I showed clear differences across the extant communities from different climate regions that are in part due to differences in environmental parameters. Because the Jehol Group currently provides the best fossil record of the Early Cretaceous terrestrial ecosystems, I applied the same approach to two Early Cretaceous mammal communities. Results show that the Early Cretaceous mammal communities have similarities and differences with extant, small-bodied communities. The differences may be due to sampling artifacts of the fossil record, non-analog paleoenvironments of the Early Cretaceous communities, and/or evolutionary ecological transitions that only occurred after the extinction of non-avian dinosaurs.

In *Chapter Five*, I provide concluding remarks that highlight the important findings from the dissertation and relate back to the central hypothesis of the dissertation

that Mesozoic mammals occupied diverse regions of ecospace in Mesozoic terrestrial ecosystems.

Together, these studies provide a new quantitative approach to the investigation of Mesozoic mammals, from species level to the clade level and the paleocommunity level. Through the dissertation, the reader should be reminded that the fossil record of Mesozoic mammals is scarce, which might bias interpretations of the patterns exhibited in these studies. As more and more Mesozoic mammals are recovered, the existing patterns may be revised.

LITERATURE CITED

Allin, E.F., and J. A. Hopson. 1992. Evolution of the auditory system in Synapsida ("mammal-like reptiles" and primitive mammals) as seen in the fossil record. Pp. 587–614 *in* D. B. Webster, R. R. Fay, and A. N. Popper, eds. The Evolutionary Biology of Hearing. Springer, New York.

Bi, S.-D., Y.-Q. Wang, J. Guan, X. Sheng, and J. Meng. 2014. Three new Jurassic euharamiyidan species reinforce early divergence of mammals. Nature 514:579–584.

Brusatte, S. L., M. A. Norell, T. D. Carr, G. M. Erickson, J. R. Hutchinson, A. M. Balanoff, G. S. Bever, J. N. Choiniere, P. J. Makovicky, and X. Xu. 2010. Tyrannosaur Paleobiology: New Research on Ancient Exemplar Organisms. Science 329:1481–1485.

Chen, M., and G. P. Wilson. 2015. A multivariate approach to infer locomotor modes in Mesozoic mammals. Paleobiology DOI: 10.1017/pab.2014.14.

Jerison, H. J. 1973. Evolution of the brain and intelligence. Academic Press, New York.

Kielan-Jaworowska, Z., R. L. Cifelli, and Z.-X. Luo. 2004. Mammals from the age of dinosaurs: origins, evolution, and structure. Columbia University Press, New York.

Krause, D. W., S. Hoffmann, J. R. Wible, E. C. Kirk, J. A. Schultz, W. von Koenigswald, J. R. Groenke, J. B. Rossie, P. M. O'Connor, E. R. Seiffert, E. R. Dumont, W. L. Holloway, R. R. Rogers, L. J. Rahantarisoa, A. D. Kemp, and H. Andriamialison. 2014. First cranial remains of a gondwanatherian mammal reveal remarkable mosaicism. Nature 515:512–517.

Lillegraven, J. A., Z. Kielan-Jaworowska, and W. A. Clemens. 1979. Mesozoic mammals: the first two-thirds of mammalian history. University of California Press, Berkeley.

Luo, Z.-X. 2007. Transformation and diversification in early mammal evolution. Nature 450:1011-1019.

Luo, Z.-X., R. L. Cifelli, and Z. Kielan-Jaworowska. 2001. Dual origin of tribosphenic mammals. Nature 409:53–57.

Luo, Z.-X., P. Chen, G. Li, and M. Chen. 2007. A new eutriconodont mammal and evolutionary development in early mammals. Nature 446:288–293.

Luo, Z.-X., Q.-J. Meng, Q. Ji, D. Liu, Y.-G. Zhang, and A. I. Neander. 2015. Mammalian evolution. Evolutionary development in basal mammaliaforms as revealed by a docodontan. Science 347:760–764.

Rowe, T. B. 1996. Coevolution of the mammalian middle ear and neocortex. Science 273: 651–654.

Rowe, T. B., T. E. Macrini, and Z. X. Luo. 2011. Fossil evidence on origin of the mammalian brain. Science 332:955–957.

Wilson, G. P., A. R. Evans, I. J. Corfe, P. D. Smits, M. Fortelius, and J. Jernvall. 2012. Adaptive radiation of multituberculate mammals before the extinction of dinosaurs. Nature 483:457–460.

CHAPTER 2:

POSTCRANIAL SKELETON OF EUTRICONODONTAN YANOCONODON ALLINI FROM THE EARLY CRETACEOUS OF HEBEI CHINA AND ITS IMPLICATIONS FOR LOCOMOTOR ADAPTATION

Postcranial skeleton of Eutriconodontan *Yanoconodon allini* from the Early Cretaceous of Hebei, China and its implications for locomotor adaptation

MENG CHEN*,[1], ZHE-XI LUO[2], and GREGORY P. WILSON[1]

[1] Department of Biology, University of Washington, Seattle, Washington, 98195, U.S.A., mengchen@uw.edu, gpwilson@uw.edu;

[2] Department of Organismal Biology and Anatomy, Chicago, Illinois, 60637, U.S.A., zxluo@uchicago.edu

ABSTRACT—A recent study hypothesized that *Yanoconodon allini* (Eutriconodonta: Jeholodentidae) from the Lower Cretaceous Yixian Formation of northeastern China had a semiaquatic locomotor mode. However, detailed description and functional study of the postcranial skeleton of *Yanoconodon* have not yet been carried out. Here, we describe and analyze the functional morphology of its postcranial skeleton. Our analyses indicate that *Yanoconodon* has a composite of adaptive features for diverse locomotor modes. Its humerus has a spindle-shaped head, an indistinct neck, and a broad and shallow intertubercular groove, all of which resemble those of non-therian mammaliaforms or cynodonts that have been interpreted as semifossorial or semiaquatic. The lack of an enlarged olecranon process of the ulna and the lack of styloid processes at the distal ends of the radius and ulna would have limited the digging efficiency of *Yanoconodon*. The triangular scapula and the pivotal pectoral girdle of *Yanoconodon* resemble those in extant mammals with some climbing ability. The femur has a spherical head with a very short neck and small greater trochanter. No malleoli are present in the distal ends of the tibia and fibula to stabilize the movement of the upper ankle joint in a parasagittal plane. The astragalus is partially superimposed on the calcaneus. Taken together, these postcranial skeletal features imply that *Yanoconodon* had a sprawling posture in both the forelimbs and hind limbs and was a generalized terrestrial mammal capable of swimming. This study documents the morphological features of the entire postcranial skeleton of *Yanoconodon* and comprehensively analyzes functions of each postcranial element. Our results are consistent with the previous locomotor inference of *Yanoconodon*.

INTRODUCTION

The Eutriconodonta is one of the most species-rich groups of Mesozoic mammals. To date, more than 30 species have been reported from the Early Jurassic to the Late Cretaceous and from all major landmasses (Kielan-Jaworowska et al., 2004; Hu et al., 2005; Meng et al., 2005, 2006; Luo et al., 2007a; Martin and Averianov, 2007; Montellano et al., 2008; Gao et al., 2010; Kusuhashi et al., 2009; Meng et al., 2011; Gaetano and Rougier, 2011, 2012). They are characterized by (i) three principal cusps aligned mesiodistally in bilaterally compressed molars and (ii) relatively precise occlusion between upper and lower molars (Lillegraven et al., 1979; Kielan-Jaworowska et al., 2004). They range in size from small-bodied taxa (~100 g; Kielan-Jaworowska et al., 2004) to the largest mammals known from the Mesozoic (~16 kg; Hu, 2006). The smaller-bodied taxa likely fed on insects and invertebrates, whereas taxa of larger body size preyed on or scavenged small vertebrates (Kielan-Jaworowska et al., 2004; Hu et al., 2005; Hu, 2006). Despite a relatively rich fossil record of eutriconodontans, most taxa are known from fragmentary fossils, mainly isolated teeth and jaw fragments and a few cranial and postcranial elements (Kielan-Jaworowska et al., 2004). Relatively complete skeletons have been reported for only seven species (Jenkins and Schaff, 1988; Ji et al., 1999; Hu et al., 2005; Hu, 2006; Luo et al., 2007a; Gao et al., 2009; Meng et al., 2006, 2011).

The incompleteness of the fossil record of eutriconodontans limited our understanding of their paleoecology and paleobiology to aspects of their feeding. However, with an increasing number of relatively complete eutriconodontan fossils discovered in recent years, it is now possible to infer locomotor mode and substrate use among some eutriconodontans (see Luo, 2007; Chen and Wilson, 2015). Qualitative and quantitative analyses of some of these fossils indicate that eutriconodontans were ecomorphologically diverse, possessing features adapted to

different habitats and locomotor strategies (Luo, 2007; Chen and Wilson, in press). The jeholodentid *Yanoconodon allini* from the Lower Cretaceous Yixian Formation of northeastern China was among those taxa analyzed and was interpreted as semiaquatic in habit (Chen and Wilson, 2015). However, the postcranial skeleton of *Yanoconodon* has not yet been fully described. Here, we describe the postcranial anatomy and functional morphology of the holotype specimen, and discuss locomotor diversity within the Eutricondonta. Our results indicate that the postcranial skeleton of *Yanoconodon* was adapted to diverse locomotor mode. It had a semi-sprawling posture in both the forelimbs and hind limbs and was mostly terrestrial but probably occasionally swam in ponds or rivers. Our results support the previous hypothesis that ecomorphological diversification of Mesozoic mammals occurred at lower taxonomic levels (Chen and Luo, 2013).

MATERIALS AND METHODS

The holotype specimen of *Yanoconodon allini* was recovered from the Lower Cretaceous (125–122 Ma; early Aptian; REF) Yixian Formation at Daluozigou locality in Fengning County, Hebei Province, China (Luo et al., 2007a). The specimen is dorsoventrally compressed in laminated siltstone and split into a main part and a counter part (NJU-P06001A, B, respectively; Figs. 1–2). The skull of NJU-P06001 is largely crushed; most of the postcranial elements are well preserved as either bony elements or molds. The specimen is housed in the collection of the Paleontological Laboratory at Nanjing University, Nanjing, China.

The monophyly of the Eutriconodonta is problematic (see e.g., Gao et al., 2010; Gaetano and Rougier, 2012). The inconsistent phylogenies of Eutriconodonta may be primarily due to a taxonomic sampling difference; the long-branch attraction of jeholodentids and gobiconodontids

may result in a monophyletic clade of eutriconodont mammals (Gao et al., 2010). In addition, the monophyly of the Jeholodentidae has also been challenged (Meng et al., 2011). Without further study to investigate such this issue, here we tentatively follow Luo et al (2007a) to place *Yanoconodon* within monophyletic Jeholodentidae of Eutriconodonta as our working hypothesis.

Previous study of *Yanoconodon* preliminarily investigated the developmental transition of three middle ear bones and the homoplastic characters in the thoraco-lumbar transition (Luo et al., 2007a). Many postcranial elements have yet to be fully analyzed and described. In this study, we focus on the characteristics of the entire postcranial skeleton of *Yanoconodon* to investigate functional and ecological implications for Early Cretaceous eutriconodontan mammals. For the anatomical terminology of the skeleton and the muscle, we follow Kielan-Jaworowska and Gambaryan (1994), and Gambaryan et al. (2002) when applicable. Otherwise, we adopt the terminology of extant mammals, such as Evans (1993). For the ankle joint, we followed Szalay (1994) and Szalay and Sargis (2001) in dividing the ankle joint into to the upper and lower ankle joints.

Institutional Abbreviations—IVPP, Institute of Vertebrate Paleontology and Paleoanthropology, Chinese Academy of Science, Beijing, China; **NJU–P**, Nanjing University–Paleontology Laboratory, Nanjing, China.

Anatomical Abbreviations—am, acromion process; **act**, acetabulum; **as**, astragalus; **at**, atlas; **ax**, axis; **C**, cervical vertebra; **Ca**; caudal vertebra; **Ct**, centrum; **cl**, clavicle; **cm**, calcaneus; **cod**, coronoid process of dentary; **cos**, coracoid process of scapula; **cou**, coronoid process of ulna; **cp**, carpal; **ct**, capitate; **cu**, cuboid; **D**, dorsal vertebra; **dt**, dentary; **dc**, distal carpal; **dcd**, dentary condyle; **dm**, dorsal margin of the scapula; **dp**, distal phalanx; **dpc**, deltopectoral crest; **ds**, dens of axis; **dr**, distal end of the radius; **ecp**, ectepicondyle; **ectc**,

ectocuneiform; **ef**, extensor fossa; **enp**, entepicondyle; **enpf**, entepicondylar foramen; **entc**, entocuneiform; **ep**, epipubis; **fd**; fibular distal end; **fe**, femur; **fh**, femoral head; **fi**, fibula; **fpe**, fibular proximal end; **gl**, glenoid fossa; **gt**, greater tubercle; **gtr**, greater trochanter; **hh**, humeral head; **hm**, hamate; **hu**, humerus; **i**, incisor; **ic**, interclavicle; **icg**, intercondylar groove; **il**, ilium; **in**, incus; **ip**, intermediate phalanx; **is**, ischium; **isf**, infraspinous fossa; **it**, ischial tuberosity; **itf**, intertrochanteric groove; **itg**, intertuberclar groove; **itl**, intermedium; **jg**, jugal; **la**, lamina of neural arch; **lcd**, lateral condyle; **lcl**, lateral centrale; **lt**, lesser tubercle; **ltr**, lesser trochanter; **lu**, lunate; **ma**, malleus; **?mb**, partial impression of sternal maubrium**; mc**, metacarpal; **mcd**, medial condyle; **mcl**, medial centrale; **metc**, mesocuneiform; ?**mm**, ?medial malleolus; **mt**, metatarsal; **mtc**, metacromion; **na**, navicular; **ob**, obturator foramen; **op**, olecranon process; **p**, pedicle of neural arch; **pb**, pubis; **ph**, phalanges; **pp**, proximal phalanx; **ps**, pisiform; **pz**, prezygapophysis; **r**, rib; **ra**, radius; **rac**, radial condyle; **rad**, radiale; **rh**, radial head; **S**, sacral vertebra; **St**, sternabra; **sa**, scapular angle; **sbs**, subscapular spine; **sbsf**, subscapular fossa; **sc**, scapula; **sp**, scapular spine; **scp**, scaphoid; **sq**, squamosal; **ssf**, supraspinous fossa; **td**, tibial distal end; **tf**, tibial fossa; **ti**, tibia; **tm**, trapezium; **tn**, trochlear notch; **tp**, trapezoid; **tpe**, tibial proximal end; **tq**, triquetrum; **tr**, transverse process; **tt**, teres tuberosity; **ul**, ulna; **ulc**, ulnar condyle; **uln**, ulnare. "**L**" and "**R**" in parenthesis refer to left and right, respectively.

DESCRIPTION AND COMPARISON

Axial skeleton

Sternebrae—Ten sternebrae (St1–St10) are preserved in both the main (NJU-P06001A) and counter parts (NJU-P06001B). Most sternebrae are negative molds aligned anteroposteriorly, and all sternebrae are displaced to the right side of the vertebral column in the main part (Figs. 1,

3A, C) but to the left side in the counterpart (Figs. 2–3B, D). The manubrium (St1) is damaged and its outline largely overlaps with the disarticulated components of the cervical vertebrae. It is hardly discernible. Sternebrae 2–6 are relatively well preserved, and each of them is bilaterally broad in the trapezoid outline that bears a narrow anterior margin and a broad posterior margin (Fig. 3B). Sternebrae 7–10, in contrast, are relatively bilaterally compressed, and their sizes decrease progressively (Fig. 3C). The xiphoid (St10) tapers posteriorly, showing a much wider anterior surface than the posterior surface. Between preceding and succeeding sternebrae, a concave fossa is present that serves as the articular recess for the distal end or the costal cartilage of the ribs.

The sternebrae of *Yanoconodon*, in general, show relatively shorter profiles in contrast to those of *Repenomamus*, which are long and bilaterally compressed (Hu, 2006). A large number of the sternebrae in *Yanoconodon*compensate for the shortening of the sternal elements to maintain the length of the thorax relative to the trunk. The sternal series is segmented, which is the prevalent morphology of the thorax among extant mammals (Lessertisseur and Saban, 1967a). The segmented condition of the sternal series is also common among premammalian cynodonts, such as the tritylondontids *Oligokyphus* and *Bienotheroides*, and Mesozoic mammals (Kühne 1956; Sun and Li, 1985; Ji et al., 1999, 2002; Luo et al., 2003, 2006, 2007a, 2007b, 2012; Luo and Ji, 2005; Hu, 2006; Meng et al., 2011; Chen and Luo, 2013; Yuan et al., 2013; Zheng et al., 2013; Zhou et al., 2013; Bi et al., 2014). One exception among Mesozoic mammals is the holotype specimen of *Zhangheotherium quinquecuspidens* (IVPP V7466; Hu et al., 1997, 1998), which possesses a fused sternal structure. This fused sternebrae condition either represents a unique (autapomorphic) morphological feature of *Z. quinquecuspidens* or a pathological condition of an individual (Chen and Luo 2013).

Cervical vertebrae—The holotype specimen (NJU-P06001; Figs. 1–3A, B) preserves seven cervicals (C1–C7), which is also the prevailing count among extant mammals (Narita and Kuratani, 2005) and other Mesozoic mammals (Chen and Luo, 2013). Unlike extant mammals, the elements of each cervical are not fused but are disarticulated in the holotype specimen. Most of the disarticulated elements are well associated with the cervicals. First cervical atlas (C1) consists of the disarticulated left and right halves of the neural arch and a centrum. The neural arch is in either anterior or posterior view; the centrum is in dorsal view (Fig. 3A). The pedicles of the neural arch bear enlarged lateral ends that would have had cranial and caudal articular facets for receiving occipital condyles anteriorly and contacting the superior articular facet of the axis (C2) posteriorly, respectively. These facets are not preserved due to the damage. The left and right neural laminae of the atlas extend laterally but meet medially in the sagittal plan of the vertebral column. The left and right laminae together form an obtuse angle (about 125º). In morganucodontids, the neural laminae (semicircular arches) of the atlas show a relatively deeper profile than those in *Yanoconodon* (Jenkins and Parrington, 1976). The neural lamina and lateral ends of the neural arch together form a pair of notches on the dorsolateral corners of the neural arch of C1 in *Yanoconodon*. A similar notch is present in *Repenomamus* and morganucodontids but deeper and more concave than that in *Yanoconodon* (Jenkins and Parrington, 1976; Hu, 2006). We interpret this notch as a homolog to the alar notch in some therian mammals (Evans, 1993). The presence of the transverse process or the "rib" in C1 remains undetermined, though a suspicious broken bony element is preserved near the left half of the neural lamina. A transverse foramen is not preserved. The vertebral foramen (canal) is half as wide as the atlas. The centrum of C1 in dorsal view shows an oval shape with a slightly convex anterior surface. The centrum has a broken fovea dentis at the dorsodistal end for receiving the dens of the axis.

The axis (C2) has a relatively long dens that protrudes anteriorly to lie on top of the fovea dentis of the atlas, forming the atlas-axis articulation as in extant mammals (Fig. 3A; Lessertisseur and Saban, 1967a). The neural arch of C2 is dorsoventrally compressed due to the preservation. Each neural lamina bears two branches projecting anteriorly and posteriorly, forming pre- and post-zygapophyses of C2, respectively, as in the multituberculate *Nemegtbaatar gobiensis* (Kielan-Jaworowska and Gambaryan, 1994) where these pre- and post-zygapophyses firmly articulate with their counterparts in the preceding and succeeding cervicals, respectively.

Cervicals 3–5 are progressively broader and shorter (Fig. 3A). Cervical 5 is the shortest (most anteroposteriorly compressed) vertebra, and it bears the most robust transverse processes among C3–C5. In C5, the laminae are separated and the centrum is oval in dorsal or ventral view. The centrum has a flat anterior surface and a slightly convex posterior surface. The neural arches of C6 and C7 are increasingly expanded bilaterally. In turn, the transverse processes of C6 and C7 become shorter than those of the preceding cervicals, which maintains an appropriate size of the neck. The spinous processes of the cervicals are broken off. Judging by the depths of the negative molds, we interpret that the spinous processes of the post-axial cervicals are short. The ribs are detached in C2–C4 but C5.

The short and broad cervical series that is prevalent in both eutriconodontans (Ji et al., 1999; Hu, 2005; Luo et al., 2007; Meng et al., 2011) and multituberculates (Kielan-Jaworowska, 1989; Kielan-Jaworowska and Gambaryan, 1994) implies that they share a short, wide neck. In extant large aquatic mammals, such as whales, the cervical series is disproportionally short relative to the trunk in comparison with their terrestrial relatives (Narita and Kuratani, 2005). Nevertheless, this adaptive morphology of the large aquatic mammals might not be comparable

to the small extinct, Mesozoic taxa. In contrast, a general shortening of the neck in subterranean rodents, particularly in those with wide heads (Hildebrand, 1985), is an adaptive morphology for digging (Stein, 2000) as seen in a number of multituberculates (see Kielan-Jaworowska et al., 2004). In addition, *Yanoconodon* and multituberculates have protruding and divergent pre- and post-zygapophyses of the cervicals; this implies that there is extensive zygapophyseal articulation among cervicals in *Yanoconodon* and multituberculates, which would reduce bilateral mobility of the neck but buttress the neck during head-lift digging.

Dorsal vertebrae—Almost all dorsal vertebrae (D1–D25) are preserved in dorsal or ventral view (Figs. 1, 2, 3B–D, 4A). The neural arches of D19–25 are displaced on the right side of the centra in the main part (NJU-P06001A; Fig. 3C) but the left side in the counter part (Fig. 3D). The total number of the dorsal vertebrae in *Yanoconodon* is 25 close to the 26 in *Repenomamus* (Hu, 2006) and more than the 22 in the closely related sister taxon *Jeholodens* and the number in other Mesozoic taxa (Ji et al., 1999; Chen and Luo, 2013). The greater number of dorsal vertebrae contributes to the trunk elongation and disproportionately short neck region in *Yanoconodon*.

In D4–D25, the centrum is wider than long. That ratio is 2:1 in D21–D25, where each centrum has a slightly concave surface on the ventral side, which is surrounded by distinctive ridges extending along the anterior and posterior margins (Figs. 1–3B, D, 4A). In D5–D11, a ventral crest extends sagittally along each centrum. The neural arches of all of the dorsal vertebrae are much narrower than those of the cervical vertebrae. The transverse processes ("diapophyses") are small, protruding laterally in D11–D13 (Fig. 3D); the transverse processes become progressively longer and larger in D14 and D15 than in the preceding ones. No transverse processes are discernible in the post-D15 dorsal vertebrae. Based on the negative

molds, we interpret the pedicles of the dorsal vertebrae as short and with pre- and post-zygapophyses in the anterior and posterior ends, respectively. The pre- and post-zygapophyses are connected by a ridge along the dorsolateral side of the pedicle (Fig. 3B, D). A transition of the zygapophyseal orientation is noticeable in D13–D17. The pre-zygapophyses orient more vertically in D14 than in D13 (Figs. 3D, 17), and the pre-zygapophyses become progressively more vertically oriented after D15. The change in orientation implies an identity transition among the dorsal vertebrae, which makes it possible to subdivide the dorsal vertebrae into the thoracic and lumbar regions (Williams et al. 1989; Evans 1993; Filler, 1987; Argot, 2003). Given the depths of the molds, we interpret the spinous processes as small in D10–D22. In D23–D25, the spinous process is unknown because no mold is preserved. Based on the small spinous processes in D10–D22, we interpret that *Yanoconodon* had a small epaxial vertebral muscle and its trunk had great bending ability. This is in contrast to the well-developed, tall spinous processes and the large, reconstructed epaxial muscles in multituberculates (Kielan-Jaworowska and Gambaryan, 1994).

All the dorsal vertebrae have associated ribs, and all the ribs are preserved in anterior or posterior view (Figs. 1, 2, 3B–D, 4A). The ribs associated with D1–D5 are short and stout and show strong curvatures. Subsequently, the ribs become progressively longer and less curved until D14. Posterior to D14, the ribs decrease in size and become tiny knobs in D25 (Figs. 3C–D, 4A). The proximal ends of the ribs of D1–D5 are enlarged and equipped with two heads, the capitulum and the tuberculum, as in extant therians (Lessertisseur and Saban, 1967a; Evans, 1993; Argot, 2003). No double heads are discernible in the ribs of D6–D25. Nevertheless, the ribs of D17–D25 have dorsoventrally expanded proximal ends, as in *Repenomamus* (Hu, 2006). No lumbar ribs are present in *Jeholodens* (Ji et al., 1999).

Sacral vertebrae—Three sacral vertebrae (S1–S3) are preserved in the type specimen (Figs. 4C, 4D). Sacral 3 is the best preserved among the three. All the centra are displaced to the right side of the neural arches in the main part in dorsal view (NJU-P06001A). They are bilaterally expanded and are wider than the centra of the dorsal vertebrae. The centra of the sacral vertebrae possess ventral crests extending anteroposteriorly in the ventral surface, dividing the ventral surface into two shallow facets. The transverse processes of the sacrals expand anteroposteriorly and laterally to increase contact area between the sacrals and the ilia in order to stabilize the pelvis. No symphysis, however, is visible in the lateral ends of the transverse processes due to damage. The spinous processes of the sacrals are as small as those of the dorsal vertebrae.

Caudal vertebrae—First eight caudal vertebrae (Ca1–Ca8) are preserved in the holotype specimen (Fig. 4B). Caudals 1–2 are preserved with the disarticulated pelvic elements, and they appear wider than the sacrals. In Ca3–Ca5, the neural arches are displaced from the centra and the transverse processes are detached from the neural arches. These transverse processes have a knob-like profile that bears an enlarged lateral end. The pre- and post-zygapophyses are oriented somehow obliquely. The pre-zygapophyses are prominent, flaring anterolaterally; the post-zygapophyses are small, projecting posteriorly. Because of the size difference between the pre- and post-zygapophyses, we interpret the articulation between caudal vertebrae as weak and, in turn, that the tail had substantial range of mobility. This mobility would be enhanced further in Ca6–Ca8, which have smaller pre- and post-zygapophyses than in Ca3–Ca5 (Fig. 4B). The spinous processes of Ca1–Ca8 are small and inclined posteriorly given to the depth of the negative molds. The morphology of the caudal vertebrae of *Yanoconodon* resembles that of other eutriconodontans (Jenkins and Parrington, 1976; Ji et al., 1999; Meng et al., 2011).

Pectoral Girdle

Clavicle—Both left and right clavicles are preserved in the holotype specimen (Figs. 1, 2, 5C–D, 6). The left clavicle is completely exposed; the medial (sternal) half of the right clavicle overlaps the right scapula. The clavicle is narrow and curved (Fig. 6A–C). About three-fifths of the length of the clavicle is bowed anteroventrally, and the medial end is slightly curved posteriorly. This curvature gives the clavicle a subtle sigmoid profile. Unlike the medial end, the enlarged lateral end of the clavicle tapers towards the lateral tip to form a flat anterodorsal facet. This facet would articulate with the acromion process of the scapula, forming a mobile joint between the clavicle and the scapula.

Interclavicle—Although the body of the interclavicle is broken and largely overlaps with the rib of C4, the outline of the interclavicle remains discernible in both the main and counter parts (Figs. 5A–B, 6A–C). The interclavicle has a rhomboid outline that has a broad body with relatively narrow anterior and posterior ends (see the reconstruction in Fig. 6A). The interclavicle body has a prominent median ridge extending anteroposteriorly and a crescentic ridge extending bilaterally on the ventral surface. The intersection of the two ridges in the center of the ventral surface bulges to forming a tubercle. This tubercle subdivides the posteroventral surface of the interclavicle into two symmetrical concave areas. The tubercle is herein termed the interclavicle prominence. Posterior to the interclavicle prominence, the posterior end articulates with the manubrium (St1) of the sternal series. Similar to *Yanoconodon*, cynodonts *Thrinaxodon* and *Massetognathus* also possess an interclavicle with a prominent interclavicle prominence (Jenkins, 1970a, 1971). In contrast, *Repenomamus* lacks the interclavicle prominence or the well-defined ridges on the ventral surface (Hu, 2006).

The anterior interclavicle has symmetrical left and right lateral extensions. The lateral

extension is short and broad with a slightly concave area. The lack of extensive overlap between the interclavicle and the clavicle indicates a non-rigid, largely mobile clavicle-interclavicle joint. Specifically, we propose two possible configurations of the contact between the clavicle and the interclavicle. In the first configuration, the concave area of the lateral extension receives the medial end of the clavicle (See reconstruction in Fig. 6A), and, in the second configuration, the medial end of the clavicle contacts the margin of the concave area. In either case, the clavicle-interclavicle joint is a mobile and pivotal joint.

The interclavicle morphology of *Yanoconodon* is distinct from that of cynodonts (Jenkins, 1971; Sues and Jenkins, 2006), the multituberculate *Kryptobaatar* (Sereno, 2006), zhangheotheriids (Hu et al., 1997, 1998; Ji and Luo, 2005), and the spalacotheriid *Akidolestes* (Chen and Luo, 2013). The latter species possesses either a cruciate- or T-shaped interclavicle without extensive lateral processes. The basal mammaliaform *Sinoconodon,* the shuotheriid *Pseudotribos,* and extant monotremes possess extensive lateral processes that immobilize the clavicle-interclavicle articulation (Klima, 1973; Luo et al., 2007b). This rigid clavicle-interclavicle joint embraces the pectoral girdle and limits the range of the shoulder movement during locomotion, such as vertical climbing. In contrast, the mobile clavicle-interclavicle joint in eutriconodontans (Ji et al., 1999; Hu, 2006), multituberculates (Gambaryan and Kielan-Jaworowska, 1997; Sereno, 2006), zhangheotheriids (Hu et al., 1997; Rougier et al., 2003; Luo and Ji, 2005; Luo et al., 2007b), and spalacotheriids (Chen and Luo, 2013) would function like the clavicle-manubrium joint in extant therians, which allows a great range of movement in the pectoral girdle (Jenkins, 1974).

Scapula—Both the left and right scapulae are well preserved in the main and counter parts (NJU-P06001A, B; Figs. 5C–F, 16). The anterior and posterior margins of the scapula are

straight and converge to form an acute angle ventrally. This convergence creates a constricted neck in the ventral end of the scapula immediately dorsal to the glenoid fossa, as in a number of Mesozoic and extant taxa (Lessertisseur and Saban, 1967b; Hu et al., 1997, 1998; Rougier et al., 2003; Luo and Ji, 2005; Hu, 2006; Chen and Luo, 2013). The vertebral (dorsal) margin of the scapula is curved dorsally. Together, the anterior, vertebral, and posterior margins form a triangular scapular plate with a well-developed scapular angle in the dorsoposterior corner. On the lateral side of the scapular plate, the distinctive rugose area extends along the vertebral margin (Fig. 5E), which would be the site for inserting rhomboid and levator muscles. The posterior margin of the scapula is curled laterally, forming the inferior lateral crest that extends along the entire length of the scapula (Fig. 5C, 5E). Anterior to the crest, the prominent scapular spine protrudes laterally and subdivides the scapula into the supraspinous and infraspinous fossae. The scapular spine is straight and extends almost three-fourths of the length of the scapular plate. The metacromion originates at the ventral end of the scapular spine and extends anteroventrally, terminating at the acromion process. The acromion process is robust and peg-like. It flares anteroventrally over the glenoid fossa (Fig. 5C–F). Bordered by the anterior scapular margin and the scapular spine, the supraspinous fossa forms a more acute angle than the scapular plate, which, in turn, forms a rectangular infraspinous fossa. The area of the infraspinous fossa is about 50% larger than the area of the supraspinous fossa. On the medial side of the scapular plate, the subscapular fossa is slightly concave and covers more than four-fifths of the area of the scapular blade (Figs. 5D, 5F, 16). The glenoid fossa of the scapula bears a small and shallow articular facet. Judging by the orientation of the natural molds, we interpret the glenoid fossa, which receives the humeral head, as facing more laterally than ventrally (Fig. 5D, 5F). The coracoid process is indistinctive and medial to the glenoid fossa (Fig. 5C–F).

The scapula of *Yanoconodon* differs from those of cynodonts, *Sinoconodon*, morganucodontids, *Haldanodon, Fruitafossor*, multituberculates, and extant monotremes in several ways (Fig. 7; Jenkins, 1971; Jenkins and Parrington, 1976; Kielan-Jaworowska and Gambaryan, 1994; Luo and Wible, 2005; Martin 2005; Sereno, 2006). In those taxa, the scapula is narrow and strap-like (likely symplesiomorphy with pre-mammalian cynodonts) and has an enormous scapular angle that flares dorsoposteriorly (Fig. 7A). In contrast, in *Jeholodens* and zhangheotheriids, the scapula has an anteroposteriorly expanded rectangular profile (Fig. 7E–F; Hu et al., 1997, 1998; Ji et al., 1999), whereas in *Repenomamus* and *Akidolestes* it is semi-circular (Fig. 7C; Hu, 2006; Chen and Luo, 2013: fig. 6). Among living therians, *Procavia* (hyrax; Lessertisseur and Saban, 1967b;) and *Petrodromus* (elephant shrew; Salton and Sargis, 2008) possess a triangular scapulae as is the case in *Yanoconodon* and *Liaoconodon* (Meng et al., 2011). The scapular spine in *Procavia* is curved towards the posterior margin at the midlength of the scapula (Lessertisseur and Saban, 1967b), and the metacromion in *Petrodromus* is greatly depressed as in the marsupial *Didelphis* and other living therians (Fig., 7; Lessertisseur and Saban, 1967b; Klima, 1987; Salton and Sargis, 2008). In *Jeholodens*, the metacromion is also highly depressed but the scapular spine splits into two crests towards the vertebral margin, forming a unique triangular area in the dorsal part of the scapula (Ji et al., 1999).

Forelimb

Humerus—The left and right humeri are well preserved in the main and counter parts (NJU-P06001A, B); only the right humerus remains in articulation with the glenoid fossa of the scapula (Figs. 1–2, 8, 16). The humerus is short and robust. The head is large and is spindle shaped in posterior view (Fig. 8B), as in premammalian cynodonts (Kühne, 1956; Jenkins, 1971; Sun and Li, 1985; Sues and Jenkins, 2006). The greater and lesser tubercles are seated medial

and lateral to the humeral head, respectively. The greater tubercle shows a larger and more elevated profile than the lesser tubercle (Fig. 8A). It continues distally, forming the deltopectoral crest that converges to the shaft at midlength of the humerus (Fig. 8A, 8C, 16). The teres crest originates distal to the lesser tubercle, extends distally, and stops at the same level as the deltopectoral crest (Fig. 8B, 8C). The tubercles, crests, and shaft together enclose a concave area, the intertubercular groove, at the anterior surface of the humerus. The intertubercular groove forms a wide and shallow area proximally and is indistinct by the midlength of the shaft (Fig. 8A, 16). The distal end of the humerus is bilaterally expanded. It is slightly wider than the proximal end. The distal end has an entepicondyle and ectepicondyle on the medial and lateral sides, respectively. The entepicondyle protrudes medially and shows a more prominent profile than the rounded ectepicondyle. Lateral to the entepicondyle, there is an oblong opening that we interpret as the entepicondylar foramen (Fig. 8A–B, 16). Judging by the positional differences of the entepicondylar foramen in anterior and posterior views, we interpret the passage of the entepicondylar foramen as oblique to the transverse axis of the distal end of the humerus. On the distal end, a shallow groove separates the radial and ulnar condyles, forming a spindle-like structure in posterior view. Above the groove, there is a shallow recess in posterior view, forming the olecranon fossa. The transverse axis of the distal end is at an angle to that of the proximal end, but no precise angle can be estimated.

The humerus of *Yanoconodon* is a composite of primitive and derived features. For example, the spindle-like humeral head resembles that in cynodonts and in morganucodontids (Kühne, 1956; Jenkins, 1973; Jenkins and Parrington, 1976; Sues and Jenkins, 2006); whereas the straight deltopectoral crest along the humeral shaft is similar to that in *Phascolarctos* (koala; Lessertisseur and Saban, 1967b). The slightly elevated greater tubercle of the humerus in

Yanoconodon contrasts to that in the docodontan *Haldanodon exspectatus* (Martin, 2005), the multituberculate *Kryptobaatar dashzevegi* (Sereno, 2006), zhangheotheriids (Rougier et al., 2003; Luo and Ji, 2005), the spalacotheriid *Akidolestes* (Chen and Luo, 2013), and the eutherian *Ukhaatherium* (Horovitz, 2003), all of which are non-elevated. The morphology of the distal end of the humerus, which lacks a trochlear articulation with the radius, resembles that in cynodonts and morganucodontids (Fig. 9; Kühne, 1956; Jenkins, 1973; Jenkins and Parrington, 1976; Sues and Jenkins, 2006). In contrast, the distal end of the humerus in multituberculates, *Repenomamus, Didelphis*, and *Tupaia* has a prominent intercondylar groove that separates the radial and the ulnar condyles (Fig. 9; Krause and Jenkins, 1983; Argot, 2001; Hu, 2006; Sereno, 2006; Hurum and Kielan-Jaworowska, 2008). In placentals, the intercondylar groove is well emarginated, forming the trochlea that embraces parasagittal motion of the elbow joint (Lessertisseur and Saban, 1967b; Evans, 1993; Boyer et al., 2010; Chester et al., 2010).

Ulna—The ulna is straight and becomes slightly widened towards the distal end (Figs. 1, 2, 8D–F, 16; Table 1). At the proximal end, it has small olecranon and coronoid processes. The olecranon process has an poorly defined anconeal process that demarcates the dorsal limit of the trochlear notch from the olecranon process. Together, the anconeal and coronoid processes define a wide and shallow trochlear notch for articulation with the distal end of the humerus. Distal to the coronoid process, the radial notch extends mediodistally, which accommodates the proximal end of the radius. Lateral to the radial notch, a broad, shallow extensor fossa extends distally and stops at the midlength of the ulna. At the distal end, a styloid process is not preserved.

Morphological features of the ulna of *Yanoconodon* are more similar to those of the tritylodontids *Oligokyphus* and *Kayentatherium* (Kühne, 1956; Sues and Jenkins, 2006) than to

those of the eutriconodontans *Gobiconodon* and *Repenomamus* and the splacotheriid *Akidolestes* (Jenkins and Schaff, 1988; Hu, 2006; Chen and Luo, 2013). The ulna is substantially curved in *Gobiconodon* and *Repenomamus* and sigmoidal in *Akidolestes* (Chen and Luo 2013); this contrasts to the straight profile in *Yanoconodon* and tritylodontids. *Yanoconodon*, however, shares the wide-open trochlear notch with all of these taxa except *Akidolestes* (Kühne, 1956; Jenkins and Schaff, 1988; Hu, 2006; Sues and Jenkins, 2006; Martin, 2005; Chen and Luo, 2013). In *Akidolestes*, a prominent coronoid process and a crest-like anconeal process restrict the trochlear notch and in turn the elbow joint. In addition, the extensor fossa appears more concave in *Akidolestes* than in eutriconodontans (Jenkins and Schaff, 1988; Hu 2006; Chen and Luo, 2013), which implies a relatively larger extensor muscle in *Akidolestes* than in eutriconodontans.

Radius—Both the left and right radii are well preserved (Figs. 1, 2, 8D–F, 16). The radius is the shortest element in the forearm (Table 1). The radius has a weak sigmoidal profile (Figs. 8D–F). The radial head is slightly enlarged, and it bears an oval rim that is obliquely oriented to the long axis of the shaft. Close to the radial head, an oblong area is present in medial view. We interpret this as an area for the attachment of the biceps brachii muscle. The distal end of the radius is bilaterally expanded, wider than the proximal end in both anterior and posterior views. It bears a rim that wraps the distal end forming a slightly convex surface. This convex surface would contact the scaphoid and the lunate to form the proximal wrist. A styloid process is not preserved at the distal end of the radius.

Carpals—Carpal elements are scattered around the proximal end of the manus in the main and counter parts (NJU-P06001A, B; Figs. 1–2, 10). Their profiles are not distinctive from each other except in size. Given the size and well-preserved molds, we reconstructed the wrist of *Yanoconodon* with two transverse rows of seven carpals (Fig. 11). The proximal row comprises

the scaphoid, lunate, and triquetrum from medial to lateral. The scaphoid has an elongate bean-like profile with rounded proximal and distal ends and flat medial and lateral surfaces. The lunate, the second largest carpal in the wrist, has a rounded triangular outline. Presumably it would contact the capitate and trapezoid distally. The triquetrum is the largest carpal in the wrist. It is rounded and bears a small and slightly concave fossa on the medial surface. The triquetrum would contact the hamate distally and the distal end of the ulna proximally.

The distal carpal row consists of the trapezium, trapezoid, capitate, and hamate from medial to lateral (Figs. 10–11). The trapezium is wide and bears small processes at the medial and lateral ends, projecting distally. The two processes form a concave facet at the distal end of the trapezium, which would articulate with the proximal end of the first metacarpal. The trapezoid has a slim bean profile and a slightly concave distal facet that would contact the proximal end of the second metacarpal. The capitate has a kidney-shaped profile and is more rounded than the trapezoid. Unlike the trapezium and trapezoid, distally the capitate bears a small flat facet for articulating with the third and fourth metacarpals. The hamate is pea-like and has several small flat facets around. Presumably, these facets would contact the triquetrum, the capitate, and the fourth and fifth metacarpals accordingly. A pisiform is not preserved.

In *Yanoconodon* none of the proximal carpals has a distinctive outline that would form rigid articulations among themselves or with the ulna, radius, or distal carpals. In contrast, the distal carpals show better-defined outlines for the articulation with the metacarpals (Figs. 10–11). Based on the width of the distal carpal row, we interpret that each of the distal carpals would contact two metacarpals, as in the reconstruction of *Kayentatherium* (Sues and Jenkins, 2006). In *Jeholodens*, *Ornithorhynchus*, *Fruitafossor*, *Akidolestes*, and therian mammals, the wrists have rigid configurations but differ from species to species in carpal morphology (Fig. 11;

Lessertisseur and Saban, 1967b; Ji et al., 1999, 2001; Luo et al. 2003; Luo and Wible, 2005). In *Akidolestes*, the hamate is the most dominant carpal and occupies entire lateral portion of both the proximal and distal carpal rows (Chen and Luo, 2013); in *Jeholodens* and *Eomaia*, the largest carpals are the bilaterally expanded scaphoid and the elongate trapezium, respectively (Fig. 11; Ji et al., 1999, 2002; Luo et al., 2003). Despite size differences, both the scaphoid and trapezium in *Yanoconodon* and *Jeholodens* are expanded bilaterally and stacked on the medial side of the wrist (Fig. 11; Ji et al., 1999, 2002).

Metacarpals and Phalanges—Five manual digits are preserved in the holotype specimen (NJU-P06001A, B; Figs. 1–2, 10). The metacarpals and the phalanges of the right manus are preserved in original anatomical position (Fig. 10A). All five metacarpals (mc1–mc5) have a dumbbell-shaped profile but they differ in length. Metacarpal 4 is the longest among the five metacarpals, followed by mc3, mc2, mc5, and mc1. Metacarpals 1 and 2 have more bilaterally expanded proximal ends than the distal ends. Metacarpal 5 is the most robust element among all metacarpals. All the metacarpals have round proximal ends but their distal ends vary in morphology (Fig. 11). In mc1, mc2, and mc5, the distal end bears a slightly convex surface, whereas that in mc3 and mc4surface is flat. The morphology of the metacarpals in *Yanoconodon* resembles that in premammalian cynodonts, *Repenomamus*, and *Akidolestes* (Jenkins, 1971; Sun and Li, 1985; Hu, 2006; Sues and Jenkins, 2006; Chen and Luo, 2013). Unlike those taxa, some Mesozoic taxa have metacarpals with relatively long shafts and small proximal and distal ends (e.g., Ji et al., 1999; Luo and Ji, 2005; Meng et al., 2013).

All proximal phalanges (pp1–pp5) except the first one are preserved in either dorsal or ventral orientation (Fig. 10). The first proximal phalanx (pp1) is in either medial or lateral view and shows the dorsoventrally enlarged proximal and distal ends with a dorsally arched shaft. All

other four proximal phalanges show transversely expanded shafts and taper distally. Given the depths of the molds, we interpret that the shafts of all proximal phalanges are wider than deep with arched ventral but flat dorsal surfaces. The distal ends of the proximal phalanges are enlarged and become vertically oriented in both the medial and lateral margins. The medial and lateral margins bear recesses for receiving the collateral ligaments. In each proximal phalanx, mediodistal to the recesses, a concave groove separates symmetrically bulged areas in the distal end, which forms the semicircular trochlea that functions as a pulley to restrict movement to the parasagittal plane at the proximal-intermediate phalangeal joint. All the intermediate phalanges have broad proximal ends, slender shafts, and rounded distal ends. The distal phalanges all have a similar outline, despite differences in size. Their dorsal margins are flat, whereas the ventral margins bear pronounced digital flexor tubercles at mid-length. In contrast to the proximal and intermediate phalanges, the distal phalanges have great depth and bear slightly concave facets on their proximal ends, which articulate with the pulley-like distal ends of the intermediate phalanges. The digital extensor tubercles are small and immediately above the articular facet.

The proximal and intermediate phalanges of *Yanoconodon* exhibit great similarities to the stout phalangeal elements of cynodonts, the docodontan *Haldanodon*, and the eutriconodontan *Liaoconodon* (Jenkins, 1971; Hopson, 1995; Damiani et al., 2003; Martin, 2005; Sues and Jenkins, 2006; Meng et al., 2011; Fernandez et al., 2013). *Yanoconodon* is the only Mesozoic mammal known to have proximal phalanges that are wider than deep. Nevertheless, the distal phalanges of *Yanoconodon* with the deep profile and pronounced digital flexor tubercle resemble those of *Gobiconodon* and *Akidolestes* (Jenkins and Schaff, 1988; Meng et al., 2011; Chen and Luo, 2013), but differ from those of *Haldanodon,* in which the digital flexor tubercle is developed ventroproximally and the digital extensor tubercle extends proximally over the pulley-

like distal end of the intermediate phalanges (Martin, 2005).

Pelvic girdle

Pelvis—The pelvis consists of the ilium, ischium, pubis, and epipubis, which are all displaced from their original anatomical positions (Figs. 1, 2, 4B–D, 16). Thus, the acetabulum is not fully preserved in the holotype. Among all pelvic elements, the ilium is the longest element and accounts for 60% of the length of the pelvis. The iliac shaft extends anteriorly and is slightly expanded anteriorly. It forms a round tuber cox at the anterior end. Posteriorly, the iliac shaft becomes slender and is constricted just anterior to the acetabular margin. The ischium is L-shaped (about 90 degree), and can be divided into dorsal and vertical (posterior) plates (Figs. 4B–D, 16). The dorsal plate is dorsoventrally expanded at its anterior end to form the posterior aspect of the acetabular margin. The expansion of the posterior plate is more substantial than in the dorsal plate and it culminates posteriorly as the dorsal ischial tuberosity. The vertical plate, perpendicular to the dorsal plate, tapers medioventrally and forms a convex posterior margin that culminates in the ventral ischial tuberosity. Presumably, the pubes and the ventromedial ends of the posterior plates of the left and right ischia would meet along the sagittal plane of the pelvis to form a symphysis; however, this symphysis is not preserved. The pubis is straight and has a concave dorsal margin. The anterodorsal end of the pubis is concave and contributes to the ventral margin of the acetabulum (Figs. 4B–D, 16). The posterior end of the pubis articulates with the ventral end of the ischial vertical plate. Together, the ischium and pubis close the obturator foramen. We reconstructed the obturator foramen as a small oval opening. Both the left and right epipubes are displaced but within the pelvic region (Figs. 4B–D, 16). They are slender and rod-like, and they are a slightly ventrally curved at midlength.

The ilium of *Yanoconodon* differs from that of *Repenomamus* and *Zhangheotherium* (Hu et

al., 1997, 1998; Hu, 2006). In *Repenomamus*, the ilium is relatively short and broad, and the iliac wing has a posterodorsal iliac spine (Hu, 2006). In *Zhangheotherium*, the ilium becomes significantly elongate and slender, and it forms an angle at the ischium (Luo and Ji, 2005). In contrast, the L-shaped (90º angle) ischium of *Yanoconodon* resembles the ischium in *Morganucodon* ("*Eozostrodon*"), *Jeholodens, Repenomamus,* and *Liaoconodon* (Jenkins and Parrington, 1976; Ji et al., 1999; Hu, 2006; Meng et al., 2011), although the width of the vertical ischial plate is twice that of the dorsal plate in *Repenomamus* and *Morganucodon* (Jenkins and Parrington, 1976; Hu, 2006). In multituberculates and *Zhangheotherium*, the ischium forms an acute angle at the enlarged dorsal ischial tuberosity (Kielan-Jaworowska and Gambaryan, 1994; Luo and Ji, 2005). In *Yanoconodon*, the pubis lacks a tuberosity for attachment of the psoas minor muscle (sensu Gambaryan et al., 2002), but it is present on the anterodorsal plates in *Akidolestes* and living monotremes (Gambaryan et al., 2002; Li and Luo, 2006; Chen and Luo, 2013). In addition, the slender, rod-like epipubis of *Yanoconodon* differs from the plate-like epipubis of monotremes, *Repenomamus*, *Zhangheotherium*, and *Akidolestes* (Gambaryan et al., 2002; Luo and Ji, 2005; Hu, 2006; Chen and Luo, 2013).

Hind limb

Femur—Both the left and right femora are well preserved (Figs. 1, 2, 12A–C). The type specimen shows a contact between the acetabular region of the pelvis and the head of the laterally oriented femur, suggesting a preservation of the original anatomical position. The femoral head is bulbous and protrudes anteromedially, immediately followed by a shallow groove, the femoral neck, distally (Fig. 12A–C). Both the greater and lesser trochanters are not well developed. The greater trochanter is elevated higher than the lesser trochanter but lower than the femoral head. The third trochanter is absent. Along the trochanters, two separate crests

originate, extend distally, and stop at the mid-shaft. Together, the crests circumscribe a broad, shallow depression, the inter-trochanteric fossa, that extends distally immediately after the femoral neck. The femoral shaft is slightly constricted mediolaterally. The distal end of the femur bears the medial and lateral condyles separated by the shallow intercondylar groove. The lateral condyle has a larger profile than the medial one, suggesting an asymmetrical knee joint in *Yanoconodon*. The epicondyles are indistinctive. No patella is preserved in the knee region.

The femur of *Haldanodon*, multituberculates, gobiconodontids, symmetrodontans, *Henkelotherium*, basal metatherians and eutherians (Krause and Jenkins, 1983; Jenkins and Schaff, 1988; Krebs, 1991; Kielan-Jaworowska and Gambaryan, 1994; Ji et al., 2002; Luo et al., 2003; Luo and Ji, 2005; Hu, 2006; Chen and Luo, 2013) differ from that of *Yanoconodon* in having a prominent spherical head, distinct long neck, well-developed trochanters, and a slender shaft. In *Haldanodon*, *Gobiconodon*, *Repenomamus, Akidolestes*, and *Henkelotherium* the well-developed lesser and greater trochanters that project dorsomedially and dorsolaterally, respectively, drastically increase the width of the proximal end of the humerus (Krause and Jenkins, 1983; Jenkins and Schaff, 1988; Krebs, 1991; Hu, 2006; Chen and Luo, 2013). In zhangheotheriids and multituberculates, the femur has a symmetrical knee joint (Krause and Jenkins, 1983; Kielan-Jaworowska and Gambaryan, 1994; Rougier et al., 2003; Luo and Ji, 2005; but see the paulchoffatiid multituberculate *Rugosodon* [Yuan et al., 2013]). This symmetrical knee joint differs from the asymmetrical configuration in *Yanoconodon*, *Akidolestes*, and monotremes (Ji et al., 1999; Gambaryan et al., 2002; Martin, 2005; Hu, 2006; Kielan-Jaworowska and Hurum, 2006; Li and Luo, 2006; Hurum and Kielan-Jaworowska, 2008; Chen and Luo, 2013).

Tibia—Similar to the femur, both the left and right tibiae are well preserved. The tibia is

short and straight, and has a rounded proximal end and a flat distal end (Figs. 12D–F, 16). The proximal end has an oval and convex facet with a rim surrounding it. The shaft slightly tapers towards midshaft, and then slightly expands medially towards the distal end. A crest for attachment of a tibiofibular interosseous ligament is not preserved. The distal end of the right tibia bears a malleolus-like structure; no malleolus-like structure is preserved in the left tibia (Fig. 12E–F, 16). Judging by the difference in length (Table 1), we interpret the malleolus-like structure in the right tibia as an artifact of damage and thus, a malleolus is not present at the distal end of the tibia of *Yanoconodon*.

The tibia of *Yanoconodon* is similar in profile to that of *Thrinaxodon*, *Repenomamus*, and *Zhangheotherium* but differs from the more curved tibia of multituberculates and *Akidolestes* (Krause and Jenkins, 1983; Kielan-Jaworowska and Gambaryan, 1994; Hu et al., 1997, 1998; Hu, 2006; Hurum and Kielan-Jaworowska, 2008; Chen and Luo, 2013). In multituberculates, the tibia is uniformly curved ("bowed") anteromedially, whereas in *Akidolestes* the tibia is sigmoid-like. The proximal end of the tibia in *Thrinaxodon* and *Zhangheotherium* has medially oblique articular facet, and this facet contacts the lateral condyle of the femur (Jenkins and Parrington, 1976; Luo and Ji, 2005). In *Haldanodon*, multituberculates, and *Repenomamus*, the proximal end of the tibia is bilaterally expanded (Krause and Jenkins, 1983; Kielan-Jaworowska and Gambaryan, 1994; Hurum and Kielan-Jaworowska, 2008; Martin, 2005; Hu, 2006). In addition, the medial malleolus is well developed in *Akidolestes*, multituberculates, and living therians (Lessertisseur and Saban, 1967a; Kielan-Jaworowska and Gambaryan, 1994; Hurum and Kielan-Jaworowska, 2008; Chen and Luo, 2013; Yuan et al., 2013).

Fibula—Both fibulae are well preserved. The fibula is straight, and it has a shorter, slenderer profile than the tibia (Fig. 12D–E, 12G). The proximal end of the fibula is slightly

enlarged and has a rounded proximal articular surface. The distal end is slightly expanded and bears a subtly convex articular facet for the calcaneus. No malleolus is present on the distal end; this absence represents a plesiomorphic feature as in cynodonts and eutriconodonts.

All the fibulae of eutriconodontans are similar (Ji et al., 1999; Hu, 2006; Meng et al., 2011). However, the fibulae of eutriconodontans differ from those of monotremes and *Akidolestes* (Gambaryan et al., 2002; Chen and Luo, 2013). In both monotremes and *Akidolestes*, the fibula is strongly curved and has a hypertrophic parafibular process fused to the proximal end of the fibulae. Likewise, in multituberculates and extant marsupials the fibula has a parafibular processes (Krause and Jenkins, 1983; Argot, 2002; Yuan et al., 2013); the parafibular process is not present in *Yanoconodon*.

Tarsals and Pes—Seven tarsals are preserved as molds and scattered in both the main and counter parts (NJU-P06001A, B; Figs. 13A–D, 14–15). The calcaneus is the largest tarsal element. The anterior aspect of the calcaneus, which bears the oblique peroneal shelf and the calcaneocuboid facet (from the lateral to the medial direction), has a semicircular outline (Fig. X). The peroneal shelf is lateral to the cuboid facet and continuous with the latter. The anterolateral portion of the calcaneus protrudes anteriorly to form the calcaneocuboid facet that articulates with the cuboid. The anterior astragalar facet is medial to the calcaneocuboid facet. The calcaneoastragalar facet is preserved with a slightly concave area on the medial margin of the calcaneus. On the ventral side, the calcaneal tuber projects ventrally and medioposteriorly. On the dorsal side, an elongate and elevated structure extends anteromedially and posterolaterally. We interpret this structure as the calcaneofibular facet, which contacts the distal end of the fibula. The sustentacular facet is oriented obliquely, and it presumably supports the ventrolateral region of the astragalus (Figs. 13–15). Posterior to the sustentacular facet, a shallow

sulcus is preserved medial to the calcaneofibular facet. We interpret the sulcus as the homolog of the calcaneal sulcus. The calcaneus of *Yanoconodon* is similar in morphology to that of *Oligokyphus* and *Morganucodon*, which have a dorsally elevated calcaneofibular facet and a ventrally bent calcaneal tuber (Szalay, 1994). In contrast, the calcaneoastragalar and the calcaneofibular facets in the latter two taxa are closely positioned to the calcaneal tuber (see Szalay, 1994).

The astragalus of *Yanoconodon* is oblong and has a uniformly convex dorsal and medial surfaces (Figs. 13–15). The medial portion of the astragalus is thicker than the lateral portion, forming an oblique plane on the ventral side. The astragalonavicular facet is at the slightly convex anterior part. A medial depression extends longitudinally on the ventral side. Taken together, we interpret the depression as the contact plane (or partially at least) between the astragalus and the calcaneus. This implies that the astragalus would not have been entirely superimposed on the top of or "side-by-side" in complete juxtaposition to the calcaneus. Thus, we reconstruct the astragalocalcaneal articulation along the sustentacular and calcaneoastragalar facets, by approximately half of the width of the astragalus (Figs. 14–15). Because the calcaneofibular facet is extensive, the distal end of the fibula would partially contact the astragalus and the calcaneus.

The navicular is square-shaped. The anterior surface of the navicular is flat, and the posterior surface is slightly concave. These two surfaces contact the proximal ends of the cuneiforms and the astragalonavicular facet of the astragalus, respectively. The cuboid is bean-shaped with an uneven anterior surface. The anterior surface can be divided into the medial and lateral facets. These facets would contact the fourth metatarsal and entocuneiform and the medial portion of the distal end of the fifth metatarsal, respectively. Three cuneiforms show oblong

outlines and decrease in size from medial to lateral. The ectocuneiform is the smallest among all the tarsals. Because of the small size of the ectocuneiform, we infer that there was no direct contact between the ectocuneiform and the fifth metatarsal. Neither the os calcares of the extra-tarsal spur or an impression of the cornu calcares (*sensu* Hurum et al., 2006) is not preserved in the type specimen.

Five metatarsals (mt2–mt5) are well preserved. The metatarsals have bilaterally expended anterior and distal ends. The proximal and intermediate pedal phalanges are dumbell-shaped and longer than wide; the shafts of the intermediate phalanges have relatively slender outlines (Figs. 13A–D, 15). Only the first distal pedal phalanx is preserved. It has a lateral profile that is similar to that of the distal manual phalanges. The digital flexor tubercle on the distal phalanx is far away from the proximal end and the digital extensor tubercle is indistinctive. No flexor ossicles are preserved.

The ankle joint of *Yanoconodon* has a similar configuration to those of premammalian cynodonts (e.g., "Manda cynodont"), the haramiyidan *Megaconus,* morganucodontids, and eutriconodontans (Figs. 14–15; Kühne, 1956; Jenkins, 1971; Jenkins and Parrington, 1976; Szalay, 1994; Ji et al., 1999; Hu, 2006; Zhou et al., 2013). Unlike those taxa, multituberculates, *Zhangheotherium*, *Akidolestes*, and therians use a different configuration for the ankle joint (Kielan-Jaworowska and Gambaryan, 1994; Horovitz, 2000; Argot, 2002; Ji et al., 2002; Luo et al., 2003; Luo and Ji, 2005; Chen and Luo, 2013). They have the astragalus largely stacked on top of the calcaneus. Thus, the calcaneus lacks or has little contact with the distal end of the fibula. The offset between the cuboid and the fifth metatarsal occurs in premammalian cynodonts, eutriconodontans (including *Yanoconodon*), and basal therians (Fig. 14; Ji et al., 1999, 2002; Hu, 2006) but multituberculates, the spalacotheriid *Akidolestes* and the living

marsupial *Didelphis* (Fig. 14; Kielan-Jaworowska and Gambaryan, 1994; Ji et al., 2002; Chen and Luo, 2013). Functionally, the offset coupled with the peroneal shelf emarginate a large notch that serves as a passage for the tendon of the peroneus longus, which represents a common morphological design in extant therians (Fig. 15; Szalay, 1994) and one that has been interpreted for multituberculates (Kielan-Jaworowska and Gambaryan, 1994). In *Akidolestes*, the analogous offset is formed by the L-shaped cuboid and would serve the same function (Fig. 15E; Chen and Luo, 2013).

DISCUSSION

Dorsal Vertebral Identity Transition

The transition from thoracic to lumbar vertebrae has been documented among several Mesozoic mammals (e.g., Hu et al., 1997; Hu, 2006; Li and Luo, 2006; Luo et al., 2007a; Zhou et al., 2013; Bi et al., 2014) and may serve as a new morphological character for distinguish different taxa. Extant mammals typically have no ribs attached to the lumbars (Narita and Kuratani, 2005; Sánchez-Villagra et al., 2007); thus, regardless of the number of dorsal vertebrae, the disruption of the rib attachment in the dorsal series indicates the transition from thoracic to lumbar vertebrae (Filler, 1986; Evans, 1993). Some Mesozoic mammals, however, have ribs attached to the entire dorsal vertebrae, forming a gradational transition between the thoracic and lumbar vertebrae (Hu, 2006; Li and Luo, 2006; Luo et al., 2007a). The gradational change of the length and profile of the rib was used for separating the thoracics from the lumbars (Li and Luo, 2006; Luo et al., 2007a).

Nevertheless, recent studies of the evolutionary development of the vertebral column indicate that the rib attachment may be a false signature for identifying the transition between the

thoracics and lumbars (Vinagre et al., 2010; Guerreiro et al., 2013). Developmental genetic studies indicate that the *Hox* genes, such as *Hox6/Hox10*, control vertebral identities and thoracolumbar transformation (e.g., Wellik and Capecchi, 2003; McIntyre et al., 2007). The gene expression of *Myf5* and *Myf6* in the hypaxial myotome mediates the rib formation in the dorsal vertebrae through an interaction with relevant enhancers (Vinagre et al., 2010; Guerreiro et al., 2013) that are downstream from *Hox6*/*Hox10* genes (Wellik and Capecchi, 2003; McIntyre et al., 2007; Wellik, 2007). The down cascade regulation induces the different formations of the rib attachment, which, in theory, may not be fully correlated with the dorsal vertebral identities as characterized in these *Hox6/Hox10* studies (Vinagre et al., 2010; Guerreiro et al., 2013). Therefore, we suggest that the rib attachment may not be a reliable indicator for identifying the thoracic-lumbar transition in the dorsal vertebrae of fossil mammals, if conflicted by the segmental identities of the vertebral centra and neural arches.

Three other morphological approaches are also used for identifying the thoracic-lumbar transition: 1) presence of independent transverse processes in the lumbars (usually not in the thoracics; Filler, 1986; Evans, 1993); 2) orientation of the contacting facets between pre- and post-zygapophyses: more vertically oriented in lumbars than in thoracics (e.g., Evans, 1993; Argot, 2003); and 3) direction of anapophysis projecting (if present). In *Yanoconodon*, the zygapophyses of the dorsal vertebrae are well preserved in the molds and the orientations of the articular facets are discernible for identifying the thoracic-lumbar transition (Fig. 17). Thus, it would be more appropriate to use the change of the orientation of the zygapophyses to recognize the thoracic-lumbar identity transition. In *Yanoconodon*, D14 is the anterior-most vertebra that shows the vertical orientation of the pre-zygapophyses; we thus interpret that D14 is a bona fide lumbar vertebrae and that the thoracic-lumbar transition occurs between D13 and D14. We revise

the numbers of the thoracic and the lumbar of *Yanoconodon* to 13 and 12, respectively. Likewise, we indicate that *Repenomamus* has 16 thoracics and ten lumbars in the dorsal series (IVPP V12549; Hu, 2006: figs. 3-8). The new interpretation of the dorsal vertebral identity in *Yanoconodon* and *Repenomamus* becomes consistent with that in *Jeholodens* (Ji et al., 1999). Furthermore, the revised identity of the dorsal vertebrae indicates that the trunk elongation in *Yanoconodon* is due to an increasing number of the lumbar vertebrae rather than the thoracic vertebrae as in afrotherians (Narita and Kuratani, 2005).

Limb Posture in *Yanoconodon*

Limb posture is associated with locomotor modes and will aid to infer the locomotor mode of *Yanoconodon*. In *Yanoconodon*, the glenoid fossa of the scapula faces ventrolaterally and articulates with a large and spindle-like humeral head (Fig. 16). The shoulder girdle lacks the "ball-in socket" glenohumeral joint that is correlated to the erect posture (Jenkins and Weijs, 1979). The humerus has some torsion and resembles those of premammalian cynodonts and Jurassic mammals that have been hypothesized to have sprawling limb posture (Jenkins, 1973). No trochlea is formed in the humeroulnar joint to reinforce the parasagittal movement of the forearm (Figs. 9, 16). These features together suggest that the forelimb of *Yanoconodon* had an abducted glenohumeral joint with a habitually flexed elbow joint in a semi-sprawling forelimb (Gambaryan and Kielan-Jaworowska; 1997; Kielan-Jaworowska and Hurum, 2006).

In the hind limb, the femur has a small head without a distinct neck, a slightly elevated greater trochanter, and an asymmetrical knee joint as in extinct premammalian cynodonts (Fig. 16; Kühne, 1956; Jenkins, 1971; Sun and Li, 1985). These features, however, are different from those in monotremes. In monotremes, the femur has the well developed lesser and greater

trochanters of nearly equal size, and the femur abducts horizontally with a highly elevated distal end (Jenkins, 1970b; Pridmore, 1985; Gambaryan et al., 2002). Thus, *Yanoconodon* may have adopted a sprawling posture as in premammalian cynodonts rather than in monotremes. We interpret that *Yanoconodon* would have had a semi-sprawling posture in both the forelimb and the hind limb.

Functional Study of Postcranial Elements of *Yanoconodon*

Pectoral Girdle—The pectoral girdle of *Yanoconodon* has derived morphological features, including a triangular scapula and a pivotal and mobile clavicle-interclavicle joint. Unlike the rigid clavicle-interclavicle joint in the terrestrial *Sinoconodon*, morganucodontids, and *Pseudotribos* (Jenkins, 1971; Klima, 1973; Jenkins and Parrington, 1976; Sun and Li, 1985; Luo et al., 2007b), the pivotal and mobile clavicle-interclavicle joint allows the pectoral girdle of *Yanoconodon* to perform a variety of movements, including the flexion and extension of the pectoral girdle as in extant therians. Sereno (2006) argued that the pivotal clavicle-interclavicle joint of the pectoral girdle in multituberculates would indicate an erect posture. However, many extinct species that have the pivotal interclavicle-clavicle joint are inferred to have sprawling forelimbs (Kielan-Jaworowska and Hurum, 2006; Chen and Luo, 2013).

Extant mammals that share the triangular scapula adopt different locomotor modes (Lessertisseur and Saban, 1967b). In living didelphids, arboreal species have a more triangular scapula with a better-developed scapular angle than in terrestrial species (Argot, 2001; Flore et al. 2009). The triangular scapula consists of an enlarged supraspinous and infraspinous fossae for inserting large supraspinatus and infraspinatus muscles that stabilize the glenohumeral joint (Jenkins and Weijs, 1979). The well-developed, scapular angle increases the lever arm of the

muscle teres major for retracting the humerus and the torque production during the extension of humerus while climbing (Marynard Smith and Savage, 1956; Jenkins and Weijs, 1979; Argot, 2001). Nevertheless, triangular scapula with similar morphology are also found in *Cynocephalus*, *Geomys*, *Pedetes*, *Procavia*, and *Trichechus* that adopt gliding, fossorial, saltatorial, scansorial, and aquatic locomotor modes, respectively (Howell, 1930; Nowak, 1999; Stein, 2000). Taken together, we interpret that the pectoral girdle of *Yanoconodon* can adduct, flex, extend, and medially rotate. These movements would allow *Yanoconodon* to perform diverse locomotions in terrestrial ecosystems.

Ulna and Radius—*Yanoconodon* has a relatively robust and short ulna and radius as in extant fossorial mammals (Hildebrand, 1985; Stein, 2000). The ulna of *Yanoconodon*, however, lacks a large olecranon process with a confined trochlear notch for securing the elbow during digging (Fig. 16; Taylor, 1974; Hildebrand et al., 1985; Stein, 2000; Argot, 2001; Sargis, 2002; Samuels and Van Valkenburgh, 2008; Samuels et al., 2012; Chen and Wilson, in press). The wide-open trochlear notch of the ulna in *Yanoconodon* resembles that in aquatic *Trichechus* (Lessertisseur and Saban, 1967b). As in *Trichechus*, the wide-open trochlear notch in *Yanoconodon* may increase the range of the elbow movement during the flexion and extension, such as swimming locomotion. Furthermore, lack of a styloid process in the distal ends of the radius and ulna increases the range of abduction and adduction of the wrist joint in *Yanoconodon*, as in premammalian cynodonts and *Haldanodon* (Kühne, 1956; Jenkins, 1971; Sun and Li, 1985; Martin, 2005; Sues and Jenkins, 2006). In arboreal animals, the abducted manus enhances the prehensility of the forelimb, which helps slow down or stop descending and prevents the animal from falling off a tree during the head-descending locomotion (Cartmill, 1985). In contrast, the presence of a styloid process prevents manus from over-abducting and

over-adducting and secures the movement of the wrist in more parasagittal plane during locomotion.

Wrist and Manus— Based on the reconstruction, *Yanoconodon* has a small wrist, a large palm, and divergent fingers, forming a funnel shape. We interpret that the funnel shape of the manus is due to the large distal ends and the small proximal ends of the metacarpals, leading phalanges to diverge distally (Figs. 10, 11). The funnel shaped manus of *Yanoconodon* resembles that of *Kayentatherium* and *Haldanodon* that are inferred to have fossorial and semiaquatic locomotor modes (Fig. 11; Martin, 2005; Sues and Jenkins, 2006; Egberth et al., 2009). In the distal phalanges, the distally placed digital flexor tubercles increase the in-lever arm for the flexion, and, in turn, the tips of the distal phalanges would produce powerful force for digging. The lateral profiles of the distal phalanges in *Yanoconodon*, however, are more similar to those of extant semiaquatic taxa than to extant fossorial taxa (sensu lato aquatic, MacLeod and Rose, 1993); the lateral profiles in *Haldanodon* show similarities to those in fossorial taxa (Hildebrand, 1985; MacLeod and Rose, 1993; Stein, 2000). Thus, we suggest that *Haldanodon* may have been more capable of digging than *Yanoconodon* was.

Ankle Joint—Lack of the malleoli in the distal ends of the tibia and fibula suggests *Yanoconodon*, perhaps also eutriconodontans as a whole (Ji et al., 1999; Hu, 2006), would have had a mobile upper ankle joint (UAJ). Theoretically, the upper ankle joint of *Yanoconodon* could not be constrained in any directions and may rotate horizontally relative to the tibia-fibula. The configuration of the UAJ is consistent with other aspects of freeing the UAJ joint in eutriconodontans (including *Yanoconodon*), such as no trochlea-like articular surfaces on the dorsal aspect of the astragalus. By contrast, the presence of the malleoli increase the stability of the UAJ and guide it in fore-aft movement (Chen and Luo, 2013). In the lower ankle joint (LAJ)

of *Yanoconodon*, half the width of the astragalus is partially superimposed on the calcaneus (Fig. 9), which resembles those of *Thrinaxodon, Oligokyphus*, and *Morganucodon* (Kühne, 1956; Jenkins, 1971; Jenkins and Parrington, 1976; Szalay, 1994). This limited superimposition would increase the mediolateral mobility in the LAJ in *Yanoconodon*, which is in contrast to the juxtaposition in premammalian cynodonts that promotes abduction and adduction in the LAJ. Therefore, the rotatable UAJ and partially superimposed LAJ increase the inversion-eversion range of the foot during locomotion (Szalay, 1994; Ji et al., 2002; Luo et al., 2003; Luo and Ji, 2005; Chen and Luo, 2013). Muizon (1998) concluded that the capability of inversion and eversion of the foot indicates that animal is capable of moving on uneven, discontinuous substrates, such as climbing. Thus, the ankle joint of *Yanoconodon* has great capabilities in performing abduction-adduction and inversion-eversion and it shows adaptive features for accommodating diverse locomotions.

Locomotor Diversity of Eutriconodont Mammals

The postcranial skeleton of *Yanoconodon* shows a composite of adaptive features for diverse locomotions, including digging and swimming. Likewise, extant small-bodied digging and swimming mammals share a number of postcranial morphologies (Chen and Wilson, in press). Fossorial mammals, however, show more forelimb-dominant locomotion than the semiaquatic ones (Samuels and Van Valkenburgh, 2008; Samuels et al., 2013; Chen and Wilson, in press), whereas some semiaquatic mammals, *Ornithorhynchus* for example, are also good diggers. Thus, we suggest *Yanoconodon* was a terrestrial mammal, capable of swimming rather than digging, given it lacks key adaptive features for digging, including the large olecranon process and confined trochlear notch in the ulna, and stout proximal and intermediate phalanges

and broad wrist in the hand. Our results are consistent with the previous locomotor inference of *Yanoconodon* (Chen and Wilson, 2015). In addition, this study provides the detailed documentation and functional analyses of the postcranial skeleton of *Yanoconodon*.

Within Eutriconodonta, *Repenomamus* and *Jeholodens* have been interpreted as adapted to semifossorial and arboreal/terrestrial locomotor modes, respectively (Chen and Wilson, in press). This contrasts with the semiaquatic locomotor mode of *Yanoconodon*. In *Jeholodens,* the derived and therian-like pectoral girdle and forelimb but plesiomorphic pelvic girdle, hind limb, and pes show adaptive features for climbing locomotion (Ji et al., 1999); in *Repenomamus* the robust postcranial elements with well-developed tubercles and crests for inserting large muscles (Hu, 2006) exhibit an adaptation for producing powerful propulsive strokes during digging locomotion (Chen and Wilson, in press). In addition, *Gobiconodon*, *Liaoconodon*, and the possible eutriconodontan *Volaticotherium* (see Gaetano and Rougier, 2011, 2012) show adaptive morphologies for terrestrial, semiaquatic, and gliding locomotion, respectively (Meng et al., 2006; Chen and Wilson, in press). Taken together, we indicate that eutriconodontans evolved diverse postcranial features for adapting to different locomotor modes more than 125 Myr ago. Given the current phylogeny, we indicate that the ecomorphological diversification not only occurred within Eutriconodonta at the ordinal level but also within Jeholodentidae at the family level. This echoes previous findings within the symmetrodontan family Spalacotheriidae and further supports the notion that ecological diversification at lower taxonomic levels was a basic feature of early mammal evolution (Chen and Luo, 2013).

ACKNOWLEDGMENTS

We thank Profs. P.-J. Chen and G. Li for generously providing this fossil for our study; A. R. Tabrum for his skillful preparation of and R. Masek for making excellent casts of the fossil; Q. Yang, X.-D. Wang, H.-C. Zhang, X.-N. Yang, Y.-K. Shi, and B.-Y. Jiang for their help with this research at NIGPAS and NJU; and A. Ish for assistance with graphics. We also would like to thank L. DeBey, D. DeMar, J. Calede, and S. Smith for providing constructive comments on early draft. Support was provided by the WRF-Hall Fellowship, University of Washington (MC) and National Science Foundation (USA), and University of Chicago (ZXL).

LITERATURE CITED

Argot, C. 2001. Functional-adaptive anatomy of the forelimb in the Didelphidae, and the paleobiology of the Paleocene marsupials *Mayulestes ferox* and *Pucadelphys andinus*. Journal of Morphology 247:51–79.

Argot, C. 2002. Functional-adaptive analysis of the hindlimb anatomy of extant marsupials and the paleobiology of the Paleocene marsupials *Mayulestes ferox* and *Pucadelphys andinus*. Journal of Morphology 253:76–108.

Argot, C. 2003. Functional-adaptive anatomy of the axial skeleton of some extant marsupials and the paleobiology of the Paleocene marsupials *Mayulestes ferox* and *Pucadelphys andinus*. Journal of Morphology 255:279–300.

Bi, S.-D., Y.-Q. Wang, j. Guan, X. Sheng, and J. Meng. 2014. Three new Jurassic euharamiyidan speciesreinforce early divergence of mammals. Nature 514:579–584.

Boyer D. M., G. V. R. Prasad, D. W. Krause, M. Godinot, A. Goswami, O. Verma, and J. J. Flynn. 2010. New postcrania of *Deccanolestes* from the Late Cretaceous of India and their bearing on the evolutionary and biogeographic history of euarchontan mammals. Naturwissenschaften 97:365–377.

Buchholtz, E. A., H. G. Bailin, S. A. Laves, J. T. Yang, M.-Y. Chan, and L. E. Drozd. 2012. Fixed cervical count and the origin of the mammalian diaphragm. Evolution & Development 14:399–411.

Cartmill, M. 1985. Climbing: pp. 73-88 in M. Hildebrand, D. M. Bramble, K. F. Liem and D. B. Wake (eds.). Functional Morphology of Vertebrates. Belknap Press of Harvard University Press, Cambridge, Massachusetts.

Chen, M., and Z.-X. Luo. 2013. Postcranial skeleton of the Cretaceous mammal *Akidolestes*

cifellii and its locomotor adaptations. Journal of Mammalian Evolution 20:159–189.

Chen, M., and G. P. Wilson. In press. A multivariate approach to infer locomotor modes in Mesozoic mammals. Paleobiology.

Chester, S. G. B., Sargis, E. J., Szalay, F. S., Archibald, J. D., and A. O. Averianov. 2010. Mammalian distal humeri from the Late Cretaceous of Uzbekistan. Acta Palaeontologica Polonica 55:199–211.

Crompton, A. W., and Z.-X. Luo. 1993. The relationships of the Liassic mammals *Sinoconodon*, *Morganucodon oehleri* and *Dinnetherium*; pp. 30–44, *in* F. S. Szalay, M. J. Novacek, and M. C. McKenna (eds.), Mammal Phylogeny. Springer-Verlag, New York.

Damiani, R., S. P. Modesto, A.Yates, and J. Neveling. 2003. Earliest evidence of cynodont burrowing. Proceedings of Royal Society (London) Series B 270:1747–1751.

Gambaryan, P. P., A. A. Aristov, J. M. Dixon, and G. Y. Zubtsova. 2002. Peculiarities of the hind limb musculature in monotremes: an anatomical description and functional approach. Russian Journal of Theriology 1 (1):1–36.

Egberts, S., T. B. Rowe, H.-D. Sues, Z.-X. Luo, and F. A. Jenkins. 2009. The first semi-aquatic synapsid from the Kayenta formation, Arizona. Journal of Vertebrate Paleontology 29(3, Supplement): 91A.

Evan, H. E. 1993. Miller's Anatomy of the Dog (3rd Edition). W. B. Saunders, Philadelphia, Pennsylvania, 1113 pp.

Fernandez, V., F. Abdala, K. J. Carlson, D. C. Cook, B. S. Rubidge, A. Yates, and P. Tafforeau. 2013. Synchrotron reveals Early Triassic odd couple: injured amphibian and aestivating therapsid share burrow. PLoS One 8(6):e64978. doi:10.1371/journal.pone.0064978.

Filler, A. G. 1986. Axial character seriation in mammals: an historical and morphological

exploration of the origin, development, use and current collapse of the homology paradigm. Ph.D. Dissertation, Harvard University, Cambridge, Massachusetts, 388 pp.

Gaetano, L. C., and G. W. Rougier, 2011. New materials of *Argentoconodon fariasorum* (Mammaliaformes, Triconodontidae) from the Jurassic of Argentina and its bearing on triconodont phylogeny. Journal of Vertebrate Paleontology 31:829–843.

Gaetano, L. C., and G. W. Rougier. 2012. First amphilestid from South America: a molariform from the Jurassic Cañadón Asfalto Formation, Patagonia, Argentina. Journal of Mammalian Evolution 19:235–248.

Gambaryan, P. P., and Z. Kielan-Jaworowska. 1997. Sprawling versus parasagittal stance in multituberculate mammals. Acta Palaeontologica Polonica 42:13–44.

Gao, C.-L., G. Wilson, Z.-X. Luo, A. Maga, Q.-J. Meng, and X.-R. Wang. 2009. A new mammal skull from the Lower Cretaceous of China with implications for the evolution of obtuse-angled molars and "amphilestid" eutriconodonts. Proceedings Biological Sciences 277:237–246.

Guerreiro, I. A., Nunes, J. M. Woltering, A. Casaca, A. Nóvoa, T. Vinagre, M. E. Hunter, D. Duboule, and M. Mallo. 2013. Role of a polymorphism in a Hox/Pax-responsive enhancer in the evolution of the vertebrate spine. Proceedings of National Academy of Sciences 110:10682–10686.

Hildebrand, M. 1985. Digging of quadrupeds; pp. 89–109 in M. Hildebrand, D. M. Bramble, K. F. Liem and D. B. Wake (eds.). Functional Morphology of Vertebrates. Belknap Press of Harvard University Press, Cambridge, Massachusetts.

Horovitz, I. 2000. The tarsus of *Ukhaatherium nessovi* (Eutheria, Mammalia) from the Late Cretaceous of Mongolia: an appraisal of the evolution of the ankle in basal therians.

Journal of Vertebrate Paleontology 20:547–560.

Horovitz, I. 2003. Postcranial skeleton of *Ukhaatherium nessovi* (Eutheria, Mammalia) from the Late Cretaceous of Mongolia. Journal of Vertebrate Paleontology 23:857–868.

Hu, Y.-M. 2006. Postcranial morphology of *Repenomamus* (Eutriconodonta, Mammalia): implications for the higher-level phylogeny of mammals. Ph.D. dissertation, The City University of New York, New York, 405 pp.

Hu, Y.-M., J. Meng, Y.-Q. Wang, and C.-K. Li. 2005. Large Mesozoic mammals fed on young dinosaurs. Nature 433:149–152.

Hu, Y.-M., Y.-Q. Wang, C.-K. Li, and Z.-X. Luo. 1998. Morphology of dentition and forelimb of *Zhangheotherium*. Vertebrata PalAsiatica 36:102–125. [Chinese 102–112; English 113–125]

Hu, Y.-M., Y.-Q. Wang, Z.-X. Luo, and C.-K. Li. 1997. A new symmetrodont mammal from China and its implications for mammalian evolution. Nature 390:137–142.

Hurum, J. H., Z.-X. Luo, and Z. Kielan-Jaworowska. 2006. Were mammals originally venomous? Acta Palaeontologica Polonica 51:1–11.

Hurum, J. H., and Z. Kielan-Jaworowska. 2008. Postcranial skeleton of a Cretaceous multituberculate mammal *Catopsbaatar*. Acta Palaeontologica Polonica 53:545–566.

Jenkins, F. A., Jr. 1970a. The Chañares (Argentina) Triassic reptile fauna VII. The postcranial skeleton of the traversodontid *Massetognathus pascuali* (Therapsida, Cynodontia). Breviora, 352:1–28.

Jenkins, F. A., Jr. 1970b. Limb movements in a monotreme (*Tachyglossus aculeatus*): a cineradiographic analysis. Science 168:1473–1475.

Jenkins, F. A., Jr. 1971. The postcranial skeleton of African cynodonts. Peabody Museum of

Natural History Bulletin 36:1–216.

Jenkins, F. A., Jr. 1973. The functional anatomy and evolution of the mammalian humero-ulnar articulation. American Journal of Anatomy 137:281–297.

Jenkins, F. A., Jr. 1974. Tree shrew locomotion and the origin of primate arborealism; pp. 85–116 in F. A. Jenkins, Jr. (ed.), Primate Locomotion. Academic Press, New York.

Jenkins, F. A., Jr., and F. Parrington. 1976. Postcranial skeletons of Triassic mamamls *Eozostrodon*, *Megazostrodon* and *Erythrotherium*. Philosophical Transactions of the Royal Society of London Series B-Biological Sciences 273:387–431.

Jenkins, F. A., Jr., and C. R. Schaff. 1988. The Early Cretaceous mammal *Gobiconodon* (Mammalia, Triconodonta) from the Cloverly Formation in Montana. Journal of Vertebrate Paleontology 8:1–24.

Jenkins, F. A., Jr., and W. A. Weijs. 1979. The functional anatomy of the shoulder in the Virginia opossum (*Didelphis virginiana*). Journal of Zoology 188:379–410.

Ji, Q., Z.-X. Luo, and S.-A. Ji. 1999. A Chinese triconodont mammal and mosaic evolution of the mammalian skeleton. Nature 398:326–330.

Ji, Q., Z.-X. Luo, C.-X. Yuan, J. R. Wible, J.-P. Zhang, and J. A. Georgi. 2002. The earliest known eutherian mammal. Nature 416:816–822.

Kemp, T. S. 1983. The relationships of mammals. Zoological Journal of the Linnean Society 77:353–384.

Kemp, T. S. 2005. The origin and evolution of mammals. Oxford University Press, Oxford, UK, 342 pp.

Kielan-Jaworowska, Z. 1989. Postcranial skeleton of a Crtetaceous Multituberculate mammal. Acta Palaeontologica Polonica 34:75–78.

Kielan-Jaworowska, Z., and P. P. Gambaryan. 1994. Postcranial anatomy and habits of Asian multituberculate mammals. Fossils and Strata 36:1–92.

Kielan-Jaworowska, Z., and H. J. Hurum. 2006. Limb posture in early mammals: sprawling or parasagittal. Acta Palaeontologica Polonica 51:393–406.

Kielan-Jaworowska, Z., R. L. Cifelli, and Z.-X. Luo (eds.). 2004. Mammals from the Age of Dinosaurs: Origins, Evolution, and Structure. Columbia University Press, New York, 630 pp.

Klima, M. 1973. Die Frühentwicklung des Schultergürtels und des Brustbeins den Monotremen (Mammalia: Prototheria). Advances in Anatomy, Embryology, and Cell Biology 47:1–80.

Klima, M. 1987. Early development of the shoulder girdle and sternum in marsupials (Mammalia: Metatheria). Advances in Anatomy, Embryology, and Cell Biology 109:1–91.

Krebs, B. 1991. [Das Skelett von *Henkelotherium guimarotae* gen. et sp. nov. (Eupantotheria, Mammalia) aus dem Oberen Jura von Portugal]. Berliner geowissenschaftliche Abhandlungen A 133:1–121. [German]

Krause, D. W., and F. A. Jenkins, Jr. 1983. The postcranial skeleton of North American multituberculates. Bulletin of the Museum of Comparative Zoology 150:199–246.

Kühne, W. G. 1956. The Liassic therapsid *Oligokyphus*. British Museum (Natural History), London, UK, 149 pp.

Kusuhashi, N., Y.-M. Hu, Y.-Q. Wang, S. Hirasawa, and H. Matsuoka. 2009. New triconodontids (Mammalia) from the Lower Cretaceous Shahai and Fuxin formations, northeastern China. Geobios 42:765–781.

Lessertisseur, J., and R. Saban. 1967a. [Squelette axial; in P.-P. Grassé (ed.) Traité de Zoologie. Tome XVI (Fascicule I)]. Mammifères: Téguments et Squelette, Masson, Paris, 89 pp.

[French]

Lessertisseur, J., and R. Saban. 1967b. [Squelette appendiculaire; in P.-P. Grassé (ed.) Traité de Zoologie. Tome XVI (Fascicule I)]. Mammifères: Téguments et Squelette, Masson, Paris, 370 pp. [French]

Li, G., and Z.-X. Luo. 2006. A Cretaceous symmetrodont therian with some monotreme-like postcranial features. Nature 439:195–200.

Lillegraven, J. A., Kielan-Jaworowska, Z., and Clemens, W. A. (eds.). 1979. Mesozoic Mammals: The First Two-thirds of Mammalian History. University of California Press, Berkeley, California, 311 pp.

Luo, Z.-X. 2007. Transformation and diversification in early mammal evolution. Nature 450:1011–1019.

Luo, Z.-X., and Q. Ji. 2005. New study on dental and skeletal features of the Cretaceous "symmetrodontan" mammal *Zhangheotherium*. Journal of Mammalian Evolution 12:337–357.

Luo, Z.-X., and J. R. Wible. 2005. A Late Jurassic digging mammal and early mammalian diversification. Science 308:103–107.

Luo, Z.-X., P.-J. Chen, G. Li, and M. Chen. 2007a. A new eutriconodont mammal and evolutionary development in early mammals. Nature 446:288–293.

Luo, Z.-X., Q. Ji, and C.-X. Yuan. 2007b. Convergent dental adaptations in pseudo-tribosphenic and tribosphenic mammals. Nature 450:93–97.

Luo, Z.-X., Q. Ji, J. R. Wible, and C.-X. Yuan. 2003. An Early Cretaceous tribosphenic mammal and metatherian evolution. Science 302:1934–1940.

MacLeod, N., and K. D. Rose. 1993. Inferring locomotor behavior in paleogene mammals via

eigenshape analysis. American Journal of Science 293A:300–355.

Martin, T., and A. O. Averianov. 2007. A previously unrecognized group of Middle Jurassic triconodontan mammals from Central Asia. Naturwissenschaften 94:43–48.

McIntyre, D. C., S., Rakshit, A. R. Yallowitz, L. Loken, L. Jeannotte, M. R. Capecchi, and D. M. Wellik. 2007. Hox patterning of the vertebrate rib cage. Development 34:2981–2989.

Meng, J., Y.-Q. Wang, and C.-K. Li. 2011. Transitional mammalian middle ear from a new Cretaceous Jehol eutriconodont. Nature 472:181–185.

Meng, J., Y.-M. Hu, Y.-Q. Wang, and C.-K. Li. 2005. A new triconodont species (Mammalia) from the Early Cretaceous Yixian Formation of Liaoning, China. Vertebrata PalAsiatica 43:1–10.

Meng, J., Y.-M. Hu, C.-K. Li, and Y.-Q. Wang. 2006. The mammal fauna in the Early Cretaceous Jehol Biota: implications for diversity and biology of Mesozoic mammals. Geological Journal 41:439–463.

Montellano, M. J. A. Hopson, and J. M. Clark. 2008. Late Early Jurassic mammaliaforms from Huizachal Canyon, Tamaulipas, México. Journal of Vertebrate Paleontology 28:1130–1143.

Muizon, C. de.1998. *Mayulestes ferox*, a borhyaenoid (Metatheria, Mammalia) from the early Palaeocene of Bolivia. Phylogenetic and palaeobiologic implications. Geodiversitas 20:19–142.

Narita, Y., and S. Kuratani. 2005. Evolution of vertebral formulae in mammals: a perspective on developmental constraints. Journal of Experimental Zoology 304B:91–106.

Pridmore, P. A. 1985. Terrestrial locomotion in monotremes (Mammalia: Monotremata). Journal of Zoology 205:53–73.

Rougier, G. W., Q. Ji, and M. J. Novacek. 2003. A new symmetrodont mammal with fur impressions from the Mesozoic of China. Acta Geologica Sinica 77:7–14.

Salton, J. A., and E. J. Sargis. 2008. Evolutionary morphology of the Tenrecoidea (Mammalia) forelimb skeleton; pp. 51–71 in E. J. Sargis and M. Dagosto (eds.), Mammalian Evolutionary Morphology. Springer, Netherlands.

Samuels, J. X., and B. Van Valkenburgh. 2008. Skeletal indicators of locomotor adaptations in living and extinct rodents. Journal of Morphology 269:1387–1411.

Samuels, J. X., J. A. Meachen, and S. A. Sakai. 2012. Postcranial morphology and the locomotor habits of living and extinct carnivorans. Journal of Morphology 274:121–146.

Sargis, E. J. 2001. The grasping behaviour, locomotion and substrate use of the tree shrews *Tupaia minor* and *T. tana* (Mammalia, Scandentia). Journal of Zoology 253:485–490.

Sargis, E. J. 2002. Functional morphology of the forelimb of tupaiids (Mammalia, Scandentia) and its phylogenetic implications. Journal of Morphology 253:10–42.

Sereno, P. C. 2006. Shoulder girdle and forelimb in multituberculates: evolution of parasagittal forelimb posture in mammals; pp. 315–366 in M.T. Carrano, T.J. Gaudin, R.W. Blob, and J. R. Wible (eds.), Amniote Paleobiology: Perspectives on the Evolution of Mammals, Birds, and Reptiles. University of Chicago Press, Chicago, Illinois.

Sereno, P. C., and M. C. McKenna. 1995. Cretaceous multituberculate skeleton and the early evolution of the mammalian shoulder girdle. Nature 377:144–147.

Sues, H.-D., and F. A. Jenkins, Jr. 2006. The postcranial skeleton of *Kayentatherium wellesi* from the Lower Jurassic Kayenta Formation of Arizona and the phylogenetic significance of postcranial Features; pp. 114–152 in M.T. Carrano, T.J. Gaudin, R.W. Blob, and J. R. Wible (eds.), Amniote Paleobiology: Perspectives on the Evolution of Mammals, Birds,

and Reptiles. University of Chicago Press, Chicago, Illinois.

Sun, A.-L., and Y.-H. Li. 1985. [The postcranial skeleton of the late tritylodont Bienotheroides]. Vertebrata PalAsiatica 23:135–151. [Chinese]

Szalay, F. S. 1994. Evolutionary history of the marsupials and an analysis of osteological characters. Cambridge University Press, Cambridge, UK, 481 pp.

Szalay, F. S., and E. J. Sargis. 2001. Model-based analysis of postcranial osteology of marsupials from the Palaeocene of Itaboraí (Brazil) and the phylogenetics and biogeography of Metatheria. Geodiversitas 23:139–302.

Taylor, M. E. 1974. The functional anatomy of the forelimb of some African Viverridae (Carnivora). Journal of Morphology 143:307–335.

Varela-Lasheras, I., Bakker, A. J., S. D. van der Mije, J. A. J. Metz, J. van Alphen and F. Galis. 2011. Breaking evolutionary and pleiotrophic constraints in mammals: on sloths, manatees and homeotic mutations. EvoDevo 2(1):1–27.

Wellik, D. M. 2007. Hox Patterning of the vertebrate axial skeleton. Developmental Dynamics 236:2454–2463.

Wellik, D. M., and M. R. Capecchi. 2003. *Hox10* and *Hox11* genes are required to globally pattern the mammalian skeleton. Science 301:363–366.

Yuan, C.-X., Q. Ji, Q.-J. Meng, A.-R. Tabrum, and Z.-X. Luo. 2013. Earliest evolution of multituberculate mammals revealed by a new Jurassic fossil. Science 341:779–783.

Zheng, X.-T., S.-D. Bi, X.-L. Wang, and J. Meng. 2013. A new arboreal haramiyid shows the diversity of crown mammals in the Jurassic period. Nature 500:199–202.

Zhou, C.-F., S.-Y. Wu, T. Martin, and Z.-X. Luo. 2013. A Jurassic mammaliaform and the earliest mammalian evolutionary adaptations. Nature 500:163–167.

FIGURES

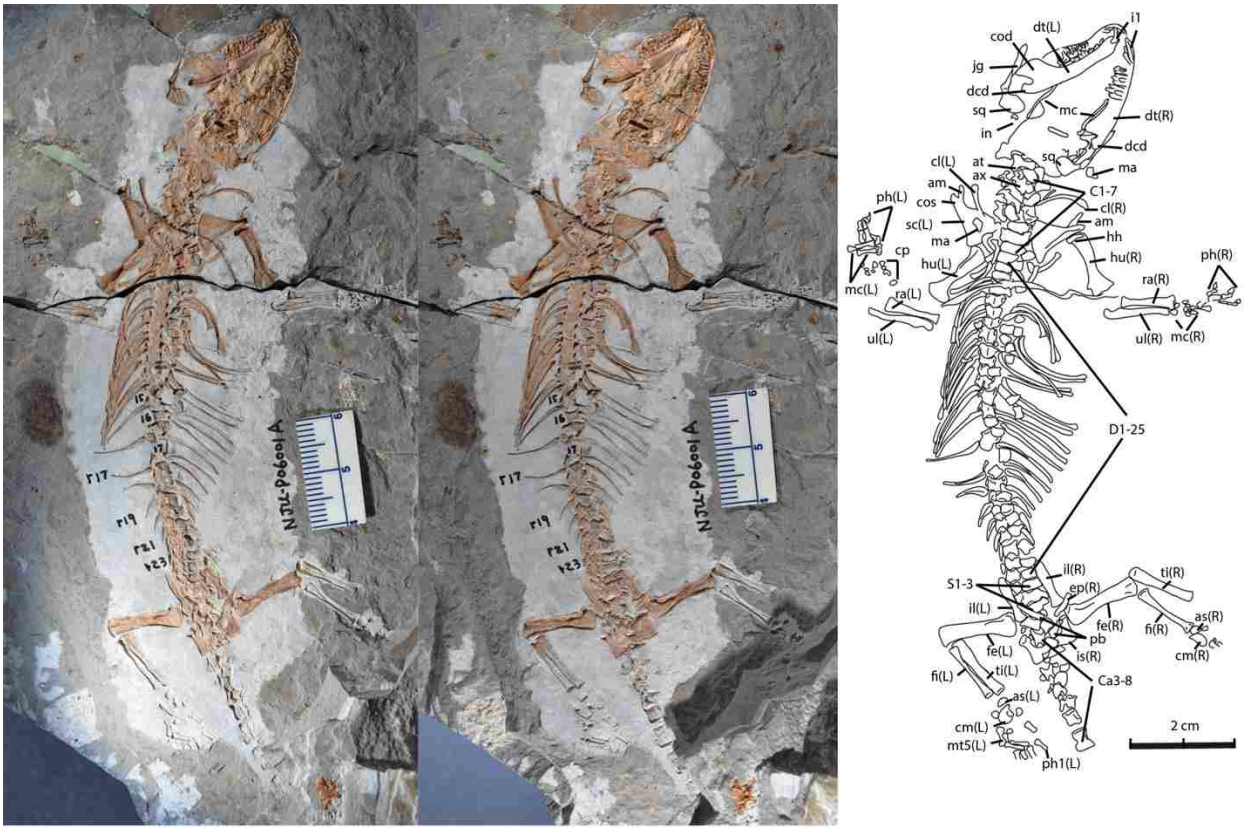

FIGURE 1. Stereophotographs and illustration of *Yanoconodon allini* in the main part, NJU-P06001A.

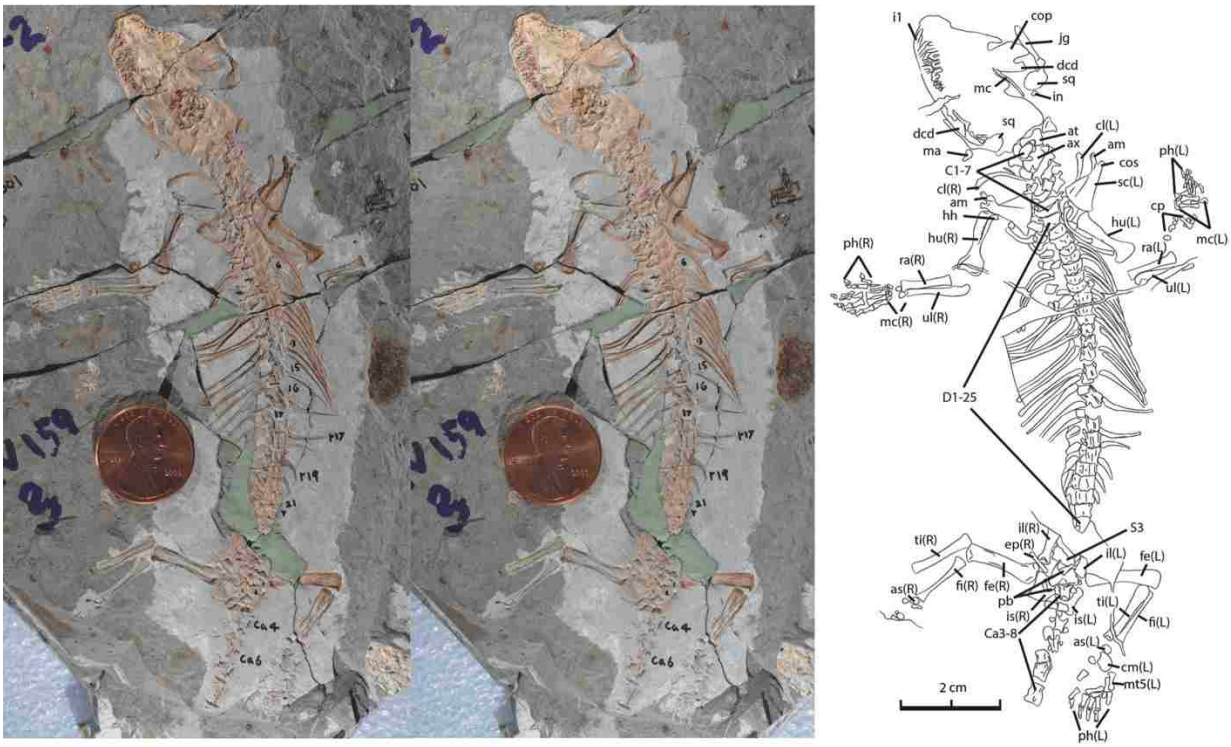

FIGURE 2. Stereophotographs and illustration of *Yanoconodon allini* in the counter part, NJU-P06001B.

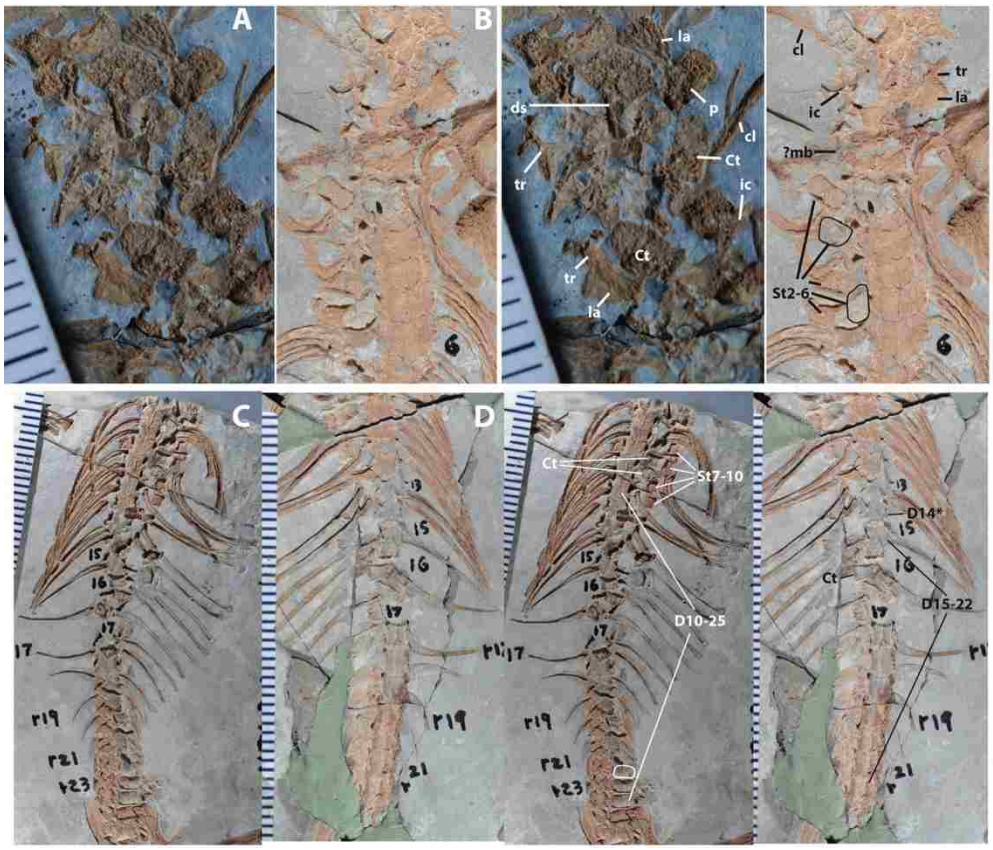

FIGURE 3. Anterior axial skeleton and pectoral girdle of *Yanoconodon allini*, NJU-P06001. **A**, stereophotographs of the cervicals in the main part; **B**, stereophotographs of the sternebrae in the counter part; **C**, **D**, stereophotographs of the dorsal vertebrae in the main and counter parts, respectively.

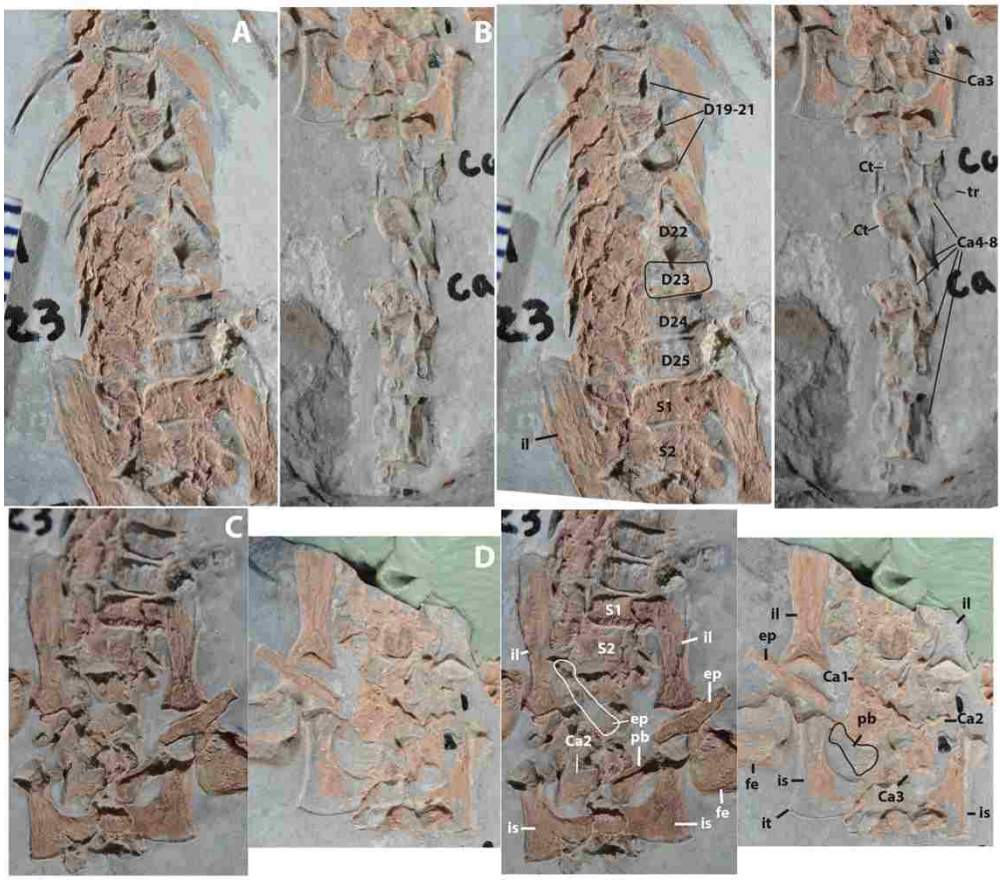

FIGURE 4. Posterior axial skeleton and pelvic girdle of *Yanoconodon allini*, NJU-P06001. **A**, stereophotographs of the dorsal vertebrae in the posterior part of vertebral column and pelvic region; **B**, stereophotographs of caudal vertebrae; **C**, **D**, stereophotographs of the pelvic girdle in the main and the counter parts, respectively.

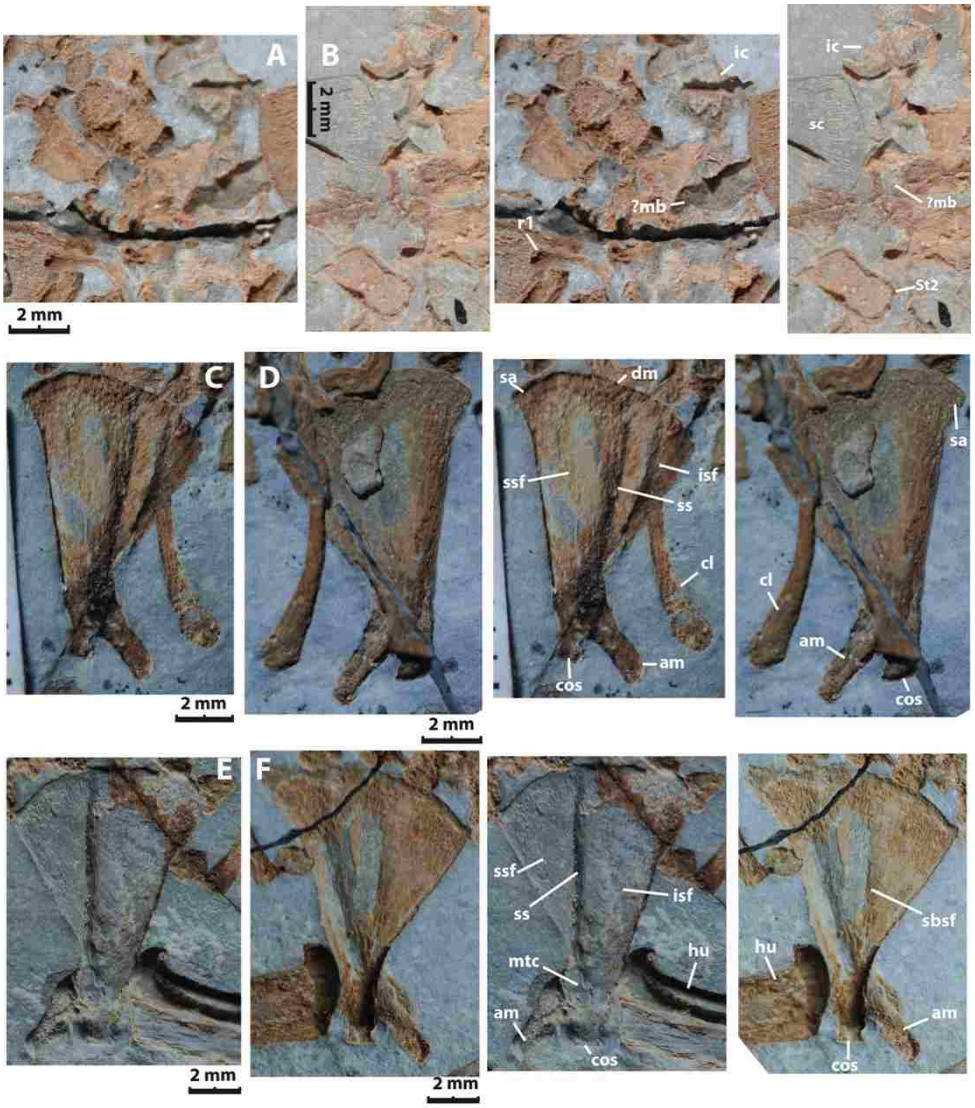

FIGURE 5. Interclavicle and scapula of *Yanoconodon allini*, NJU-P06001. **A**, **B**, paired stereophotographs of the interclavicle; **C**, **D**, paired stereophotographs of the left scapula in the main and counter parts, respectively; **E**, **F**, paired stereophotographs of the right scapula in the counter and main parts, respectively.

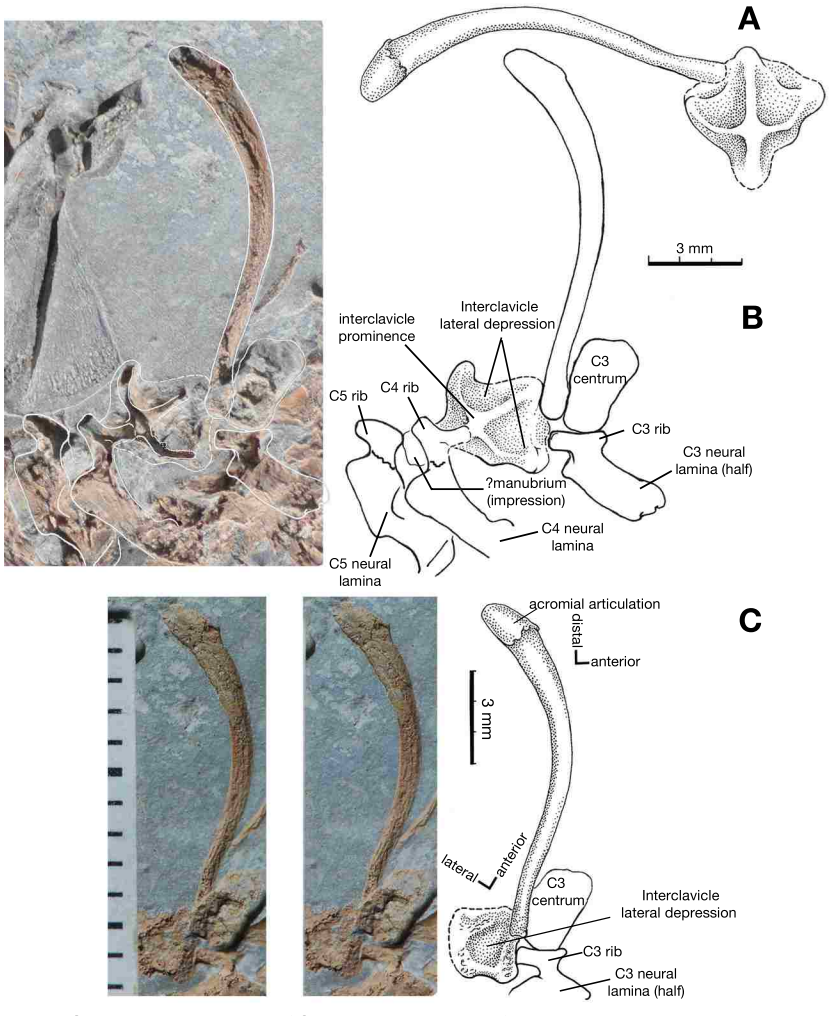

FIGURE 6. Reconstructions of clavicle and interclavicle of *Yanoconodon allini*, NJU-P06001. **A**, composite reconstruction of the clavicle and interclavicle in conjectural articulation. **B**, photograph and structural identification of outlines of impression (after preparation) of the interclavicle and the left clavicle. **C**, stereophotographs (flipped so depressions shown as positive reliefs) of the left clavicle and the interclavicle (before preparation to expose the details of impression and outlines).

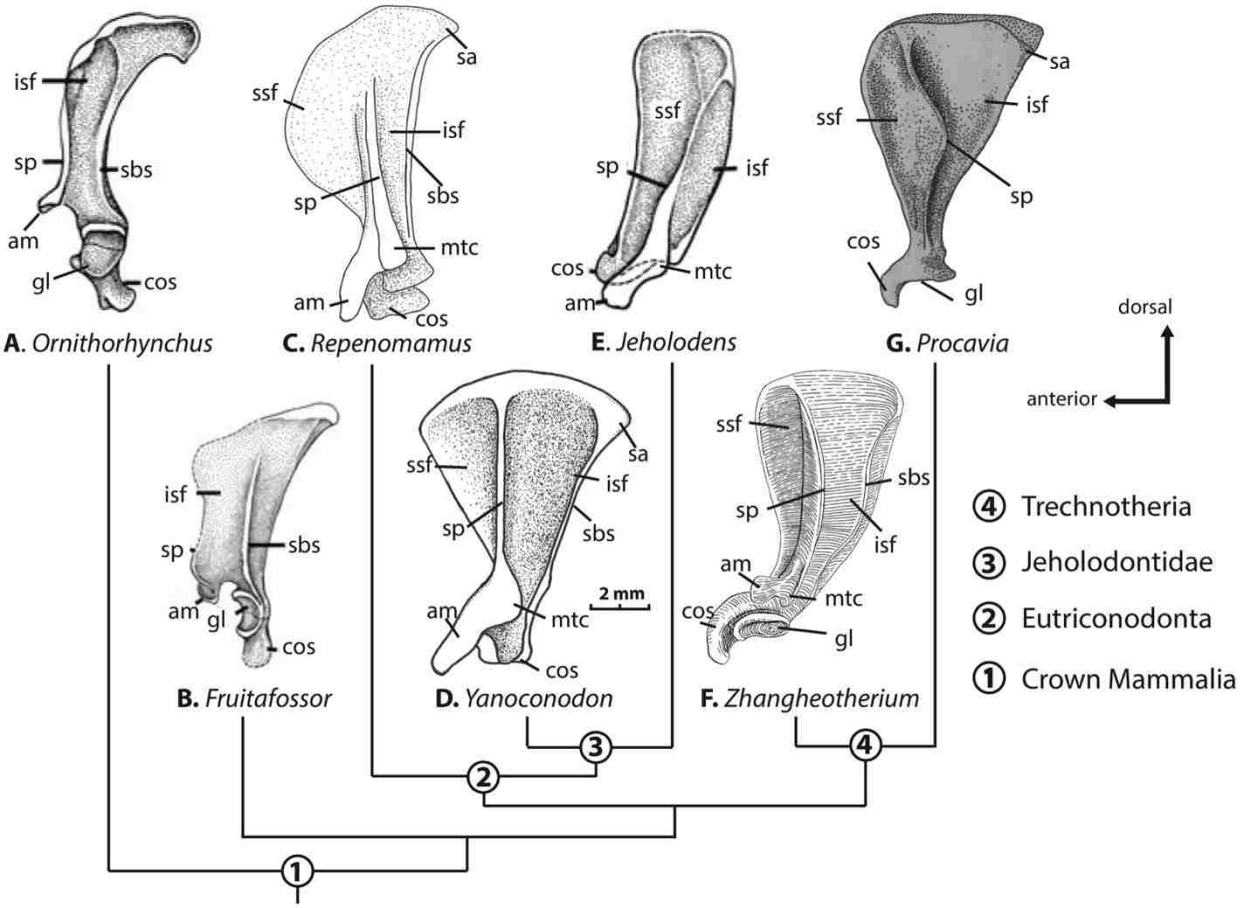

FIGURE 7. Comparison of the scapulae of extant and Mesozoic mammals (left scapulae). **A**, monotreme *Ornithorhynchus* (lateral view, Ji et al., 1999); **B**, basal mammal *Fruitafossor* (ventrolateral view; Luo and Wible, 2005); **C**, eutriconodontan *Repenomamus* (lateral view; reconstruction from Hu, 2006); **D**, jeholodontid *Yanoconodon*. **E**, jeholodontid *Jeholodens* (lateral view; Ji et al., 1999); **F**, symmetridontan *Zhangheotherium* (lateral view; Chen and Luo, 2012); **G**, placental *Procavia* (lateral view; Lessertisseur and Saban 1967b).

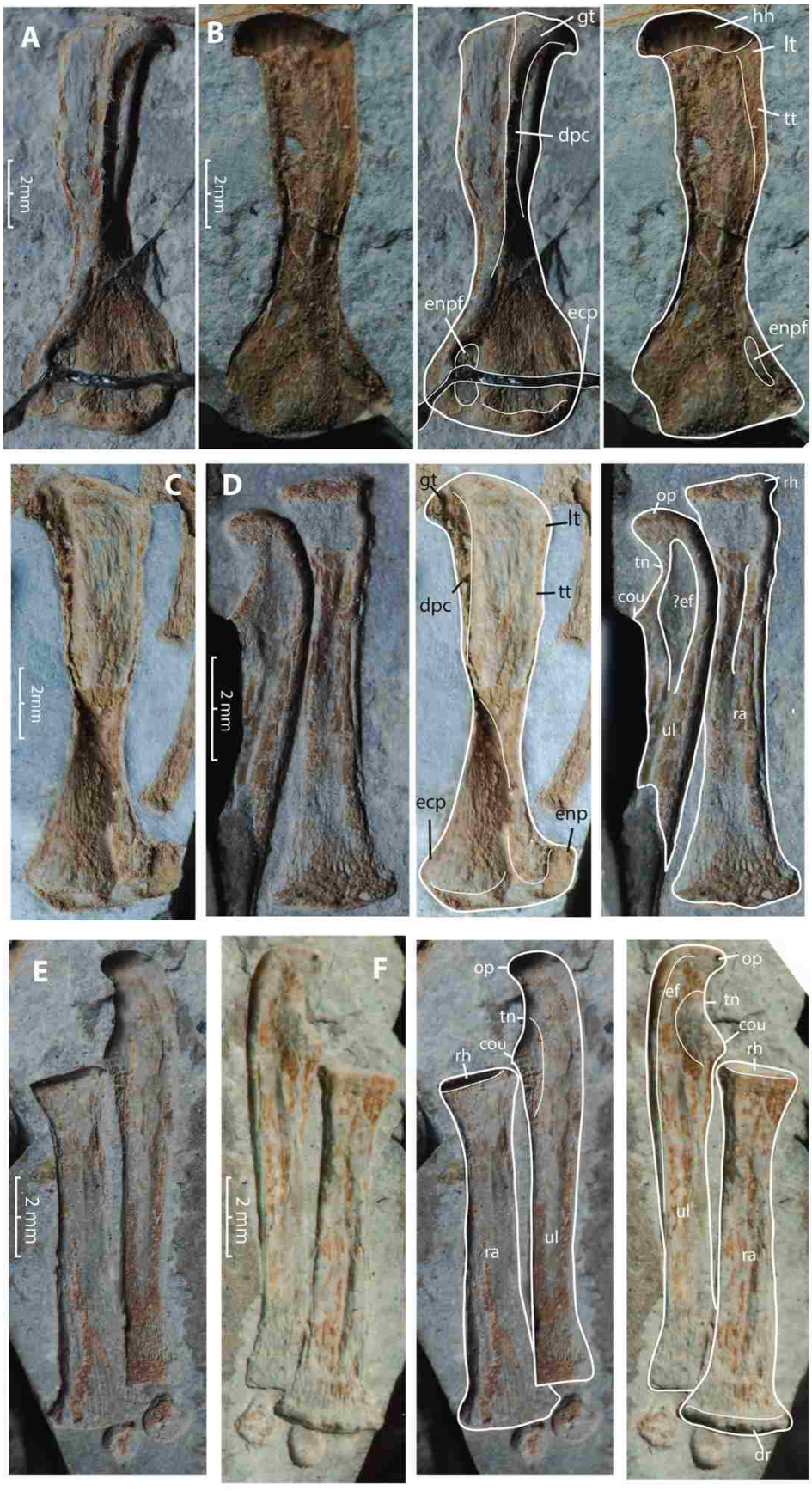
A
2mm
B
2mm
gt
dpc
enpf
ecp
hh
lt
tt
enpf
C
2mm
D
2 mm
gt
lt
dpc
tt
ecp
enp
op
rh
tn
cou
?ef
ra
ul
E
2 mm
F
2 mm
op
tn
cou
rh
ra
ul
op
ef
tn
cou
rh
ul
ra
dr

FIGURE 8. Humerus, ulna and radius of the eutriconodontan *Yanoconodon allini,* NJU-P06001. **A**, **B**, paired stereophotographs of the right humerus in the counter and the main parts, respectively; **C**, stereophotographs of the left humerus in the main part; **D**, stereophotographs of the left radius and ulna in the counter part; **E**, **F**, stereophotographs of the right radii and ulnae in the counter and main parts, respectively.

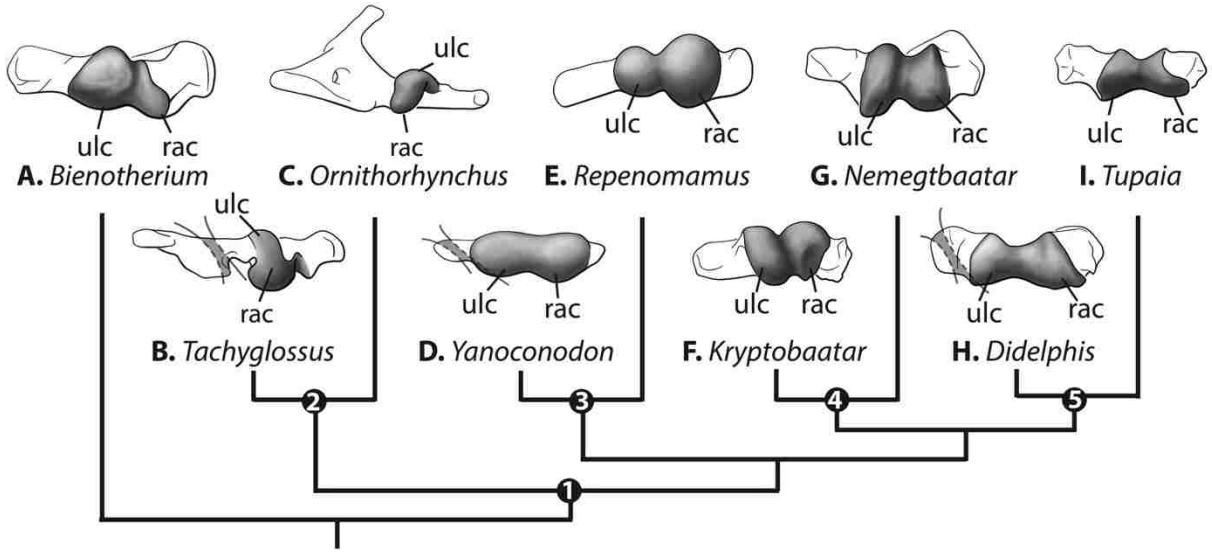

FIGURE 9. Comparison of the distal humeri of *Yanoconodon allini*, NJU-P06001, and other mammals (right humeri). **Node 1**, Crown Mammalia; **node 2**, Momotremata; **node, 3**, Eutriconodonta; **node 4**, Multituberculata; **node 5**, Theria. **A**, premammalian cynodont *Bienotherium* (redrawn from Sereno, 2006); **B**, monotreme *Tachyglossus* (Jenkins, 1973); **C**, *Ornithorhynchus*; **D**, *Yanoconodon*; **E**, *Repenomamus*; **F**, *Kryptobaatar* (redrawn from Senero, 2006); **G**, *Nemegtbaatar* (redrawn from Senero, 2006); **H**, *Didelphis* (redrawn from Sereno, 2006); I, *Tupaia* (Jenkins, 1973). Not to scale.

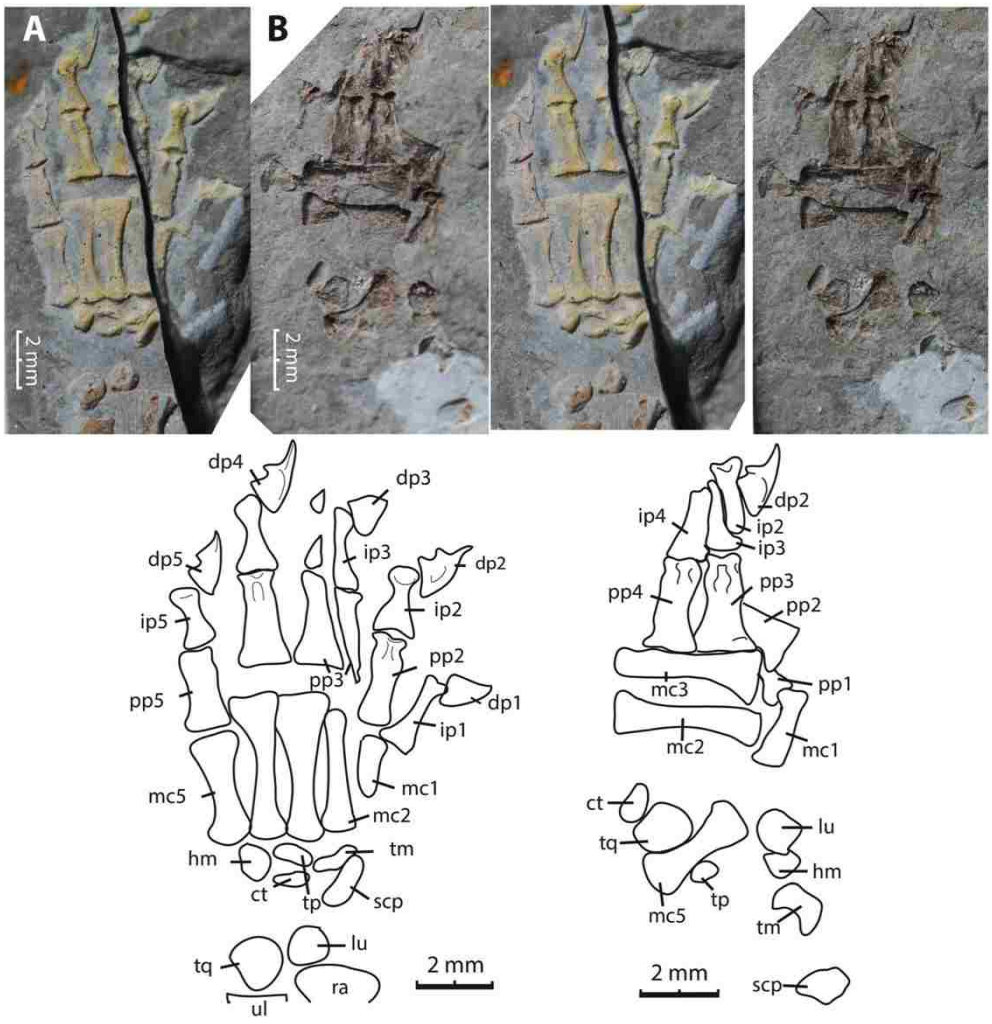

FIGURE 10. Manus of *Yanoconodon allini*, NJU-P06001. **A**, **B,** paired stereophotographs of the right manus in the counter part and the left manus in the main part.

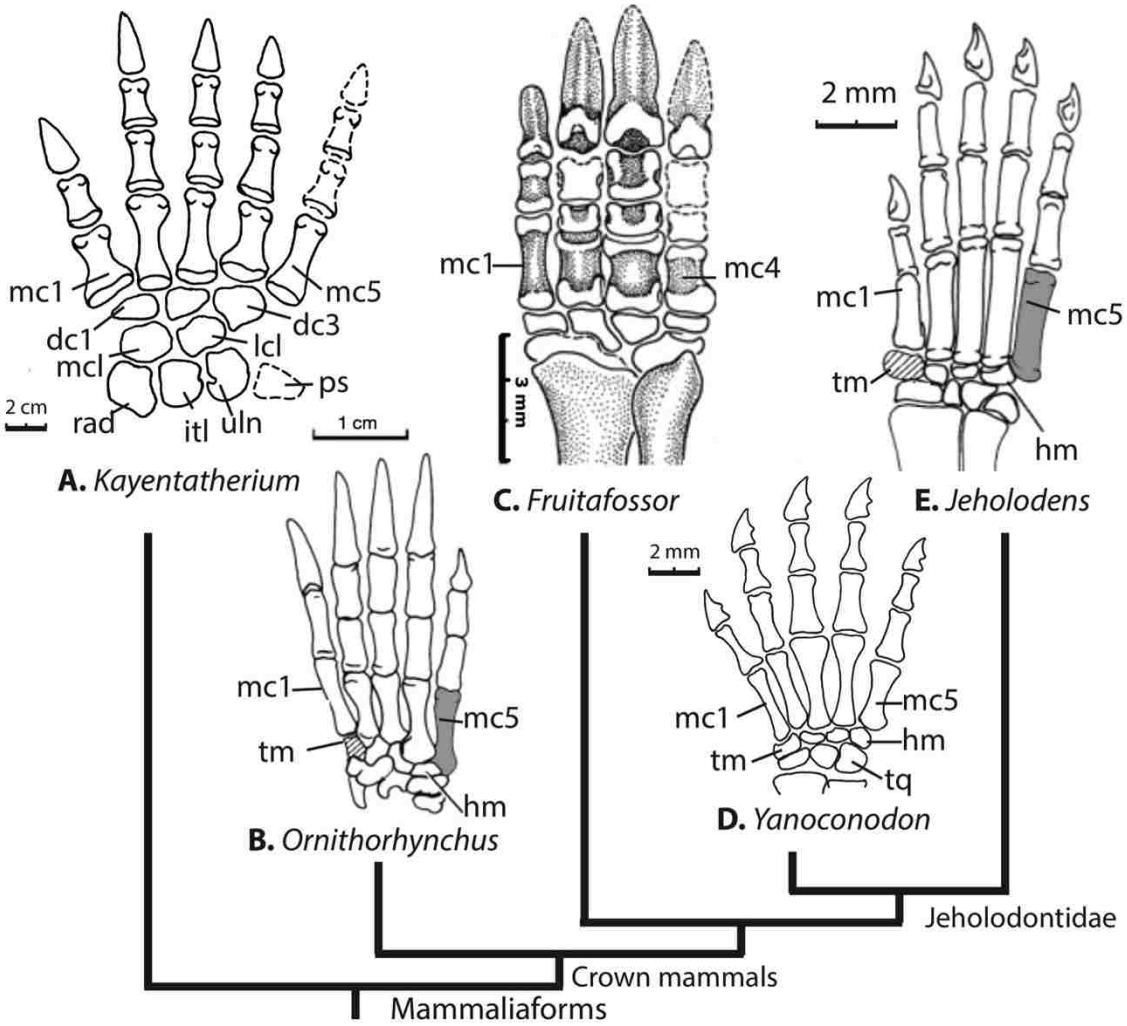

FIGURE 11. Comparison of manus of *Yanoconodon allini*, NJU-P06001. **A**, premammalian cynodont *Kayentatherium* (adopted with modification from Sues and Jenkins, 2006); **B**, monotreme *Ornithorhynchus* (dorsal view, Ji et al., 2002); **C**, basal mammal *Fruitafossor* (dorsal view, Luo and Wible, 2005); **D**, jeholodontid *Yanoconodon* (ventral view); **D**, jeholodontid *Jeholodens* (dorsal view; Ji et al., 1999).


A
B
fh
gtr
ltr
fh
ltr
2 mm
2 mm
mcd
lcd
C
D
gtr
fh
ltr
tpe
fpe
ti
fi
2 mm
2 mm
td
fd
E
F
G
fpe
tpe
tpe
fpe
fi
ti
ti
fi
2 mm
2 mm
2 mm
fd
td
td
?mm
fd

FIGURE 12. Femur, tibia and fibula of *Yanoconodon allini*, NJU-P06001. **A**, **B**, stereophotographs of the left and right femora in the counter and main parts, respectively; C, the paired photographs of left femur in main part; **D**, **E**, stereophotographs of the left fibula and tibia in the counter and main parts, respectively; **F**, **G**, stereophotographs of the right tibia and fibula in the main part, respectively.

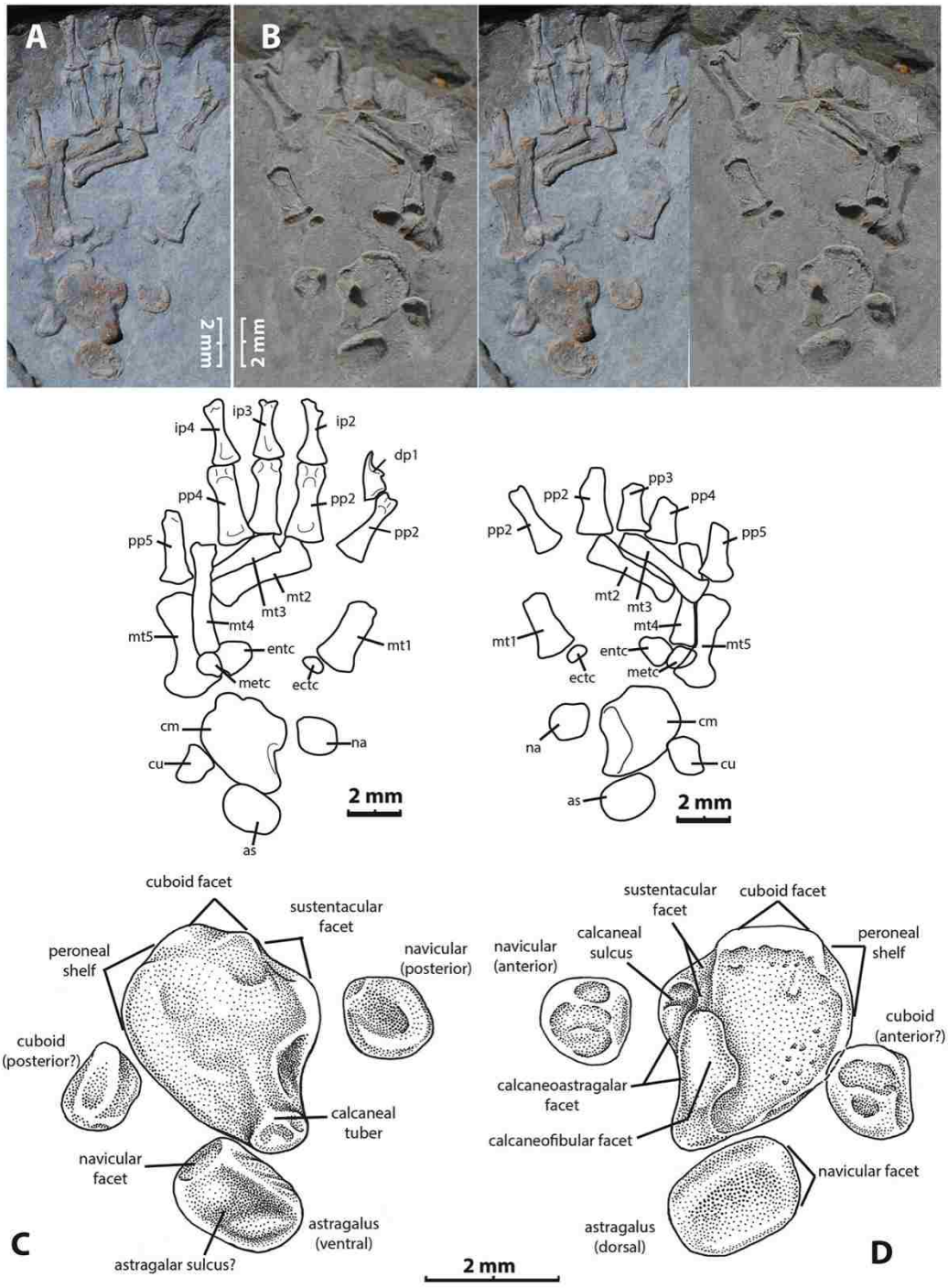

FIGURE 13. Hind foot of *Yanoconodon allini,* NJU-P06001. **A**, **B**, stereophotographs of the left pes in the counter and the main parts, respectively; **C**, ventral views of the calcaneus and the astragalus, likely the posterior view of the cuboid and navicular; **D**, dorsal view of the calcaneus and the astragalus, likely the anterior view of the cuboid and the navicular.

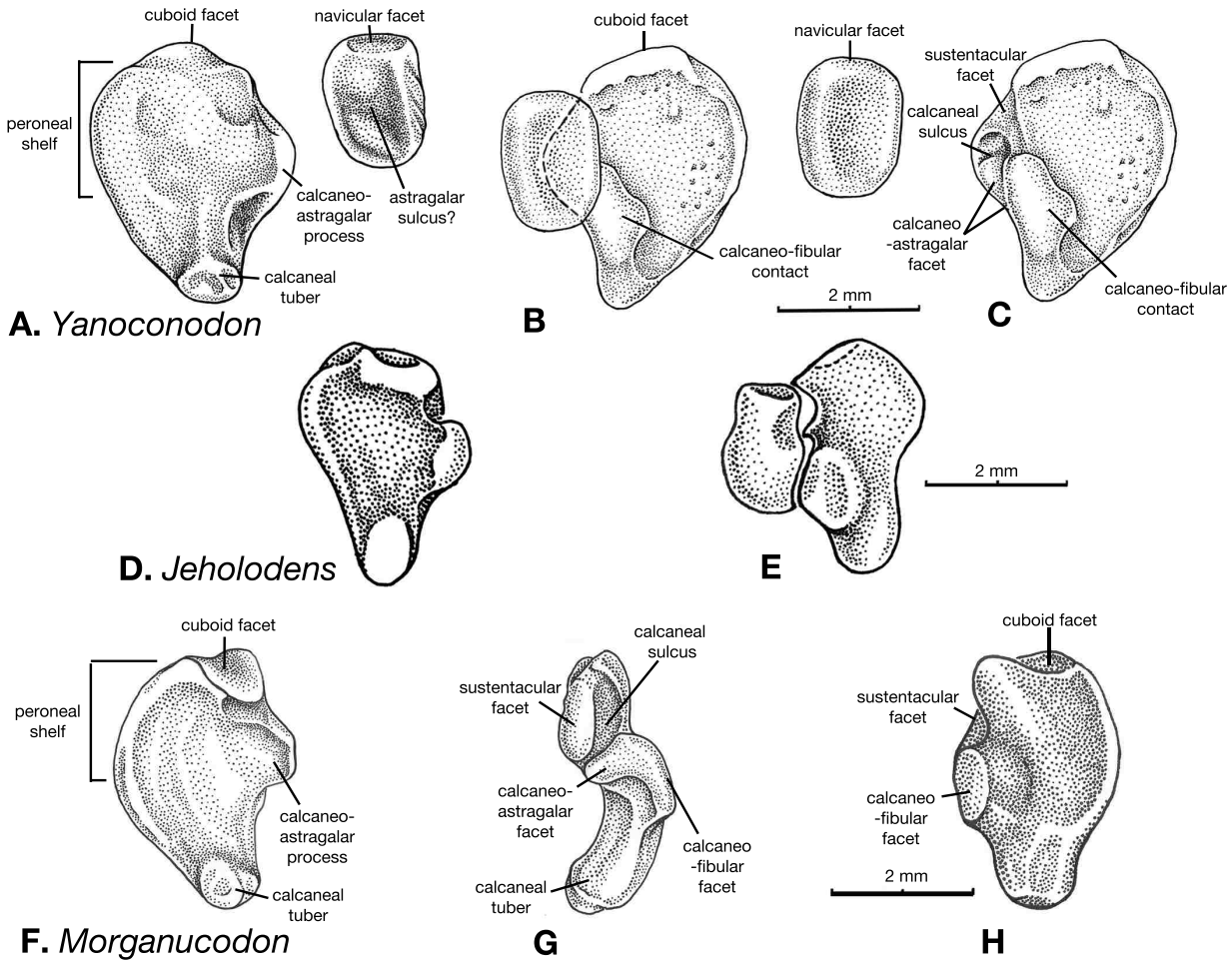

FIGURE 14. Restoration and comparative morphology of the astragalus and calcaneus of *Yanoconodon allini*, NJU-P06001. **A**, ventral aspect of the calcaneus and astragalus; **B**, dorsal aspect of the right astragalus and the right calcaneus; restoration of a partially superposition on the calcaneus by the astragalus that is slightly oblique dorsal view; **C**, dorsal aspect of the astragalus and calcaneus (the articulating features for astragalus shown as originally exposed); **D**, **E**, *Jeholodens*: ventral aspect of the calcaneus (D) and dorsal aspect of the astragalus and the calcaneus with the former partially superpositioned on the latter, as preserved (E; from Ji et al., 1999; Luo and Wible, 2005); **F**, **G**, and **H**, *Morganucodon*: right calcaneus in ventral (F), medial (G) and dorsal (H) views (redrawn from Szalay, 1994; Luo and Wible, 2005; Zhou et al., 2013).

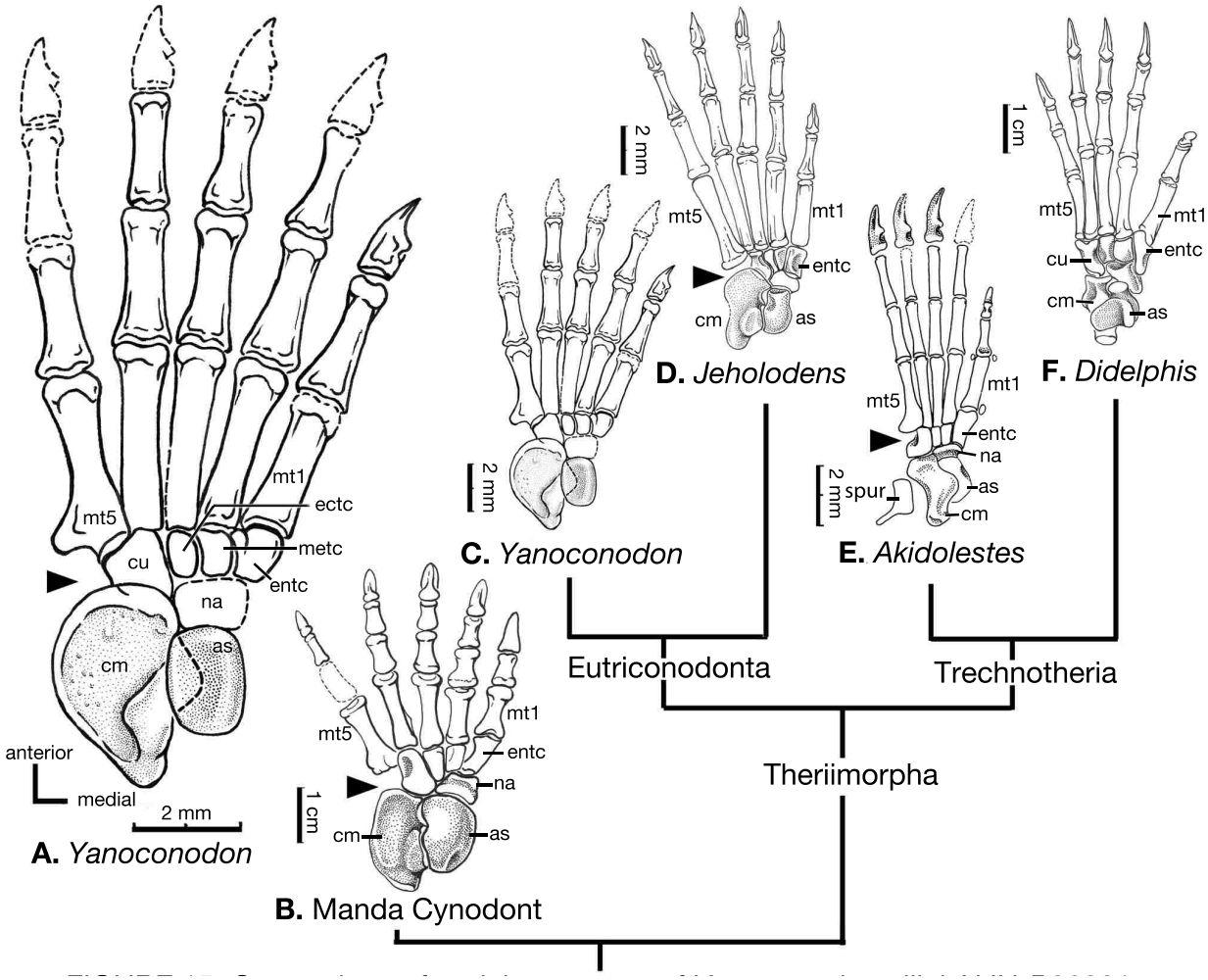

FIGURE 15. Comparison of the pedal structure of *Yanoconodon allini,* NJU-P06001. **A**, composite reconstruction of *Yanoconodon*; **B**, premammalian cynodont (”Manda cynodont”, dorsal view); **C**, jeholodontid *Yanoconodon* (ventral view); **D**, jeholodontid *Jeholodens* (dorsal view Ji et al., 1999); **E**, spalacotheriid *Akidolestes* (ventral view; Chen and Luo, 2013); **F**, marsupial *Didelphis* (dorsal view). Triangle symbol, “cuboid notch” for the passage of the long peroneal tendon.

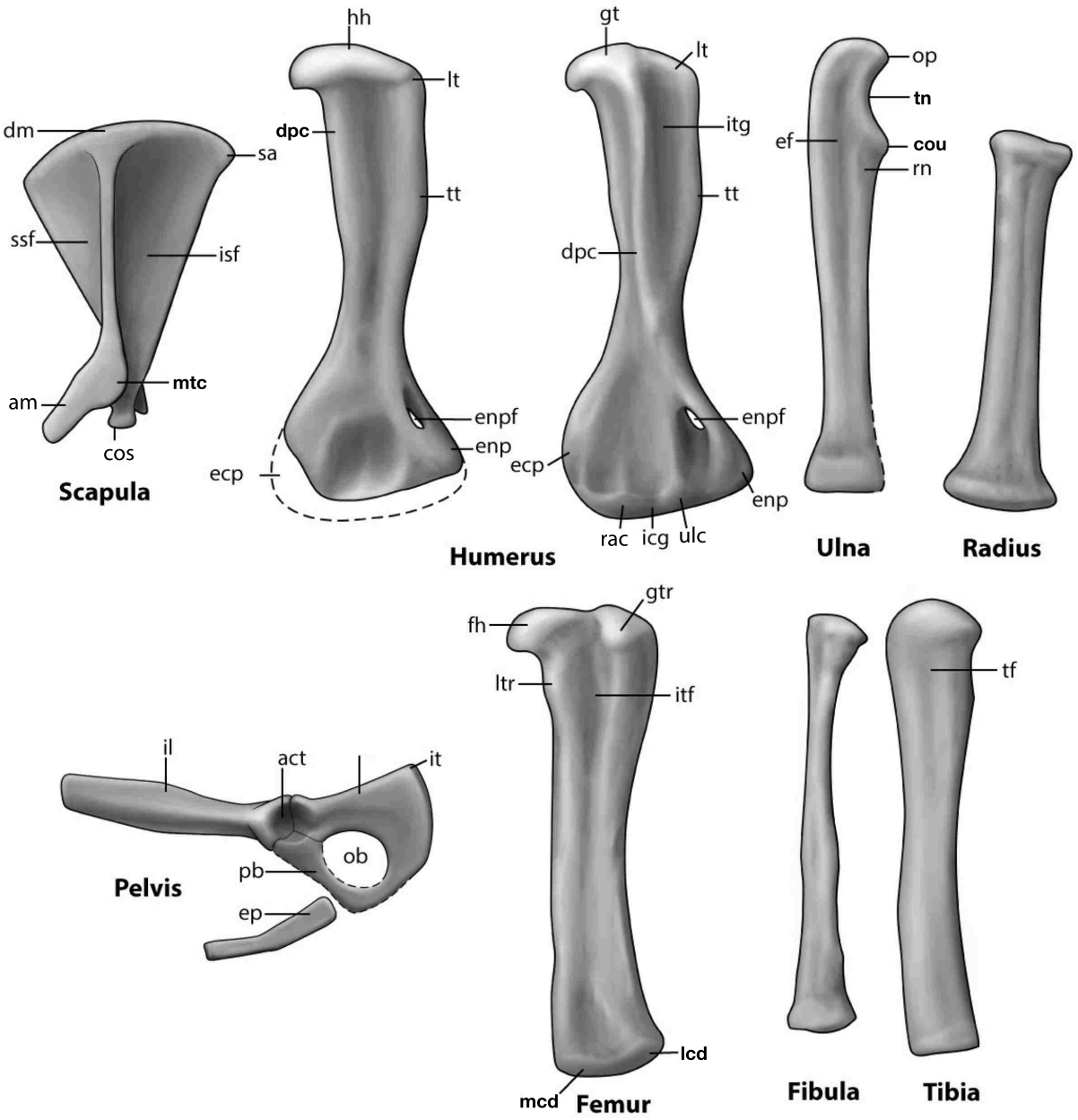

FIGURE 16. Illustration and reconstruction of the postcranial elements of *Yanoconodon allini,* NJU-P06001.

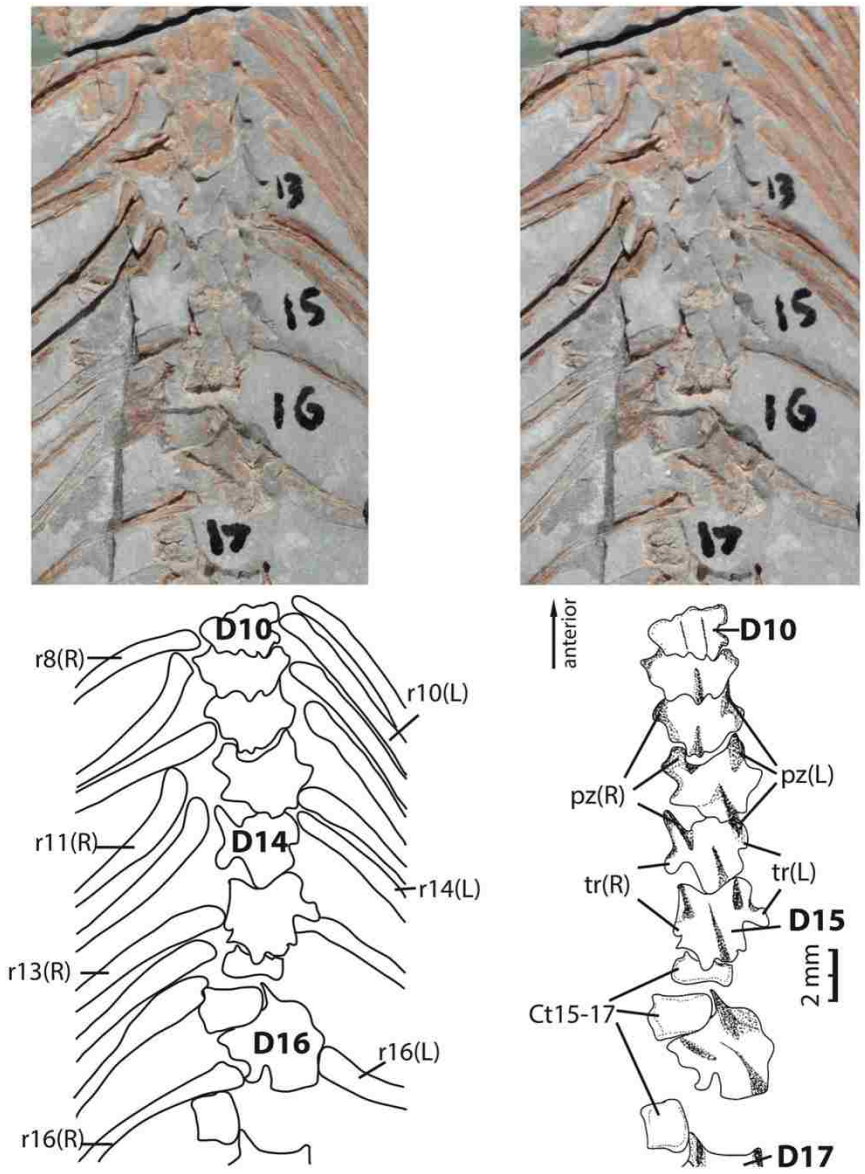

FIGURE 17. Gradational transition between thoracic and lumbar vertebral region of *Yanoconodon allini,* NJU-P06001. Distinctive change to the vertical orientation of prezygapophyses, and elongate transverse process occur at dorsal 14, but not the loss of dorsal rib.

TABLES

Table 1 Postcranial measurements of eutriconodontan *Yanocondon allini* (cm).

Postcranial Skeletal elements	Left		Right	
	Length	Width	Length	Width
Scapula	1.022	0.612	1.04	0.58
Humerus	1.248	0.164	1.241	0.166
Ulna	1.181	0.132	1.174	0.1
Radius	0.958	0.159	0.978	0.139
Metacarpal I	-	-	0.207	0.053
Metacarpal II	0.309	-	-	-
Metacarpal III	0.373	0.054	0.365	0.038
Metacarpal IV	0.37	0.056	0.367	0.038
Metacarpal V	0.28	0.062	0.294	0.049
Proximal phalanx I	0.211	0.041	-	-
Proximal phalanx II	0.225	0.073	0.243	0.099
Proximal phalanx III	0.22	-	0.226	0.081
Proximal phalanx IV	0.24	0.084	-	-
Proximal phalanx V	0.2	0.083	-	-
Intermediate phalanx II	0.174	0.05	-	-
Intermediate phalanx III	0.199	-	-	-
Intermediate phalanx IV	0.187	0.043	-	-
Intermediate phalanx V	0.144	0.041	-	-
Distal phalanx I	0.093	0.086	-	-
Distal phalanxII	0.14	0.098	-	-
Distal phalanx III	-	-	-	-
Distal phalanx IV	0.161	0.096	0.195	-
Distal phalanx V	0.157	0.091	-	-
Illium	0.821		0.866	
Ischium	0.523		0.587	

Pubis	0.401		0.481	
Epipubis	0.512			
Femur	1.397	0.225	1.407	0.245
Tibia	1.28	0.158	1.268	0.148
Fibula	1.119	0.088	1.157	0.092
Calcaneus	-	-	0.336	0.266
Metatarsal I	-	-	0.227	0.078
Metatarsal II	-	-	0.324	0.068
Metatarsal III	-	-	0.362	0.065
Metatarsal IV	-	-	0.39	0.043
Metatarsal V	-	-	0.362	0.068
Proximal phalanx I	-	-	0.214	0.042
Proximal phalanx II	-	-	0.255	0.071
Proximal phalanx III	-	-	0.249	0.069
Proximal phalanx IV	-	-	0.261	0.066
Proximal phalanx V	-	-	0.252	0.067
Intermediate phalanx II	-	-	0.211	0.045
Intermediate phalanx III	-	-	0.203	0.033
Intermediate phalanx IV	-	-	0.212	0.031
Distal phalanx I	-	-	0.146	0.08

"-", not applicable due to damage.

CHAPTER 3:

A MULTIVARIATE APPROACH TO INFER LOCOMOTOR MODES IN MESOZOIC MAMMALS

Paleobiology, page 1 of 33
DOI: 10.1017/pab.2014.14

A multivariate approach to infer locomotor modes in Mesozoic mammals

Meng Chen and Gregory P. Wilson

Abstract.—Ecomorphological diversity of Mesozoic mammals was presumably constrained by selective pressures imposed by contemporary vertebrates. In accordance, Mesozoic mammals for a long time had been viewed as generalized, terrestrial, small-bodied forms with limited locomotor specializations. Recent discoveries of Mesozoic mammal skeletons with distinctive postcranial morphologies have challenged this hypothesis. However, ecomorphological analyses of these new postcrania have focused on a single taxon, a limited region of the skeleton, or have been largely qualitative.

For more comprehensive locomotor inference in Mesozoic mammals, we applied multivariate analyses to a morphometric data set of extant small-bodied mammals. We used 30 osteological indices derived from linear measurements of appendicular skeletons of 107 extant taxa that sample 15 orders and eight locomotor modes. Canonical variate analyses show that extant small-bodied mammals of different locomotor modes have detectable and predictable morphologies. The resulting morphospace occupation reveals a morphofunctional continuum that extends from terrestrial to scansorial, arboreal, and gliding modes, reflecting an increasingly slender postcranial skeleton with longer limb output levers adapted for speed and agility, and extends from terrestrial to semiaquatic/semifossorial and fossorial modes, reflecting an increasingly robust postcranial skeleton with shorter limb output levers adapted for powerful, propulsive strokes. We used this morphometric data set to predict locomotor mode in ten Mesozoic mammals within the Docodonta, Multituberculata, Eutriconodonta, "Symmetrodonta," and Eutheria. Our results indicate that these fossil taxa represent five of eight locomotor modes used to classify extant taxa in this study, in some cases confirming and in other cases differing from prior ecomorphological assessments. Together with previous locomotor inferences of 19 additional taxa, these results show that by the Late Jurassic mammals had diversified into all but the saltatorial and active flight locomotor modes, and that this diversification was greatest in the Eutriconodonta and Multituberculata, although sampling of postcranial skeletons remains uneven across taxa and through time.

Meng Chen and Gregory P. Wilson. Department of Biology, University of Washington, Seattle, Washington 98195, U.S.A. E-mail: mengchen@uw.edu; gpwilson@uw.edu

Accepted: 14 October 2014
Supplemental materials deposited at Dryad: doi:10.5061/dryad.870j3

Introduction

During the Mesozoic Era, mammals underwent critical morphological transformations that shaped their evolution and ecology and likely those of modern mammals (e.g., Kielan-Jaworowska et al. 2004). Previous studies of these transformations have mostly focused on the skull and dentition (e.g., tri-ossicular middle ear [Allin and Hopson 1992; Rowe 1996], tribosphenic molar [Luo et al. 2001a,b], and encephalization [Jerison 1973; Rowe et al. 2011]). Inferences about the evolution of locomotor complexes, locomotor diversity, and the role of locomotion and substrate use in resource partitioning among Mesozoic mammals have historically been hampered by a fossil record of mostly dental specimens, some cranial material, and very few postcranial skeletons (e.g., Kielan-Jaworowska et al. 2004). However, in the last three decades, a large number of relatively complete skeletons of early mammals have been reported, most notably from the Upper Jurassic and Cretaceous of Asia (e.g., Kielan-Jaworowska and Gambaryan 1994; Hu et al. 1997; Ji et al. 1999, 2006; Horovitz 2003; Luo et al. 2003, 2007; Meng et al. 2006; Hurum and Kielan-Jaworowska 2008; Yuan et al. 2013; Zhou et al. 2013).

Based on anatomical and functional insights from these newly recovered, more complete fossils, Luo (2007) challenged the traditional notion that all Mesozoic mammals were small-bodied, ecologically generalized, terrestrial forms. Instead, he proposed that Mesozoic mammals occupied a broad range of ecological

 0094-8373/15/4004-0006

categories, approaching the diversity found among modern communities of small-bodied mammals. Here, we aim to (i) develop a robust quantitative approach to infer locomotion and substrate use in Mesozoic mammals and (ii) apply it to select taxa to assess the breadth of locomotor specializations among Mesozoic mammals.

Background

Today's mammals include more than 5000 species in 29 orders (Wilson and Reeder 2005) that range from the tiny (~2 g), aerial bumblebee bat to the titanic ($\sim 100 \times 10^3$ kg), fully aquatic blue whale. They inhabit a broad range of habitats from the bottom of the oceans to inhospitable deserts and mountain snow lines (Wilson and Reeder 2005). This diversity is in part due to morphological evolution of the postcranial skeleton. Not only does the rigid postcranial skeleton structurally support an animal's body mass and outline its shape, but it also acts through coordinated neuromuscular pathways to move the animal through its environment (e.g., Grillner and Wallén 1985; Kardong 2009).

Whereas numerous methods have been developed to infer feeding ecology in fossil mammals (e.g., microwear, dental complexity, geometric morphometrics [Ungar and Williamson 2000; Wilson et al. 2012; Evans 2013; Wilson 2013]), few quantitative approaches have been developed to infer mammalian locomotion and substrate use and fewer have been applied to Mesozoic mammals. Those that have been developed use the relationship between postcranial morphology and locomotion/substrate use in living forms as an analogue (e.g., Van Valkenburgh 1987; Stein 1988; Sargis 2001a, 2002a,b; Gingerich 2003; Elissamburu and Vizcaíno 2004; O'Keefe and Carrano 2005; Kirk et al. 2008; Polly 2008, 2011; Samuels and Van Valkenburgh 2008; Fröbisch and Reisz 2009; Samuels et al. 2013). Unfortunately, most of these studies have focused on (i) no more than a few skeletal elements (e.g., distal phalanges [MacLeod and Rose 1991], autopodial skeleton [Weisbecker and Schmid 2007], third digit ray [Kirk et al. 2008]); (ii) a narrow phylogenetic scope (e.g., Tupaiidae [Sargis 2001a, 2002a,b], Diprotodontia [Weisbecker and Warton 2006], Rodentia [Samuels and Van Valkenburgh 2008]); (iii) single or few locomotor modes (e.g., fossorial mode [Hopkins and Davis 2009]; and/or (iv) mostly large-bodied taxa (>5 kg; e.g., Van Valkenburgh 1987; Gingerich 2003; Samuels et al. 2013). None have focused on a phylogenetically broad sample of small-bodied mammals (≤5 kg) that could be used as an analogue for Mesozoic mammals.

Here, we describe and validate a new method to quantitatively infer locomotor mode in small-bodied fossil mammals. This method uses functionally relevant, linear measurements that are broadly distributed across the appendicular skeleton. Relative to other measurement schemes that focus on only one or a few postcranial elements, our more extensive scheme (i) accounts for conflicting locomotor signatures from different parts of the skeleton, and (ii) enables discrimination among locomotor modes that share similar values for one or a few osteological indices. Moreover, we sampled nearly half of all mammalian orders and eight locomotor modes. The inclusion of a broad diversity of taxa in each mode minimizes the phylogenetic overprint that can confound ecomorphological associations. From this data set, we analyzed linear measurement ratios, using canonical variate analysis. Our results show that the different locomotor modes occupy distinct regions of the morphospace, indicating that postcranial morphology can be used to predict locomotor mode in small-bodied mammals. Thus, we used this approach and data set to infer locomotor mode in a taxonomically and morphologically diverse sample of Mesozoic mammals.

Materials and Methods

Taxa

Our extant mammalian data set includes measurements from 107 extant species from 15 orders: Afrosoricida, Carnivora, Cingulata, Dasyuromorphia, Didelphimorphia, Diprotodontia, Erinaceomorpha, Lagomorpha, Macroscelidea, Monotremata, Peramelemorphia, Primates, Rodentia, Scandentia, and Soricomorpha (Fig. 1, Supplementary Table 1). For each species, we sampled one adult individual. Additional sampling and strict sampling of

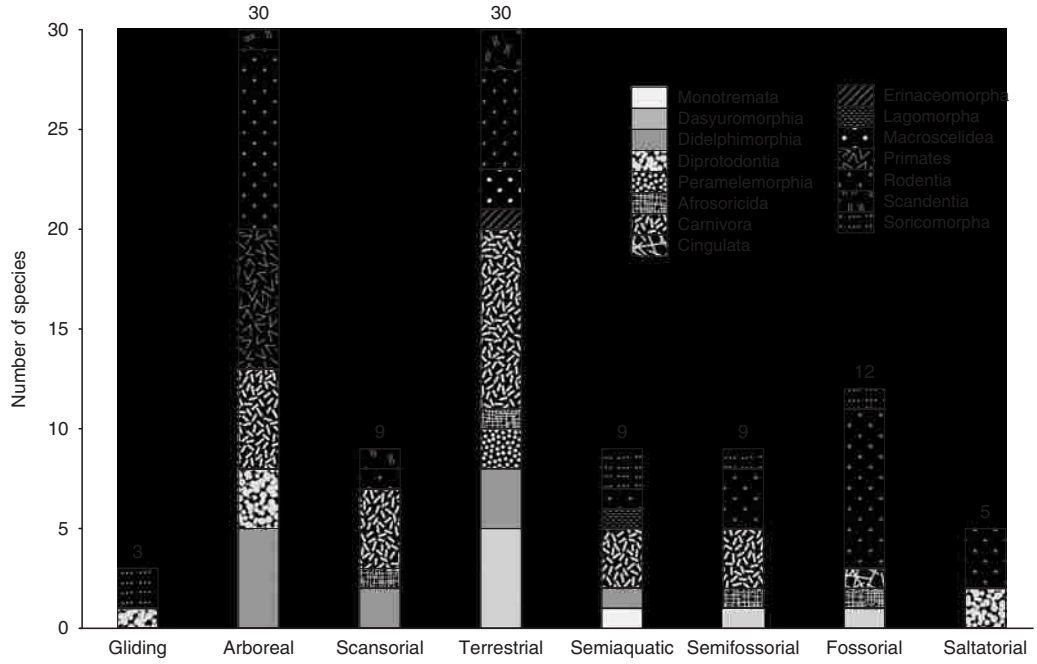

FIGURE 1. Taxonomic sampling of extant small-bodied mammals in each locomotor mode in our data set. Numbers indicate the total number of species of each locomotor order that are included.

only field-collected specimens unfortunately were hampered by variability in the degree of completeness and quality of preservation among museum specimens of the same species. However, whenever possible we examined additional specimens of the same species to confirm that the postcranial morphology of our measured specimen was representative for that species. Skeletons were identified as those of adults based on dental eruption pattern, epiphyseal fusion, or both. Although the degree of sexual dimorphism among small-bodied mammals is usually minor, we attempted to control for it by measuring specimens of male individuals whenever possible. We selected mostly small-bodied species (≤5 kg, following Bourlière 1975; Stoddart 1979; Degen 1997; Merritt 2010) to reflect the typical body size of most Mesozoic mammals (e.g., Lillegraven et al. 1979; Kielan-Jaworowska et al. 2004). A few select species have body masses up to 16 kg (e.g., *Vulpes vulpes*), which represent the estimated upper limit for Mesozoic mammals (e.g., *Repenomamus giganticus* [Hu 2006]). Species were also selected to cover a broad range of locomotor strategies. We excluded flying mammals (i.e., bats) from our extant mammalian data set because flying mammals have not yet been reported from the Mesozoic. Owing to their high taxonomic richness and abundance, rodents and carnivorans are particularly well represented in museum collections and, in turn, our data set (Fig. 1). See Supplementary Table 1 for details.

We also measured postcranial skeletons of ten fossil taxa that broadly sample the phylogenetic diversity and evolutionary history of Mesozoic mammals. The sample consists of four eutriconodontans, one multituberculate, two symmetrodontans, and one eutherian, all from northeastern Asia; one docodontan from Western Europe (Portugal); and the enigmatic *Fruitafossor* from North America. Most included specimens are published: the Late Jurassic *Fruitafossor windscheffeli* (Luo and Wible 2005); the Late Jurassic docodontan *Haldanodon exspectatus* (Martin 2005, 2013); the Late Jurassic multituberculate *Rugosodon eurasiaticus* (Yuan et al. 2013); the Early Cretaceous eutriconodontans *Jeholodens jenkinsi* (Ji et al. 1999), *Repenomamus robustus* (Hu et al. 2005; Hu 2006), and *Yanoconodon allini* (Luo et al. 2007); the Early Cretaceous symmetrodontan *Akidolestes cifellii* (Li and Luo 2006; Chen and Luo 2013); and the Early Cretaceous eutherian

TABLE 1. Inferred locomotor modes of Mesozoic mammals. Abbreviations: ELM, eight-locomotor-mode analysis; FLM, five-locomotor-mode analysis; NI, number of osteological indices; NM, number of measurements; *p*, posterior probability.

					Inferred locomotor mode	
Taxon	Order	Specimen no.	NM	NI	ELM (*p*)	FLM (*p*)
Haldanodon exspectatus	Docodonta	Gui Mam 30/79	21	21	A/Sf/T (56.6%/41.6%/1.8%)	Sf (100%)
Fruitafossor windscheffeli	N/A	LACM 150948	25	23	F (100%)	N/A
Repenomamus robustus	Eutriconodonta	IVVP V12728	28	22	Sf (100%)	Sf (100%)
Liaoconodon sp.	Eutriconodonta	BMNH PM001139	35	24	Sa (100%)	Sa (99.7%)
Yanoconodon allini	Eutriconodonta	NJU-P06001	30	27	Sa (99.7%)	Sa (99.9%)
Jeholodens jenkinsi	Eutriconodonta	GMV 2139	40	25	A (98.8%)	A/T (73.9%/21.2%)
Rugosodon eurasiaticus	Multituberculata	BMNH PM001142	35	24	A (98.8%)	Sc (94.8%)
Akidolestes cifellii	"Symmetrodonta"	NIGPAS 139381	35	27	Sf (99.3%)	Sf (99.8%)
Zhangheotherium sp.	"Symmetrodonta"	DMNH 2874	27	16	Sf/Sc/A/T (32.6%/26.2%/20.0%/11.6%)	Sc/T (71.3%/12.2%)
Eomaia scansoria	Eutheria	CAGS01-IG1	31	24	A/Sc/T (68.6%/16.5%/11.3%)	A (93.2%)

See *Methods and Materials* for abbreviations of institutions and locomotor modes.

Eomaia scansoria (Ji et al. 2002). We also included two unpublished specimens from the Early Cretaceous: the eutriconodontan *Liaoconodon* sp. indet. and symmetrodontan *Zhangheotherium* sp. indet. Among the ten Mesozoic taxa, eight have previously been assigned to locomotor modes based on a more traditional comparative anatomy approach (Hu et al. 1997, 1998; Ji et al. 1999, 2002; Luo and Wible 2005; Martin 2005; Hu 2006; Li and Luo 2006; Luo et al. 2007; Chen and Luo 2013; Yuan et al. 2013) (Table 1). Because the degree of completeness varies among these specimens, each taxon has a unique set of available postcranial measurements. Thus, when inferring locomotor mode in these fossil taxa, we could not use a universal morphometric data set of extant small-bodied mammals, but instead individually pruned the modern data set to reflect the measurements available for each fossil specimen.

Extant specimens were accessed in the mammal collections of the American Museum of Natural History (AMNH), New York, New York; the Field Museum of Natural History (FMNH), Chicago, Illinois; the Smithsonian Institution National Museum of Natural History (NMNH), Washington, D.C.; and the University of Washington's Burke Museum of Natural History and Culture (UWBM), Seattle, Washington. Eight of the fossil specimens are housed in Chinese institutions: the Beijing Museum of Natural History (BMNH), Beijing; the Chinese Academy of Geological Sciences, Institute of Geology (CAG-IG), Beijing; the Institute of Vertebrate Paleontology and Paleoanthropology, Chinese Academy of Science (IVPP), Beijing; the National Geological Museum of China (GMV), Beijing; the Dalian Museum of Natural History (DMNH), Dalian; the Nanjing Institute of Geology and Paleontology, Chinese Academy of Science (NIGPAS), Nanjing; the Nanjing University (NJU), Nanjing. The other two fossil specimens are housed in the Museu Geológico (Gui Mam), Lisbon, Portugal, and the Los Angeles County Museum (LACM), Los Angeles, California, U.S.A.

Locomotor Modes

We used natural history compendia and the primary literature (e.g., Howell 1930; Nowak 1999, 2005; Wilson and Reeder 2005;

TABLE 2. Definitions of locomotor modes of small-bodied mammals that were used in this study (modified from Hildebrand and Goslow 1998; Polly 2007; Samuels and Van Valkenburgh 2008; Samuels et al. 2012).

Locomotor mode	Descriptive definition
Gliding	Bridge gaps between trees by gliding usually with patagium
Arboreal	Spend most of the time in trees foraging, traveling, resting, but occasionally travel on the ground
Scansorial	Capable of climbing for escape, eating, or leisure, and probably spend a considerable time both in the trees and on the ground
Terrestrial	Spend most of time on the ground, but able to swim, climb, and burrow occasionally, but not specialized for those
Semiaquatic	Capable of swimming for dispersal, escape, or foraging as well as on the ground
Semifossorial	Regularly dig for food or to build burrows for shelter, but do not exclusively live underground
Fossorial	Efficiently dig burrows for shelter or foraging underground exclusively
Saltatorial	Capable of jumping using both hind limbs simultaneously for high-speed transportation over long distance

Samuels and Van Valkenburgh 2008; Samuels et al. 2013) (Supplementary Table 1) to assign each extant species to one of eight locomotor modes: gliding (G), arboreal (A), scansorial (Sc), terrestrial (T), semifossorial (Sf), fossorial (F), semiaquatic (Sa), or saltatorial (S) (Table 2). These modes are commonly used in those natural history compendia and the primary literature. Owing to limited availability, most small-bodied primates included in this study are callitrichines that have a specialized arboreal locomotion relative to other primates. Because of the adaptations involved in gliding from tree to tree, we treated gliding mammals as a separate locomotor mode, although they commonly have an arboreal lifestyle.

Postcranial Measurements and Indices

We took 45 linear measurements of the appendicular postcranial skeleton (Fig. 2, Supplementary Table 2). Some of these measurements have been included in other studies, where they were shown to be functionally relevant or important for discriminating among locomotor strategies (Supplementary Table 2) (e.g., Van Valkenburgh 1987; Beard 1993; Sargis 2001a, 2002a,b; Samuels and Van Valkenburgh 2008; Samuels et al. 2013). We primarily used Mitutoyo Digimatic Digital Calipers (±0.05 mm accuracy) to collect these measurements. For very small elements, we captured high-resolution images with a digital camera (Nikon D80) and then obtained measurements using NIH ImageJ 64 software for Mac (±0.01 mm accuracy). This method was also used for measuring the postcranial elements of the fossil mammals on high-resolution photographs of *Akidolestes cifellii, Jeholodens jenkinsi, Liaoconodon* sp., *Repenomamus robustus, Rugosodon eurasiaticus, Yanoconodon allini*, and *Zhangheotherium* sp., and published figures of *Eomaia scansoria* (Ji et al. 2002), *Fruitafossor windscheffeli* (Luo and Wible 2005), and *Haldanodon exspectatus* (Martin 2005).

To reduce the size correlation within the data matrix, we converted the linear measurements to ratios of bony elements or bony features (osteological indices). Some of the osteological indices reflect functional morphology (Samuels and Van Valkenburgh 2008). For example, the Olecranon Process Length Index (OPLI) captures the relative length of the input-lever of the forearm; an increase in OPLI would imply a greater capacity to generate output forces by the triceps brachii, which is a common adaptation to semiaquatic, semifossorial, and fossorial modes. Sokal and Rohlf (2012) cautioned that statistical analyses of ratios might potentially violate the assumptions of normality and homoscedasticity for parametric tests as well as some other problems noted by Emerson (1985). However, Carrano (1999) argued that without a uniform denominator, spurious intercorrelation might not cause a statistical problem. Arcsine transformation has been forwarded as a solution to this potential statistical violation (Sokal and Rohlf 2012), but our data set includes ratios greater than 1.0 that are not amenable to arcsine transformation. Previous studies have produced robust ecomorphological inferences of fossil taxa by using raw osteological indices (Van Valkenburgh 1987; Van Valkenburgh

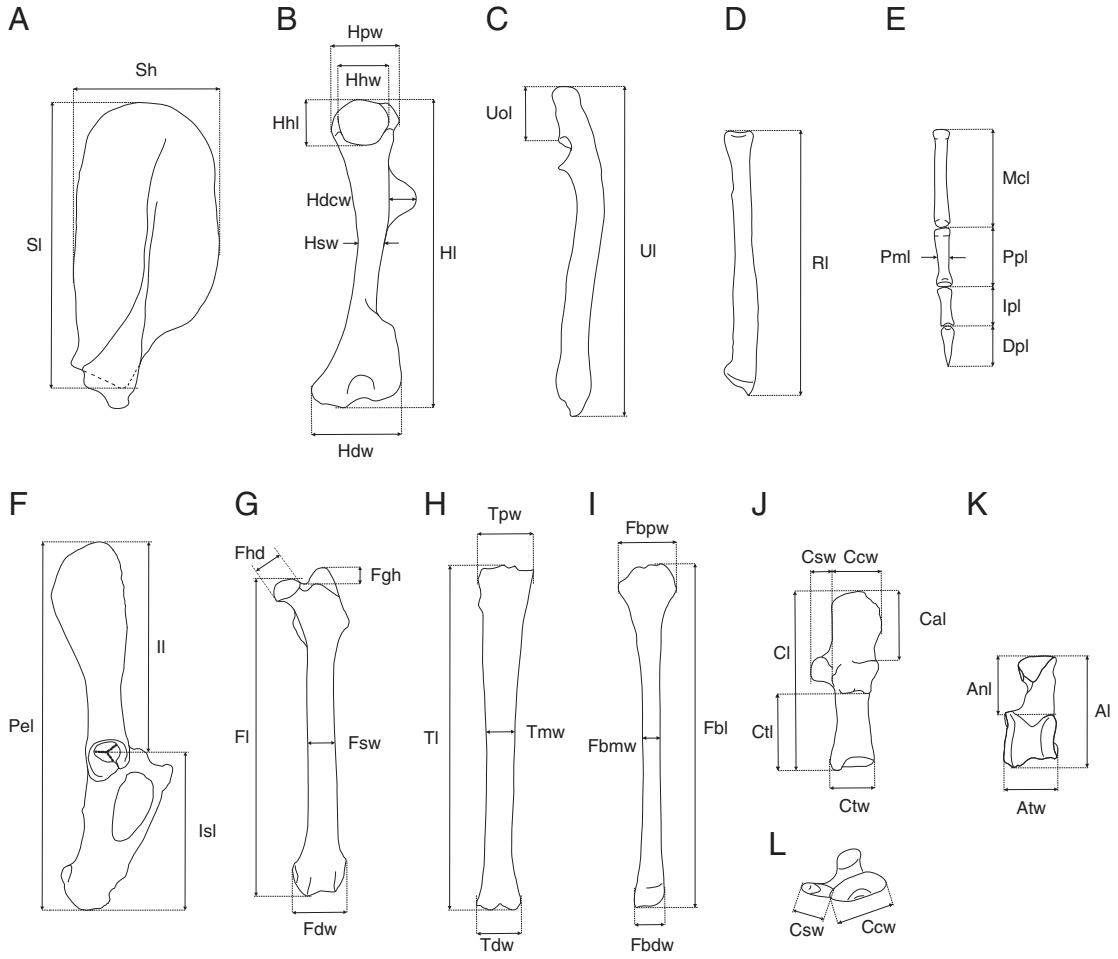

FIGURE 2. Schematic of the linear measurements obtained from the appendicular skeleton of extant and extinct small-bodied mammals. A, Scapula (lateral view). B, Humerus (posterior view). C, Ulna (lateral view). D, Radius (posterior view). E, Ray III of manus (dorsal view). F, Pelvis (lateral view). G, Femur (anterior view). H, Tibia (anterior view). I, Fibula (anterior or lateral view). J, Calcaneus (dorsal view). K, Astragalus (dorsal view). L, Calcaneus (anterior view). See Supplementary Table 2 for full descriptions of the postcranial skeletal measurements. A, C, D, E, G, H, I, and L are from the left side, and B, F, J, and K are from the right side.

and Koepfli 1993; Elissamburu and Vizcaíno 2004) or transformed osteological indices (Samuels and Van Valkenburgh 2008; Bover et al. 2010; Samuels et al. 2013) in their multivariate analyses. On this basis, we converted the 45 linear measurements from our modern data set to 56 osteological indices (Table 3), and then determined how well each raw osteological index discriminated among locomotor modes (see *Statistical Analyses*, below). For ease of communication and interpretation, we grouped the osteological indices into three major types: (1) robustness indices, which describe the robustness of postcranial elements; (2) morphofunctional indices, which reflect functional aspects of morphology, such as length of an input lever, and (3) proportional indices, which describe the shape or relative size of a postcranial element (Bover et al. 2010).

Statistical Analyses

To test whether there were significant differences across the eight locomotor modes in each osteological index, we carried out 56 univariate analyses of variance (ANOVA). Then, we used the osteological indices that were significantly different across eight locomotor modes ($p < 0.001$) in the canonical variate analysis

(CVA) to determine the linear combination of variables that maximize segregation among our eight locomotor modes. To enhance segregation among some tightly clustered locomotor modes, we also successively pruned the data sets down to five and three locomotor modes for two additional CVAs. We refer to these analyses as the eight-, five-, and three-locomotor-mode analyses, respectively. The same prior probability was given to each locomotor mode in the CVA to correct the uneven sampling of the eight locomotor modes. Together, the CVAs identify morphological signatures (via osteological indices) of the appendicular skeleton for each locomotor mode in our extant mammalian data set. We used the first three canonical functions (CFs) in the eight-locomotor-mode analysis to calculate the morphological variance, the mean of the squared-distance from each data point to the centroid, within each locomotor mode.

We then used this training set as a basis to predict locomotor habit in ten Mesozoic mammal species for which we obtained the same linear measurements. We initially conducted the multivariate analyses for each Mesozoic species, using the modern data set comprising all eight locomotor modes. In that analysis, more specialized locomotor modes (gliding, saltatorial, or fossorial) are well segregated, but the remaining modes (arboreal, scansorial, terrestrial, semiaquatic, and semifossorial) cluster together. Because *Fruitafossor* is the only Mesozoic taxon likely to have had an extremely specialized locomotor mode (fossorial [Luo and Wible 2005]), we conducted secondary analyses on the other nine fossil mammals by removing the specialized modes from the data set (five-locomotor-mode analysis). We chose not to perform a three-locomotor-mode analysis because it would preemptively narrow the possible locomotor inferences. The ANOVA and CVA were carried out using RStudio 0.98.501 (R core v3.1.0 64-bit). For the ANOVA, we used built-in functions in R, and for the CVA, we used R package MASS 7.3-31 (Venables and Ripley 2002).

To visualize the locomotor morphospace occupied by the extant small-bodied mammals in our data set, we plotted the CF1, CF2, and CF3 scores in bivariate plots. In all of our analyses, the first three CFs account for more than 85% of the variance (Supplementary Tables 3, 6, and 8 show the variance explained by each CF in each analysis).

Results

Morphological Variation among Locomotor Modes

ANOVA results indicate that 30 of the 56 osteological indices are significantly different across eight locomotor modes ($p < 0.001$) (Table 4). We suggest that these indices capture the morphological variation that is important for characterizing the eight locomotor modes.

Among our locomotor modes, gliding, arboreal, fossorial, and saltatorial mammals exhibit more-specialized morphological signatures (Table 5, Fig. 3A,B). Given that certain arboreal supports cannot withstand great amounts of weight, many gliding and arboreal mammals have minimized their body mass and have enhanced their locomotor dexterity and precision for movement in the trees in order to reduce the risk of falling from trees. Thus, they have more-gracile bony elements than taxa that exhibit different locomotor modes. In turn, most of the morphological signatures of the arboreal and gliding modes reflect low robustness indices, including (i) a slender humerus with small and round humeral head (HRI, HHRI, and HHw:Hpw; see Table 3 for definition), (ii) a weakly developed humeral deltopectoral crest (DI), (iii) a small olecranon process of the ulna (OPLI), (iv) a small palm with slender, elongate phalanges (PRTI and PI), (v) an elongate ilium (IRI), (vi) a gracile femur and tibia (FRI and TRI), (vii) a small greater trochanter (GI), and (viii) an elongated calcaneal body and a shortened calcaneal tuber (CBRI and CTRI). Scansorial taxa, which are capable of climbing but do not inhabit trees, are intermediate in form between arboreal and terrestrial taxa and possess a relatively long forelimb (IM). Terrestrial mammals have a moderately built (i) deltopectoral crest of the humerus (DI), (ii) olecranon process of the ulna (OPLI), and (iii) greater trochanter of the femur (GI), as well as a relatively short (iv) ulna (Ul:Hl; see Table 3 for definition) and (v) phalanges (PI and MRTI).

TABLE 3. List of the osteological indices that were used in this study and derived from linear measurements of the appendicular skeleton of small-bodied mammals. Codes for the types of osteological indices: 1, robustness index; 2, morphofunctional index; 3, proportional index.

No.	Osteological index	Abbr.	Equation	Description	Selected references for example	Index type
1	Scapular shape index	SI	Sh:Sl	Scapular height divided by scapular length	Sargis 2002a	2
2			Sl:Hl	Scapular length divided by humeral length		3
3	Humerus robustness index	HRI	Hsw:Hl	Humeral mid-shaft transverse diameter divided by humeral length	Elissamburu and Vizcaíno 2004; Samuels and Van Valkenburgh 2008; Bover et al. 2010; Samuels et al. 2013	1
4	Humeral proximal end index	HPI	Hpw:Hl	Humeral proximal end width divided by humeral length		1
5	Humeral epicondylar index	HEB	Hdw:Hl	Humeral epicondylar width divided by humeral length	Elissamburu and Vizcaíno 2004; Samuels and Van Valkenburgh 2008; Bover et al. 2010; Samuels et al. 2013	1
6			Hsw:Hpw	Transverse diameter of humerus divided by humeral proximal end width		3
7	Humeral head robustness index	HHRI	HHl:Hl	Humeral head length divided by humeral length		1
8	Humeral head shape index	HHSI	HHw:HHl	Humeral head width divided by humeral head length	Sargis 2002a	2
9			HHw:Hpw	Humeral head width divided by humeral proximal end width		3
10			Hpw:Hdw	Humeral proximal end width divided by humeral distal width		3
11			HHw:Hdw	Humeral head width divided by humeral distal end width		3
12			Hsw:Hdw	Transverse diameter of humerus divided by humeral distal end width		3
13			Hdw:Sh	Humeral epicondylar width divided by scapular length		3
14			Hdcw:Hpw	Deltopectoral crest width divided by humeral proximal end		3
15	Deltopectoral crest index	DI	Hdcw:Hsw	Deltopectoral crest width divided by the mid-shaft width of humerus		1
16			Hdcw:Hdw	Deltopectoral crest width divided by humeral distal end		3
17			Ul:Hl	Ulnar length divided by humeral length		3
18	Olecranon Process Length Index	OPLI	Uol:Ul	Olecranon process length divided by ulna length	Sargis 2002a	2
19			Uol:Hl	Olecranon process length divided by humeral length		2
20	Brachial Index	BI	Rl:Hl	Radial length divided by humeral length	Sargis 2002a; Samuels and Van Valkenburgh 2008; Bover et al. 2010; Samuels et al. 2013	3

TABLE 3. Continued

No.	Osteological index	Abbr.	Equation	Description	Selected references for example	Index type
21			Rl:Ul	Radial length divided by ulnar length		3
22			Uol:Rl	Olecranon process length divided by radial length		2
23	Palm robustness index	PRTI	Mcl:(Hl + Rl)	Metacarpal length divided by lengths of humerus and radius		2
24	Metacarpal robustness index	MRI	Mcw:Mcl	Transverse diameter metacarpal bone of digit ray III divided by its length		1
25	Proximal phalangeal robustness index	PPRI	Ppw:Ppl	Transverse diameter of proximal phalanx of digit ray III divided by its length		1
26	Intermediate phalangeal robustness index	IPRI	Ipw:Ipl	Transverse diameter of intermediate phalanx of digit ray III divided by its length		1
27	Distal phalangeal robustness index	DPRI	Dpw:Dpl	Transverse diameter of distal phalanx of digit ray III divided by its length		1
28			Dpl:Mcl	Distal phalanx length of digit ray III divided by humeral length		3
29	Phalangeal index	PI	(Ppl + Ipl): Mcl	Lengths of proximal and intermediate phalanges of digit ray III divided by metacarpal length	Beard 1993; Lemelin 1999; Argot 2001; Bloch and Boyer 2002; Ji et al. 2002; Luo et al. 2003; Chen and Luo 2008; Kirk et al. 2008; Chen and Luo 2013	2
30	Phalangeal robustness index	PRI	(Ppl + Ipl + Dpl):Mcl	Lengths of all phalanges divided of digit ray III by metacarpal length		1
31	Manual robustness index	MRTI	(Mcl + Ppl + Ipl + Dpl): (Hl + Rl)	Manual length divided by lengths of humerus and radius		1
32	Ilium robustness index	IRI	Il:Pel	Ilium length divided by entire pelvic length	Sargis 2002b	1
33			Il:Isl	Ilium length divided by ischium length		3
34	Gluteal Index	GI	FGh:Fl	Proximal extension of greater trochanter divided by femoral length	Sargis 2002b; Samuels and Van Valkenburgh 2008; Bover et al. 2010; Samuels et al. 2013	2
35	Femoral robustness index	FRI	Fsw:Fl	Transverse diameter divided by femur length	Elissamburu and Vizcaíno 2004; Samuels and Van Valkenburgh 2008; Bover et al. 2010; Samuels et al. 2013	1
36	Femoral head robustness index	FHRI	Fhd:Fsw	Femoral head diameter divided by femoral midshaft width		1
37			Fsw:Fdw	Transverse diameter of femur divided by the femoral distal end width		3
38	Crural Index	CI	Tl:Fl	Tibial length divided by fibular length	Sargis 2002b; Samuels and Van Valkenburgh 2008; Bover et al. 2010; Samuels et al. 2013	3
39	Intermembral index	IM	(Hl + Rl): (Tl + Fl)	Lengths of the humerus and radius divided by lengths of the femur and tibia.	Sargis 2002a; Samuels and Van Valkenburgh 2008; Bover et al. 2010; Samuels et al. 2013	3

TABLE 3. Continued

No.	Osteological index	Abbr.	Equation	Description	Selected references for example	Index type
40			Tmw:Tpw	Transverse diameter of tibia divided by tibial proximal end width		3
41			Tdw:Tpw	Tibial distal end width divided by tibial proximal end width		3
42	Tibial robustness index	TRI	Tmw:Tl	Transverse diameter of tibia divided by tibial length	Elissamburu and Vizcaíno 2004; Samuels and Van Valkenburgh 2008; Bover et al. 2010; Samuels et al. 2013	1
43	Fibular robustness index	FBRI	Fbsw:Fbl	Transverse diameter of fibula divided by fibular length		3
44			Fbsw:Fbpw	Transverse diameter of fibula divided by fibular proximal end width		3
45			Fbdw:Fbpw	Fibular distal end width divided by fibular proximal end width		1
46	Fibular proximal end robustness index	FPRI	Fbpw:Fbl	Robustness of the proximal end of fibula		1
47	Fibular distal end robustness index	FDRI	Fbdw:Fbl	Robustness of the distal end of fibula		1
48	Astragalar neck robustness index	ANRI	Anl:Al	Astragalar neck length divided by astragalar length		1
49	Astragalar trochlea robustness index	ATRI	Atw:Al	Astragalar trochlea width divided by astragalar length		1
50	Calcaneal body robustness index	CBRI	Cal:Cl	Calcaneal body length divided by calcaneal length		1
51	Calcaneal tuber robustness index	CTRI	Ctl:Cl	Calcaneal tuber length divided by calcaneal length		3
52			Cal:Ctl	Calcaneal body length divided by calcaneal tuber length	Bassarova et al. 2009	3
53	Sustentacular robustness index	SRI	Csw:Ccw	Sustentacular process width divided by calcaneal cuboid facet width		1
54	Cuboid facet robustness index	CFRI	Ccw:Cl	Cuboid facet width divided by calcaneal length	Bassarova et al. 2009	1
55			Ctw:Ccw	Calcaneal tuber facet width divided by cuboid facet width		3
56	Tuber facet robustness index	TFRI	Ctw:Cl	Tuber facet width divided by calcaneal length		1

TABLE 4. Means, standard deviations, and results of the univariate ANOVA tests of each osteological index for each locomotor mode. Abbreviations: A, arboreal; F, fossorial; G, gliding; S, saltatorial; Sc, scansorial; Sa, semiaquatic; Sd, standard deviation; Sf, semifossorial; T, terrestrial. Shaded osteological indices were used in canonical variate analyses.

	Mean of each locomotor mode										Multivariate ANOVA Test			
Index No.	G	A	Sc	T	Sa	Sf	F	S	Total Mean	Sd	Sum Square	Mean Square	*F*-value	Pr (>F)
1	0.490	0.580	0.549	0.544	0.558	0.546	0.576	0.512	0.556	0.101	0.05005	0.00715	0.693	0.6778
2	0.590	0.675	0.731	0.759	0.854	0.811	0.948	1.024	0.774	0.164	1.1629	0.166136	9.8412	2.90E-09***
3	0.067	0.083	0.080	0.078	0.098	0.099	0.132	0.090	0.089	0.032	0.03048	0.0043543	5.3921	2.94E-05***
4	0.163	0.182	0.198	0.205	0.260	0.237	0.318	0.246	0.219	0.069	0.19802	0.028289	8.9938	1.51E-08***
5	0.210	0.248	0.227	0.237	0.332	0.303	0.404	0.308	0.274	0.110	0.3419	0.048843	5.1845	4.67E-05***
6	0.413	0.458	0.413	0.381	0.378	0.416	0.403	0.358	0.410	0.060	0.11757	0.0167953	6.4443	2.94E-06***
7	0.123	0.130	0.130	0.135	0.151	0.157	0.188	0.160	0.143	0.029	0.037058	0.0052941	9.8473	2.86E-09***
8	0.990	1.068	1.170	1.114	1.179	1.049	0.880	1.080	1.074	0.210	0.709	0.101287	2.532	0.01938*
9	0.763	0.765	0.778	0.728	0.662	0.688	0.561	0.692	0.714	0.105	0.44207	0.063153	8.5048	4.01E-08***
10	0.790	0.746	1.433	0.889	0.849	0.797	0.823	0.816	0.870	0.558	3.4409	0.49156	1.6488	0.1306
11	0.607	0.571	1.102	0.646	0.571	0.549	0.463	0.562	0.623	0.433	2.5614	0.36591	2.0975	0.05066
12	0.327	0.340	0.626	0.336	0.319	0.326	0.324	0.288	0.355	0.261	0.7319	0.104553	1.591	0.1468
13	0.733	0.637	0.564	0.762	0.720	0.694	0.848	0.592	0.702	0.630	0.726	0.10377	0.2482	0.9717
14	0.140	0.171	0.117	0.135	0.166	0.216	0.323	0.294	0.182	0.127	0.42461	0.060659	4.709	0.0001359***
15	0.337	0.378	0.273	0.345	0.429	0.548	0.839	0.836	0.450	0.336	3.4588	0.49411	5.7317	1.39E-05***
16	0.110	0.123	0.118	0.121	0.129	0.178	0.268	0.240	0.149	0.108	0.28046	0.040066	4.1151	0.000524***
17	1.270	1.098	1.092	1.112	1.171	1.112	1.213	1.494	1.145	0.146	0.84943	0.121348	8.5648	3.55E-08***
18	0.080	0.114	0.131	0.144	0.157	0.169	0.257	0.142	0.148	0.060	0.19747	0.0282103	15.383	1.74E-13***
19	0.103	0.126	0.144	0.158	0.183	0.190	0.310	0.206	0.170	0.075	0.32911	0.047016	17.165	1.08E-14***
20	1.123	0.928	0.904	0.939	0.921	0.872	0.841	1.218	0.933	0.135	0.66033	0.094333	7.2949	4.81E-07***
21	0.880	0.846	0.832	0.851	0.788	0.787	0.693	0.814	0.819	0.093	0.275	0.039285	6.0792	6.48E-06***
22	0.093	0.137	0.158	0.172	0.202	0.216	0.390	0.174	0.189	0.106	0.6209	0.0887	15.634	1.17E-13***
23	0.100	0.135	0.167	0.157	0.178	0.166	0.149	0.126	0.150	0.034	0.029793	0.0042562	4.6302	0.0001624***
24	0.130	0.122	0.107	0.115	0.127	0.134	0.358	0.162	0.149	0.176	0.60631	0.086616	3.2025	0.004232**
25	0.137	0.164	0.183	0.247	0.222	0.323	0.634	0.390	0.270	0.269	2.1855	0.312221	5.6335	1.72E-05***
26	0.170	0.230	0.251	0.362	0.314	0.396	0.512	0.568	0.335	0.175	1.1799	0.168551	8.1129	8.87E-08***
27	0.150	0.189	0.169	0.198	0.206	0.186	0.205	0.166	0.191	0.055	0.01885	0.0026928	0.9003	0.5095
28	0.530	0.417	0.423	0.441	0.401	0.666	1.712	0.946	0.617	0.909	17.851	2.5502	3.6235	0.001614*
29	1.560	1.289	0.957	0.859	1.043	0.913	1.311	0.996	1.085	0.433	4.5297	0.6471	4.1628	0.0004699***
30	2.090	1.704	1.382	1.300	1.442	1.579	3.024	1.942	1.701	1.270	28.221	4.0316	2.7976	0.01065*
31	0.310	0.364	0.393	0.358	0.433	0.420	0.482	0.368	0.387	0.078	0.1983	0.0283284	6.3666	3.47E-06***
32	0.617	0.615	0.591	0.594	0.546	0.593	0.572	0.530	0.591	0.043	0.060826	0.0086895	6.409	3.17E-06***
33	1.647	1.625	1.476	1.475	1.420	1.621	1.467	1.182	1.515	0.274	1.2413	0.177322	2.6097	0.01628*
34	0.057	0.049	0.044	0.059	0.058	0.060	0.088	0.066	0.058	0.025	0.015091	0.00215587	4.3552	0.0003032***
35	0.063	0.075	0.079	0.086	0.113	0.099	0.117	0.082	0.088	0.022	0.024423	0.003489	13.886	2.03E-12***
36	1.400	1.305	1.229	1.178	1.160	1.271	1.183	1.048	1.225	0.191	0.5843	0.083466	2.5263	0.01963*
37	0.427	0.431	0.431	0.448	0.436	0.432	0.476	0.438	0.441	0.062	0.02172	0.0031026	0.7876	0.5993
38	1.150	1.048	1.032	1.119	1.288	1.096	1.043	1.410	1.110	0.158	0.96524	0.137891	8.0702	9.68E-08***
39	0.837	0.773	0.830	0.766	0.761	0.813	0.783	0.414	0.764	0.106	0.69634	0.099477	19.965	<2.20E-16***
40	0.337	0.325	0.338	0.355	0.326	0.309	0.333	0.408	0.338	0.054	0.047962	0.0068517	2.5897	0.01703*
41	0.553	0.604	0.647	0.621	0.618	0.640	0.609	0.590	0.615	0.100	0.03415	0.0048789	0.474	0.8513
42	0.047	0.053	0.060	0.060	0.064	0.062	0.074	0.056	0.060	0.013	0.0046989	0.00067128	4.8558	9.76E-05***

TABLE 4. Continued

Index No.	Mean of each locomotor mode									Multivariate ANOVA Test			
	G	A	Sc	T	Sa	Sf	F	S	Total Mean	Sd	Sum Square	Mean Square	*F*-value	Pr (>F)
43	0.020	0.032	0.029	0.029	0.030	0.034	0.042	0.014	0.031	0.018	0.0034658	0.00049511	1.606	0.1425
44	0.260	0.289	0.277	0.276	0.250	0.324	0.269	0.204	0.277	0.139	0.05964	0.0085202	0.4213	0.887
45	0.630	0.581	0.804	0.687	0.728	0.631	0.569	0.642	0.649	0.242	0.5374	0.076773	1.3351	0.2419
46	0.077	0.122	0.108	0.107	0.128	0.118	0.153	0.070	0.116	0.045	0.036663	0.0052376	2.8421	0.00624**
47	0.047	0.065	0.074	0.070	0.083	0.070	0.084	0.044	0.070	0.024	0.010041	0.00143445	2.6925	0.01351*
48	0.483	0.501	0.428	0.454	0.457	0.452	0.467	0.452	0.467	0.076	0.05818	0.0083118	1.4828	0.1821
49	0.697	0.713	0.722	0.770	0.690	0.752	0.728	0.902	0.741	0.180	0.2133	0.030475	0.938	0.4809
50	0.380	0.392	0.324	0.368	0.342	0.361	0.294	0.274	0.356	0.071	0.13533	0.0193334	4.7702	0.000118***
51	0.337	0.350	0.399	0.404	0.403	0.368	0.471	0.518	0.396	0.087	0.22423	0.032033	5.555	2.05E-05***
52	1.137	1.238	0.880	0.956	0.891	1.012	0.640	0.546	0.979	0.447	4.5866	0.65522	3.9184	0.000821***
53	0.733	0.807	0.598	0.655	0.688	0.656	0.779	0.724	0.715	0.235	0.5779	0.082561	1.5461	0.1607
54	0.300	0.284	0.330	0.293	0.296	0.332	0.294	0.274	0.297	0.062	0.02911	0.0041583	1.1004	0.3689
55	0.767	0.947	0.888	0.954	0.959	0.914	1.014	0.972	0.946	0.187	0.1984	0.028343	0.7959	0.5925
56	0.227	0.264	0.288	0.270	0.283	0.301	0.280	0.254	0.273	0.041	0.021511	0.003073	1.9056	0.0765

*$p<0.1$, **$p<0.01$, ***$p<0.001$

At the opposite extreme, fossorial mammals possess the most robustly built postcranial skeletons of the eight locomotor modes. They tend to have (i) an enlarged scapula (SI), (ii) a robust and longer forelimb with a prominent humeral deltopectoral crest and a relatively wide humeral distal end (HEB, HRI, and DI), (iii) an ulna with an enlarged olecranon process (OPLI), (iv) a robust hand with shortened proximal and intermediate phalanges and elongate distal phalanges (PPRI, IPRI, PI, and MRTI), (v) a shortened ilium (IRI), (vi) a robust femur with an elevated greater trochanter (FRI and GI), (vii) a shortened and robustly built tibia and fibula (TRI), (viii) a reduced astragalar neck and calcaneal body (CBRI), and (ix) an elongate calcaneal tuber (CTRI). Semi-fossorial mammals have similar morphological signatures but to a lesser degree and without the reduction of the ilium found in fossorial taxa. Semiaquatic mammals also tend to be robustly built, having (i) an anteroposteriorly compressed scapula (SI), (ii) a robust humerus with bilaterally expanded proximal and distal ends (HEB, HRI, and Hpw:Hl; see Table 3 for definition), (iii) a well-developed humeral deltopectoral crest (DI), (iv) an enlarged hand (MRTI), (v) a shortened ilium (IRI), (vi) a robust hind limb with a pronounced greater trochanter of the femur (FRI, GI, and TRI), and (vii) an elongate tibia and fibula (CI).

Distinct from all other locomotor modes, saltatorial mammals mainly travel by bipedal hopping and are characterized by (i) a greatly reduced forelimb and an elongated hind limb (IM), (ii) gracile limb elements (HRI, FRI, and TRI), (iii) a relatively shortened humerus (BI), (iv) a relatively large hand (MRTI), (v) a shortened ilium (IRI), (vi) a poorly developed greater trochanter of the femur (GI), (vii) a shortened calcaneal body (CBRI), and (viii) an elongate calcaneal tuber (CTRI).

Predicted Locomotor Modes of Small-bodied Extant Mammals

Eight-Locomotor-Mode Analysis.—This CVA included all locomotor modes in our data set (Fig. 4A, Supplementary Fig. 1A). Together, the first three canonical functions (CFs) account for 85.50% of the variance in the data set

TABLE 5. Morphological signatures of each locomotor mode. Abbreviations: G, gliding; A, arboreal; F, fossorial; S, saltatorial; Sc, scansorial; Sa, semiaquatic; Sf, semifossorial; T, terrestrial. Symbols: ++, relatively robust; +, relatively large, long, or wide; -, relatively small, short, or slender; --, relatively very small or extremely gracile; = =, equal; =, intermediate; *, varies; fd, forelimb dominated; hd, hind limb dominated.

	Locomotor mode							
Morphological signature	G	A	Sc	T	Sa	Sf	F	S
Scapular length	+	-	*	+	+	*	*	-
Deltopectoral crest width	- -	-	-	*	+	+	++	-
Olecranon process length	- -	-	-	*	+	+	++	-
Palm size	-	-	*	+	-	*	- -	-
Proximal and intermediate phalangeal length	-	-	*	+	-	*	- -	-
Distal phalangeal robustness	-	-	-	-	+	*	++	+
Ilium length	+	+	=	*	-	+	-	-
Greater trochanter length	-	-	-	*	+	+	++	-
Forelimb robustness	- -	-	*	*	+	+	++	-
Hind limb robustness	- -	-	*	*	+	+	++	-
Limb use domination	fd	= =	fd	= =	*	*	fd	hd

(CF1 = 49.13%, CF2 = 25.83%, CF3 = 10.54%; Supplementary Table 3). In the morphospace formed by the CF1 vs. CF2 scores, the gliding, fossorial, and saltatorial mammals are well separated from each other and the remaining locomotor modes. Their centroids are at the extremes of the morphospace. In contrast, the remaining five locomotor modes overlap in the morphospace and their centroids are clustered near the origin. The morphological variance of each locomotor mode shows that gliding taxa have the smallest variance, followed by scansorial, arboreal, terrestrial, saltatorial, semiaquatic, semifossorial, and fossorial taxa (Fig. 4C, Supplementary Table 4).

CF1 is strongly positively correlated with Ul:Hl (see Table 3 for definition), the brachial index (BI), and the crural index (CI), and negatively correlated with the Intermembral (IM) indices (Fig. 4B, Supplementary Fig. 1B). The saltatorial species are well separated from other modes along CF1 due to a high CI and a low IM (high CF1 scores). CF2 is negatively correlated with numerous robustness, morpho-functional, and proportional indices of the forelimb, which separates the fossorial, semi-fossorial, and saltatorial mammals from other modes in the morphospace. These indices include Sl:Hl (see Table 3 for definition), the humeral robustness index (HRI), the humeral proximal robustness index (HPEI), the humeral epicondylar index (HEB), Hsw:Hpw (see Table 3 for definition), the humeral head robustness index (HHRI), Hdcw:Hpw, the deltopectoral index (DI), Hdcw:Hdw, the olecranon process length index (OPLI), Uol:Hl, Uol:Rl (see Table 3 for definition), the robustness index of proximal and intermediate phalanges (PPRI and IPRI), and the manual robustness index (MRTI), as well as a few hind limb indices, such as the gluteal index (GI), the femoral robustness index (FRI), the calcaneal tuber robustness index (CTRI). CF2 is positively correlated with HHw:Hpw, Rl:Ul (see Table 3 for definition), the ilia robustness index (IRI), and the calcaneal body robustness index (CBRI) (Fig. 4B). CF3 is negatively correlated with HRI, three deltopectoral-crest-related indices, OPLI, the phalangeal index (PI), and GI, and positively correlated with the palm robustness index (PRTI) (Supplementary Fig. 1B). CF3 successfully separates scansorial and terrestrial mammals from fossorial and saltatorial mammals.

The CVA correctly classified 89.72% of the individuals (100% of gliding, semifossorial, and saltatorial taxa; 93.93% of arboreal taxa; 88.89% of scansorial and semiaquatic taxa; 86.67% of terrestrial taxa; and 75.00% of fossorial taxa). In total, 11 of 107 species were misclassified (Supplementary Table 5) and the majority of misclassified taxa are from arboreal, scansorial, terrestrial, and semifossorial locomotor modes.

Five-Locomotor-Mode Analysis.—Removing the gliding, fossorial, and saltatorial modes from the CVA improved the segregation of the remaining five locomotor modes (Supplementary Fig. 2A, C). The first three CFs accounted for 93.36% of the variance

(CF1 = 48.30%, CF2 = 27.61%, CF3 = 17.45%; Supplementary Table 6). In the plot of CF1 vs. CF2 (Supplementary Fig. 2A), the locomotor modes appear to be separated farther apart, relative to the distribution of these modes in the eight-locomotor-mode analysis. Although the arboreal, terrestrial, semifossorial, and semiaquatic modes are well separated from

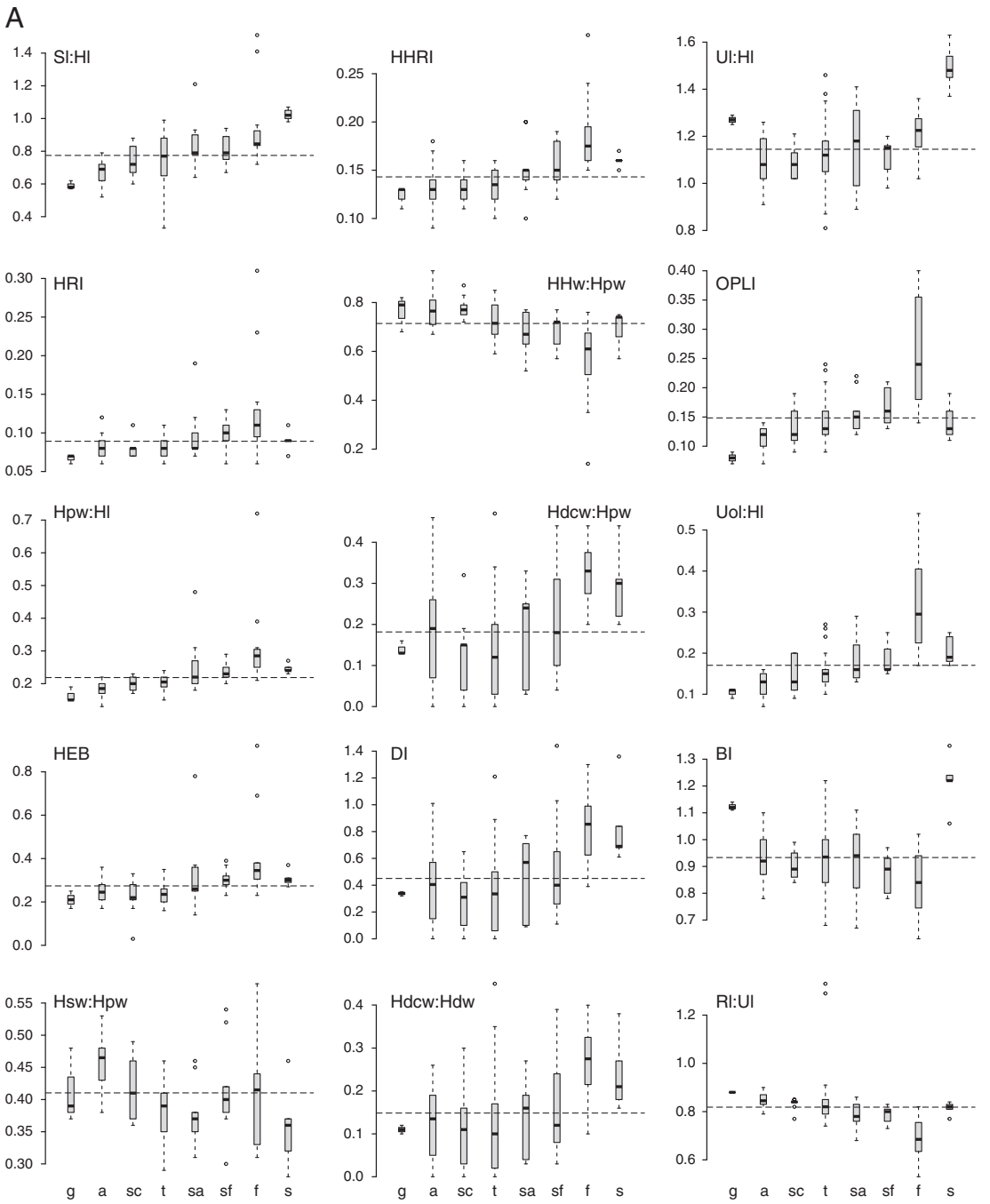

FIGURE 3. A, B. Boxplots of 30 osteological indices for our extant small-bodied mammal data set. Abbreviations: g, gliding; a, arboreal; sc, scansorial; t, terrestrial; sa, semiaquatic; sf, semifossorial; f, fossorial; s, saltatorial. See descriptions of the osteological indices in Table 3.

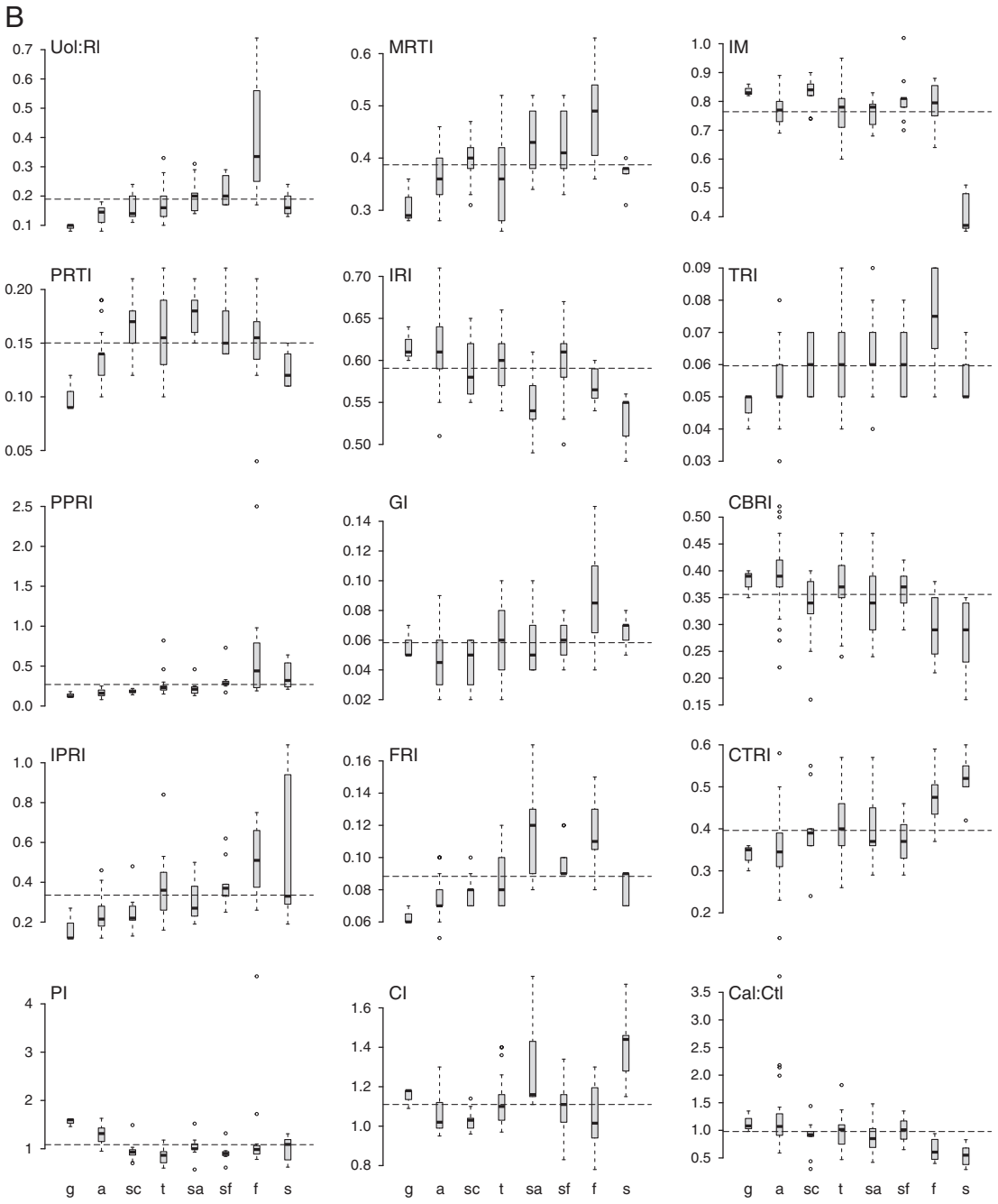

FIGURE 3. Continued.

each other, the scansorial mode still overlaps with the arboreal and terrestrial modes.

In the structure matrix, the structure coefficients indicate that CF1 is highly correlated with two robustness and two morphofunctional indices: the olecranon process length index (OPLI), the proximal phalangeal robustness index (PPRI), the intermediate phalangeal robustness index (IPRI), and the phalangeal index (PI) (Supplementary Table 6). These four indices are also highly correlated with CF2 and CF3, suggesting that they play a significant role

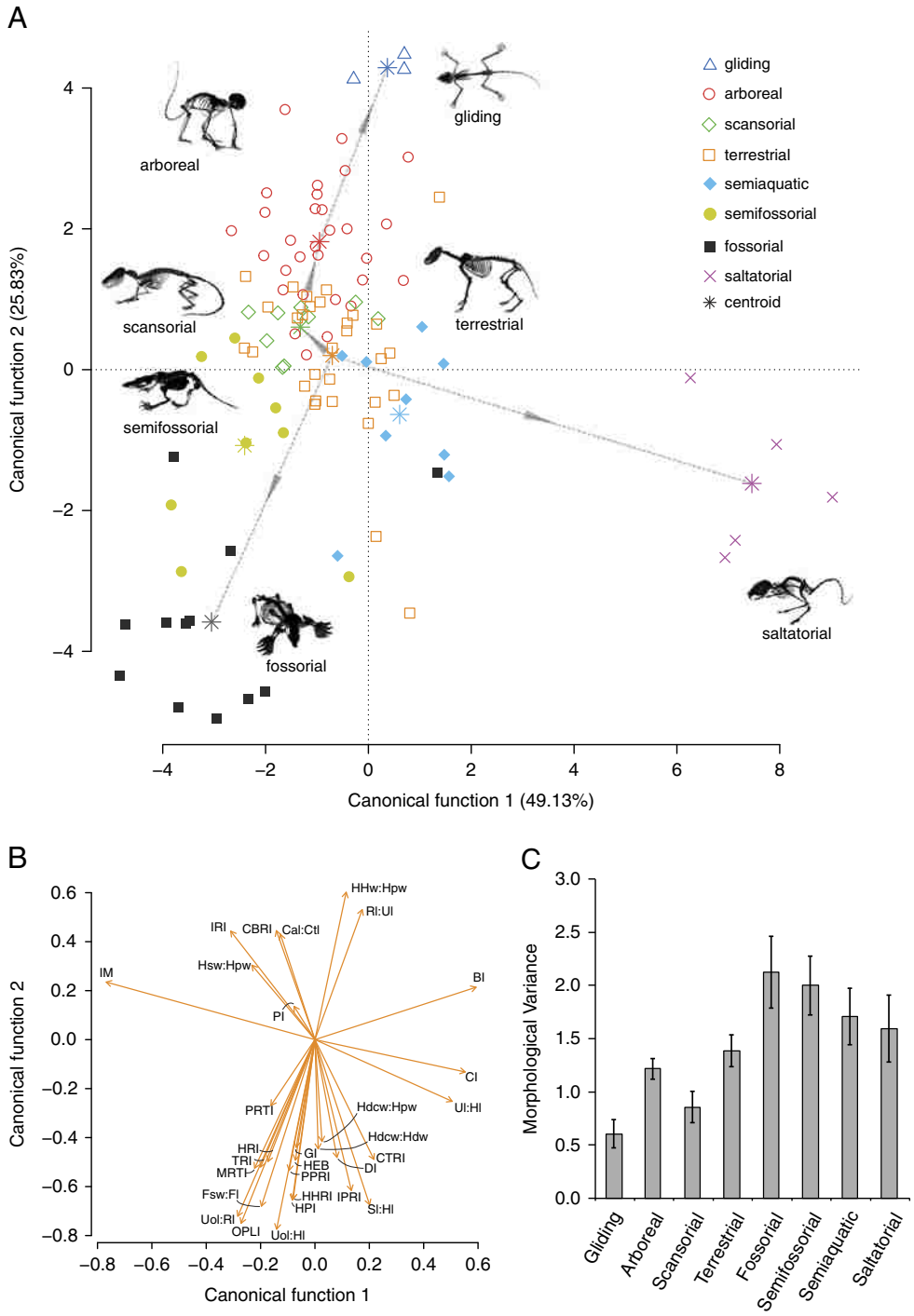

FIGURE 4. Ordination of locomotor modes of small-bodied extant mammals in the eight-locomotor-mode analysis. A, Plot of canonical functions (CF) 1 and 2 from the canonical variate analysis (CVA). Dashed lines with arrows show axes of morphofunctional continua among locomotor modes. B, Plot of structure correlations between the osteological indices and the CF1 and CF2. C, Morphological variances among eight locomotor modes. The morphological variance is calculated by using the mean of the distances between species in a locomotor mode and their corresponding centroid, using first three CF scores in each locomotor mode.

in segregating among the five locomotor modes. On CF1, the semifossorial taxa have high scores and are well separated from the other four taxa. Most of the semiaquatic taxa have very low CF1 scores and separate themselves from the other four locomotor modes. Together, the five locomotor modes form a morphological gradient along CF1, from semiaquatic to arboreal/scansorial/terrestrial and semifossorial modes (Supplementary Fig. 2A,C).

Along CF2, the morphological gradient extends from semiaquatic to semifossorial, terrestrial, and arboreal/scansorial modes (Supplementary Fig. 2A). Each locomotor mode overlaps to varying degrees with the adjacent locomotor modes. CF2 is correlated with numerous indices as well as the four osteological indices that were strongly correlated with CF1 (Supplementary Table 6, Supplementary Fig. 2B). It is negatively correlated with Sl:Hl, the humeral robustness index (HRI), the humeral proximal end robustness index (HPEI), the humeral epicondylar index (HEB), Hsw:Hpw, the humeral head robustness index (HHRI), HHw:Hpw, Uol:Hl, Uol:Rl, the palm robustness index (PRTI), the manual robustness index (MRTI), the femoral robustness index (FRI), and the tibial robustness index (TRI), and positively correlated with HHw:Hpw and the ilium robustness index (IRI).

CF3 is negatively correlated with Hsw:Hpw, the calcaneal body robustness index (CBRI), and Cal:Ctl (see Table 3 for definition), and positively correlated with the olecranon process length index (OPLI) and calcaneal tuber robustness index (CTRI) (Supplementary Table 6, Supplementary Fig. 2D). CF3 segregates the five locomotor modes into three groups, from arboreal to semiaquatic/semifossorial and scansorial/terrestrial (Supplementary Fig. 2C).

The CVA correctly classified 95.40% of the individuals (100% of semifossorial, 96.67% of arboreal, 96.67% of terrestrial, 88.89% of scansorial, and 88.89% of semiaquatic). Four of the 11 species that were misclassified in the eight-locomotor-mode analysis remain misclassified here (Supplementary Table 7).

Three-Locomotor-Mode Analysis.—To further understand the morphological differences among arboreal, scansorial, and terrestrial taxa, we removed all other locomotor modes from the CVA. The results indicate that two canonical functions account for 100% of variance in the data set (Supplementary Table 8). The plot of CF1 vs. CF2 shows unambiguous segregation of the three locomotor modes (Supplementary Fig. 3).

CF1 accounts for 55.93% of the variance and separates the three locomotor modes into three discrete groups in the morphospace (Supplementary Fig. 3A). The scansorial mode plots intermediate between the arboreal and terrestrial modes. Given the structure matrix, CF1 positively correlates with Sl:Hl, the humeral proximal end index (HPI), the olecranon process index (OPLI), Uol:Hl, Uol:Rl, the palm robustness index (PRTI), the proximal phalangeal robustness index (PPRI), the intermediate phalangeal robustness index (IPRI), the femoral robustness index (FRI), the crural index (CI), the tibial robustness index (TRI), and the calcaneal tuber robustness index (CTRI), and negatively correlates with Hsw:Hpw, HHw:Hpw, the phalangeal index (PI), and the Cal:Ctl (Supplementary Table 8, Supplementary Fig. 3B). CF2, which accounts for the remaining 44.07% of the variance, separates the scansorial mode from the arboreal/terrestrial modes. It negatively correlates with the palm robustness index (PRI), intermembral index (IM), and positively correlates with calcaneal body robustness index (CBRI) (Supplementary Table 8, Supplementary Fig. 3B).

The CVA correctly classified 97.10% of the individuals (100% of terrestrial, 96.67% of arboreal, and 88.89% of scansorial taxa; Supplementary Table 9). The only misclassified taxa are *Rattus andamanensis* and *Heliosciurus rufobrachium*, which were also misclassified in the five- and eight-locomotor-mode analyses.

Predicted Locomotor Mode of Mesozoic Mammals

We used the above CVAs of extant small-bodied mammals as a framework for inferring the locomotor mode of ten Mesozoic mammal species that are known from relatively complete postcranial skeletons. The results of the eight-locomotor-mode analysis indicate that *Fruitafossor*, *Repenomamus*, and *Liaoconodon* were likely adapted for fossorial, semifossorial, and semiaquatic lifestyles, respectively, given the 100% posterior probabilities. Our analysis also yielded high posterior probabilities (>95%)

for *Rugosodon*, *Jeholodens*, *Yanoconodon*, and *Akidolestes* as arboreal, arboreal, semiaquatic, and semifossorial mammals, respectively. The locomotor inferences for *Haldanodon* were ranked in order of decreasing posterior probability, as follows (Table 1): arboreal (56.6%), semifossorial (41.6%), and terrestrial (1.8%), suggesting that this analysis cannot clearly determine whether this taxon is arboreal or semifossorial. For *Eomaia*, the posterior probabilities of the locomotor inferences were ranked as follows: arboreal (68.6%), scansorial (16.5%), and terrestrial (11.3%), whereas for *Zhangheotherium*, the posterior probabilities were ranked from semifossorial (32.6%), to scansorial (26.2%), arboreal (20.0%), and terrestrial (11.6%), suggesting that the locomotor modes of *Eomaia* and *Zhangheotherium* cannot not be determined by an eight-locomotor-model analysis.

The results of the five-locomotor-mode analysis, supported by high posterior probabilities, indicate that *Haldanodon* (100%) and *Eomaia* (93.2%) are likely semifossorial and arboreal mammals, respectively. The results also suggest that *Rugosodon* (94.8%) and *Zhangheotherium* (71.25%) were both scansorial mammals rather than arboreal as inferred by the eight-locomotor-mode analysis. Moreover, the results indicate that *Jeholodens* had some morphological features that are adapted to terrestrial locomotion (21.2%). The inferred locomotor adaptations of *Yanoconodon*, *Liaoconodon*, and *Akidolestes* from the five-locomotor-mode analysis are consistent with the inferences from the eight-locomotor-mode analysis (semiaquatic, semiaquatic, and semifossorial, respectively).

Discussion

The Link between Postcranial Morphology and Locomotor Mode in Extant Small-Bodied Mammals

Different locomotor modes place different mechanical and energetic demands on the appendicular skeleton of vertebrates (Tucker 1970, 1975; Hildebrand et al. 1985; Biewener 1989, 1990, 2003). Adaptation to these demands is associated with morphological modifications. These modifications tend to be pronounced in mammals, which have higher metabolic requirements and thus greater need for efficient movement across the landscape than do most other vertebrates (McNab 2002). Because total energetic costs of locomotion scale with body size (see McNab 1990; Biewener 2003), larger-bodied mammals would seem to have higher selective pressures than small-bodied mammals, presumably resulting in distinct morphological adaptations to locomotor mode. Moreover, preservation bias and collecting methods favor recovery of larger skeletal elements in the fossil record. For these reasons, paleontologists have tended to focus on inferring locomotor mode in large-bodied fossil mammals over small-bodied ones, quantitatively establishing the link between postcranial morphology and locomotion by using extant analogues (Van Valkenburgh 1987; Janis et al. 2002; Polly 2008, 2011; Bassarova et al. 2009; Samuels et al. 2013). The underlying assumption is that in small-bodied mammals this link would be subtle or indistinguishable and that scansoriality is an obligatory locomotion in small-bodied mammals (Jenkins 1974; Jenkins and Parrington 1976). However, multiple studies have shown that the same biomechanical selective forces operate on both small- and large-bodied mammals (Szalay 1984; Sargis 2001b; Szalay and Sargis 2001). Nonetheless, few studies have attempted to quantitatively infer locomotion in smaller-bodied fossil mammals (but see Samuels and Van Valkenburgh 2008; Hopkins and Davis 2009). Here, we tested this assumption by attempting to establish a link between postcranial morphology and locomotor mode in a sample of small-bodied extant mammals of diverse locomotor modes and phylogenetic histories, using multivariate analysis of morphometric data from postcranial skeletons.

The results from our multivariate analyses show that the link between postcranial morphology and locomotor mode in small-bodied mammals is indeed subtle but detectable. The eight-locomotor-mode analysis segregated the most specialized locomotor groups (gliding, fossorial, and saltatorial), leaving the remaining locomotor groups (arboreal, scansorial, terrestrial, semiaquatic, and semifossorial) in a cluster (Fig. 4A, Supplementary Fig. 1A). Despite this clustering, the CVA correctly classified nearly 90% of the extant taxa into their

correct locomotor modes. A secondary analysis (five-locomotor-mode analysis), which excluded the most specialized locomotor groups, further segregated the semifossorial and semiaquatic groups from the main cluster of terrestrial, arboreal, and scansorial taxa (Supplementary Fig. 2A,C). Prediction of locomotor group membership improved to better than 95% in this analysis. The cluster of terrestrial, scansorial, and arboreal taxa persisted, but this is not surprising in light of variable definitions of scansoriality and variable assignment of extant taxa to these modes in the literature (Kingdon 1997; Iwaniuk et al. 1999; Nakagawa et al. 2007; Kelt and Meyer 2009; Shattuck and Williams 2010; Chen and Luo 2013). Moreover, an individual mammal's perception of its substrate likely scales with body size (but see Szalay and Sargis 2001); for example, during ground locomotion across uneven substrate, some small-bodied terrestrial mammals, such as an island mouse (*Nesomys rufus*), might require a degree of climbing, whereas large-bodied mammals, such as a red fox (*Vulpes vulpes*), can cross the same substrate without climbing. This phenomenon can further blur formal distinctions among locomotor modes. Nevertheless, in our third analysis (three-locomotor-mode analysis), the terrestrial, scansorial, and arboreal modes were fully separated from each other (Supplementary Fig. 3A) and over 97% of the sampled taxa were correctly classified to their respective locomotor mode. Taken together, these results provide promise for inferring locomotion in small-bodied fossil mammals. The most specialized locomotor modes (gliding, fossorial, and saltatorial) have very distinctive postcranial morphologies that are readily detectable in our eight-locomotor-mode analysis, and the more subtle morphological differences among less specialized groups become perceptible as specialized modes are progressively removed from the analyses (five-locomotor-mode and then three-locomotor-mode analyses).

The large morphological variance *within* locomotor modes contributes to the difficulty in distinguishing *among* locomotor modes. This morphological variance stems from phylogenetic and functional diversity in our data set. By design, we sampled a phylogenetically broad range of taxa for each locomotor mode in hopes that our analyses would detect a robust signal of functional adaptations rather than a narrow subset of shared derived features (synapomorphies). Our results show that this approach was successful. At a higher taxonomic level, our analysis accurately segregated the large samples of marsupials, carnivorans, and rodents according to locomotor mode not phylogeny (Fig. 5), a result that is consistent with previous studies (Van Valkenburgh 1987; Iwaniuk et al. 1999; Weisbecker and Warton 2006; Weisbecker and Schmid 2007; Samuels and Van Valkenburgh 2008; Bassarova et al. 2009; Samuels et al. 2013). The merit of this approach extends to the subgenus level, where, for example, four species of *Tupaia* (*T. longipes* and *T. tana* [both terrestrial], *T. glis* [scansorial], and *T. minor* [arboreal]) were segregated in the ecomorphospace according to their locomotor modes (Fig. 5). A trade-off of having phylogenetic diversity within locomotor-mode samples is the associated increase in morphological diversity that results from divergent evolutionary histories. Although this variance inherently limits our ability to distinguish among locomotor modes relative to more phylogenetically uniform samples (e.g., a fossorial group of only rodents), it enables robust locomotor inference for a phylogenetically broader range of extinct taxa.

Additional morphological variance results from functional diversity within locomotor modes, most notably within the fossorial, semifossorial, and semiaquatic samples (Fig. 4C). Fossorial and semifossorial samples include taxa that employ diverse digging modes, from chisel-tooth, to scratch, head-lift, humeral-rotation, and combinations thereof (Hildebrand 1985; Hildebrand and Goslow 1998; Stein 2000; Hopkins and Davis 2009). Likewise, some semiaquatic mammals emphasize forelimb propulsion (e.g., *Neovison vison* in surface swimming [Dunstone 1979]), whereas others (e.g., *Chironectes minimus* [Howell 1930; Marshall 1978] and *Ondatra zibethicus* [Fish 1993]) emphasize hind limb propulsive paddling. In turn, the associated postcranial adaptations of these taxa within the same locomotor mode can vary substantially (e.g., humeral-rotation diggers tend to have a more bilaterally expanded humerus than scratch diggers). Inclusion of this functional diversity in our data set dilutes the

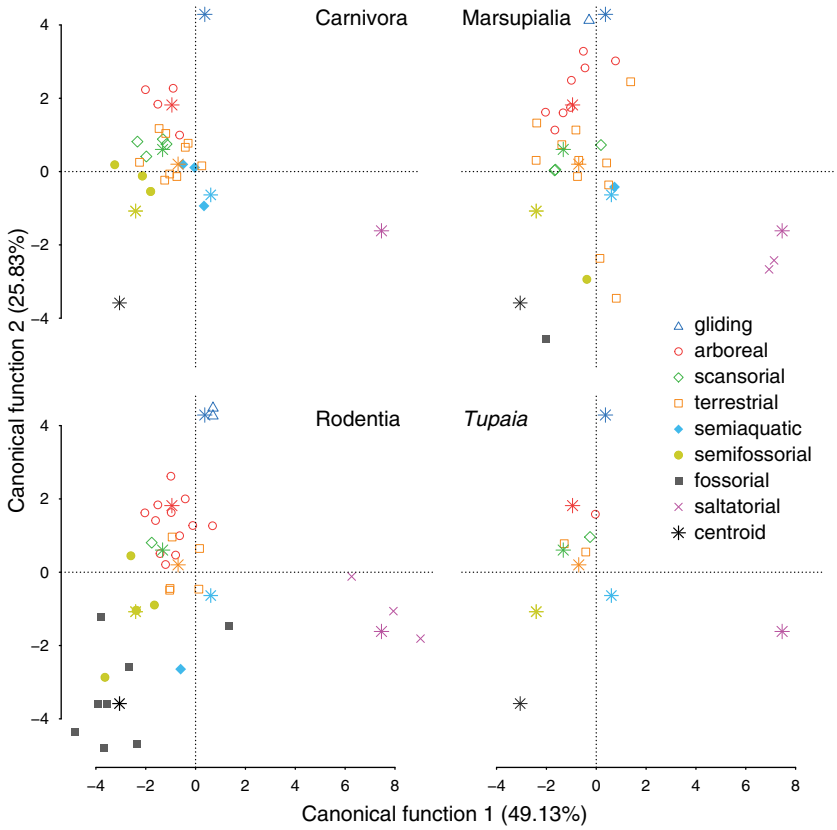

FIGURE 5. CVA plots (first two functions) of eight-locomotor-mode analyses for Carnivora, Rodentia, Marsupialia, and *Tupaia*. Rodents use eight locomotor modes, whereas marsupials and carnivorans use six and four locomotor modes, respectively. Species of the genus *Tupaia* use arboreal, scansorial, and terrestrial locomotor modes. The centroids represent the centroids of the full dataset.

morphological signal of any one locomotor mode (i.e., makes it less uniform), but it better reflects the reality among extant small-bodied mammals and improves our ability to capture locomotor diversity in fossil taxa. The saltatorial mode also exhibits large morphological variance, but for a different reason. Saltatorial taxa commonly show a striking elongation of their hind limbs for bipedal hopping, whereas their forelimbs are only minimally involved in locomotion. As a result, the forelimbs of saltatorial taxa often evolve for other activities (e.g., food manipulation, digging). This evolutionary independence of the forelimb not only increases the morphological variance in this group, but it can also complicate locomotor inferences. For example, several saltatorial taxa (e.g., *Potorous tridactylus*, *Aepyprymnus rufescens*, *Jaculus jaculus*) exhibit forelimb adaptations associated with scratch digging, which if analyzed without hind limb indices would lead to their classification as members of the semifossorial group. This result highlights the importance of analyzing an anatomically broad set of indices rather than a few that focus on select anatomical elements (e.g., only the forelimb) whenever possible; however, we acknowledge that small-bodied mammal fossils are typically less complete than those in our sample. Moreover, it should be noted that the accuracy of locomotor predictions using our multivariate approach decreases as the number of available postcranial measurements decreases.

A couple of caveats to future application of this morphometric approach should be noted. First, allometric scaling has profound influence on morphological and ecological adaptation of mammals. It may produce major differences

between large- and small-bodied mammals in their morphological adaptation to the same locomotor mode (e.g., the arboreal marsupial *Caluromys* versus the arboreal primate *Hylobates*; McMahon 1975; Alexander 1985). Thus, for robust locomotor inference of extinct taxa, the analogue extant species in the morphometric data set should be of comparable body size to the fossil taxa. Second, the coverage of locomotor modes in the morphometric data set also affects locomotor inference of extinct mammals. For example, inclusion of too many locomotor modes in the morphometric data set, especially highly specialized ones like fossorial and saltatorial modes, could result in poor segregation of locomotor modes in the ecomorphospace plots (although prediction error may still be low). In contrast, incomplete coverage of locomotor modes in the morphometric data set could in some cases lead to inaccurate locomotor prediction of extinct mammals. Thus, the composition of the analogue extant taxa in the morphometric data set should be carefully chosen based on initial morphological assessment of the fossil taxon. For example, if the fossil taxon lacks the obvious morphological signatures associated with gliding, the effectiveness of the analysis to discriminate among the non-gliding modes for this taxon would be improved by removal of gliders from the morphometric data set, thus improving the inferential power of the analysis. In sum, the morphometric data set of extant taxa and the analyses should be tailored to the fossil taxa of interest whenever possible.

Morphofunctional Continuum among Locomotor Modes

The eight locomotor modes in our analyses not only possess distinct postcranial morphologies but also ordinate in the ecomorphospace (Fig. 4A, Supplementary Fig. 1A) according to shared biomechanical properties. In the eight-locomotor-mode analysis, CF1 segregates locomotor modes by forelimb to hind limb proportions, i.e., facultative bipeds (saltatorial) versus quadrupeds (all other modes). CF2 generally ordinates locomotor modes according to mechanical advantage. Modes that emphasize force over speed (fossorial, semifossorial, semiaquatic) have robustly built appendicular skeletons and short output levers (low CF2 scores), whereas modes that emphasize speed over force (gliding, arboreal) have more gracile appendicular skeletons and long output levers (high CF2 scores). The saltatorial mode is the exception to this pattern. Despite having hind limb adaptations for bipedal hopping (speed), several saltatorial taxa have forelimb adaptations for digging (force) that lead to low CF2 scores, comparable to other modes that emphasize the strength and magnitude of output forces, such as fossorial, semifossorial, and semiaquatic.

Within this morphofunctional continuum of locomotor modes, the terrestrial mode lies near the origin (Fig. 4A, Supplementary Fig. 1A). As morphological features become progressively more gracile (increasing CF2 scores), the continuum extends from the terrestrial mode to the scansorial, arboreal, and gliding modes. The decreasing robustness of postcranial elements reduces body mass, which is generally correlated with increased flexibility of skeletal elements and joints of these mammals. This enhances the dexterity and precision of movement in mammals that move among trees, simultaneously mitigating the risk of falling during climbing. The scansorial mode is intermediate between terrestrial and arboreal modes (Fig. 4A, Supplementary Figs. 2A, 3A) and shares numerous morphological features with these other modes. The only distinctive morphological feature of the scansorial mode is a more elongate forelimb (high IM) than that of terrestrial and arboreal taxa. This forelimb elongation suggests that scansorial taxa have more forelimb-dominated locomotion than the arboreal and terrestrial taxa. This would functionally correlate with the ability of scansorial mammals to ascend and descend (Polly 2007). In the arboreal mode, the postcranial elements are even more slender and exhibit greater reduction of crests and tubercles than in the scansorial and terrestrial modes. The latter modification enables greater mobility at the joints, thereby increasing agility for arboreal locomotion (Cartmill 1985; Argot 2001, 2002; Sargis 2001a, 2002a,b). Relative to scansorial and terrestrial modes, arboreal taxa also have more elongate digits and smaller palms (high PI and low PRTI, respectively), both of

which correlate with prehensility (Jouffroy and Lessertisseur 1979; Cartmill 1985; Van Valkenburgh 1987; Jouffroy et al. 1993; Lemelin 1999; Argot 2001, 2002; Sargis 2001a, 2002a,b; Bloch and Boyer 2002; Weisbecker and Warton 2006; Kirk et al. 2008; Weisbecker and Schmid 2007; Boyer et al. 2013). In the gliding mode, the appendicular skeleton is exceptionally gracile and lacks prominent crests and tubercles. These modifications further reduce body mass and further increase joint mobility for gliding locomotion (Samuels and Van Valkenburgh 2008).

In the opposite direction, the morphofunctional continuum extends from the terrestrial mode to the semiaquatic/semifossorial and fossorial modes with morphological features becoming progressively more robust (decreasing CF2 scores) (Fig. 4A). This aspect of the continuum reflects the need to withstand the increasingly high mechanical stresses incurred in these locomotor modes (Lanyon and Rubin 1985; Biewener 1989). The trend toward increasingly more robust elements is coupled with a trend toward increasingly greater area for muscle attachment (e.g., high HRI, HPI, OPLI, MRTI, FRI, and TRI). The postcranial elements of fossorial taxa are the most robust of all locomotor modes. The semifossorial and semiaquatic modes are intermediate on this aspect of the continuum. However, separation along CF1 indicates important functional differences between semifossorial and semiaquatic modes. Relative to semiaquatic taxa, semifossorial taxa tend to have shorter limb output levers (e.g., less elongate radius, ulna and tibia [high BI and CI]) (Croft and Anderson 2008; Samuels and Van Valkenburgh 2008; Samuels et al. 2013). This slight morphological difference likely reflects the greater propulsive forces needed for a digging stroke against soil versus a swimming stroke against water. Moreover, within the semifossorial mode, the output lever of the forelimb is smaller than that of the hind limb (BI higher than CI), which indicates that power of the digging stroke in semifossorial (and fossorial) taxa resides in the forelimb rather than the hind limb. In contrast, the relative lengths of the ulna and tibia vary in semiaquatic taxa. This likely reflects differences in primary swimming strategies among semiaquatic taxa, from forelimb-, to hind-limb-, and all-limb-dominated modes. In fossorial taxa, postcranial elements are even more robust and the relative size of the manus is substantially larger than in the semifossorial and semiaquatic modes. These more extreme morphological adaptations (relative to semifossorial taxa) reflect a more subterranean existence, in which these animals often develop elaborate tunnel systems (Hildebrand 1985; Hildebrand and Goslow 1998; Stein 2000).

The morphofunctional continuum also extends from the terrestrial to saltatorial mode. Saltatorial taxa have forelimbs that are reduced relative to their elongate hind limbs (increasing CF1 scores) (Fig. 4A). This change in morphology relative to the terrestrial mode reflects a shift toward rapid and simultaneous extension of both hind limbs in bipedal hopping. Energetically, bipedal hopping is a more efficient mode of transportation over long distances than the seven other locomotor modes (McNab 2002). In saltatorial taxa, the ischium is elongate relative to the ilium (low IRI). Although this morphological change would seem to increase the input lever for the hip extensors, a proximal insertion of these muscles on the tibia only maintains the same input lever length relative to non-jumping mammals (Emerson 1985). Instead, the enlarged hip extensor muscles increase the output force during the propulsive stroke (Gambaryan 1974; Alexander et al. 1981; Emerson 1985). Moreover, the elongate tibia (high CI) results in a longer output lever of the hind limb musculature, thereby increasing the speed of the propulsive stroke. Together, these changes to the pelvis and hind limb optimize jumping ability in saltatorial taxa. In contrast, the forelimbs of three saltatorial taxa (*Potorous tridactylus*, *Aepyprymnus rufescens*, *Jaculus jaculus*) show adaptations for scratch digging. Despite slender elongate hind limbs (e.g., low FRI, TRI), the forelimbs of these three taxa are relatively robust with well-developed crests and tubercles (e.g., high HRI, HHRI, DI). These enlargements increase the attachment area for large muscles and the resistance against high stresses incurred during scratch digging. These changes of the forelimb are independent of those of the hind limbs. Their differences point to a modularity of development and a modularity in locomotor function between the forelimb and hind limb of

these saltatorial mammals. It is noteworthy that locomotor inferences based on only the forelimb or only the hind limb could be misleading.

Taken together, our results show that the morphofunctional differences among locomotor modes are best described as a continuum rather than as discrete features. Moreover, we hypothesize that the pattern of evolutionary transformations from one locomotor mode to another could mirror this continuum rather than consist of random or more distant evolutionary jumps across the morphofunctional space (Carrano 1999). Testing this hypothesis within a phylogenetic comparative framework and with developmental insight is beyond the scope of this paper but is an area for future work.

Ecological Diversification of Mesozoic Mammals

Paleontologists used to view Mesozoic mammals as mostly generalized, small-bodied, nocturnal insectivores (e.g. Lillegraven et al. 1979), seemingly restricted to these limited ecological roles by selection pressures (e.g., predation, competition) imposed by dinosaurs (Van Valen and Sloan 1977; Stucky 1990). This view, however, has begun to fade in the face of recent discoveries of relatively complete mammal fossils (e.g., *Zhangheotherium*, *Yanoconodon*, *Eomaia*) and large-scale quantitative analyses of ecomorphology (Wilson et al. 2012; Wilson 2013; Grossnickle and Polly 2013). In his review of Mesozoic mammal evolution, Luo (2007: Fig. 2) identified five ecomorphs (semiaquatic carnivore/omnivore, terrestrial carnivore/scavenger, fossorial colonial insectivore, scansorial/climbing insectivore, and gliding insectivore/omnivore) present among Mesozoic mammals, in addition to the conventional "terrestrial-generalized insectivore/omnivore/herbivore" category. This more generous view of the ecomorphological diversity of Mesozoic mammals, however, was based on ecomorph assignments from previous studies that variously employed qualitative and quantitative approaches. Subsequently, Wilson et al. (2012) and Grossnickle and Polly (2013) separately documented an expansion in the range of feeding ecomorphs among some mammals (e.g., multituberculates) during the late Mesozoic. In each study, the authors used a robust quantitative approach to a synoptic craniodental data set. However, despite the accumulation of postcranial data in recent years, a similar approach has not been taken to infer the diversity of locomotor modes among Mesozoic mammals. For example, several studies using the phalangeal index (PI) have tested for arboreality vs. scansoriality vs. terrestriality in individual Mesozoic mammals (e.g., Ji et al. 2002; Chen and Luo 2013; Zhou et al. 2013; Zheng et al. 2013), but have quantitatively analyzed few other informative aspects of postcranial morphology. Thus, our study provides the first comprehensive quantitative test of locomotor diversity in Mesozoic mammals, focusing on a phylogenetically broad sample of ten taxa with relatively well-preserved postcranial skeletons. Because locomotor mode has previously been inferred for several of these taxa, our analysis also provides a separate test of those ecomorphological analyses.

From our multivariate analysis of the morphometric data in this modest sample of fossil mammals, we infer the presence of at least five locomotor modes (arboreal, scansorial, semiaquatic, semifossorial, and fossorial) among Mesozoic mammals (Table 1). The Early Cretaceous *Eomaia*, one of the earliest eutherian mammals, was previously inferred as arboreal or scansorial on the basis of the phalangeal index (PI) and comparative anatomical study of its postcranial skeleton (Ji et al. 2002). The ambiguity in this assignment reflects the difficulty in distinguishing arboreal and scansorial modes in extant small-bodied mammals by using osteological features (Jenkins 1974; Schilling and Fischer 1999). Indeed, we also found that in our extensive extant data set the morphological transformation from scansorial to arboreal is gradational with respect to our indices (Fig. 3A,B). For example, in adapting for climbing and branch-working, both arboreal and scansorial mammals have relatively slender limb elements without well-developed tubercles and crests. In our CVAs, the morphological differences between arboreal and scansorial taxa were apparent only in the three-locomotor-mode analysis (Supplementary Fig. 3A). In that analysis, scansorial taxa separate from arboreal taxa on the basis of their more elongate

forelimbs, larger palms, and more elongate phalanges. This characterization does not fit what is observed in *Eomaia*, and, in turn, our analysis predicted that *Eomaia* was arboreal not scansorial (Fig. 6, Supplementary Figs. 4, 5). This assignment is also consistent with other indicators of arboreality (e.g., well-developed scapular acromion and coracoid process [Argot 2001]) that were not captured by our indices but were recognized by Ji et al. (2002) in their study of *Eomaia*.

The Early Cretaceous eutriconodontan *Jeholodens* was previously inferred to be a terrestrial mammal capable of climbing on uneven substrates (Ji et al. 1999). It has a number of plesiomorphic features of the pelvic girdle and hind limb that are primarily associated with terrestrial locomotion in premammalian cynodonts (Ji et al. 1999). However, our multivariate analyses indicate that *Jeholodens* was an arboreal taxon that spent more time in the trees than on the ground (Table 1, Fig. 6, Supplementary Figs. 4, 5). This locomotor inference is consistent with the more derived pectoral girdle and forelimb of *Jeholodens* (Ji et al. 1999). The pectoral girdle has a mobile scapuloclavicular joint and a non-rigid claviculo-interclavicle joint, which together form a mobile and pivotal joint. Its scapula bears a well-demarcated triangular fossa on the dorsoposterior margin that forms a large area of attachment for the teres major muscle (Ji et al. 1999). This muscle functions in the retraction of the forelimb, a motion that is especially important in climbing (Salton and Sargis 2008). In addition to these features, our CVA indicates that the tubercles and processes of the humerus, ulna, and femur (e.g., the lesser and greater tubercles, the olecranon process, and greater trochanter, respectively) are relatively reduced in *Jeholodens*, a condition commonly associated with scansorial and arboreal locomotion. Moreover, *Jeholodens* has a relatively large hand, comparable in size to those of extant small-bodied arboreal and scansorial mammals, implying that the hand was prehensile. Together, these lines of evidence support our interpretation that *Jeholodens* was an arboreal mammal.

The basalmost multituberculate *Rugosodon* from the Middle Jurassic of China was previously inferred as a terrestrial mammal, on the basis of the phalangeal index (PI) and slenderness index (=inverse of our phalangeal robustness index; Yuan et al. 2013). However, as noted by those authors in their supplementary information, the PI of *Rugosodon* plots with terrestrial didelphids, diprodonts, sciuromorph rodents, and euarchontans (Weisbecker and Warton 2006; Kirk et al. 2008) as well as scansorial and arboreal hystricognath rodents and carnivorans (Weisbecker and Schmid 2007; Kirk et al. 2008). In our analyses, the PI of *Rugosodon* is 1.05, which is at the lower limit for arboreal taxa and within the range of our scansorial and terrestrial taxa. Our intermediate phalangeal robustness index (~0.26), which corresponds to the inverse of the intermediate phalangeal slender index of Yuan et al. (2013), places *Rugosodon* in the range of arboreal and scansorial taxa. In light of the subtle morphometric gradation from terrestrial to scansorial to arboreal taxa, it is not surprising that individual osteological indices do not sufficiently distinguish among these locomotor modes. However, using our more comprehensive morphometric scheme in our multivariate analysis, we predict with high posterior probability that *Rugosodon* was a scansorial mammal that was adapted for both climbing and ground walking (Table 1, Fig. 6, Supplementary Figs. 4, 5).

The symmetrodontan *Zhangheotherium quinquecuspidens* was previously inferred as a ground-dwelling mammal on the basis of anatomical observations of the forelimb (Hu et al. 1997, 1998). However, our CVAs classify an unpublished specimen of *Zhangheotherium* (species undetermined) as scansorial. The analyses indicate that *Zhangheotherium* had a relatively large hand with elongate metacarpals and phalanges. The hand proportions are similar to those of extant scansorial taxa, whereas the robustness of the phalanges closely resembles that of extant arboreal taxa. The new specimen of *Zhangheotherium* also has a small olecranon process of the ulna, a feature that is common among both scansorial and arboreal mammals. However, our CVAs indicate that *Zhangheotherium* has other features that differ from those of scansorial mammals. Specifically, extant scansorial taxa tend to have

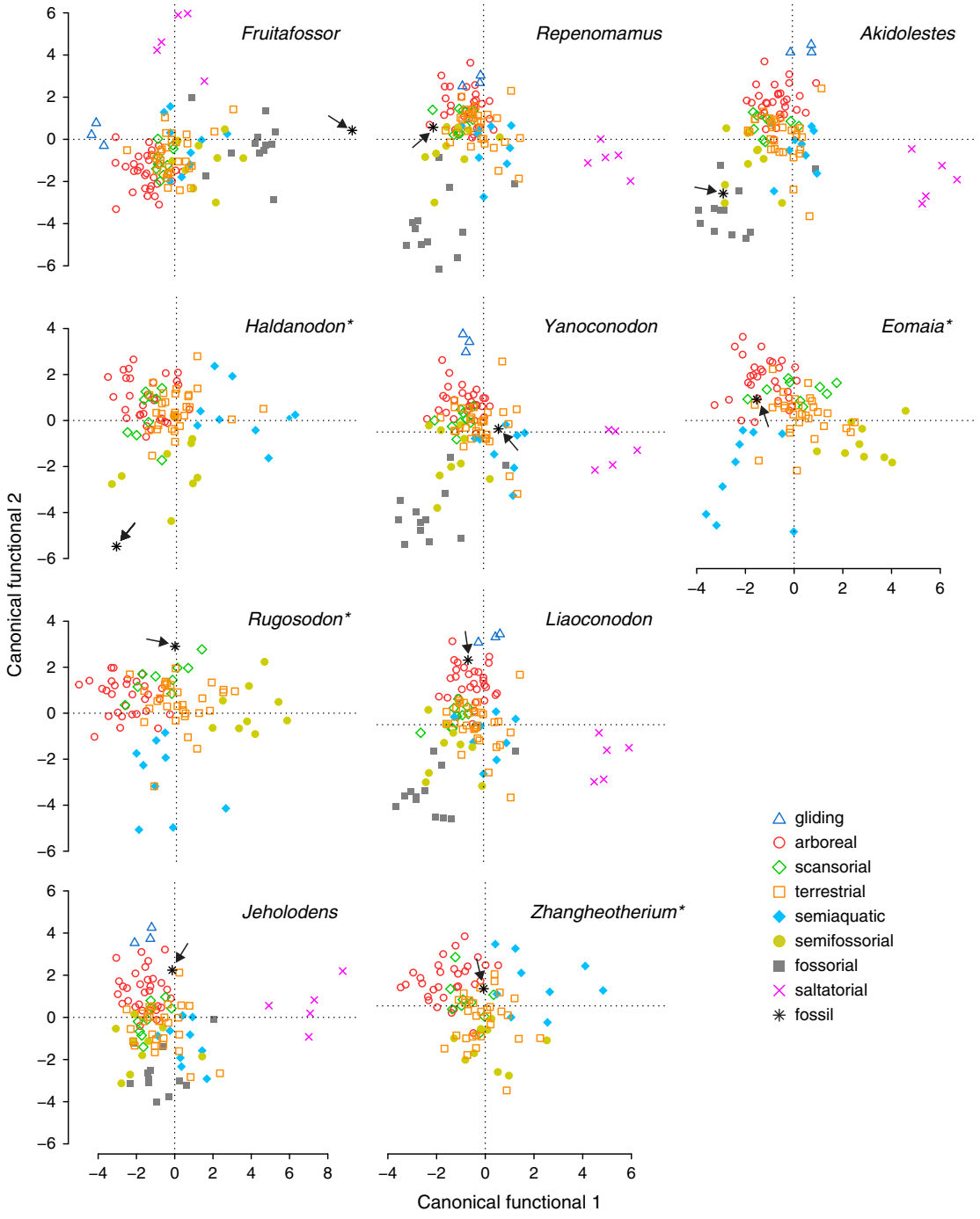

FIGURE 6. Ordinations of ten Mesozoic mammals in the locomotor morphospace. Because each Mesozoic taxon has a unique morphometric data set, each multivariate analysis produced a unique locomotor ordination in the morphospace. Arrows indicate where each fossil taxon plots. An asterisk after the taxon name indicates that the five-locomotor-mode analysis was used for the plot.

elongate forelimbs for ascending and descending trees. In contrast, *Zhangheotherium* has relatively elongate hind limbs, which in extant small-bodied mammals is correlated with hind limb-dominated locomotion, such as hopping or hind-limb-paddle swimming. Moreover, metatarsals II

and III of *Zhangheotherium* are anteroposteriorly elongate and bilaterally expanded, implying that this unpublished specimen of *Zhangheotherium* had a large plantar area of the foot. This region of the foot was missing in the holotype specimen (Hu et al. 1997, 1998). We note, however, that because of poor preservation of the unpublished specimen, we were able to include only 16 osteological indices. Thus, we tentatively follow the locomotor inference of the CVAs to interpret *Zhangheotherium* as a scansorial mammal from the Early Cretaceous (Table 1, Fig. 6, Supplementary Figs. 4, 5).

Full descriptions and functional morphological analyses of the postcranial skeleton of *Yanoconodon* and *Liaoconodon* have not yet been published, but our analyses of the morphometric data indicate that both of these Early Cretaceous eutriconodontans were semiaquatic (Table 1, Fig. 6, Supplementary Figs. 4, 5). Another Mesozoic mammal that was not included in our analysis, the Middle Jurassic docodontan *Castorocauda*, has also been interpreted as semiaquatic (Ji et al. 2006). Despite the shared locomotor assignment, these two eutriconodontans and *Castorocauda* have clear differences in postcranial morphology that indicate different swimming strategies. *Castorocauda* possesses dorsoventrally compressed caudal vertebrae with bifurcated transverse processes that are similar to those of the river otter *Lontra canadensis* and a broad, scaly tail that resembles that of the modern beaver, *Castor canadensis* (Ji et al. 2006); this might imply that, like the modern beaver, *Castorocauda* occasionally used its tail for sculling (Howell 1930). In contrast, *Yanoconodon* and *Liaoconodon* lack those specialized swimming adaptations of the caudal vertebrae, but possess other features of semiaquatic mammals. Their relatively robust limb elements are well suited to resist the stresses incurred during the propulsive swimming stroke. *Yanoconodon* and *Liaoconodon* also have relatively large hands and feet, which presumably facilitated paddling even without webbed fingers. Moreover, the phalanges of the manus of *Yanoconodon* diverge distally, forming a funnel shape, which may be correlated with swimming locomotion. Although we did not analyze indices of the axial skeleton, the elongate trunk of these two eutriconodontans may also be an adaption for swimming, as in the semiaquatic American mink, *Neovison vison*.

Three Mesozoic taxa are inferred as semifossorial: the Late Jurassic docodontan *Haldanodon exspectatus*, the Early Cretaceous eutriconodontan *Repenomamus robustus*, and the Early Cretaceous symmetrodontan *Akidolestes cifellii* (Table 1, Fig. 6; Supplementary Figs. 4, 5). *Akidolestes* was initially inferred as a scansorial mammal by Chen and Luo (2013), on the basis of qualitative comparisons to living arboreal and terrestrial marsupials. In contrast, the interpretation forwarded here, which we argue is more robust because it is based on quantitative multivariate analysis of an extensive data set of extant small-bodied mammals specimens, indicates that *Akidolestes* was a semifossorial mammal. In general, the postcranial skeletons of all three taxa have well-developed tubercles and crests of the forelimbs and hind limbs for attachment of relatively large muscles as in extant digging mammals. The diaphyses of their limb elements are more slender than those of fossorial taxa, as reflected by their robustness index values, which are closer to those of extant semifossorial taxa than those of fossorial taxa. Nevertheless, the postcranial morphologies of these three semifossorial fossil mammals differ from one another. As a stem mammal, the docodontan *Haldanodon* retains some plesiomorphic postcranial features that are shared with, for example, premammalian cynodonts, morganucodontans, and monotremes (Kühne 1956; Klima 1973; Sun and Li 1985; Jenkins and Parrington 1976; Martin 2005; Sues and Jenkins 2006), but are lost in more nested mammalian taxa, like *Repenomamus* and *Akidolestes*. For example, *Haldanodon* has an hourglass-shaped humerus that bears a broad proximal head and a well-developed deltopectoral crest, which is similar to that of the short-beaked echidna, *Tachyglossus aculeatus* (Martin 2005). In contrast, the humerus of *Akidolestes* is relatively longer and less robust than that of *Haldanodon.* Its distal end bears a trochlear articular facet for the ulna (Chen and Luo 2013), as in living therians but absent in *Haldanodon*. Furthermore, the degree of torsion along the humeral diaphysis differs between *Haldanodon* (60°) and *Akidolestes* (40°),

corresponding, respectively, to a more sprawling posture vs. a more parasagittal one. In general, the postcranial elements of *Repenomamus* (Hu 2006) show an intermediate stage of development between the less robust postcranial elements of *Akidolestes* and the more robust postcranial elements of *Haldanodon*. In other aspects, *Repenomamus* strongly differs from *Haldanodon* and *Akidolestes*. The scapula of *Repenomamus* has curved anterior and dorsal margins, whereas *Haldanodon* and *Akidolestes* have scapulae with straight margins. This degree of morphological variance among semifossorial Mesozoic mammals parallels the large morphological variance in our sample of semifossorial extant taxa, and likewise probably stems from a combination of phylogenetic diversity and functional diversity.

The Late Jurassic *Fruitafossor windscheffeli* has uncertain phylogenetic affinities among stem mammals, but its locomotor mode is unequivocally fossorial, as inferred by our analysis and the analysis of Luo and Wible (2005) (Table 1, Fig. 6; Supplementary Fig. 4). *Fruitafossor* possesses a number of adaptations for digging, including a bilaterally expanded humerus with well-developed tubercles and crests forming a large area for muscle attachment, an enlarged olecranon process of the ulna that increases the size of the input lever, hypertrophied manual elements for efficiently removing soil, and elongate distal phalanges for effectively loosening soil (Hildebrand 1985; Stein 2000; Hopkins and Davis 2009). Luo and Wible (2005) further suggested that the dental and vertebral anatomy of *Fruitafossor* is convergent with that of extant xenarthran diggers that use a scratch digging sub-mode (Hildebrand 1985). *Fruitafossor* is similar in many shoulder girdle and limb features to *Tachyglossus*, which has been known to use scratch digging and hook-and-pull digging (Augee et al. 2006). Additionally, we note that the scapula and forelimb of *Fruitafossor* are comparable to moles that are humeral-rotation diggers (*sensu* Hildebrand 1985; Hildebrand and Goslow 1998), such as the extant mole *Scapanus*.

Taken together, our locomotor inferences of these ten Mesozoic taxa and those from previous studies of 19 other taxa begin to paint a more complete picture of the temporal and phylogenetic pattern of locomotor diversification among Mesozoic mammals (Fig. 7). The Late Triassic record of mammalian postcranial skeletons is limited to a single taxon, the stem mammal *Morganucodon*, which has been interpreted as a generalized terrestrial mammal (Jenkins and Parrington 1976). By the late Middle Jurassic, we see substantial locomotor diversification: the gliding ?eutricondontan *Volaticotherium* (Meng et al. 2006), the arboreal haramiyidan *Arboroharamiya* (Zheng et al. 2013), the terrestrial haramiyidan *Megaconus* (Zhou et al. 2013), and the semiaquatic docodontan *Castorocauda* (Ji et al. 2006). The Late Jurassic may represent a peak in locomotor diversification, in which the docodontan *Haldanodon,* the stem mammal *Fruitafossor*, the multituberculate *Rugosodon*, and the basal cladotherian *Henkelotherium* (Krebs 1991; Vázquez-Molinero et al. 2001; Jäger et al. 2013) further expand the range of locomotor modes to include semifossorial, fossorial, scansorial, and arboreal, respectively.

Then, in the Early Cretaceous, there are examples of repeated, independent evolution of these six locomotor modes in different lineages (Fig. 7). The eutriconodontans *Yanoconodon* and *Liaoconodon*, like the Middle Jurassic *Castorocauda*, were semiaquatic forms, although they may have differed from *Castorocauda* in swimming strategy. Moreover, the eutriconodontan *Jeholodens* (arboreal), the multituberculate *Sinobaatar* (arboreal [Hu and Wang 2002]), the symmetrodontan *Zhangheotherium* (scansorial), the eutherian *Eomaia* (arboreal), and the metatherian *Sinodelphys* (scansorial/arboreal) show climbing adaptations like Late Jurassic *Arboroharamiya* and *Henkelotherium*; the eutriconodontan *Gobiconodon ostromi* shows ground-dwelling adaptations (terrestrial); and the symmetrodontan *Akidolestes* and the eutriconodontan *Repenomamus* show burrowing adaptations (semifossorial), although they may have had sub-modes distinct from each other and from the Late Jurassic *Haldanodon*. In the Late Cretaceous, the range of locomotor modes further expanded to include the saltatorial mode. The multituberculates *Catopsbaatar*, *Kryptobaatar*, and *Nemegtbaatar* (Kielan-Jaworowska and Gambaryan 1994; Hurum and Kielan-Jaworowska 2008) and the

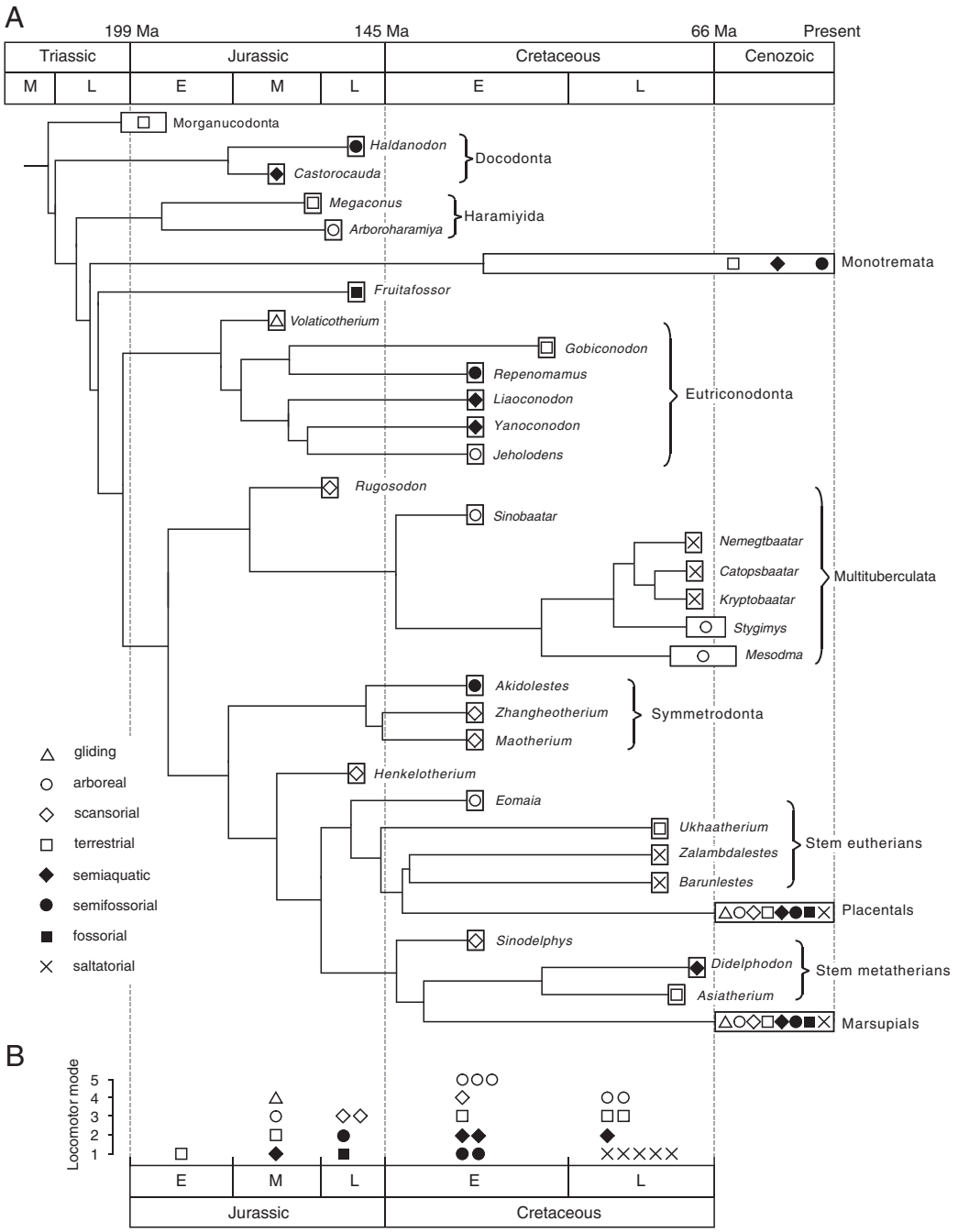

FIGURE 7. Locomotor diversification of mammals from the Early Jurassic to the present. A, Distribution of locomotor modes across the phylogeny of Mesozoic mammals (phylogeny is based on Kielan-Jaworowska and Hurum 2001, Luo 2007, Yuan et al. 2013, Zheng et al. 2013, and Zhou et al. 2013). We followed the placement of Haramiyida in Zhou et al. 2013 (but see Zheng et al. 2013 for a different placement). Stratigraphic ranges of taxa (rectangles bounding symbols) are based on Kielan-Jaworowska et al. (2004) and the primary literature. We mapped the inferred locomotor mode of 29 Mesozoic taxa that have relatively well-preserved postcranial skeletons, of which ten were analyzed in this study (see Table 1). The locomotor inferences of the other 19 taxa are based on previous functional morphological studies (see text). B, Distribution of locomotor modes through time, from the Early Jurassic to the Late Cretaceous. Symbols indicate which locomotor modes were present in each time interval and the number of taxa from that locomotor mode.

eutherians *Zalambdalestes* and *Barunlestes*, all from Asia, have been interpreted as saltatorial and/or terrestrial runners (Kielan-Jaworowska 1978; Chester et al. 2010, 2012). In contrast, the Late Cretaceous and Paleogene multituberculates *Mesodma* and *Stygimys* from North America may have employed an arboreal mode (Krause and Jenkins 1983), whereas the eutherian *Ukhaatherium* (Horovitz 2003; Kielan-Jaworowska et al. 2004) and the metatherian *Asiatherium* (Kielan-Jaworowska et al. 2004), both from Asia, have been interpreted as terrestrial, and the Late Cretaceous metatherian *Didelphodon* has been interpreted as possibly semiaquatic on the basis of isolated elements that can only be tentatively associated (Szalay 1994; Longrich 2004; but see Fox and Naylor 2006 and Borths and Hunter 2008).

This pattern of locomotor diversification among Mesozoic mammals also differed across clades (Fig. 7). The Multituberculata, arguably the most successful clade of Mesozoic mammals (Wilson et al. 2012), has a relatively small sample of postcranial fossils that have led to sometimes-divergent interpretations of locomotor modes among Mesozoic multituberculates (e.g., Gambaryan and Kielan-Jaworowska 1997; Sereno 2006). Accordingly, multituberculates may have diversified into arboreal, scansorial, terrestrial, as well as saltatorial forms during the Mesozoic (Krause and Jenkins 1983; Kielan-Jaworowska and Gambaryan 1994; Hu and Wang 2002; Sereno 2006; Yuan et al. 2013). Another highly successful clade, the Eutriconodonta, had representatives of at least four locomotor modes: arboreal (this study), terrestrial (Jenkins and Schaff 1988), semiaquatic (this study), and semifossorial modes (Hu 2006; this study); and if assignment of *Volaticotherium* to the Eutriconodonta is upheld (Gaetano and Rougier 2011, 2012), it would add a gliding form to this clade. As such, eutriconodontans may have achieved the greatest locomotor diversity of any mammal clade up until the Early Cretaceous. In contrast, only four locomotor modes have been inferred for the Metatheria (arboreal, scansorial, terrestrial, and possibly semiaquatic [Szalay 1994; Luo et al. 2002; Horovitz 2003; Kielan-Jaworowska et al. 2004; Longrich 2004; Chester et al. 2010, 2012]), and only two for the Docodonta (semiaquatic and semifossorial [Ji et al. 2006; this study]), "Symmetrodonta" (semifossorial and terrestrial [Hu et al. 1997, 1998; Luo and Ji 2005; this study]), and Eutheria (arboreal and saltatorial [Kielan-Jaworowska 1978; this study]). In sum, Mesozoic mammals did achieve greater locomotor diversity than is generally appreciated, as hypothesized by Luo (2007), but it seems that this diversification was not fully under way until the Late Jurassic and even then it did not include all clades. We emphasize, however, that our picture of locomotor diversification among Mesozoic mammals should be viewed as a conservative estimate. With the pace of discovery of relatively complete Mesozoic mammal skeletons showing no signs of slowing down, we expect that in the not too distant future many of the temporal and phylogenetic gaps presented here could be filled in.

Conclusions

In this paper, our multivariate analyses of a large postcranial morphometric data set show that extant small-bodied mammals of different locomotor modes have subtle but detectable and functionally relevant morphological differences. Ordination of these locomotor modes via linear canonical variate analysis illustrates what we term a morphofunctional continuum; that is, a gradient of locomotor modes reflecting their biomechanical requirements and adaptations under natural selection. We speculate that the pattern of evolutionary transformations from one locomotor mode to another, at least in small-bodied mammals, may be best explained in the context of this morphofunctional continuum, as well as external selective pressures that these small-bodied mammals faced in the Mesozoic (e.g., vegetational structure, predation, competition [Wing and Tiffney 1987]). We applied our more comprehensive, multivariate approach to locomotor inference to postcranial skeletons of ten Mesozoic mammal taxa. In some cases, our results confirmed previous locomotor inferences, and in other cases differed from them. Viewing these interpretations along with other robust studies serves to further shift the paradigm away from the notion that the Mesozoic represented the "dark ages" for mammalian evolution (Luo 2007). Instead, it

appears that by the Late Jurassic mammals had diversified into seven of the eight locomotor modes that we recognized in this study. The degree of locomotor diversification varied across Mesozoic mammal clades, but seems to have been most pronounced in the Eutriconodonta and the Multituberculata, although sampling of postcranial skeletons is still a major issue.

Acknowledgments

We would like to thank D. Lunde (Smithsonian Institute National Museum of Natural History), E. Westwig (American Museum of Natural History), W. Stanley and R. Banasiak (Field Museum of Natural History), and J. Bradley (University of Washington Burke Museum of Natural History and Culture) for access to and assistance with the mammal collections at their respective institutions. We are indebted to Z.-X. Luo (University of Chicago); Q.-J. Meng, Z.-H. Zeng, L.-D. Liu, and D. Liu (Beijing Museum of Natural History); Q. Ji and Q.-X. Yuan (Chinese Academy of Geological Science); C.-L Gao (Dalian Museum of Natural History); P.-J. Chen and G. Li (Nanjing Institute of Geology and Paleontology); and X.-N. Yang, Y.-K. Shi, and B.-Y. Jiang (Nanjing University) for providing access to some of the Mesozoic fossil specimens included in this study. We are grateful for valuable suggestions and discussions offered by Z.-X. Luo, D. Polly, J. Samuels, and C. Sidor. We also thank members of the Wilson Lab (J. Calede, L. DeBey, D. DeMar Jr., and S. Smith) for useful comments on earlier drafts of this manuscript. We thank three reviewers, S. Chester, T. Martin, and Z.-X. Luo, for their comments and suggestions and helping us improve this manuscript. We gratefully acknowledge funding for this project to M.C by the Washington Research Foundation-Hall Fellowship and to G.W. and M.C. from the University of Washington Department of Biology.

Literature Cited

Alexander, R. M. 1985. Body support, scaling, and allometry. Pp. 26–37 *In* Hildebrand et al. 1985.

Alexander, R. M, A. S. Jayes, G. M. Maloiy, and E. M. Wathuta. 1981. Allometry of the leg muscles of mammals. Journal of Zoology 194:539–552.

Allin, E.F., and J. A. Hopson. 1992. Evolution of the auditory system in Synapsida ("mammal-like reptiles" and primitive mammals) as seen in the fossil record. Pp. 587–614 *In* D. B. Webster, R. R. Fay, and A. N. Popper, eds. The evolutionary biology of hearing. Springer, New York.

Argot, C. 2001. Functional-adaptive anatomy of the forelimb in the Didelphidae, and the paleobiology of the Paleocene marsupials *Mayulestes ferox* and *Pucadelphys andinus*. Journal of Morphology 247:51–79.

——. 2002. Functional-adaptive analysis of the hindlimb anatomy of extant marsupials and the paleobiology of the Paleocene marsupials *Mayulestes ferox* and *Pucadelphys andinus*. Journal of Morphology 253:76–108.

Augee, M., B. Gooden, and A. Musser. 2006. Echidna: extraordinary egg-laying mammal. CSIRO Publishing, Collingwood, Australia.

Bassarova, M., C. M. Janis, and M. Archer. 2009. The calcaneum—on the heels of marsupial locomotion. Journal of Mammalian Evolution 16:1–23.

Beard, K. C. 1993. Origin and evolution of gliding in Early Cenozoic Dermoptera (Mammalia, Primatomorpha). Pp. 63–90 *In* R. D. E. MacPhee, ed. Primates and their relatives in phylogenetic perspective. Plenum, New York.

Biewener, A. A. 1989. Mammalian terrestrial locomotion and size. Bioscience 39:776–783.

——. 1990. Biomechanics of mammalian terrestrial locomotion. Science 250:1097.

——. 2003. Animal locomotion. Oxford University Press, Oxford.

Bloch, J. I., and D. M. Boyer. 2002. Grasping primate origins. Science 298:1606–1610.

Boyer, D. M., G. S. Yapuncich, S. G. B. Chester, J. I. Bloch, and M. Godinot. 2013. Hands of early primates. Yearbook of Physical Anthropology 57:33–78.

Borths, M., and J. P. Hunter. 2008. Gimme shelter? Locomotor trends and mammalian survivorship at the K/Pg boundary. Journal of Vertebrate Paleontology 28:54–55A.

Bourlière, F. 1975. Mammals, small and large: the ecological implications of size. Pp. 1–8 *in* F. B. Golley, K. Petrusewicz, and L. Ryszkowski, eds. Small mammals: their productivity and population dynamics. Cambridge University Press, Cambridge.

Bover, P., J. A. Alcover, J. J. Michaux, L. Hautier, and R. Hutterer. 2010. Body shape and life style of the extinct Balearic dormouse *Hypnomys* (Rodentia, Gliridae): new evidence from the study of associated skeletons. PLoS ONE 5(12):e15817. doi:10.1371/journal.pone.0015817.

Carrano, M. T. 1999. What, if anything, is cursor? Categories versus continua for determining locomotor habit in mammals and dinosaurs. Journal of Zoology 247:29–42.

Cartmill, M. 1985. Climbing. Pp. 73–88 *In* Hildebrand et al. 1985.

Chen, M., and Z.-X. Luo. 2013. Postcranial skeleton of the Cretaceous mammal *Akidolestes cifellii* and its locomotor adaptations. Journal of Mammalian Evolution 20:159–189.

Chester, S. G. B., E. J. Sargis, F. S. Szalay, J. D. Archibald, and A. O. Averianov. 2010. Mammalian distal humeri from the Late Cretaceous of Uzbekistan. Acta Palaeontologica Polonica 55:199–211.

Chester, S. G. B., E. J. Sargis, F. S. Szalay, J. D. Archibald, and A. O. Averianov. 2012. Therian femora from the Late Cretaceous of Uzbekistan. Acta Palaeontologica Polonica 57:53–64.

Croft, D. A., and L. C. Anderson. 2008. Locomotion in the extinct notoungulate *Protypotherium*. Palaeontologia Electronica 11: 1–20.

Degen, A. A. 1997. Ecophysiology of small desert mammals. Springer, Berlin.

Dunstone, N. 1979. Swimming and diving behavior of the mink (*Mustela vison* Schreber). Carnivore 2:56–61.

Elissamburu, A., and S. F. Vizcaíno. 2004. Limb proportions and adaptations in caviomorph rodents (Rodentia: Caviomorpha). Journal of Zoology 262:145–159.

Emerson, S. B. 1985. Jumping and leaping. Pp. 58–72 *in* Hildebrand et al. 1985.

Evans, A. R. 2013. Shape descriptors as ecometrics in dental ecology. Hystrix, Italian Journal of Mammalogy 24:133–140.

Fish, F. E. 1993. Influence of hydrodynamic design and propulsive mode on mammalian swimming energetics. Australian Journal of Zoology 42:79–101.

Fox, R. C., and B. G. Naylor. 2006. Stagodontid marsupials from the Late Cretaceous of Canada and their systematic and functional implications. Acta Palaeontologica Polonica 51: 13–36.

Fröbisch, J., and R. R. Reisz. 2009. The Late Permian herbivore *Suminia* and the early evolution of arboreality in terrestrial vertebrate ecosystems. Proceedings of Royal Society of London B 276:3611–3618.

Gaetano, L. C., and G. W. Rougier. 2011. New materials of *Argentoconodon fariasorum* (Mammaliaformes, Triconodontidae) from the Jurassic of Argentina and its bearing on triconodont phylogeny. Journal of Vertebrate Paleontology 31:829–843.

——. 2012. First amphilestid from South America: a molariform from the Jurassic Cañadón Asfalto Formation, Patagonia, Argentina. Journal of Mammalian Evolution 19:235–248.

Gambaryan, P. P. 1974. How mammals run: anatomical adaptations. Wiley, New York.

Gambaryan, P. P., and Z. Kielan-Jaworowska. 1997. Sprawling versus parasagittal stance in multituberculate mammals. Acta Palaeontologica Polonica 42:13–44.

Gingerich, P. D. 2003. Land-to-sea transition in early whales: evolution of Eocene Archaeoceti (Cetacea) in relation to skeletal proportions and locomotion of living semiaquatic mammals. Paleobiology 29:429–454.

Grillner, S., and P. Wallén. 1985. The ionic mechanisms underlying N-methyl-D-aspartate receptor-induced, tetrodotoxin-resistant membrane potential oscillations in lamprey neurons active during locomotion. Neuroscience Letter 60:289–294.

Grossnickle, D. M., and P. D. Polly. 2013. Mammal disparity decreases during the Cretaceous angiosperm radiation. Proceedings of the Royal Society of London B 280:20132110. doi: 10.1098/rspb.2013.2110.

Hildebrand, M. 1985. Digging in quadrupeds. Pp. 89–109 *in* Hildebrand et al. 1985.

Hildebrand, M., and G. Goslow. 1998. Analysis of vertebrate structure. Wiley, New York.

Hildebrand, M., D. M. Bramble, K. F. Liem, and D. B. Wake, eds. 1985. Functional vertebrate morphology. Harvard University Press, Cambridge.

Hopkins, S. S. B., and E. B. Davis. 2009. Quantitative morphological proxies for fossoriality in small mammals. Journal of Mammalogy 90:1449–1460.

Horovitz, I. 2003. Postcranial skeleton of *Ukhaatherium nessovi* (Eutheria, Mammalia) from the Late Cretaceous of Mongolia. Journal of Vertebrate Paleontology 23:857–868.

Howell, A. B. 1930. Aquatic mammals. Charles C. Thomas, Springfield, Ill.

Hu, Y.-M. 2006. Postcranial morphology of *Repenomamus* (Eutriconodonta, Mammalia): implications for the higher-level phylogeny of mammals. Ph.D. dissertation. City University of New York, New York.

Hu, Y.-M., and Y.-Q. Wang. 2002. *Sinobaatar* gen. nov.: first multituberculate from the Jehol Biota of Liaoning, northeast China. Chinese Science Bulletin 47:933–938.

Hu, Y.-M., Y.-Q. Wang, Z.-X. Luo, and C.-K. Li. 1997. A new symmetrodont mammal from China and its implications for mammalian evolution. Nature 390:137–142.

Hu, Y.-M., Y.-Q. Wang, C.-K. Li, and Z.-X. Luo. 1998. Morphology of dentition and forelimb of *Zhangheotherium*. Vertebrata PalAsiatica 36:102–125.

Hu, Y.-M., J. Meng, Y.-Q. Wang, and C.-K. Li. 2005. Large Mesozoic mammals fed on young dinosaurs. Nature 433:149–152.

Hurum, J. H., and Z. Kielan-Jaworowska. 2008. Postcranial skeleton of a Cretaceous multituberculate mammal *Catopsbaatar*. Acta Palaeontologica Polonica 53:545–566.

Iwaniuk, A. N., S. M. Pellis, and I. Q. Whishaw. 1999. The relationship between forelimb morphology and behaviour in North American carnivores (Carnivora). Canadian Journal of Zoology 77:1064–1074.

Janis, C. M., J. M. Theodor, and B. Boisvert. 2002. Locomotor evolution in camels revisited: a quantitative analysis of pedal anatomy and the acquisition of the pacing gait. Journal of Vertebrate Paleontology 22:110–121.

Jäger, K., Z.-X. Luo, and T. Martin. 2013. CT scanning and 3D image analysis of the postcranial skeleton of *Henkelotherium guimarotae* (Cladotheria, Mammalia) from the Late Jurassic of Portugal and its locomotor adaptations. Society of Vertebrate Paleontology 73rd, Program and Abstracts, p. 147. Journal of Vertebrate Paleontology (online supplement), October 2013.

Jenkins, F. A. 1970. Limb movements in a monotreme (*Tachyglossus aculeatus*): a cineradiographic analysis. Science 168:1473–1475.

——. 1974. Tree shrew locomotion and arborealism. Pp. 85–115 *in* F. A. Jenkins, ed. Primate locomotion. Academy Press, New York.

Jenkins, F. A., and F. Parrington. 1976. Postcranial skeletons of Triassic mammals *Eozostrodon*, *Megazostrodon* and *Erythrotherium*. Philosophical Transactions of the Royal Society of London B 273:387–431.

Jenkins, F. A., and C. R. Schaff. 1988. The Early Cretaceous mammal *Gobiconodon* (Mammalia, Triconodonta) from the Cloverly Formation in Montana. Journal of Vertebrate Paleontology 8:1–24.

Jerison, H. J. 1973. Evolution of the brain and intelligence. Academic Press, New York.

Ji, Q., Z.-X. Luo, and S.-A. Ji. 1999. A Chinese triconodont mammal and mosaic evolution of the mammalian skeleton. Nature 398:326–330.

Ji, Q., Z.-X. Luo, C.-X. Yuan, J. R. Wible, J.-P. Zhang, and J. A. Georgi. 2002. The earliest known eutherian mammal. Nature 416:816–822.

Ji, Q., Z.-X. Luo, C.-X. Yuan, and A. R. Tabrum. 2006. A swimming mammaliaform from the Middle Jurassic and ecomorphological diversification of early mammals. Science 311:1123–1127.

Jouffroy, F. K., and J. Lessertisseur. 1979. Relationships between limb morphology and locomotor adaptations among prosimians: an osteometric study. Pp. 143–181 *In* M. E. Morbeck, H. Preuschoft, and N. Gomberg, eds. Environment, behavior, and morphology: dynamic interactions in primates. Gustav Fischer, New York.

Jouffroy, F. K., M. Godinot, and Y. Nakano. 1993. Biometrical characteristics of primate hands. Pp. 133–171 *In* H. Preuschoft and D. J. Chivers, eds. Hands of primates. Springer, New York.

Kardong, K. V. 2009. Vertebrates: comparative anatomy, function, evolution. McGraw-Hill, New York.

Kelt, D. A., and M. D. Meyer. 2009. Body size frequency distributions in African mammals are bimodal at all spatial scales. Global Ecology and Biogeography 18:19–29.

Kielan-Jaworowska, Z. 1978. Evolution of the therian mammals in the Late Cretaceous of Asia. Part III. Postcranial skeleton in Zalambdalestidae. Acta Palaeontologia Polonica 38:5–41.

Kielan-Jaworowska, Z., and P. P. Gambaryan. 1994. Postcranial anatomy and habits of Asian multituberculate mammals. Fossil and Strata 36:1–92.

Kielan-Jaworowska, Z., R. L. Cifelli, and Z.-X. Luo. 2004. Mammals from the age of dinosaurs: origins, evolution, and structure. Columbia University Press, New York.

Kingdon, J. 1997. The Kingdon field guide to African mammals. Academic Press, San Diego.

Kirk, E. C., P. Lemelin, M. W. Hamrick, D. M. Boyer, and J. I. Bloch. 2008. Intrinsic hand proportions of euarchontans and other mammals: implications for the locomotor behavior of plesiadapiforms. Journal of Human Evolution 55:278–299.

Klima, M. 1973. Die Frühentwicklung des Schultergürtels und des Brustbeins bei den Monotremen (Mammalia: Prototheria). Advances in Anatomy, Embryology and Cell Biology 47:1–80.

Krause, D. W., and F. A. Jenkins. 1983. The postcranial skeleton of North American multituberculates. Bulletin of the Museum of Comparative Zoology 150:199–246.

Krebs, B. 1991. Das Skelett von *Henkelotherium guimarotae* gen. et sp. nov. (Eupantotheria, Mammalia) aus dem Oberen Jura yon Portugal. Berliner Geowissenschaftliche Abhandlungen A 133: 1–121.

Kühne, W. G. 1956. The Liassic therapsid *Oligokyphus*. British Museum (Natural History), London.

Lanyon, L. E., and C. T. Rubin. 1985. Functional adaptation in skeletal structures. Pp. 1–25 *In* Hildebrand et al. 1985.

Lemelin, P. 1999. Morphological correlates of substrate use in didelphid marsupials: implications for primate origins. Journal of Zoology 247:165–175.

Li, G., and Z.-X. Luo. 2006. A Cretaceous symmetrodont therian with some monotreme-like postcranial features. Nature 439: 195–200.

Lillegraven, J. A., Z. Kielan-Jaworowska, and W. A. Clemens. 1979. Mesozoic mammals: the first two-thirds of mammalian history. University of California Press, Berkeley.

Longrich, N. 2004. Aquatic specialization in mammals from the Late Cretaceous of North America. Journal of Vertebrate Paleontology 24(Suppl. to No. 3): 84A.

Luo, Z.-X. 2007. Transformation and diversification in early mammal evolution. Nature 450:1011–1019.

Luo, Z.-X., and Q. Ji. 2005. New study on dental and skeletal features of the Cretaceous "symmetrodontan" mammal *Zhangheotherium*. Journal of Mammalian Evolution 12:337–357.

Luo, Z.-X., and J. R. Wible. 2005. A Late Jurassic digging mammal and early mammalian diversification. Science 308: 103–107.

Luo, Z.-X., R. L. Cifelli, and Z. Kielan-Jaworowska. 2001a. Dual origin of tribosphenic mammals. Nature 409:53–57.

Luo, Z.-X., A. W. Crompton, and A.-L. Sun. 2001b. A new mammaliaform from the early Jurassic and evolution of mammalian characteristics. Science 292:1535–1540.

Luo, Z.-X., Q. Ji, J. R. Wible, and C.-X. Yuan. 2003. An Early Cretaceous tribosphenic mammal and metatherian evolution. Science 302:1934–1940.

Luo, Z.-X., P.-J. Chen, G. Li, and M. Chen. 2007. A new eutriconodont mammal and evolutionary development in early mammals. Nature 446:288–293.

MacLeod, N., and K. D. Rose. 1993. Inferring locomotor behavior in Paleogene mammals via eigenshape analysis. American Journal of Science 293A:300–355.

Martin, T. 2005. Postcranial anatomy of *Haldanodon exspectatus* (Mammalia, Docodonta) from the Late Jurassic (Kimmeridgian) of Portugal and its bearing for mammalian evolution. Zoological Journal of the Linnean Society 145:219–248.

——. 2013. Mammalian postcranial bones from the Late Jurassic of Portugal and their implications for forelimb evolution. Journal of Vertebrate Paleontology 33:1432–1441.

Marshall, L. G. 1978. *Chironectes minimus*. Mammalian Species 109:1–6.

McMahon, T. A. 1975. Using body size to understand the structural design of animals: quadrupedal locomotion. Journal of Applied Physiology 39:619–627.

McNab, B. K. 1990. Physiological significance of body size. Pp. 11–24 *In* J. D. Damuth and B. J. MacFadden, eds. Body size in mammalian paleobiology: estimation and biological implications. Cambridge University Press, Cambridge.

——. 2002. The physiological ecology of vertebrates: a view from energetics. Cornell University Press, New York.

Meng, J., Y.-M. Hu, Y.-Q. Wang, X.-L. Wang, and C.-K. Li. 2006. A Mesozoic gliding mammal from northeastern China. Nature 444:889–893.

Merritt, J. F. 2010. The biology of small mammals. Johns Hopkins University Press, Baltimore.

Nakagawa, M., H. Miguchi, K. Sato, S. Shoko, and T. Nakashizuka. 2007. Population dynamics of arboreal and terrestrial small mammals in a tropical rainforest, Sarawak, Malaysia. Raffles Bulletin of Zoology 55:389–395.

Nowak, R. M. 1999. Walker's mammals of the world. Johns Hopkins University Press, Baltimore.

——. 2005. Walker's marsupials of the world. Johns Hopkins University Press, Baltimore.

O'Keefe, F. R, and M. T. Carrano. 2005. Correlated trends in the evolution of the plesiosaur locomotor system. Paleobiology 31:656–675.

Polly, P. D. 2007. Limbs in mammalian evolution. Pp. 245–268 *In* B. K. Hall, ed. Fins into limbs: evolution, development and transformation. University of Chicago Press, Chicago.

——. 2008. Adaptive zones and the pinniped ankle: a three-dimensional quantitative analysis of carnivoran tarsal evolution. Pp. 167–196 *In* E. J. Sargis and M. Dagosto, eds. Mammalian evolutionary morphology. Springer, Dordrecht.

——. 2011. Tiptoeing through the trophics: geographic variation in carnivoran locomotor ecomorphology in relation to environment. Pp. 374–410 *In* A. Goswami and A. R. Friscia, eds. Carnivoran evolution: new views on phylogeny, form and function. Cambridge University Press, Cambridge.

Rowe, T. B. 1996. Coevolution of the mammalian middle ear and neocortex. Science 273:651–654.

Rowe, T. B., T. E. Macrini, and Z. X. Luo. 2011. Fossil evidence on origin of the mammalian brain. Science 332:955–957.

Salton, J. A. and E. J. Sargis. 2008. Evolutionary morphology of the Tenrecoidea (Mammalia) forelimb skeleton. Pp. 51–77 *In* E. J. Sargis and M. Dagosto, eds. Mammalian evolutionary morphology. Springer, Dordrecht.

Samuels, J. X., and B. Van Valkenburgh. 2008. Skeletal indicators of locomotor adaptations in living and extinct rodents. Journal of Morphology 269:1387–1411.

Samuels, J. X., J. A. Meachen, and S. A. Sakai. 2013. Postcranial morphology and the locomotor habits of living and extinct carnivorans. Journal of Morphology 274:121–146.

Sargis, E. J. 2001a. The grasping behaviour, locomotion and substrate use of the tree shrews *Tupaia minor* and *T. tana* (Mammalia, Scandentia). Journal of Zoology 253:485–490.

——. 2001b. A preliminary qualitative analysis on the axial skeleton of tupaiids (Mammalia, Scandentia): functional morphology and phylogenetic implications. Journal of Zoology, London 253:473–483.

——. 2002a. Functional morphology of the forelimb of tupaiids (Mammalia. Scandentia) and its phylogenetic implications. Journal of Morphology 253:10–42.

——. 2002b. Functional morphology of the hindlimb of tupaiids (Mammalia. Scandentia) and its phylogenetic implications. Journal of Morphology 254:149–185.

Schilling, N., and M. S. Fischer. 1999. Kinematic analysis of treadmill locomotion of tree shrews, *Tupaia glis* (Scandentia: Tupaiidae). Zeitschrift für Säugetierkunde (International Journal of Mammalian Biology) 64:1–25.

Sereno, P. 2006. Shoulder girdle and forelimb in multituberculates: evolution of parasagittal forelimb posture in mammals. Pp. 315–366 *In* M. T. Carrano, T. J. Gaudin, R. W. Blob, and J. R. Wible, eds. Amniote paleobiology: perspectives on the evolution of mammals, birds, and reptiles. University of Chicago Press, Chicago.

Shattuck, M. R., and S. A. Williams. 2010. Arboreality has allowed for the evolution of increased longevity in mammals. Proceedings of the National Academy of Sciences USA 107:4635–4639.

Shimer, H. W. 1903. Adaptations to aquatic, arboreal, fossorial, and cursorial habits in mammals. III. Fossorial adaptations. American Naturalist 37:819–825.

Sokal, R. R., and F. J. Rohlf. 2012. Biometry: the principles and practice of statistics in biological research, 4th ed. W. H. Freeman, New York.

Stein, B. R. 1988. Morphology and allometry in several genera of semiaquatic rodents (*Ondatra, Nectomys*, and *Oryzomys*). Journal of Mammalogy 69:500–511.

——. 2000. Morphology of subterranean rodents. Pp. 19–61 *In* E. A. Lacey, J. L. Patton, and G. N. Cameron, eds. Life underground: the biology of subterranean rodents. University of Chicago Press, Chicago.

Stoddart, D. M. 1979. Ecology of small mammals. Chapman and Hall, London.

Stucky, R. K. 1990. Evolution of land mammal diversity in North America during the Cenozoic. Current Mammalogy 2:375–432.

Sues, H.-D., and F. A. Jenkins. 2006. The postcranial skeleton of *Kayentatherium wellesi* from the Lower Jurassic Kayenta Formation of Arizona and the phylogenetic significance of postcranial features. Pp. 114–152 *In* M. T. Carrano, T. J. Gaudin, R. W. Blob, and J. R. Wible, eds. Amniote paleobiology: perspectives on the evolution of mammals, birds, and reptiles. University of Chicago Press, Chicago.

Sun, A., and Y. Li. 1985. The postcranial skeleton of the late tritylodont Bienotheroides. Vertebrata PalAsiatica 23:135–151.

Szalay, F. S. 1984. Arboreality: is it homologous in metatherian and eutherian mammals? Evolutionary Biology 18:215–258.

——. 1994. Evolutionary history of the marsupials and an analysis of osteological characters. Cambridge University Press, New York.

Szalay, F. S., and E. J. Sargis. 2001. Model-based analysis of postcranial osteology of marsupials from the Palaeocene of Itaboraí (Brazil) and the phylogenetics and biogeography of Metatheria. Geodiversitas 23:139–302.

Tucker, V. A. 1970. Energetic cost of locomotion in animals. Comparative Biochemistry and Physiology 34:841–846.

——. 1975. The energetic cost of moving about. American Scientist 63:413–419.

Ungar, P. S., and M. Williamson. 2000. Exploring the effects of tooth wear on functional morphology: a preliminary study using dental topographic analysis. Palaeontologia Electronica 3:1–18.

Van Valen, L., and R. E. Sloan. 1977. Ecology and the extinction of the dinosaurs. Evolutionary Theory 2:37–64.

Van Valkenburgh, B. 1987. Skeletal indicators of locomotor behavior in living and extinct carnivores. Journal of Vertebrate Paleontology 7:162–182.

Van Valkenburgh, B., and K. P. Koepfli. 1993. Cranial and dental adaptations to predation in canids. Symposium of the Zoological Society of London 65:15–37.

Vázquez-Molinero, R., T. Martin, M. S. Fischer, and R. Frey. 2001. Comparative anatomical investigations of the postcranial skeleton of *Henkelotherium guimarotae* Krebs, 1991 (Eupantotheria, Mammalia) and their implications for its locomotion. Zoosystematics and Evolution 77:207–216.

Venables, W. N., and B. D. Ripley. 2002. Modern applied statistics with S. Springer, New York.

Weisbecker, V., and S. Schmid. 2007. Autopodial skeletal diversity in hystricognath rodents: functional and phylogenetic aspects. Mammalian Biology – Zeitschrift für Säugetierkunde 72:27–44.

Weisbecker, V., and D. I. Warton. 2006. Evidence at hand: diversity, functional implications, and locomotor prediction in intrinsic hand proportions of diprotodontian marsupials. Journal of Morphology 267:1469–1485.

Wilson, G. P. 2013. Mammals across the K/Pg boundary in northeastern Montana, U.S.A.: dental morphology and body-size patterns reveal extinction selectivity and immigrant-fueled ecospace filling. Paleobiology 39:429–469.

Wilson, D. E., and D. M. Reeder. 2005. Mammal species of the world: a taxonomic and geographic reference. Johns Hopkins University Press, Baltimore.

Wilson, G. P., A. R. Evans, I. J. Corfe, P. D. Smits, M. Fortelius, and J. Jernvall. 2012. Adaptive radiation of multituberculate mammals before the extinction of dinosaurs. Nature 483: 457–460.

Wing, S. L., and B. H. Tiffney. 1987. Interactions of angiosperms and herbivorous tetrapods through time. Pp. 203–224 *In* E. M. Friis, W. G. Chaloner, and P. R. Crane, eds. The origins of angiosperms and their biological consequences. Cambridge University Press, New York.

Yuan, C.-X., Q. Ji, Q.-J. Meng, A. R. Tabrum, and Z.-X. Luo. 2013. A new Jurassic mammal and origins of diverse feeding and locomotor adaptation multituberculate mammals. Science 341:779–783.

Zheng, X.-T., S.-D. Bi, X.-L. Wang, and J. Meng. 2013. A new arboreal haramiyid shows the diversity of crown mammals in the Jurassic period. Nature 500:199–202.

Zhou, C.-F., S.-Y. Wu, T. Martin, and Z.-X. Luo. 2013. A Jurassic mammaliaform and the earliest mammalian evolutionary adaptations. Nature 500:163–167.

Supplementary Materials

For

"Inferring locomotor mode in Mesozoic mammals"

(Submitted to Paleobiology, 17 April, 2014)

Meng Chen and Gregory P. Wilson

Department of Biology

University of Washington

Seattle, Washintong 98195, U.S.A.

E-mail: mengchen@uw.edu; gpwilson@uw.edu.

Supplementary Table 1. List of extant small-bodied mammal taxa with referred locomotor modes in our dataset for morphometric analysis. Abbreviations: A, arboreal; F, fossorial; LM, locomotor mode; S, saltatorial; Sa, semiaquatic; Sc, scansorial; Sf, semifossorial; T, terrestrial.

No.	Taxon	Order	Family	LM	References
	Monotreme				
67	*Ornithorhynchus anatinus*	Monotremata	Ornithorhynchidae	Sa	Howell 1930; Grant and Fanning 1989; Gingerich, 2003
	Marsupial				
78	*Antechinus swainsonii*	Dasyuromorphia	Dasyuridae	T	Nowak 1999
82	*Dasycercus byrnei*	Dasyuromorphia	Dasyuridae	T	Nowak 1999
35	*Dasypus novemcinctus*	Dasyuromorphia	Dasyuridae	F	Samuels and Van Valkenburgh 2008
83	*Dasyurus hallucatus*	Dasyuromorphia	Dasyuridae	T	Nowak 1999
84	*Dasyurus viverrinus*	Dasyuromorphia	Dasyuridae	T	Nowak 1999
103	*Sarcophilus laniarius*	Dasyuromorphia	Dasyuridae	T	Van Valkenburgh 1987
71	*Myrmecobius fasciatus*	Dasyuromorphia	Myrmecobiidae	Sf	Christensen et al. 1984; Copper 2011
5	*Caluromys derbianus*	Didelphimorphia	Didelphidae	A	Argot 2001
6	*Caluromys philander*	Didelphimorphia	Didelphidae	A	Nowak 1999
61	*Chironectes minimus*	Didelphimorphia	Didelphidae	Sa	Howell 1930; Marshall 1978; Gingerich 2003
51	*Didelphis marsupialis*	Didelphimorphia	Didelphidae	Sc	Argot 2001
52	*Didelphis virginiana*	Didelphimorphia	Didelphidae	Sc	Argot 2001
11	*Gracilinanus microtarsus*	Didelphimorphia	Didelphidae	A	Delciellos and Vieira 2006
15	*Marmosa robinsoni*	Didelphimorphia	Didelphidae	A	Nowak 1999
91	*Metachirus nudicaudatus*	Didelphimorphia	Didelphidae	T	Argot 2001; Delciellos and Vieira 2006
16	*Micoureus demerarae*	Didelphimorphia	Didelphidae	A	Nowak 1999
93	*Monodelphis domestica*	Didelphimorphia	Didelphidae	T	Nowak 1999; Kirk et al. 2008
101	*Philander opossum*	Didelphimorphia	Didelphidae	T	Kirk et al. 2008
45	*Petaurus breviceps*	Diprotodontia	Petauridae	G	Smith 1973; Nowak 1999; Körtner and Geiser 2000
29	*Trichosurus vulpecula*	Diprotodontia	Phalangeridae	A	Nowak 1999
46	*Aepyprymnus rufescens*	Diprotodontia	Potoroidae	S	Bassarova et al. 2009

50	*Potorous tridactylus*	Diprotodontia	Potoroidae	S	Bassarova et al. 2009
12	*Hemibelideus lemuroides*	Diprotodontia	Pseudocheiridae	A	Nowak 1999
22	*Pseudocheirus peregrinus*	Diprotodontia	Pseudocheiridae	A	Bassarova et al. 2009
99	*Perameles nasuta*	Peramelemorphia	Peramelidae	T	Nowak 1999
90	*Isoodon macrourus*	Peramelemorphia	Peramelinae	T	Bassarova et al. 2009
	Placental				
31	*Amblysomus hottentotus*	Afrosoricida	Chrysochloridae	F	Nowak 1999
53	*Echinops telfairi*	Afrosoricida	Tenrecidae	Sc	Endo et al. 2006
77	*Hemicentetes semispinosus*	Afrosoricida	Tenrecidae	Sf	Endo et al. 2006
92	*Microgale talazaci*	Afrosoricida	Tenrecidae	T	Endo et al. 2006
80	*Cerdocyon thous*	Carnivora	Canidae	T	Nowak 1999
107	*Vulpes Vulpes*	Carnivora	Canidae	T	Larivie´re and Pasitschniak-Arts 1996; Meachen-Samuels 2010
56	*Oncifelis geoffroyi*	Carnivora	Felidae	Sc	Iwaniuk et al. 2000
102	*Prionailurus planiceps*	Carnivora	Felidae	T	Meachen-Samuels 2010
59	*Urocyon cinereoargenteus*	Carnivora	Felidae	Sc	Van Valkenburgh 1987; Julie Meachen-Samuels 2010
81	*Crossarchus alexanidri*	Carnivora	Herpestidae	T	Van Valkenburgh 1987
88	*Herpestes brachyurus*	Carnivora	Herpestidae	T	Gebo and Rose 1993
89	*Herpestes edwardsi*	Carnivora	Herpestidae	T	Nowak 1999
57	*Suricata suricatta*	Carnivora	Herpestidae	Sc	van Staaden 1994; Iwaniuk et al. 1999
70	*Mephitis mephitis*	Carnivora	Mephitidae	Sf	Wade-Smith and Verts 1982; Van Valkenburgh 1987; Samuels and Van Valkenburgh 2008
60	*Aonyx cinerea*	Carnivora	Mustelidae	Sa	Gingerich 2003
87	*Galictis cuja*	Carnivora	Mustelidae	T	Yensen and Tarifa 2003
54	*Gulo gulo*	Carnivora	Mustelidae	Sc	Van Valkenburgh 1987; Pasitschniak-Arts and Larivie´re 1995
63	*Lontra canadensis*	Carnivora	Mustelidae	Sa	Gingerich 2003
94	*Mustela erminea*	Carnivora	Mustelidae	T	Nowak 1999
95	*Mustela putorius*	Carnivora	Mustelidae	T	Nowak 1999
64	*Neovision vison (Mustela*	Carnivora	Mustelidae	Sa	Howell 1930; Larivie´re 1999; Gingerich 2003

	vison)				
74	*Spilogale putorius*	Carnivora	Mustelidae	Sf	Heinrich and Houde 2006
76	*Taxidea taxus berlandieri*	Carnivora	Mustelidae	Sf	Van Valkenburgh 1987; Samuels and Van Valkenburgh 2008
17	*Nandinia binotata*	Carnivora	Nandiniidae	A	Nowak 1999
9	*Genetta maculata*	Carnivora	Viverridae	A	Iwaniuk et al. 2000
18	*Paguma larvata*	Carnivora	Viverridae	A	Nowak 1999
19	*Paradoxurus hermaphroditus*	Carnivora	Viverridae	A	Nowak 1999
21	*Prionodon linsang*	Carnivora	Viverridae	A	Van Valkenburgh 1987
36	*Euphractus sexcinctus*	Cingulata	Dasypodidae	F	Redford and Wetzel 1985; Nowak 1999
85	*Echinosorex gymnura*	Erinaceomorpha	Erinaceidae	T	Nowak 1999
68	*Sylvilagus aquaticus*	Lagomorpha	Leporidae	Sa	Gingerich 2003
86	*Elephantulus rufescens*	Macroscelidea	Macroscelididae	T	Nowak 1999
100	*Petrodromus tetradactylus*	Macroscelidea	Macroscelididae	T	Nowak 1999
1	*Callimico goeldii*	Primates	Cebidae	A	Nowak 1999
2	*Callithrix argentata*	Primates	Cebidae	A	Nowak 1999
3	*Callithrix geoffroyi*	Primates	Cebidae	A	Nowak 1999
4	*Callithrix pygmaea*	Primates	Cebidae	A	Nowak 1999
25	*Saguinus oedipus*	Primates	Cebidae	A	Nyakatura et al. 2008
26	*Saimiri sciureus*	Primates	Cebidae	A	Nowak 1999
13	*Leontopithecus chrysomela*	Primates	Leontopithecus	A	Nowak 1999
32	*Aplodontia rufa*	Rodentia	Aplodontiidae	F	Samuels and Van Valkenburgh 2008
34	*Cryptomys hottentotus*	Rodentia	Bathyergidae	F	Samuels and Van Valkenburgh 2008
79	*Cavia porcellus*	Rodentia	Caviidae	T	Nowak 1999
38	*Microtus pennsylvanicus*	Rodentia	Cricetidae	F	Nowak 1999
96	*Neotoma bryanti*	Rodentia	Cricetidae	T	Nowak 1999
66	*Ondatra zibethicus*	Rodentia	Cricetidae	Sa	Howell 1930; Gingerich, 2003
75	*Synaptomys cooperi*	Rodentia	Cricetidae	Sf	Linzey 1983; Nowak 1999
47	*Allactaga mongolica*	Rodentia	Dipodidae	S	Samuels and Van Valkenburgh 2008

49	*Jaculus jaculus*	Rodentia	Dipodidae	S	Nowak 1999
37	*Geomys pinetis*	Rodentia	Geomyidae	F	Nowak 1999
39	*Pappogeomys merriami*	Rodentia	Geomyidae	F	Nowak 1999
42	*Thomomys bottae*	Rodentia	Geomyidae	F	Nowak 1999
10	*Glis glis (Myoxus Glis)*	Rodentia	Gliridae	A	Nowak 1999
33	*Chaetodipus fallax*	Rodentia	Heteromyidae	F	Lackey, 1996
48	*Dipodomys deserti*	Rodentia	Heteromyidae	S	Samuels and Van Valkenburgh 2008
14	*Lophiomys ibeanus*	Rodentia	Lophiomyinae	A	Nowak 1999
23	*Rattus andamanensis*	Rodentia	Muridae	A	Smith et al 2010
104	*Tatera*	Rodentia	Muridae	T	Nowak 1999
7	*Eliurus webbi*	Rodentia	Nesomyidae	A	Nowak 1999
97	*Nesomys rufus*	Rodentia	Nesomyidae	T	Nowak 1999
72	*Octodon degus*	Rodentia	Octodontidae	Sf	Nowak 1999
98	*Octodontomys gliroides*	Rodentia	Octodontidae	T	Nowak 1999
69	*Cynomys ludovicianus*	Rodentia	Sciuridae	Sf	Nowak 1999
8	*Funisciurus pyrropus*	Rodentia	Sciuridae	A	Van Valkenburgh 1987
43	*Glaucomys sabrinus*	Rodentia	Sciuridae	G	Samuels and Van Valkenburgh 2008
44	*Glaucomys volans*	Rodentia	Sciuridae	G	Nowak 1999
55	*Heliosciurus rufobrachium*	Rodentia	Sciuridae	Sc	Nowak 1999
20	*Paraxerus cepapi*	Rodentia	Sciuridae	A	Samuels and Van Valkenburgh 2008
24	*Ratufa bicolor*	Rodentia	Sciuridae	A	Nowak 1999
27	*Sciurus aberti*	Rodentia	Sciuridae	A	Nowak 1999
28	*Sciurus carolinensis*	Rodentia	Sciuridae	A	Nowak 1999
40	*Rhizomys sumatrensis*	Rodentia	Spalacidae	F	Nowak 1999
58	*Tupaia glis*	Scandentia	Tupaiidae	Sc	Van Valkenburgh 1987
105	*Tupaia longipes*	Scandentia	Tupaiidae	T	Kirk et al. 2008
30	*Tupaia minor*	Scandentia	Tupaiidae	A	Sargis 2001; Kirk et al. 2008
106	*Tupaia tana*	Scandentia	Tupaiidae	T	Sargis 2001; Kirk et al. 2008

73	*Solenodon paradoxus*	Soricomorpha	Solenodontidae	Sf	Nowak 1999
65	*Neomys fodiens*	Soricomorpha	Soricidae	Sa	Gingerich 2003
62	*Galemys pyrenaicus*	Soricomorpha	Talpidae	Sa	Gingerich 2003
41	*Scapanus orarius*	Soricomorpha	Talpidae	F	Hildbrand 1985; Nowak 1999

Supplementary Table 2. Descriptions of linear measurements of postcranial skeleton of extant small-bodied and extinct Mesozoic mammals in our dataset.

Skeletal segments	Measurement (Abbreviation)	Description of osteological measurement
Scapula	Scapular length (Sl)	Maximal length from the glenoid fossa to the distal end of the scapula
	Scapular height (Sh)	Maximal dorsoventral height of the scapula
Humerus	Humerus head length (HHl)	Anterior edge of the articular surface of the humerus head to posterior edge
	Humerus head width (HHw)	Medial edge of the articular surface of the humerus head to lateral edge
	Humerus distal end width (Hdw)	Maximal width between two distal epicondyles of the humerus
	Humerus length (Hl)	Maximal length between proximal and distal ends of the humerus
	Humerus proximal width (Hpw)	Maximal width of proximal end of the humerus
	Humerus mid-shaft width (Hsw)	Shaft width at the half humerus length
	Deltopectoral crest width (Hdcw)	Maximal width between medial and lateral edges of deltopectoral crest
Ulna	Ulna length (Ul)	Maximal length of ulna between proximal and distal ends
	Ulna olecranon process length (Uol)	Maximal length between proximal end of ulna and top margin of semilunar notch
Radius	Radius length (Rl)	Maximal length between proximal and distal ends of radius
Manus	Metacarpal length (Mcl)	Maximal length between proximal and distal ends of metacarpals
	Metacarpal width (Mcw)	Width of middle shaft of metacarpals
	Proximal phalangeal length (Ppl)	Maximal length between proximal and distal ends of proximal phalanges
	Proximal phalangeal width (Ppw)	Width of middle shaft of proximal phalanges
	Intermediate phalangeal length (Ipl)	Maximal length between proximal and distal ends of intermediate phalanges
	Intermediate phalangeal width (Ipw)	Width of middle shaft of intermediate phalanges
	Distal phalangeal length (Dpl)	Maximal length between proximal and distal ends of distal phalanges
	Distal phalangeal width (Dpw)	Width of middle shaft of distal phalanges
Pelvis	Ilium length (Il)	Maximal length between anterior tip and suture point in acetabulum of pelvis
	Ischium length (Isl)	Maximal length between the suture point in acetabulum and posterior end of pelvis
	Pelvic length (Pel)	Maximal length between anterior and posterior ends of pelvis
Femur	Femoral head depth (Fhd)	Proximal edge of head to distal edge
	Femoral distal width (Fdw)	Maximal width between epicondyles at the distal end of femur
	Femoral great trochanter height (FGh)	Maximal length between proximal end and root of great trochanter
	Femoral length (Fl)	Maximal length between head and distal end of femur
	Femoral mid-shaft width (Fsw)	Width of middle shaft of femur
Tibia	Tibia distal width (Tdw)	Maximal width of distal end of tibia
	Tibia length (Tl)	Maximal length between proximal and distal ends
	Tibia middle shaft width (Tmw)	Width of middle shaft tibia
	Tibia proximal width (Tpw)	Maximal width of proximal end of tibia

Fibula	Fibular distal end width (Fbdw)	Width of distal end of fibula
	Fibular length (Fbl)	Maximal length between proximal and distal ends of fibula
	Fibular mid-shaft width (Fbmw)	Width of middle shaft of fibula
	Fibula proximal width (Fpw)	Maximal width of proximal end of fibula
Astragalus	Astragalar length (Al)	Maximal length between anterior and posterior ends of astragalus
	Astragalar neck length (Anl)	Maximal length between anterior and most-posterior ends of astragalus
	Astragalar trochlea width (Atw)	Width of mediolateral of trochlea
Calcaneus	Calcaneal body length (Cal)	Length between anterior point of trochlea pernoealis and anterior end of calcaneus
	Calcaneal Cuboidal width (Ccw)	Maximal width of cuboidal facet
	Calcaneal length (Cl)	Maximal length between anterior and posterior ends of calcaneus
	Calcaneal tuber length (Ctl)	Length between posterior point of trochlea peronealis to the posterior end of calcaneus
	Calcaneal tuber width (Ctw)	Maximal mediolateral width of calcaneal tuber
	Calcaneal sustentacular width (Csw)	Maximal mediolateral width of the sustentaculum

Supplementary Table 3. Structure matrix, eigenvalues, and proportions of the variance explained by each function of the canonical variate analysis in the eight-locomotor-mode analysis.

	Canonical Function (CF)		
	CF1	CF2	CF3
Sl:Hl	0.201	-0.674	-0.176
Hsw:Hl	-0.173	-0.498	-0.314
Hpw:Hl	-0.08	-0.651	-0.268
Hdw.Hl	-0.072	-0.492	-0.269
Hsw:Hpw	-0.232	0.304	-0.106
HHl:Hl	-0.083	-0.655	-0.392
HHw:Hpw	0.115	0.602	0.339
Hdcw:Hpw	0.026	-0.416	-0.428
Hdcw:Hsw	0.081	-0.481	-0.43
Hdcw:Hdw	0.012	-0.446	-0.392
Ul:Hl	0.505	-0.252	-0.383
Uol:Ul	-0.272	-0.75	-0.369
Uol:Hl	-0.141	-0.774	-0.453
Rl:Hl	0.593	0.214	-0.109
Rl:Ul	0.174	0.531	0.306
Uol:Rl	-0.284	-0.721	-0.443
Mcl:(Hl+Rl)	-0.162	-0.269	0.447
Ppw:Ppl	-0.095	-0.534	-0.405
Ipw:Ipl	0.134	-0.616	-0.249
(Ppl+Ipl):Mcl	-0.077	0.136	-0.415
(Mcl+Ppl+Ipl+Dpl):(Hl+Rl)	-0.222	-0.525	-0.154
Il:Pel	-0.31	0.443	-0.047
FGh:Fl	-0.069	-0.44	-0.381
Fsw:Fl	-0.197	-0.68	-0.056
Tl:Fl	0.553	-0.132	0.167
(Hl+Rl):(Tl+Fl)	-0.768	0.235	0.082
Tmw:Tl	-0.2	-0.52	-0.105
Cal:Cl	-0.142	0.445	0.221
Ctl:Cl	0.217	-0.489	-0.208
Cal:Ctl	-0.127	0.43	0.159
Eigenvalue	11.923	8.646	5.523
Variance cumulative (%)	49.13	74.96	85.50

Supplementary Table 4. Canonical function scores of eight-locomotor-mode analysis and distances between taxa and the centroids of corresponding locomotor modes. Abbreviation: A, arboreal; Sa, semiaquatic; Sc, scansorial; Sf, semifossorial; T, terrestrial.

Taxon No.	Locomotor Mode	CF1	CF2	CF3	Distance
43	G	0.6985	4.4776	-1.9571	0.3797
44	G	0.6959	4.2635	-2.4697	0.6009
45	G	-0.2872	4.1263	-1.4718	0.8377
1	A	-0.7513	1.9811	-0.1648	0.4563
2	A	-1.0344	2.2860	0.1297	0.4830
3	A	-2.6642	1.9737	0.2704	1.7218
4	A	0.3518	2.0693	0.6952	1.4119
5	A	-0.9973	2.4901	-0.8515	1.2590
6	A	0.7736	3.0194	-0.4302	2.1976
7	A	0.6802	1.2676	0.0459	1.7289
8	A	-0.9784	1.6279	0.6144	0.4460
9	A	-0.3391	0.9040	1.7595	1.8984
10	A	-0.6406	0.9960	0.6673	0.9891
11	A	-1.0303	1.7498	0.9041	0.7002
12	A	-0.5154	3.2823	-1.5746	2.3508
13	A	-1.9788	2.5115	-0.2665	1.3295
14	A	-1.4278	0.5090	1.0689	1.6354
15	A	-1.6602	1.1334	0.4424	1.0123
16	A	-2.0357	1.6198	-0.2159	1.1830
17	A	-0.9002	2.2721	-0.1711	0.5965
18	A	-1.5145	1.8378	0.2794	0.5684
19	A	-2.0114	2.2346	0.0345	1.1536
20	A	-0.8008	0.4682	0.8548	1.5021
21	A	-1.2718	1.0663	1.7468	1.7389
22	A	-0.4517	2.8283	-0.3890	1.2773
23	A	-1.2048	0.2106	0.0245	1.6376
24	A	-1.6064	1.4103	-0.7710	1.2497
25	A	-0.9912	2.6193	0.2955	0.8073
26	A	-1.6218	3.6947	0.5441	2.0211
27	A	-0.1141	1.2739	-0.1401	1.0577
28	A	-0.4151	2.0007	-0.0057	0.6063
29	A	-1.3301	1.6025	0.5298	0.5399
30	A	-0.0343	1.5830	0.4248	0.9695
51	Sc	0.1892	0.7245	0.3805	1.6343
52	Sc	-1.6395	0.0528	0.9573	0.6363
53	Sc	-1.6697	0.0328	1.1807	0.6956

54	Sc	-1.9748	0.4116	1.2620	0.7327
55	Sc	-1.7595	0.8064	0.5291	0.6638
56	Sc	-1.3121	0.8834	1.3951	0.4945
57	Sc	-2.3325	0.8172	1.6963	1.2515
58	Sc	-0.2485	0.9599	0.3071	1.3209
59	Sc	-1.1649	0.7497	1.1758	0.2862
78	T	0.4990	-0.3643	1.2217	1.3480
79	T	0.1596	0.6473	1.3675	1.0415
80	T	0.2485	0.1568	1.3363	1.0131
81	T	-0.7530	-0.1349	1.9202	0.9907
82	T	1.3820	2.4500	-1.0240	3.6683
83	T	-0.7024	0.3067	0.8771	0.1542
84	T	-1.3822	0.7345	0.5902	0.9518
85	T	-0.0022	-0.7625	1.8773	1.4856
86	T	-0.7026	-0.4521	1.9914	1.1960
87	T	-1.0397	-0.0663	2.1761	1.2621
88	T	-2.2500	0.2528	1.8105	1.7525
89	T	-1.2400	-0.2342	2.0665	1.2798
90	T	0.8040	-3.4570	0.3178	4.0130
91	T	0.4173	0.2350	1.2071	1.1412
92	T	-1.9549	0.8899	1.2325	1.4497
93	T	-2.3883	1.3245	0.8804	2.0287
94	T	-0.4126	0.6625	1.9388	1.0943
95	T	-0.3007	0.7731	0.8870	0.7063
96	T	-1.1352	0.8958	0.2740	1.0872
97	T	-1.0242	-0.4437	0.2432	1.0376
98	T	-1.0406	-0.4912	0.5849	0.8705
99	T	0.1484	-2.3682	1.1580	2.7120
100	T	-0.9407	0.9603	1.0728	0.7999
101	T	-0.8161	1.1338	0.1625	1.2517
102	T	-1.1981	1.0403	0.5626	1.0639
103	T	-2.4116	0.3064	0.3187	1.8391
104	T	0.1312	-0.4619	-0.3813	1.7362
105	T	-1.2838	0.7791	0.6508	0.8869
106	T	-0.4207	0.5516	0.9269	0.4540
107	T	-1.4646	1.1746	1.4437	1.3169
60	Sa	-0.5116	0.1964	3.7938	2.2817
61	Sa	0.7324	-0.4205	0.8086	1.2056
62	Sa	1.0435	0.6086	1.3011	1.4870
63	Sa	0.3377	-0.9375	2.8086	0.9148
64	Sa	-0.0394	0.1107	1.3235	1.1908
65	Sa	1.4750	-1.2081	3.2068	1.6015
66	Sa	-0.5994	-2.6441	-0.5832	3.4786

67	Sa	1.5673	-1.5149	3.5760	2.0530
68	Sa	1.4625	0.0850	1.6580	1.1661
69	Sf	-2.5976	0.4488	0.5129	1.5428
70	Sf	-3.8352	-1.9212	1.9271	2.0972
71	Sf	-2.1357	-0.1195	1.1088	1.0981
72	Sf	-0.3777	-2.9401	1.7645	2.9743
73	Sf	-1.6531	-0.8951	-0.2086	1.1527
74	Sf	-2.3795	-1.0399	1.8971	1.2538
75	Sf	-1.8034	-0.5423	2.2892	1.8320
76	Sf	-3.6372	-2.8671	-1.8731	3.3249
77	Sf	-3.2454	0.1866	-1.6202	2.7251
31	F	-3.4822	-3.5673	-4.1215	1.8357
32	F	-3.7841	-1.2344	0.5161	3.7675
33	F	1.3452	-1.4599	-1.5171	4.9512
34	F	-4.8381	-4.3456	-2.0412	1.9647
35	F	-2.0051	-4.5735	-3.7736	2.0346
36	F	-4.7203	-3.6179	-3.7323	2.1753
37	F	-3.5466	-3.6064	-2.1681	0.5234
38	F	-2.6807	-2.5751	-0.7057	1.9533
39	F	-3.9300	-3.5967	-2.9249	1.0569
40	F	-3.6895	-4.7949	-1.1180	1.8333
41	F	-2.9486	-4.9481	-3.9202	2.0928
42	F	-2.3412	-4.6796	-2.5385	1.3219
46	S	6.9349	-2.6686	1.0395	1.9511
47	S	7.9377	-1.0614	-0.2749	0.7719
48	S	6.2625	-0.1167	-0.2005	1.9444
49	S	9.0250	-1.8110	-2.2949	2.3768
50	S	7.1348	-2.4232	-0.8572	0.9337

Supplementary Table 5. Classification matrix of the canonical variate analysis in eight-locomotor-mode analysis. Abbreviation: A, arboreal; F, fossorial; G, gliding; S, saltatorial; Sa, semiaquatic; Sc, scansorial; Sf, semifossorial; T, terrestrial.

Observed Mode	% Correct	Inferred Locomotor Mode							
		G	A	Sc	T	Sa	Sf	F	S
G	100.00	3	0	0	0	0	0	0	0
A	93.33	0	28	1	1	0	0	0	0
Sc	88.89	0	1	8	0	0	0	0	0
T	86.67	1	1	2	26	0	0	0	0
Sa	88.89	0	0	0	1	8	0	0	0
Sf	100.00	0	0	0	0	0	9	0	0
F	75.00	0	0	0	1	0	2	9	0
S	100.00	0	0	0	0	0	0	0	5
Total	89.72	4	30	11	29	8	11	9	5

Supplementary Table 6. Structure matrix, eigenvalues, and proportions of the variance explained by each function of the canonical variate analysis in the five-locomotor-mode analysis.

	Canonical Function (CF)		
	CF1	CF2	CF3
Sl:Hl	0.116	-0.553	0.269
Hsw:Hl	0.101	-0.371	-0.164
Hpw:Hl	0.091	-0.684	0.186
Hdw:Hl	0.019	-0.433	-0.144
Hsw:Hpw	-0.064	0.474	-0.595
HHl:Hl	0.217	-0.454	0.004
HHw:Hpw	-0.125	0.589	-0.077
Hdcw:Hpw	0.118	-0.084	-0.212
Hdcw:Hsw	0.152	-0.167	-0.136
Hdcw:Hdw	0.158	-0.096	-0.038
Ul:Hl	-0.06	-0.206	0.016
Uol:Ul	0.31	-0.524	0.306
Uol:Hl	0.263	-0.561	0.272
Rl:Hl	-0.119	0.054	0.012
Rl:Ul	-0.075	0.283	0.026
Uol:Rl	0.284	-0.556	0.244
Mcl:(Hl+Rl)	0.058	-0.423	0.378
Ppw:Ppl	0.425	-0.357	0.241
Ipw:Ipl	0.376	-0.38	0.336
(Ppl+Ipl):Mcl	-0.366	0.356	-0.768
(Mcl+Ppl+Ipl+Dpl):(Hl+Rl)	0.031	-0.355	0.006
Il:Pel	0.128	0.503	-0.236
FGh:Fl	0.147	-0.24	0.103
Fsw:Fl	0.058	-0.758	0.149
Tl:Fl	-0.156	-0.61	0.118
(Hl+Rl):(Tl+Fl)	0.147	0.083	0.106
Tmw:Tl	0.088	-0.335	0.281
Cal:Cl	0.017	0.169	-0.305
Ctl:Cl	-0.022	-0.17	0.337
Cal:Ctl	-0.03	0.214	-0.348
Eigenvalue	9.799	7.409	5.891
Variance cumulative (%)	48.30	75.91	93.36

Supplementary Table 7. Classification matrix of the canonical variate analysis in the five-locomotor-mode analysis. Abbreviation: A, arboreal; Sa, semiaquatic; Sc, scansorial; Sf, semifossorial; T, terrestrial.

Observed Mode	% Correct	Inferred Locomotor Mode				
		A	Sc	T	Sa	Sf
A	96.67	29	0	1	0	0
Sc	88.89	1	8	0	0	0
T	96.67	0	1	29	0	0
Sa	88.89	0	0	1	8	0
Sf	100.00	0	0	0	0	9
Total	95.40	30	9	31	8	9

Supplementary Table 8. Structure matrix, eigenvalues, and proportions of the variance explained by each function of the canonical variate analysis in the three-locomotor-mode analysis.

	Canonical Function (CF)	
	CF1	CF2
Sl:Hl	0.402	-0.077
Hsw:Hl	-0.196	0.021
Hpw:Hl	0.487	-0.098
Hdw:Hl	-0.109	0.141
Hsw:Hpw	-0.763	0.09
HHl:Hl	0.132	0.061
HHw:Hpw	-0.304	-0.209
Hdcw:Hpw	-0.161	0.154
Hdcw:Hsw	-0.062	0.154
Hdcw:Hdw	-0.007	0.021
Ul:Hl	0.063	0.049
Uol:Ul	0.47	-0.051
Uol:Hl	0.454	-0.05
Rl:Hl	0.053	0.12
Rl:Ul	0.03	0.085
Uol:Rl	0.419	-0.055
Mcl:(Hl+Rl)	0.35	-0.32
Ppw:Ppl	0.47	0.088
Ipw:Ipl	0.554	0.14
(Ppl+Ipl):Mcl	-0.842	0.242
(Mcl+Ppl+Ipl+Dpl):(Hl+Rl)	-0.057	-0.232
Il:Pel	-0.283	0.179
FGh:Fl	0.254	0.188
Fsw:Fl	0.395	0.036
Tl:Fl	0.373	0.219
(Hl+Rl):(Tl+Fl)	-0.061	-0.399
Tmw:Tl	0.322	-0.158
Cal:Cl	-0.183	0.399
Ctl:Cl	0.335	-0.137
Cal:Ctl	-0.303	0.222
Eigenvalue	9.553	8.479
Variance cumulative (%)	55.93	100.00

Supplementary Table 9. Classification matrix of the canonical variate analysis in the three-locomotor-mode analysis. Abbreviation: A, arboreal; Sc, scansorial; T, terrestrial.

Observed Mode	% Correct	Predicted locomotor category		
		A	Sc	T
A	96.67	29	0	1
Sc	88.89	1	8	0
T	100.00	0	0	30
Total	97.10	30	8	31

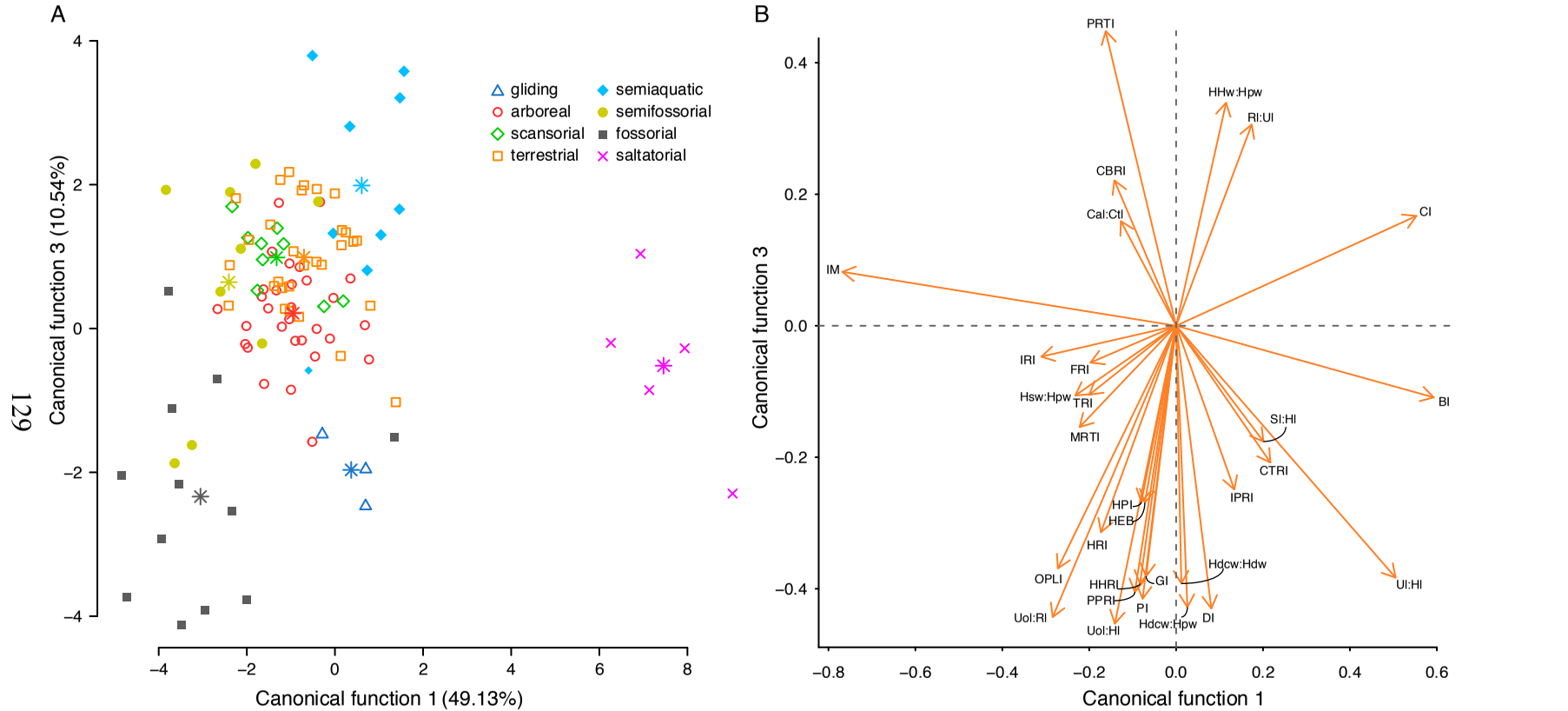

Supplementary Figure 1. A, plot of canonical functions (CFs) 1 and 3 from the canonical variate analysis (CVA) in the eight-locomotor-mode analysis. B, plot of structure correlations between the osteological indices and the CF1 and CF3. *, centroid of the locomotor mode.

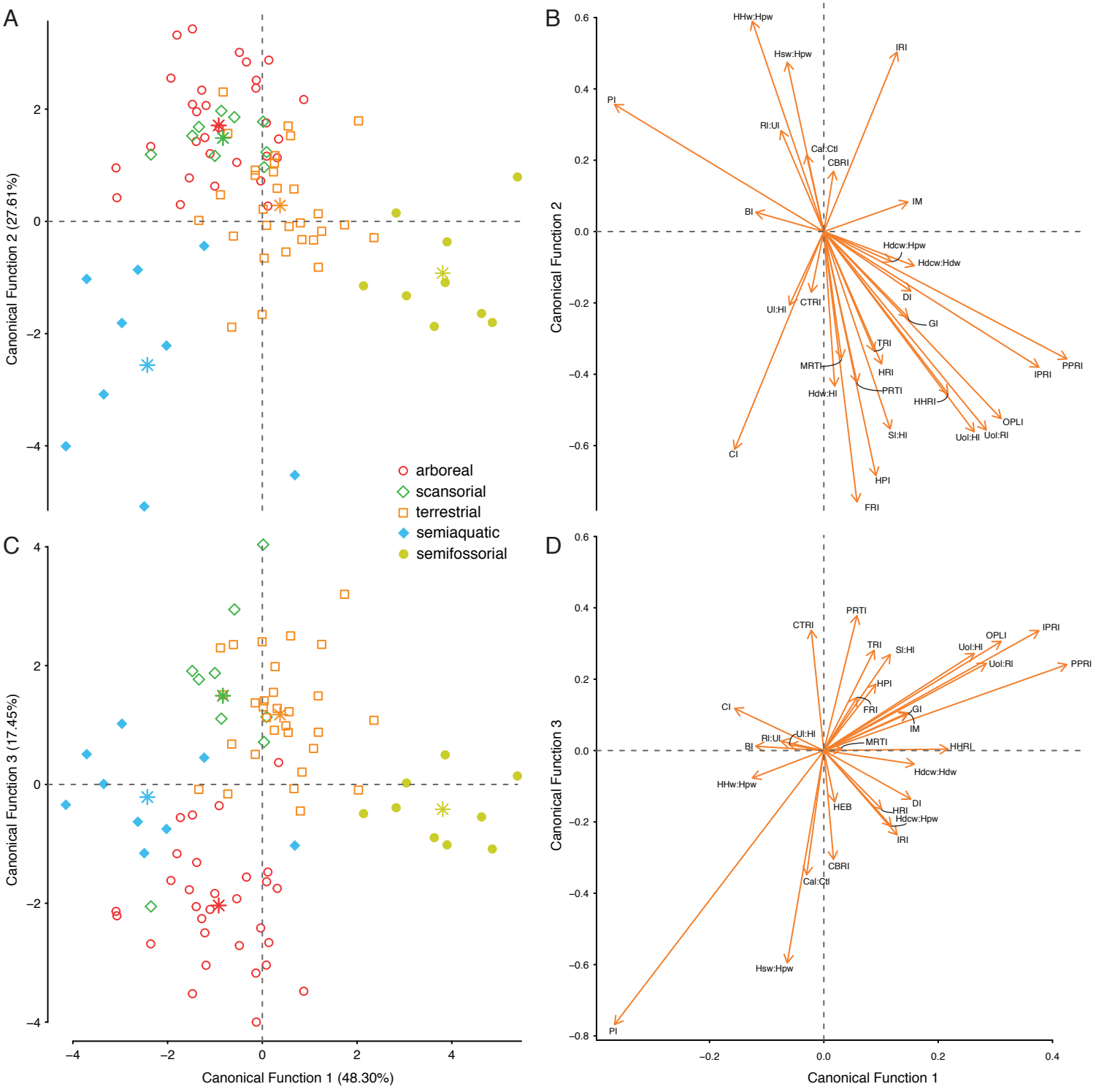

Supplementary Figure 2. A, plot of canonical functions (CFs) 1 and 2 from the canonical variate analysis (CVA) in the five-locomotor-mode analysis. B, plot of structure correlations between the osteological indices and the CF1 and CF2. C, plot of canonical functions (CFs) 1 and 3 from the canonical variate analysis (CVA) in the eight-locomotor-mode analysis. D, plot of structure correlations between the osteological indices and the CF1 and CF3. *, centroids of the locomotor modes.

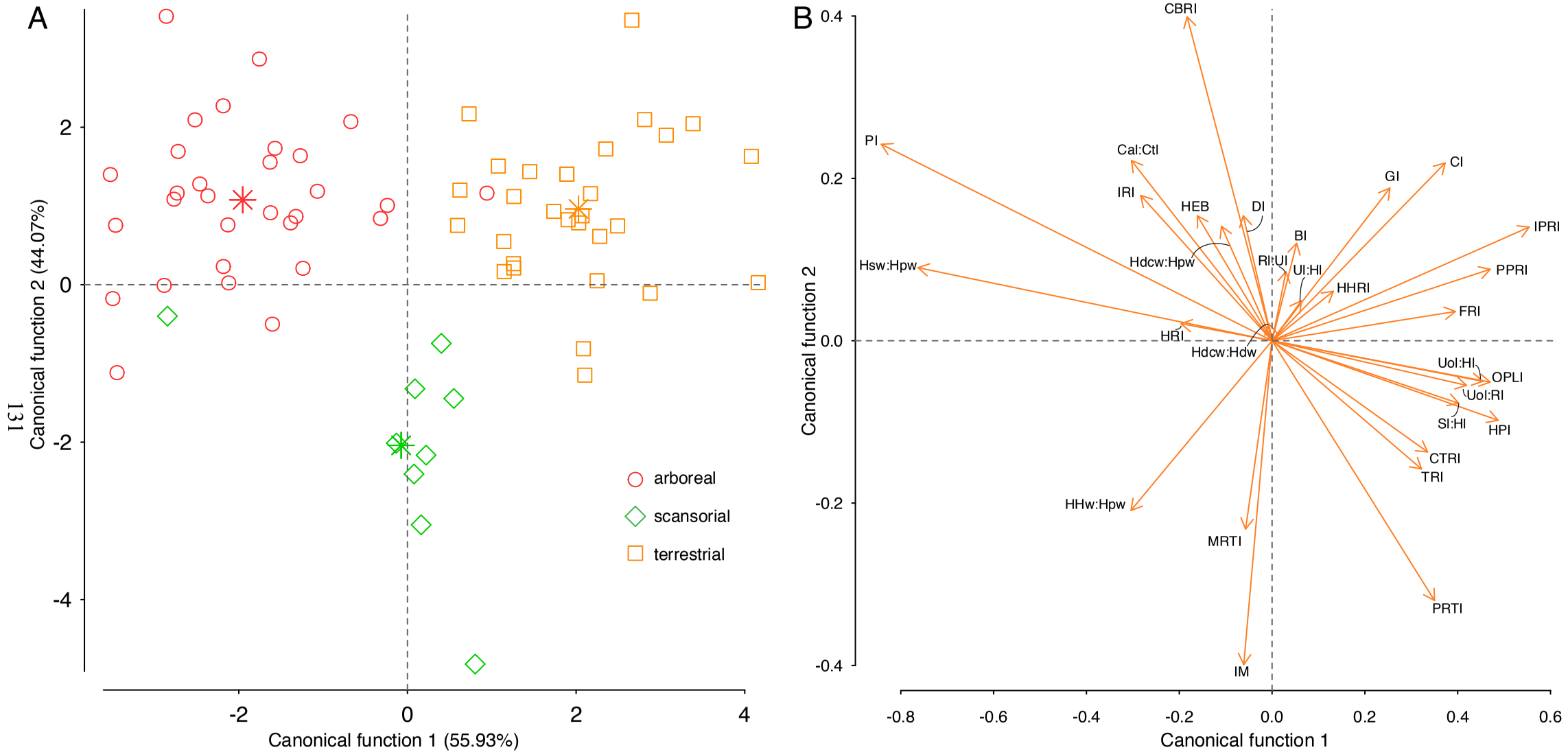

Supplementary Figure 3. A, plot of canonical functions (CFs) 1 and 2 from the canonical variate analysis (CVA) in the three-locomotor model analyses. B, plot of structure correlations between the osteological indices and the CF1 and CF2. *, centroid of the locomotor mode.

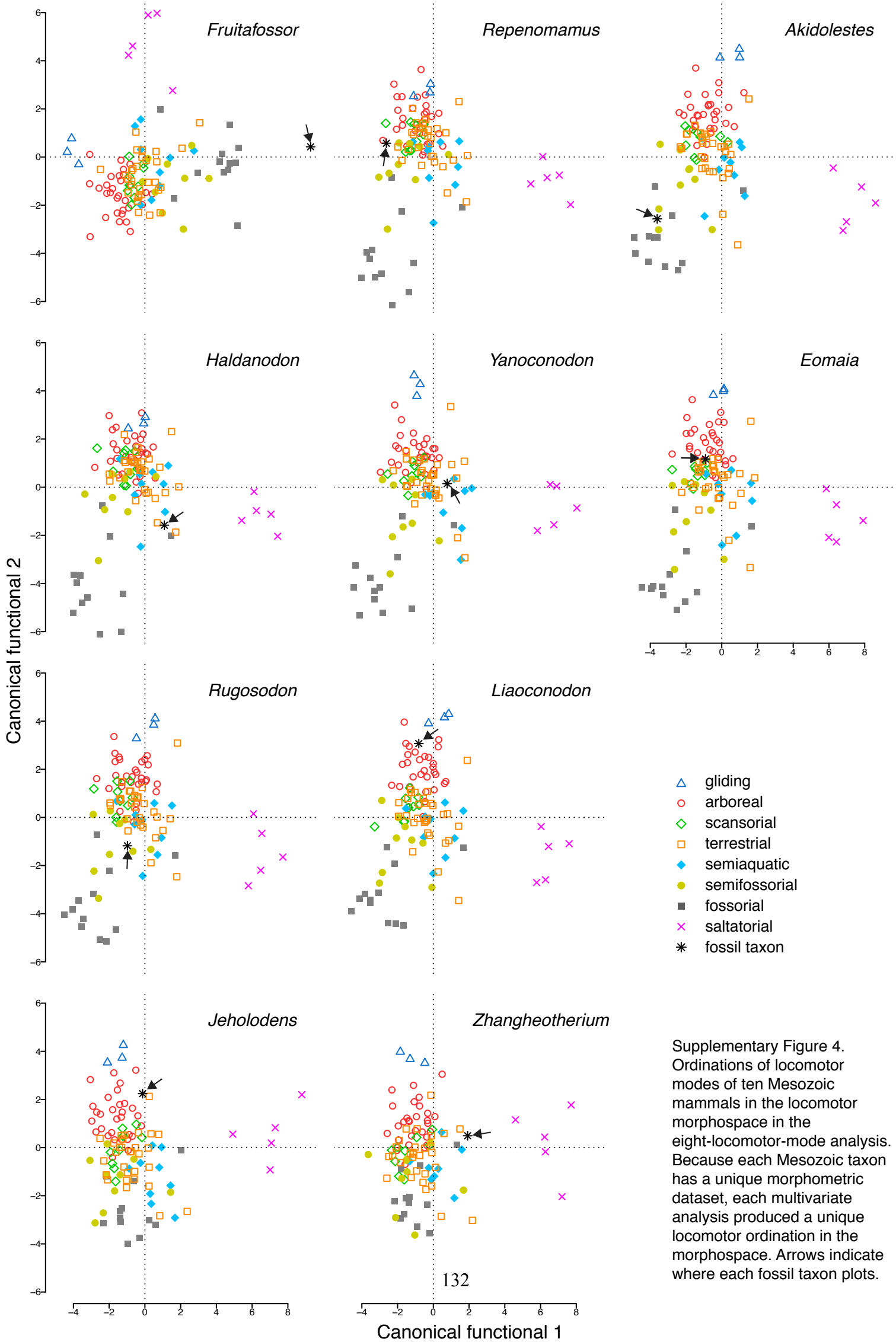

Supplementary Figure 4. Ordinations of locomotor modes of ten Mesozoic mammals in the locomotor morphospace in the eight-locomotor-mode analysis. Because each Mesozoic taxon has a unique morphometric dataset, each multivariate analysis produced a unique locomotor ordination in the morphospace. Arrows indicate where each fossil taxon plots.

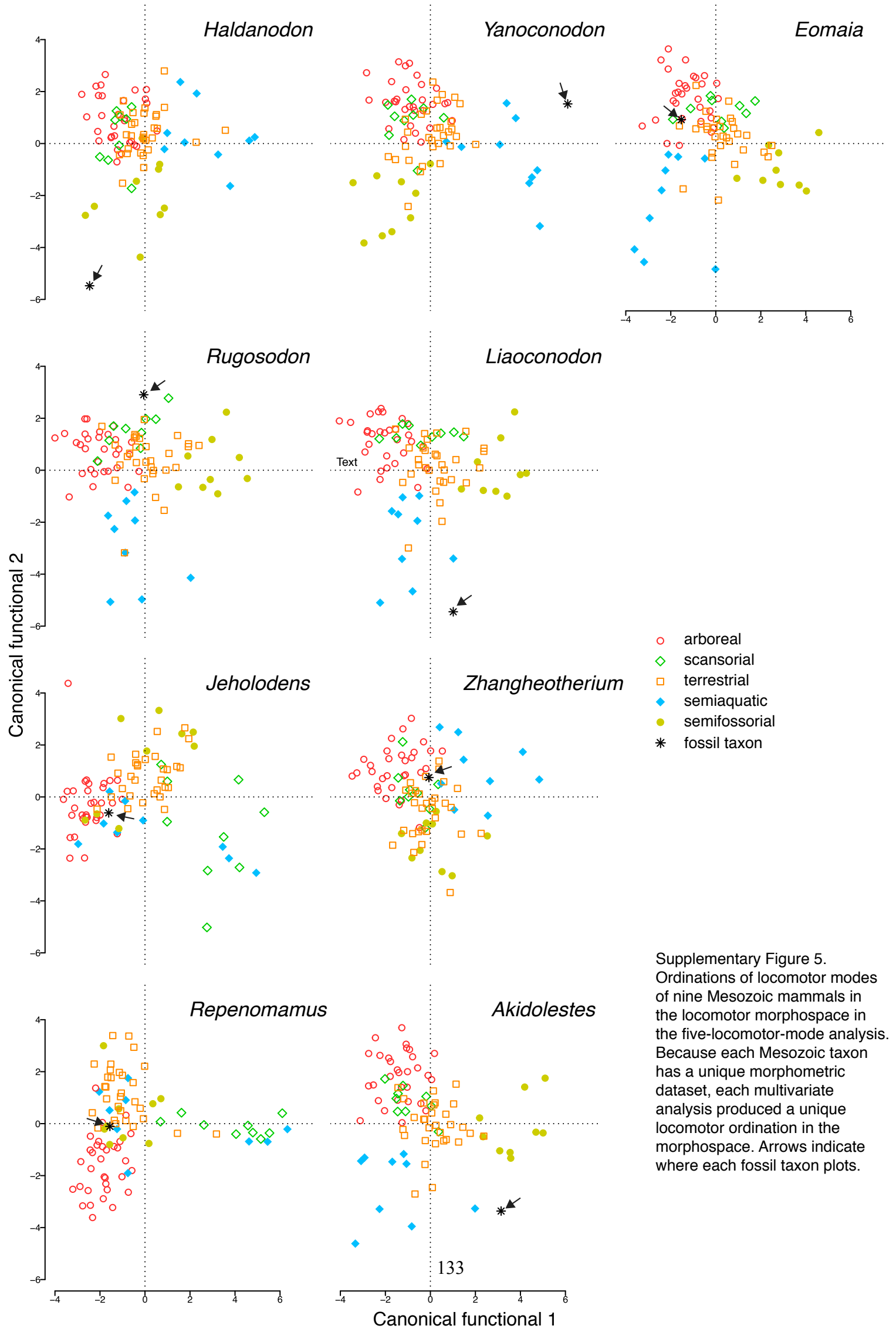

Supplementary Figure 5. Ordinations of locomotor modes of nine Mesozoic mammals in the locomotor morphospace in the five-locomotor-mode analysis. Because each Mesozoic taxon has a unique morphometric dataset, each multivariate analysis produced a unique locomotor ordination in the morphospace. Arrows indicate where each fossil taxon plots.

Literature Cited

Argot, C. 2001. Functional-adaptive anatomy of the forelimb in the Didelphidae, and the paleobiology of the Paleocene marsupials *Mayulestes ferox* and *Pucadelphys andinus*. Journal of Morphology 247:51–79.

Bassarova, M., C. M. Janis, and M. Archer. 2009. The calcaneum–on the heels of marsupial locomotion. Journal of Mammalian Evolution 16:1–23.

Bishop, K. L. 2007. Aerodynamic force generation, performance and control of body orientation during gliding in sugar gliders (*Petaurus breviceps*). Journal of Experimental Biology 210:2593–2606.

Christensen, P., K. Maisey, and D. H. Perry. 1984. Radio-tracking the numbat, *Myrmecobius fasciatus*, in the Perup Forest of western Australia. Australia Wildlife Research 11:275–288.

Cooper, C. E. 2011. *Myrmecobius fasciatus* (Dasyuromorphia: Myrmecobiidae). Mammalian Species 43:129–140.

Delciellos, A. C., and M. V. Vieira. 2006. Arboreal walking performance in seven didelphid marsupials as an aspect of their fundamental niche. Austral Ecology 31:449–457.

Endo, H., T. Yonezawa, F. Rakotondraparany, M. Sasaki, and M. Hasegawa. 2006. The adaptational strategies of the hindlimb muscles in the Tenrecidae species including the aquatic web-footed tenrec (*Limnogale mergulus*). Annals of Anatomy 188:383–390.

Fish, F. E. 1984. Mechanics, power output and efficiency of the swimming muskrat (*Ondatra zibethicus*). Journal of Experimental Biology 110:183– 201.

Gebo, D., and K. Rose. 1993. Skeletal morphology and locomotor adaptation in *Prolimnocyon atavus*, an early Eocene hyaenodontid creodont. Journal of Vertebrate Paleontology

13:125–144.

Gingerich, P. D. 2003. Land-to-sea transition in early whales: evolution of Eocene Archaeoceti (Cetacea) in relation to skeletal proportions and locomotion of living semiaquatic mammals. Paleobiology 29:429–454.

Goldingay, R. L. 2000. Gliding mammals of the world: diversity and ecological requirements. Pp. 5–40 *in* R. L. Goldinggay, and J. S. Scheibe, eds. Biology of gliding mammals. Filander Verlag, Fürth.

Grant, T., and D. Fanning. 1989. The platypus: a unique mammal. New South Wales University Press, Kensington, Australia.

Heinrich, R., and P. Houde. 2006. Postcranial anatomy of *Viverravus* (Mammalia, Carnivora) and implications for substrate use in basal Carnivora. Journal of Vertebrate Paleontology 26:422–435.

Hildebrand, M. 1985. Digging in quadrupeds. Pp. 89–109 *in* M. Hildebrand, D. M. Bramble, K. F. Liem, and D. B. Wake, eds. Functional Vertebrate Morphology. Harvard University Press, Cambridge, Mass.

Hopkins, S. S. B., and E. B. Davis. 2009. Quantitative morphological proxies for fossoriality in small mammals. Journal of Mammalogy 90:1449–1460.

Howell, A. B. 1930. Aquatic mammals. Charles C. Thomas, Springfield, Illinois.

———. 1932. The saltatorial rodent *Dipodomys*: The functional and comparative anatomy of its muscular and osseous systems. Proceedings of the American Academy of Arts and Science 67:377–536.

———. 1937. The swimming mechanism of the platypus. Journal of Mammalogy 18:217–222.

Iwaniuk, A. N., S. M. Pellis, and I. Q. Whishaw. 1999. The relationship between forelimb

morphology and behaviour in North American carnivores (Carnivora). Canadian Journal of Zoology 77:1064–1074.

Iwaniuk, A., and S. Pellis. 2000. The relative importance of body size, phylogeny, locomotion, and diet in the evolution of forelimb dexterity in fissiped carnivores (Carnivora). Canadian Journal of Zoology 78:1110–1125.

Kirk, E. C., P. Lemelin, M. W. Hamrick, D. M. Boyer, and J. I. Bloch. 2008. Intrinsic hand proportions of euarchontans and other mammals: implications for the locomotor behavior of plesiadapiforms. Journal of Human Evolution 55:278–299.

Körtner, G., and F. Geiser. 2000. Torpor and activity patterns in free-ranging sugar gliders *Petaurus breviceps* (Marsupialia). Oecologia 123:350–357.

Lackey, J. A. 1996. *Chaetodipus fallax*. Mammalian Species 517:1–6.

Larivie´re, S. 1999. *Mustela vison*. Mammalian Species 608:1–9.

Larivie´re, S., and M. Pasitschniak-Arts. 1996. *Vulpes vulpes*. Mammalian Species 537:1–11.

Linzey, A. V. 1983. *Synaptomys cooperi*. Mammalian Species 210:1–5.

Marshall, L. G. 1978. *Chironectes minimus*. Mammalian Species 109:1–6.

Meachen-Samuels, J. 2010. Comparative scaling of humeral cross-sections of felids and canids using radiographic images. Journal of Mammalian Evolution 17:193–209.

Nowak, R. M. 1999. Walker's mammals of the world. Johns Hopkins University Press, Baltimore.

Nowak, R. M. 2005. Walker’s marsupials of the world. Johns Hopkins University Press, Baltimore.

Nyakatura, J. A., M. S. Fischer, and M. Schmidt. 2008. Gait parameter adjustments of cotton-top tamarins (*Saguinus oedipus*, Callitrichidae) to locomotion on inclined arboreal substrates.

American Journal of Physical Anthropology 135:13–26.

Pasitschniak-Arts, M., and S. Larivie´re. 1995. *Gulo gulo*. Mammalian Species 499:1–10.

Redford, K. H., and R. M. Wetzel. 1985. *Euphractus sexcinctus*. Mammalian Species 252: 1–4.

Samuels, J. X., and B. Van Valkenburgh. 2008. Skeletal indicators of locomotor adaptations in living and extinct rodents. Journal of Morphology 269:1387–1411.

Sargis, E. J. 2001. The grasping behaviour, locomotion and substrate use of the tree shrews *Tupaia minor* and *T. tana* (Mammalia, Scandentia). Journal of Zoology 253:485–490.

Smith, M. J. 1973. *Petaurus breviceps*. Mammalian Species 30:1–5.

Smith, A. T., Y. Xie, R. S. Hoffmann, D. Lunde, J. MacKinnon, D. E. Wilson, and W. C. Wozencraft, eds. 2010. A guide to the mammals of China. Princeton University Press, Princeton.

Stein, B. R. 1988. Morphology and allometry in several genera of semiaquatic rodents (*Ondatra, Nectomys*, and *Oryzomys*). Journal of Mammalogy 69:500–511.

Taylor, M. E. 1974. The functional anatomy of the forelimb of some African Viverridae (Carnivora). Journal of Morphology 143: 307–336.

Thorington, R. W. Jr., and L. R. Heaney. 1981. Body proportions and gliding adaptations of flying squirrels (Petauristinae). Journal of Mammalogy 62:101–114.

van Staaden, M. J. 1994. *Suricata suricatta*. Mammalian Species 483:1–8.

Van Valkenburgh, B. 1987. Skeletal indicators of locomotor behavior in living and extinct carnivores. Journal of Vertebrate Paleontology 7:162–182.

Wade-Smith, J., and B. J. Verts. 1982. *Mephitis mephitis*. Mammalian Species 173:1–7.

Yensen, E., and T. Tarifa. 2003. *Galictis cuja*. Mammalian Species 728:1–8.

CHAPTER 4:

THE NON-ANALOG ECOLOGICAL STRUCTURE OF EARLY CRETACEOUS JEHOL MAMMAL COMMUNITIES

The non-analog ecological structure of Early Cretaceous Jehol mammal communities

Meng Chen[a,b,1] and Gregory P. Wilson[a,b]

[a] Department of Biology, University of Washington, Box 351800, Seattle WA 98195-1800, USA

[b] Department of Geology, Burke Museum of Natural History and Culture, Box 353010, Seattle WA 98195-0001, USA

Author contributions: M.C. and G.P.W. designed research; M.C. performed analyses; M.C. and G.P.W. analyzed the data and wrote the paper.

The authors declare no conflict of interest

[1]To whom correspondence may be addressed. E-mail: mengchen@uw.edu and gpwilson@uw.edu

Abstract.– Most mammalian taxa of the Lower Cretaceous Jehol Group are preserved as nearly complete fossil skeletons. This fossil record currently represents our best opportunity to move beyond the study of the autecology of individual species to analysis of Mesozoic mammal communities. Contextual information, such as abiotic factors and other biotic factors, is well constrained for the Jehol Group, enabling analysis of linkages between intrinsic and extrinsic factors that might have shaped the ecological structure of these ancient mammal communities. I quantified ecological structure of two mammalian communities from the Jehol Group and 28 extant small-bodied mammal communities from tropical, arid, temperate, and cold environments using diet, body size, and locomotor mode. I used the resulting dataset to compare ecological structure among extant mammal communities and Mesozoic mammal communities. I used ecological disparity and ecological diversity as parameters to characterize ecospace occupations for each mammal community. Results indicate that environmental factors play essential roles in shaping ecological structure of extant small-bodied mammal communities. Small-bodied mammal communities in tropical regions have more clustered ecospace occupations, reflected by low ecological disparity and high ecological diversity, in contrast with mammalian communities from arid and cold environments, which have more scattered ecospace occupations as reflected by high ecological disparity and low ecological diversity. Results also indicate that the ecological diversity and disparity of the two Early Cretaceous mammal communities are comparable to extant small-bodied mammal communities from tropical and arid environments, respectively. The significantly different ecological structure of the extant small-bodied and Early Cretaceous mammal communities might be primarily due to sampling biases of the fossil record, non-analog Early Cretaceous environments, and/or evolutionary ecology differences of species compositions among extinct and extant mammalian communities.

Introduction

Mammals arose in the Late Triassic (ca. 220 Ma; Kielan-Jaworowska et al., 2004) at about the same time as dinosaurs (Brusatte et al., 2010). Through the Mesozoic Era, they became taxonomically rich (>320 species) and geographically widespread across Laurasia and Gondwana (Lillegraven et al., 1979; Kielan-Jaworowska et al., 2004). Although they were long thought of as ecologically constrained to roles as mostly small-bodied, generalized, nocturnal insectivores (e.g., Simpson, 1937; Van Valen and Sloan, 1977), recent discoveries of exquisitely preserved fossils (see e.g., Luo, 2007) and comprehensive ecomorphological analyses (e.g., Wilson et al., 2012; Wilson, 2013; Grossnickle and Polly, 2013) have shown that instead Mesozoic mammals evolved an array of ecologies comparable to that of extant, small-bodied mammals, namely from colonial-insect feeding diggers to insectivorous gliders, terrestrial scavengers, and semiaquatic carnivores (Luo, 2007; Chen and Wilson, 2015). Moreover, these diverse forms independently arose multiple times independently in different mammalian lineages during the Mesozoic. Still, we know little about how these ecomorphs were distributed across Mesozoic mammal communities. In the context of dinosaur-dominated terrestrial ecosystems and perhaps non-analog environmental conditions, was the ecological structure of Mesozoic mammal communities fundamentally different from that of small-bodied mammal communities today?

The fossil record of the Lower Cretaceous Jehol Group in northeastern China currently represents our best opportunity to quantify ecological structure of Mesozoic mammal communities (Meng, 2014). Most mammalian taxa from the Jehol Group are preserved as nearly complete fossil skeletons (Chang et al., 2003; Zhou et al., 2003; Meng et al., 2006; Meng, 2014; Zhou, 2014), such that robust paleoecological inferences are possible. To quantify ecological structure in two mammalian communities from the Jehol Group, we plotted ecospace occupation

of constituent species based on inferred body size, diet, and locomotor categories. Contextual information, such as other biotic factors (e.g. vertebrates, invertebrates, and plants) and the abiotic factors (e.g., climate), is well constrained for this study area (Zhou, 2014), enabling us to analyze linkages between intrinsic and extrinsic factors that may have shaped the ecological structure of these ancient mammal communities. We compared these communities to 28 extant, small-bodied mammal communities from tropical, arid, temperate, and cold regions. Our results indicate that these Early Cretaceous mammal communities were on par with modern mammal communities in terms of the ecological diversity and disparity but they significantly differed in ecological structure, implying that variables that shaped communities might have been different in the Mesozoic compared to today.

Materials and Methods

Extant Small-bodied Mammal Communities and Mesozoic Mammal Communities. Because most Mesozoic mammals were small bodied (Kielan-Jaworowska et al., 2004), extant small-bodied mammals (< 5kg) are appropriate analogs for them (Chen and Wilson, 2015). Thus, we assembled a dataset of 28 extant small-bodied mammal communities from the primary literature (Fig. S1; Table S2). Because flying mammals have not been documented in the Mesozoic, we excluded flying mammals from our extant dataset. We assigned each extant small-bodied mammal community to one of four climate regions (tropical, arid, temperate, and cold environments; see Peel et al., 2007; Table S3). Twenty-two out of 28 small-bodied mammal communities have available mean annual temperature (MAT) and annual precipitation (APT) data that we used for assessing the relationships between ecological structure and climate.

To study ecological structure of Mesozoic mammal communities, we assembled two

Early Cretaceous mammal communities from the northeastern China Jehol Group (Zhou, 2014; Table S4): the Dawangzhangzi-Jiufotang (DJ) community, which has seven mammalian species, and the Jianshangou-Lujiatun (JL) community, which has ten mammalian species. During the Early Cretaceous in the Jehol Group, phreatomagmatic volcanic events produced mass-mortality assemblages of well-preserved vertebrates (Chang et al., 2003; Zhou et al., 2003; Zhou, 2014), which may represent autochthonous fossil deposition. The DJ and JL communities each consist of two fossil assemblages from within the Jehol Group. The DJ fossil assemblages are temporally constrained to 120–122 Ma by radiometric ages, and the JL fossil assemblages are temporally constrained to 125–128 Ma. As in any study of the fossil record, the time averaging of the assembled Early Cretaceous mammal communities may bias the interpretation of evolutionary and ecological patterns of mammal communities in this study. However, we contend that the restricted temporal scope and mode of fossilization of the fossil assemblages support their use in the analysis of the ecological structure of Mesozoic mammal communities.

Ecological Structure. We used three ecological variables (body size, diet, and locomotor mode) to assess ecological structure of our extant and extinct mammalian communities. These ecological variables play important roles in explaining the structure of extant and extinct animal communities (Fleming, 1973; Andrews et al., 1979; Van Valkenburgh, 1994) as well as community stability (see McCann, 2000). The distribution of body sizes shows physiological differences among community members (Eisenberg, 1981; McNab, 1990); the range of diets illustrates the range of foods available; and locomotor preferences may reflect vegetational structure and survival strategies. These three ecological traits are well documented for extant small-bodied mammals and can be inferred for a number of Mesozoic mammals (e.g. Damuth and MacFadden, 1990; Kielan-Jaworowska et al., 2004; Luo, 2007).

We attained the ecological trait data of extant species using the primary literature or natural history compendia (e.g., Kingdon, 1997; Nowak, 1999). To estimate body size of extinct taxa, we used length measurements from the mandible, humerus, and femur (Foster, 2009; Campione and Evans, 2012). We divided $\log_2$-transformation body mass into six ranks (body size rank 1–6). We classified diet and locomotor mode into six (carnivore, insectivore, omnivore, frugivore, granivore, herbivore) and eight (gliding, arboreal, scansorial, terrestrial, semiaquatic, semifossorial, fossorial, saltatorial) categories, respectively. In extant mammals, the complexity of the cheek tooth row can be quantified as the orientation patch count (OPC). Diet correlates with OPC: higher OPC values (>~200) are associated with more herbivorous diets in contrast with lower OPC values (=~100) for more carnivorous diets (Evans et al., 2007). Thus, we ranked diet categories on an ordinal scale from 1 (carnivore) to 6 (herbivore). To order locomotor modes, we rely on multivariate morphometric analyses that have successfully classified eight locomotor modes among small-bodied mammals (Chen and Wilson, 2015). The locomotor modes are arrayed along a morphofunctional continuum from agility- and speed-based modes (gliding, arboreal) to power-based modes (semiaquatic, fossorial) (Chen and Wilson, 2015). The saltatorial mode is anomalous because it reflects both power- and speed-directed locomotion in the forelimbs and hind limbs, respectively. Accordingly, we rank locomotor mode categories on an ordinal scale from 1 (gliding) to 7 (fossorial) and 8 (saltatorial) (Table S1).

We characterized the ecological structure of each mammalian community by two parameters, ecological disparity and ecological diversity. Ecological disparity represents the magnitude of differences in ecological traits among each species in a community (Jernvall et al., 1996). For example, the didelphid marsupial *Marmosa elegans*, which is between 33 g and 128 g in body mass, eats insects, and uses scansorial locomotion, has an ecological assignment of 2-2-

3, reflecting the ordinal values for each ecological trait. The ecological assignment of the rodent *Abrocoma bennetti* is 3-6-3. The ecological distance between *M. elegans* and *A. bennetti* is calculated as |2-3|+|2-6|+|3-3|=5. The ecological disparity of a community would then be the mean pair-wise ecological distance between all species pair combinations in a community. In contrast, ecological diversity measures the number of the unique ecological assignments within each community (Fig. 2a, b, c, d). Ecological diversity describes the number of occupations in a given ecospace (e.g., full vs. empty). The ecological diversity resembles the functional richness index using ordinal variables (Villeger et al., 2008; Schleuter et al., 2010). However, the purpose of estimating ecological diversity in this study differs from the purpose of the functional richness index, which aims to capture the ecospace occupation with the smallest convex hull volume to enclose all species (Schleuter et al., 2010). We visualized the ecospace occupations of each mammal community by plotting the ecological assignment of constituent species in cube plots.

As a result of intraspecific variation, body size of mammalian species is sometimes given as a range in the literature (e.g., 18–45g). To account for this, we used both maximum and minimum body size for each species when calculating the ecological disparity and ecological diversity for small-bodied mammal communities. We found that there was no statistical significant difference between datasets using maximum and minimum body size for the ecological disparity and ecological diversity except for the ecological disparity of the temperate regions (p<0.05). However, this had no effect on major patterns of the ecological structure of extant small-bodied mammal communities in the four climate regions. Thus, we chose to report the ecological disparity and ecological diversity using the lowest body size.

Assess influence of environments. To understand how what factors might have influenced the ecological structure of small-bodied mammal communities, we investigated how ecological

structure correlates with latitude, longitude, APT and MAT. We used these four variables for several reasons. Latitudinal biodiversity gradients are well documented across many taxonomic groups (Buckley et al., 2010; Davies and Buckley, 2011; Hawkins et al., 2011). Longitude is also important, as vegetational structure and, in turn, the habitats of small-bodied mammal communities often vary with longitude. For example, the Sahara desert and tropical rainforests of Central America, which range across similar latitudes, differ drastically in biodiversity because of their distinct environments. MAT and APT affect geographical distributions of small-bodied mammal species, which have variable physiological tolerances to temperature (Merritt, 2010). Both temperature and precipitation are also highly correlated with evapotranspiration, which influences vegetation structure, primary productivity, and seasonal availability of plant resources (Cox and Moore, 1985; Whittaker, 1975; Badgley and Fox, 2000). Thus, MAT and APT are important drivers for patterning mammalian diversity at a global scale (Cooper et al., 2011; Davies and Buckley, 2011; Davies et al., 2011; Hawkins et al. 2012). These variables were also chosen because they can be obtained or approximated for the Early Cretaceous mammalian communities (Enkin et al., 1992; Amiot et al. 2011; Pen and Huang 2013).

We compiled the environmental data for each extant mammal community using data from the published literature and National Oceanic and Atmospheric Administration (NOAA; Supplementary Materials). Most environmental data refer to the same year when the original field study of small-bodied mammal community was conducted (Table S2). We excluded the few mammal communities that lack environmental data from the correlation analyses. For the two Early Cretaceous mammal communities, we used paleoenvironmental data estimated by Amiot et al. (2011) and Pen and Huang (2013) (Table S2).

Statistical Analyses. To test whether the differences in ecological structure of sampled small-bodied mammal communities is due to chance, we performed two different sets of statistical analyses. The χ^2 test was used to test for correlations between each ecological trait and four different climates in order to determine whether climates have influence on ecological traits of our sampled extant small-bodied mammal communities. The Mantel test (1956) was used to investigate the relationship between the ecological structure and climate. To conduct the Mantel test, we calculated a Bray-Curtis distance matrix for ecological disparity and Euclidean distance matrices for ecological diversity and climate variables (APT and MAT; Tables S11–S13). Because the sample sizes of extant small-bodied mammal communities are small in the four climate regions, we performed six pair-wise two-sample bootstrap tests. These tests examine the resampled distribution on expected mean differences (Kowalewski and Novack-Gottshall, 2010) of ecological disparity and diversity to test whether the ecological structure of small-bodied mammal communities in, for example, tropical and arid regions truly differ from each other. We also performed the same two-sample bootstrap tests to compare the ecological structure of the Early Cretaceous and extant small-bodied mammal communities. In addition, we applied single and multiple regression models to investigating which of the environmental factors has a statistically significant, unique contribution to the ecological structure of extant small-bodied mammals. We used corrected Akaike Information Criterion (AICc) and the proportion of explained variation to assess each model because our sample sizes are relatively small. Then we applied the most appropriate models to predict the ecological structure of the Early Cretaceous mammal communities. All statistical analyses were carried out using open source software R 3.1.2 with appropriate statistical packages, such as “vegan”, “MASS”, and “ade4”.

Results

We found that small-bodied mammal communities of the four climate regions have distinct ecological structures (Fig. 1). We also found that environmental differences may have a great influence on body size (χ^2=94.04, df=15, p<0.001), diet (χ^2=178.73, df=15, p<0.001), and locomotor mode (χ^2=138.18, df=21, p<0.001; Table S3). In addition, Mantel tests indicate that the ecological structure of small-bodied mammal communities show positive correlations with climate (ecological disparity: r=0.231, p=0.0028; ecological diversity: r =0.332, p=0.0058). Ecological disparity and ecological diversity, which were used to characterize ecospace occupation, are distinct across the four climate regions (Fig. 1; Table S4). The small-bodied mammal communities in tropical and arid regions show distinct ecological structures from those of the other two regions. Mammal communities in tropical regions have the lowest mean ecological disparity (3.52) but the highest mean ecological diversity (12.44); whereas mammal communities in arid regions have high mean ecological disparity (4.73) but the lowest mean ecological diversity (6.75). The results of *t*-tests indicate both temperate and cold regions show no statistically significant differences in ecological diversity or disparity (P>0.05; Table S5): relatively high mean ecological disparity and ecological diversity. The results of the two-sample bootstrap tests are consistent with the results of the *t*-tests (Figs. S1-2). Likewise, statistical analyses indicate that the ecological disparity and diversity of the Early Cretaceous mammal communities show some similarities to those in tropical and arid regions, respectively (Figs. S3–6; Table S5).

The cube plots, which graphically illustrate the ecospace occupation of each species in each mammal community, show the ecological differences across the four regions (Fig. 2a–d). In the tropical region, the ecospace occupation of small-bodied mammal communities is tightly

clustered (Fig. 2a), reflecting low ecological disparity; whereas the high density of filled spaces in the cube plot reflects the high ecological diversity. Specifically, the most commonly filled parts of the ecospace are the body mass range from 32–128 g, the omnivore dietary category, and the terrestrial locomotor mode (Fig. 2a, e). In contrast, in the arid region, the ecospace occupation is more scattered and sparsely filled (Fig. 2b), reflecting high ecological disparity but low ecological diversity. There is no apparently dominant category in each ecological trait in arid regions (Fig. 2f). In temperate regions, the ecospace of small-bodied mammal communities is more filled than those in tropical and arid regions. (Fig. 2c), reflecting high ecological disparity and diversity. The most densely filled parts of the ecospace are the body mass range under 32 g, the omnivore dietary category, and the terrestrial locomotor mode (Fig. 2g). The ecological occupation in cold regions is scattered and sparsely filled (Fig. 2d), reflecting high ecological disparity. However, the high density of filled spaces in the cube plot reflects high ecological diversity in cold regions. The environmental models indicate that the differences of the ecological structures (e.g., clustered *versus* scattered) are highly correlated with latitude (for ecological disparity: AICc=-13.061, adjusted r^2=0.651, F=40.13, p<0.000; Tables S6–S7) and annual precipitation (for ecological diversity: AICc=123.566, adjusted r^2=0.322, F=10.99, p=0.003; Tables S8-S9).

The ecological structure of the DJ and JL communities in the Jehol Group (Table S10) differ from extant small-bodied mammal communities (Figs. 3a, S3–S6). The ecological structure of the DJ community was dominated by mammals under 128 g with insectivorous diets (Fig. 3b), whereas the ecological structure of the JL community had a greater number of larger bodied (512–2048g), carnivorous mammals with a scansorial locomotor mode (Fig. 3c). Ecological disparities of the DJ and JL communities (means values 3.62 and 3.27, respectively)

significantly differ from those in arid, temperate and cold regions (p<0.05); the ecological diversities fall in the range of mammalian communities from the arid and temperate regions. Together, the most common ecological traits among the two Early Cretaceous mammal communities are body sizes under 128 g, insectivorous diet, and scansorial locomotor mode (Fig. 3b-c). Using the environmental models derived from the extant small-bodied mammal communities, we would predict the Early Cretaceous mammal communities to have ecological disparity between 3.15 and 3.91 and ecological diversity between 6.23 and 8.31; both of these are fairly close to the observed values (Tables S6, S8). These predictions suggest that the assembled Early Cretaceous mammal communities might resemble a true mammalian community in ecological structure in the Early Cretaceous.

Discussion

Taphonomy undoubtedly influenced the taxonomic and ecological composition of the mammalian fossil assemblages of the Jehol Group; for example, preservation potential may vary with ecological (e.g., aquatic habitats) and morphological (e.g. body size) factors (Behrensmeyer et al., 2000). Thus, we might expect that in our fossil assemblages larger bodied taxa are more commonly preserved than smaller bodied taxa (Valentine et al., 2006). However, Mitchell and Makovicky (2014) found that taphonomy alone failed to explain the ecological vacancies observed in the Jehol avifanua; a relevant finding considering that Jehol mammals and birds have similar body size ranges. Thus, we contend that taphonomic processes may have influenced the ecological structure of two Early Cretaceous mammal communities, but those effects were likely not large enough to produce the differences in ecological structure with the extant small-bodied

mammal communities; those might be best explained by differences in evolutionary ecology and environments.

Differences of evolutionary ecology

The taxonomic compositions of the two Early Cretaceous communities are predominated by eutriconodontans and symmetrodontans, two mammalian groups that have no living descendants (Table S10). Morphologically, eutriconodontans and symmetrodontans have primitive dental morphologies that share few morphological features with tribosphenic molars of therian mammals. They possess either a three-cusp-in-a-line or a three-cusp-in-a-reversed-triangle arrangement. Both of these arrangements are best suited for insectivorous and carnivorous diets (Fig. 3b-c; Kielan-Jaworowska et al., 2004). In therian mammals, the tribosphenic molar allows for the slicing functions of the eutriconodontans and symmetrodontans but also allows for crushing and grinding (Luo et al., 2007). This molar form thus opened up omnivorous and herbivorous dietary niches not available to the eutriconodontans and symmetrodontans. Thus, without numerous therian mammals, the dietary diversity of two Early Cretaceous mammal communities is decreased.

In contrast to the diet, a great diversity of locomotor modes were present in the two Early Cretaceous mammal communities. There were few terrestrial taxa but more specialized taxa (e.g., arboreal and semiaquatic taxa in the DJ and scansorial taxa in the JL)(Fig. 3b-c). These locomotor strategies might increase their survivorship against predation and competition from contemporary vertebrates, such as carnivorous dinosaurs (Stucky, 1990; Matsukawa et al., 2014). Moreover, diverse locomotor modes enable mammals to access food resources in different parts of the environment than other vertebrates that were otherwise similar in body size and diet.

Low dietary but high locomotor diversity suggests that the dietary and locomotor diversification might have been decoupled in the Early Cretaceous. This may have resulted from distinctive ecological pressures imposed on Mesozoic mammals. During the Mesozoic, dinosaurs were the most dominant vertebrates in terrestrial ecosystems and presumably imposed ecological pressures (e.g., predation, competition) on mammals (Stucky, 1990). Likely to avoid predation, most Mesozoic mammals were small in size. This small size and their mostly primitive dental morphologies further constrained Mesozoic mammals to mostly insectivorous diets (e.g., Kielan-Jaworowska et al., 2004). However, small body size did not hinder the morphological evolution of postcranial skeleton. Mesozoic mammals evolved a diverse array of postcranial morphologies reflecting a diversity of locomotor modes, as in extant small-bodied mammals (e.g., Chen and Wilson, 2015). After the removal of non-avian dinosaurs as well as many non-tribosphenic mammals, tribosphenic mammals were released from the previous ecological pressures for small body size and evolved diverse diets for utilizing different food resources. Together, these indicate that the ecological structure of mammalian communities might have undergone a fundamental shift after the removal of non-avian dinosaurs.

Paleoenvironmental influence

Today net primary productivity (NPP) that affects the distribution of food resources on global and local scales and affects the temporal seasonality of food availability. Temperature and precipitation are correlated with latitude (Peel et al., 2007) and NPP (Cramer et al., 1999), suggesting that environmental factors indirectly shape the ecological structure of mammal communities. It follows that environmental factors would have also impacted the ecological structure of Early Cretaceous mammal communities.

In the Early Cretaceous, global climates were generally warm and interrupted by cold intervals (Larson and Erba, 1999; Grocke et al., 2005). However, the Jehol mammal fauna in northeastern China may have experienced a regional environment different from the global average. Wood and dinosaur fossil evidence suggest cold climates persisted in the Early Cretaceous during deposition of the Jehol Group (Amiot et al., 2011; Xu et al., 2012; Zhou, 2014). Sedimentological studies, in contrast, suggest that during deposition of the Jehol Group climates were temperate and humid (Sha et al., 2008; Ohta et al., 2011) with semi-arid climate intervals (Fürsich et al., 2007; Pen and Huang, 2014). Thus, no consensus has been reached on the paleoenvironmental reconstruction of the Jehol Group. However, the discrepancy in paleoenvironmental inferences for the Jehol Group may be the result of temporal and spatial heterogeneity of the paleoenvironment. Taken together, we interpret that climates were temperate to cold during deposition of the Jehol Group in the Early Cretaceous, recognizing that there might have been some diversity of habitats in the Jehol Group (Li and Liu, 1999; Zhu, 2000; Ding et al., 2003a, b; Ding and Zhang, 2004; Zhang et al., 2004; Li, 2010; Zhang et al., 2010). In addition, the occurrences of frequent volcanic eruptions and large lakes have been inferred in the Jehol Group (Faux and Padian, 2007; Pan et al., 2012; Jiang et al., 2014). Frequent volcanic eruption has a great impact on ecosystem (del Moral and Grishin, 1999) and thereby may further partition the paleoenvironments in the Jehol Group into a number of small diverse habitats. Together, these indicate the paleoenvironment of the Early Cretaceous Jehol Group might not be represented in our dataset of extant mammalian communities and thus would be non-analog.

Sampling issues of this study

Well-preserved mammalian fossil fauna are rare, particularly in the Mesozoic. The Jehol Group currently provides our best-sampled mammalian faunas. Still, each locality has yielded less than ten species (Meng et al., 2006), and each of these localities likely represents a unique paleoenvironment from a slightly different time point. Thus, we cannot be certain that the results from DL and JZ communities are generalizable to Mesozoic mammal communities or even Early Cretaceous mammal communities.

Today small-bodied mammal communities from the four climate regions differ in ecological structure. Likewise, Early Cretaceous mammal communities might differ in the same fashion. Moreover, the Jehol Group spans from 131–120 Ma, which might create an enormous number of different habits during the nine-million-year span, each which presumably shaped mammalian communities differently. Together, temporal and spatial differences might create a number of different Mesozoic mammal communities in the Jehol Group. Likewise, this thought process can be applied to all fossil mammal faunas. The most well-documented Late Cretaceous mammal communities are from the Gobi Desert, which had an arid and aeolian paleoenvironment. We might predict this community to have high ecological disparity but low ecological diversity, in contrast to the more tropical Eocene mammal communities, which might be expected to have low ecological disparity but high ecological diversity. Each mammal community represents a snapshot from a specific environment at a particular time, and the comparison of the ecological structures of two communities cannot reflect the evolution of mammal communities from the Late Cretaceous to Eocene. Therefore, the effect of biased sampling of paleoenvironments must be considered when interpreting evolutionary and ecological patterns from the fossil record.

Conclusions

Environmental factors play essential roles in shaping ecological structure of extant small-bodied mammal communities. Extant small-bodied mammal communities worldwide show distinct ecological structures across the four major climate regions. Small-bodied mammal communities in tropical regions have more clustered ecospace occupations, reflected by low ecological disparity and high ecological diversity, in contrast with mammalian communities from arid and cold environments, which have more scattered ecospace occupations as reflected by high ecological disparity and low ecological diversity. The ecological diversity and disparity of the two Early Cretaceous mammal communities are both low, which are comparable to extant small-bodied mammal communities from tropical and arid regions, respectively. Thus, the ecological structure of two Early Cretaceous mammal communities differ from those of extant small-bodied mammal communities. The resulting differences might be primarily due to sampling biases of the fossil record, non-analog Early Cretaceous environments, and/or evolutionary ecology differences of species compositions among extinct and extant mammalian communities.

Acknowledgements

We would like to thank A. Behrensmeyer, I. Breckheimer, L. B. Buckley, D. Grossnikle, J. Hille Ris Lambers, Z.-X. Luo, K. Lyons, C. A. Sidor, and C. A.E. Strömberg for valuable suggestions and discussions. We also thank members of the Wilson Lab (A. Brannick, J. Calede, L. DeBey, D. DeMar Jr., and S. Smith) for discussing earlier ideas of this project. We gratefully acknowledge funding for this project to M.C by the Washington Research Foundation-Hall Fellowship and Burke Museum of Natural History and Culture Vertebrate Paleontology Fellowship and to G.W. and M.C. from the University of Washington Department of Biology.

Literature Cited

Andrews, P., J. M. Lord, and E. M. N. Evans. 1979. Patterns of ecological diversity in fossil and modern mammalian faunas. Biological Journal of the Linnean Society 11:177–205.

Amiot, R., X. Wang, Z. Zhou, X. Wang, E. Buffetaut, C. Lécuyer, Z. Ding, F. Fluteau, T. Hibino, and N. Kusuhashi. 2011. Oxygen isotopes of East Asian dinosaurs reveal exceptionally cold Early Cretaceous climates. Proceedings of the National Academy of Sciences 108:5179–5183.

Badgley, C., and D. L. Fox. 2000. Ecological biogeography of North American mammals: species density and ecological structure in relation to environmental gradients. Journal of Biogeography 27:1437–1467.

Behrensmeyer, A. K., S. M. Kidwell, and R. A. Gastaldo. 2000. Taphonomy and Paleobiology. Paleobiology 26:103–147.

Brusatte, S. L., M. A. Norell, T. D. Carr, G. M. Erickson, J. R. Hutchinson, A. M. Balanoff, G. S. Bever, J. N. Choiniere, P. J. Makovicky, and X. Xu. 2010. Tyrannosaur Paleobiology: New Research on Ancient Exemplar Organisms. Science 329:1481–1485.

Buckley, L. B., T. J. Davies, D. D. Ackerly, N. J. B. Kraft, S. P. Harrison, B. L. Anacker, H. V. Cornell, E. I. Damschen, J. A. Grytnes, B. A. Hawkins, C. M. McCain, P. R. Stephens, and J. J. Wiens. 2010. Phylogeny, niche conservatism and the latitudinal diversity gradient in mammals. Proceedings of the Royal Society B: Biological Sciences 277:2131–2138.

Campione, N. E., and D. C. Evans. 2012. A universal scaling relationship between bodymass and proximal limb bone dimensions inquadrupedal terrestrial tetrapods. BMC Biology 10:60.

Chang, M.-M., P.-J. Chen, Y.-Q. Wang, and Y. Wang. 2003. The Jehol Biota: the emergence of feathered dinosaurs, beak birds and flowering plants. Shanghai Scientific and Technical Publishers: Shanghai.

Chen, M., and G. P. Wilson. 2015. A multivariate approach to infer locomotor modes in Mesozoic mammals. Paleobiology DOI: 10.1017/pab.2014.14.

Cooper, N., R. P. Freckleton, and W. Jetz. 2011. Phylogenetic conservatism of environmental niches in mammals. Proceedings of the Royal Society B: Biological Sciences 278:2384–2391.

Cox, C. B., and P. D. Moore. 1985. Biogeography: an ecological and evolutionary approach, 4th Ed. Blackwell, Oxford.

Cramer, W., D. W. Kicklighter, A. Bondeau, B. Moore, G. Churkina, B. Nemry, A. Ruimy, and A. L. Schloss. 1999. Intercomparison, the Participants of the Potsdam NPP Model. Comparing Global Models of Terrestrial Net Primary Productivity (NPP): Overview and Key Results. Global Change Biology 5(Suppl. 1):1–15.

Damuth, J. D., and B. J. McFadden. 1990. Body Size in Mammalian Paleobiology: Estimation and Biological Implications, Cambridge University Press.

Davies, T. J., and L. B. Buckley. 2011. Phylogenetic diversity as a window into the evolutionary and biogeographic histories of present-day richness gradients for mammals. Philosophical Transactions of the Royal Society B 366:2414–2425.

Davies, T. J., L. B. Buckley, R. Grenyer, and J. L. Gittleman. 2011. The influence of past and present climate on the biogeography of modern mammal diversity. Philosophical Transactions of the Royal Society B: Biological Sciences 366:2526–2535.

Ding, Q.-H., and L.-D. Zhang. 2004. Spore-pollen flora as the indicator of paleoclimate condition in the Yixian Formation, western Liaoning Province. Acta Micropalaeontologica Sinica 21:332–341. (In Chinese with English abstract)

Ding, Q.-H., L.-D. Zhang, S.-Z. Guo, C.-J. Zhang, Y.-D. Peng, B. Jia, S.-W. Chen, and D.-H. Xing. 2003a. Paleoclimatic and palaeoenvironmental proxies of the Yixian Formation in the Beipiao area, western Liaoning. Geological Bulletin of China 22:186–191. (In Chinese with English abstract)

Ding, Q.-H., L.-D. Zhang, S.-Z. Guo, C.-J. Zhang, Y.-D. Peng, B. Jia, S.-W. Chen, and D.-H. Xing. 2003b. Study on the paleoecology of Yixian Formation in Beipiao area, western Liaoning province, China. Geology and Resources 12:9–18. (In Chinese with English abstract)

Eisenberg, J. F. 1981. The mammalian radiations, University of Chicago Press, Chicago, IL.

Enkin, R. J., Z. Yang, Y. Chen, and V. Courtillot. 1992. Paleomagnetic constraints on the geodynamic history of the major blocks of China from the Permian to the present. Journal of Geophysical Research: Solid Earth (1978–2012) 97:13953–13989.

Evans, A. R., G. P. Wilson, M. Fortelius, and J. Jernvall. 2007. High-level similarity of dentitions in carnivorans and rodents. Nature 445:78–81.

Faux, C. M. and K. Padian. 2007. The opisthotonic posture of vertebrate skeletons: postmortem contraction or death throes? Paleobiology 33:201–26.

Fleming, T. H. 1973. Numbers of mammal species in North and Central American forest communities. Ecology 54:555–563.

Foster, J. R. 2009. Preliminary body mass estimates for mammalian genera of the Morrison Formation (Upper Jurassic, North America). PaleoBios 28:114–122.

Fürsich, F. T., J. Sha, B. Jiang, and Y. Pan. 2007. High resolution palaeoecological and taphonomic analysis of Early Cretaceous lake Group, western Liaoning (NE-China). Palaeogeography Palaeoclimatology Palaeoecology 253:434–457.

Grocke, D. R., G. D. Price, S. A. Robinson, E. Y. Baraboshkin, J. Mutterlose, and A. H. Ruffell. 2005. The Upper Valanginian (Early Cretaceous) positive carbon-isotope event recorded in terrestrial plants. Earth and Planetary Science Letter 40:495–509.

Grossnickle, D. M., and P. D. Polly, P. D. 2013. Mammal disparity decreases during the Cretaceous angiosperm radiation. Proceedings of the Royal Society B: Biological Sciences 280:20132110.

Hawkins, B. A., C. M. McCain, T. J. Davies, L. B. Buckley, B. L. Anacker, H. V. Cornell, E. I. Damschen, J.-A. Grytnes, S. Harrison, R. D. Holt, N. J. B. Kraft, and P. R. Stephens. 2011. Different evolutionary histories underlie congruent species richness gradients of birds and mammals. Journal of Biogeography 39:825–841.

Hu, Y.-M., J. Meng, Y.-Q. Wang, and C.-K. Li. 2005. Large Mesozoic mammals fed on young dinosaurs. Nature 433:149–152.

Jiang, B.-Y., F. T. Fürsich, and M. Hethke. 2012. Depositional evolution of the Early Cretaceous Sihetun Lake and implications for regional climatic and volcanic history in western Liaoning, NE China. Sedimentary Geology 257:31–44.

Jiang, B.-Y., G. E. Harlow, K. Wohletz, Z.-H. Zhou, and J. Meng. 2014. New evidence suggests pyroclastic flows are responsible for the remarkable preservation of the Jehol biota. Nature Communications 5:3151.

Jernvall, J., J. P. Hunter, and M. Fortelius. 1996. Molar Tooth Diversity, Disparity, and Ecology in Cenozoic Ungulate Radiations. Science 274:1489–1492.

Kielan-Jaworowska, Z., R. L. Cifelli, and Z.-X. Luo. 2004. Mammals from the age of dinosaurs: origins, evolution, and structure. Columbia University Press, New York.

Kingdon, J. 1997. The Kingdon field guide to African mammals. Academic Press, San Diego.

Kowalewski, M., and P. Novack-Gottshall. 2010. Resampling methods in paleontology. Pp. 19–54 in J. Alroy and G. Hunt, eds. Quantitative methods in paleobiology. The Paleotological Society, Chicago, Illinois.

Larson, R. L., and E. Erba. 1999. Onset of the mid-Cretaceous greenhouse in the Barremian-Aptian: igneous events and the biological, sedimentary, and geo- chemical responses. Paleoceanography 14:663–78.

Li, W.-B. 2010. Palynological assemblage from the Zhuangchengzi Beds of Yixian Formation in Jinjiagou, Yixian. Acta Palaeontologica Sinica 49:44–53. (In Chinese with English abstract)

Li, W.-B., and Z.-Z. Liu. 1999. Sporomorph assemblage from the basal Yixian Formation in western Liaoning and its geological age. Palaeoworld 11:68–79. (In Chinese with English abstract)

Lillegraven, J. A., Z. Kielan-Jaworowska, and W. A. Clemens. 1979. Mesozoic mammals: the first two-thirds of mammalian history. University of California Press, Berkeley.

Luo, Z.-X. 2007. Transformation and diversification in early mammal evolution. Nature 450:1011–1019.

Luo, Z.-X., Q. Ji, and C.-X. Yuan. 2007. Convergent dental adaptations in pseudo-tribosphenic and tribosphenic mammals. Nature 450:93–97.

Matsukawa, M., K. Shibata, K. Sato, X.-U. Xing, and M. G. Lockley. 2014. The Early Cretaceous terrestrial ecosystems of the Jehol Group based on food-web and energy-flow models. Biological Journal of the Linnean Society 113:836–853.

Mantel, N. 1967. The detection of disease clustering and a generalized regression approach. Cancer Research 27:209–220.

Meng, J. 2014. Mesozoic mammals of China: implications for phylogeny and early evolution of mammals. National Science Review 1:521–542.

Meng, J., Y.-M. Hu, C.-K. Li, and Y.-Q. Wang. 2006. The mammal fauna in the Early Cretaceous Jehol Biota: implications for diversity and biology of Mesozoic mammals. Geological Journal 41:439–463.

Merritt, J. F. 2010. The biology of small mammals. Johns Hopkins University Press, Baltimore.

McCann, K. S. 2000. The diversity–stability debate. Nature 405:228–233.

McNab, B. K. 1990. The physiological significance of body size. Pp. 11–23 in Damuth and MacFadden 1990.

Mitchell, J. S., and P. J. Makovicky. 2014. Low ecological disparity in Early Cretaceous birds. Proceedings of the Royal Society B: Biological Sciences 281:20140608–20140608.

del Moral, R., and S. Y. Grishin. 1999. Volcanic disturbances and ecosystem recovery. Pp. 137-160 in L. R. Wale, ed. Ecosystems of disturbed ground. Elsevier Science, Amsterdam, Netherlands.

Nowak, R. M. 1999. Walker's mammals of the World. Johns Hopkins University Press.

Ohta, T., G. Li, H. Hirano, T. Sakai, T. Kozai, T. Yoshikawa, and A. Kaneko. 2011. Early Cretaceous Terrestrial Weathering in Northern China: Relationship between Paleoclimate

Change and the Phased Evolution of the Jehol Group. The Journal of Geology 119:81–96.

Pan, Y.-H., J.-G. Sha, F. T. Fürsich, Y.-Q. Wang, X.-L. Zhang, and X.-G Yao. 2012. Dynamics of the lacustrine fauna from the Early Cretaceous Yixian Formation, China: implications of volcanic and climatic factors. Lethaia 45:299–314.

Pan, Y.-Y., and C.-M. Huang. 2014. Quantitative reconstruction of early cretaceous paleoclimate using paleosol carbonates in China. Carbonates Evaporites 29:327–335.

Peel, M. C., B. L. Finlayson, and T. A. McMahon. 2007. Updated world map of the Köppen-Geiger climate classification. Hydrology and Earth System Sciences Discussions 4:439–473.

Sha, J.-G., H. Hirano, X. Yao, and Y. Pan. 2008. Late Mesozoic transgressions of eastern Heilongjiang and their significance in tectonics, and coal and oil accumulation in northeastern China. Palaeogeography, Palaeoclimatology, Palaeoecology 263:119–130.

Simpson, G. G. 1937. The beginning of the age of mammals. Biological Reviews 12:1-46.

Stucky, R. K. 1990. Evolution of land mammal diversity in North America during the Cenozoic. Current Mammalogy 2:375–432.

Valentine, J. W., D. Jablonski, S. M. Kidwell, and K. Roy. 2006. Assessing the fidelity of the fossil record by using marine bivalves. Proceedings of the National Academy of Sciences 103:6599–6604.

Van Valen, L., and R. E. Sloan. 1977. Contemporaneity of late Cretaceous extinctions. Nature 270:193.

Van Valkenburgh, B. 1994. Ecomorphological analysis of fossil vertebrates and their paleocommunities. Pp.140–166 in Ecological Morphology: Integrative Organismal Biology. Wainwright and Reilly, eds. The University of Chicago Press, Chicago, IL.

Walther, G.-R., E. Post, P. Convey, A. Menzel, C. Parmesan, T. J. Beebee, J.-M. Fromentin, O. Hoegh-Guldberg, and F. Bairlein. 2002. Ecological responses to recent climate change. Nature 416:389–395.

Whittaker, R. H. 1975. Communities and ecosystems, 2nd Ed. Macmillan, New York, NY.

Wilson, G. P. 2013. Mammals across the K/Pg boundary in northeastern Montana, U.S.A.: dental morphology and body-size patterns reveal extinction selectivity and immigrant-fueled ecospace filling. Paleobiology 39:429–469.

Wilson, G. P., A. R. Evans, I. J. Corfe, P. D. Smits, M. Fortelius, and J. Jernvall. 2012. Adaptive radiation of multituberculate mammals before the extinction of dinosaurs. Nature 483:457–460.

Xu, X., K.-B. Wang, K. Zhang, Q.-Y. Ma, L.-D. Xing, C. Sullivan, D.-Y. Hu, S.-Q. Cheng, and S. Wang. 2012. A gigantic feathered dinosaur from the Lower Cretaceous of China.Nature 484:92–95.

Zhang, H.-C., B. Wang, and Y. Fang. 2010. Evolution of insect diversity in the Jehol Group. Science China Earth Sciences 53:1908–1917.

Zhang, L.-D., C.-Z. Jin, S.-Z. Guo, C.-J. Zhang, Y.-D. Peng, S.-W. Chen, D.-H. Xing, Q.-H. Ding and Y.-J. Zheng. 2004. The precious fossil-bearing beds of Yixian Formation in Beripiao-Yixian area: their ages and correlation. Geology and Resources 13:193–201. (In Chinese with English abstract)

Zhou, Z.-H. 2006. Evolutionary radiation of the Jehol Biota: chronological and ecological perspectives. Geological Journal 41:377–393.

Zhou, Z.-H, and Y. Wang. 2010. Vertebrate diversity of the Jehol Biota as compared with other lagerstätten. Science China Earth Sciences 53:1894–1907.

Zhou, Z., P. M. Barrett, and J. Hilton. 2003. An exceptionally preserved Lower Cretaceous ecosystem. Nature 421:807–814.

Zhou, Z.-H. 2014. The Jehol Group, an Early Cretaceous terrestrial Lagerstatte: new discoveries and implications. National Science Review 1:543–559.

Zhu, W.-Q. 2000. Preliminary studies on the palaeoclimate in Yixian Formation, western Liaoning Province, China. Chinese Bulletin of Botany 17:292–294. (In Chinese with English abstract)

Figures

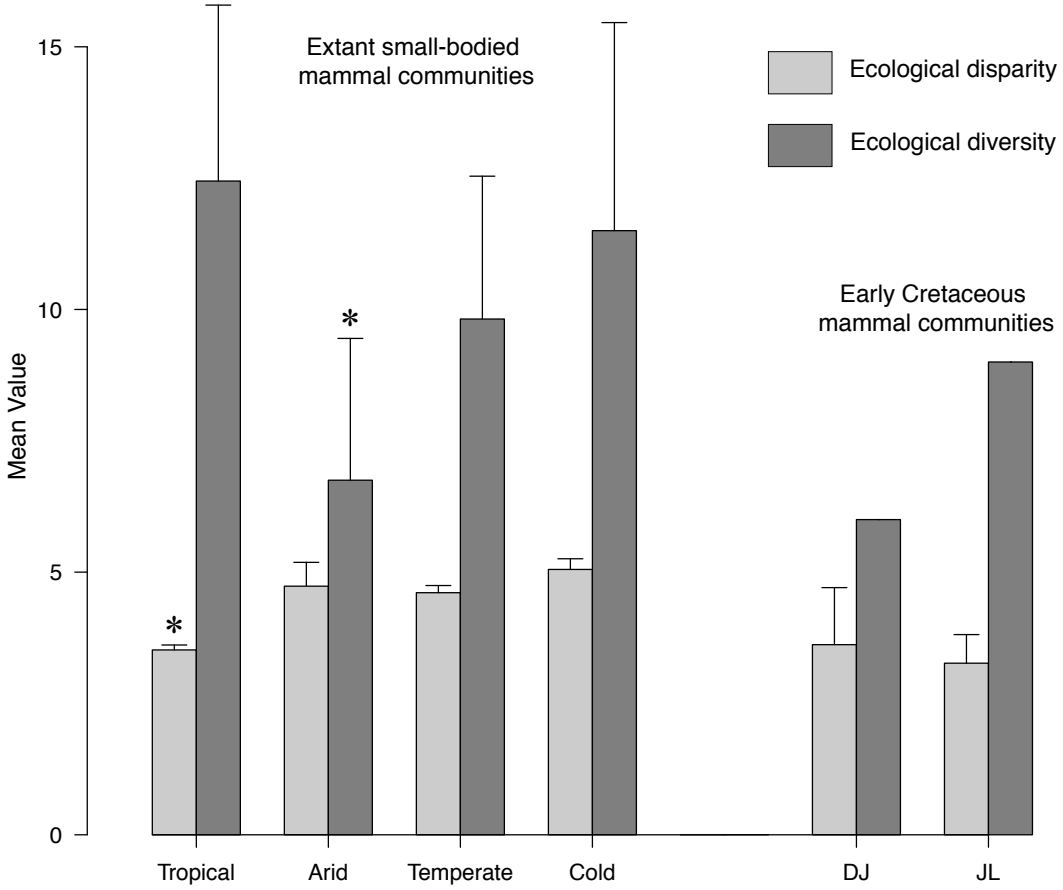

Figure 1. Ecological structures (ecological disparity and ecological diversity) of two Early Cretaceous and 28 extant small-bodied mammal communities. Extant small-bodied mammal communities have been divided into tropical, arid, temperate, cold regions (see Materials and Methods). Abbreviations: DJ, Dawangzhangzi-Jiufotang community; JL, Jianshangou-Lujiatun community. Asterisk refers to that the ecological disparity or ecological diversity in the specific climate region is significantly different from in others (p<0.05).

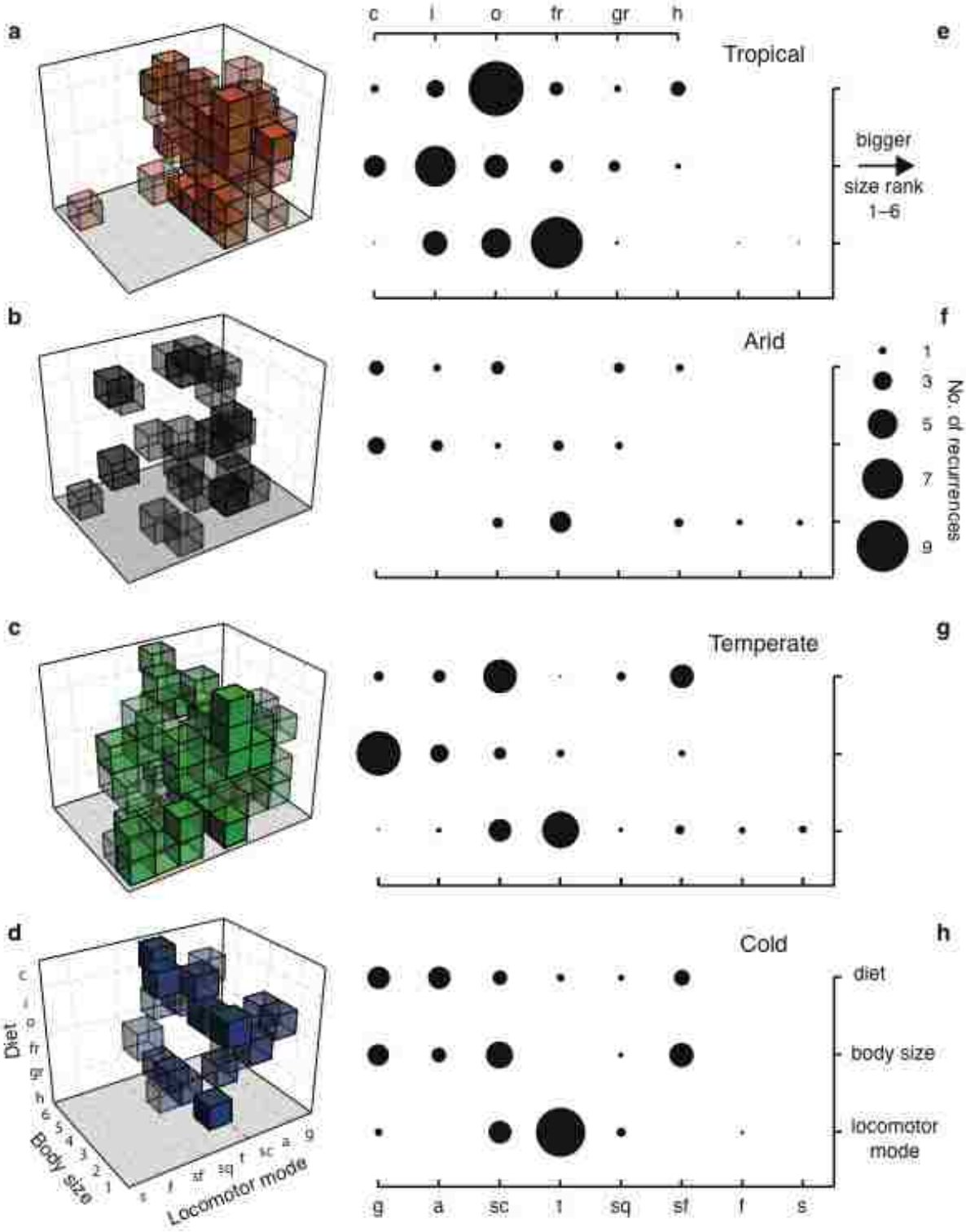
a
b
c
d
e
f
g
h
c
i
o
fr
gr
h
Tropical
bigger
size rank
1–6
Arid
No. of recurrences
1
3
5
7
9
Temperate
Cold
diet
body size
locomotor
mode
g
a
sc
t
sq
sf
f
s
Diet
Body size
Locomotor mode

Figure 2. Three-dimensional cube plots of ecological structures and descriptive plots of ecological traits of 28 extant small-bodied mammal communities from four climate regions. **a-d**, structures of ecological structures of extant small-bodied mammal communities in four climate regions using three ecological traits (body size, diet, and locomotor mode). **e-h**, comparisons of different categories within each ecological trait across four climate regions. Dark color refers recurrence of the ecological structures; the darker the cube is, the more the recurrences are. Circle size refers to the mean number of the recurrence of the category of each ecological trait. The larger size of the circle, the more dominate within the ecological trait.

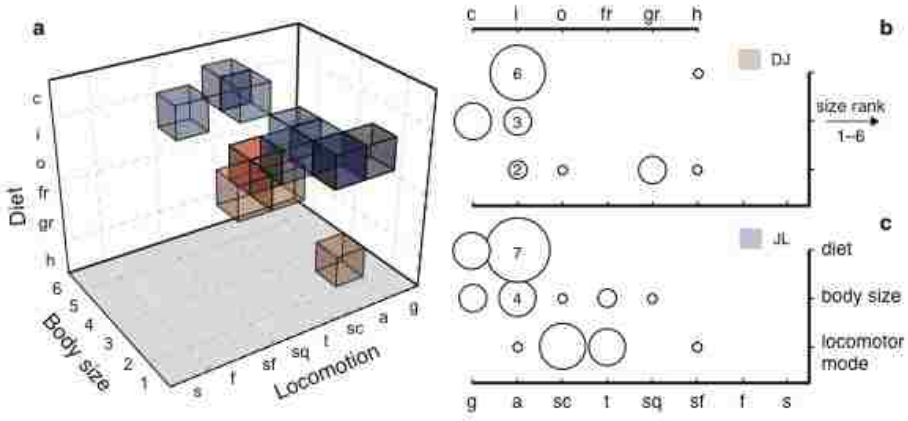

Figure 3. Ecological structures of two Early Cretaceous mammal communities. DJ, Dawangzhangzi-Jiufotang community; JL, Jianshangou-Lujiatun community. **a**, three-dimensional plots of ecological structures of two Early Cretaceous mammal communities; **b-c**, comparisons of different categories within each ecological trait across four climate regions. Dark color refers recurrence of the ecological structures; the darker the cube is, the more the recurrences are. The number inside cycle refers to the number of recurrences of the category of each ecological trait.

Supplementary Materials

For

"The non-analog ecological structure of Early Cretaceous Jehol mammal communities"

Meng Chen[a,b] and Gregory P. Wilson[a,b]

[a] Department of Biology, University of Washington, Box 351800, Seattle WA 98195-1800, USA

[b] Department of Geology, Burke Museum of Natural History and Culture, Box 353010, Seattle WA 98195-0001, USA

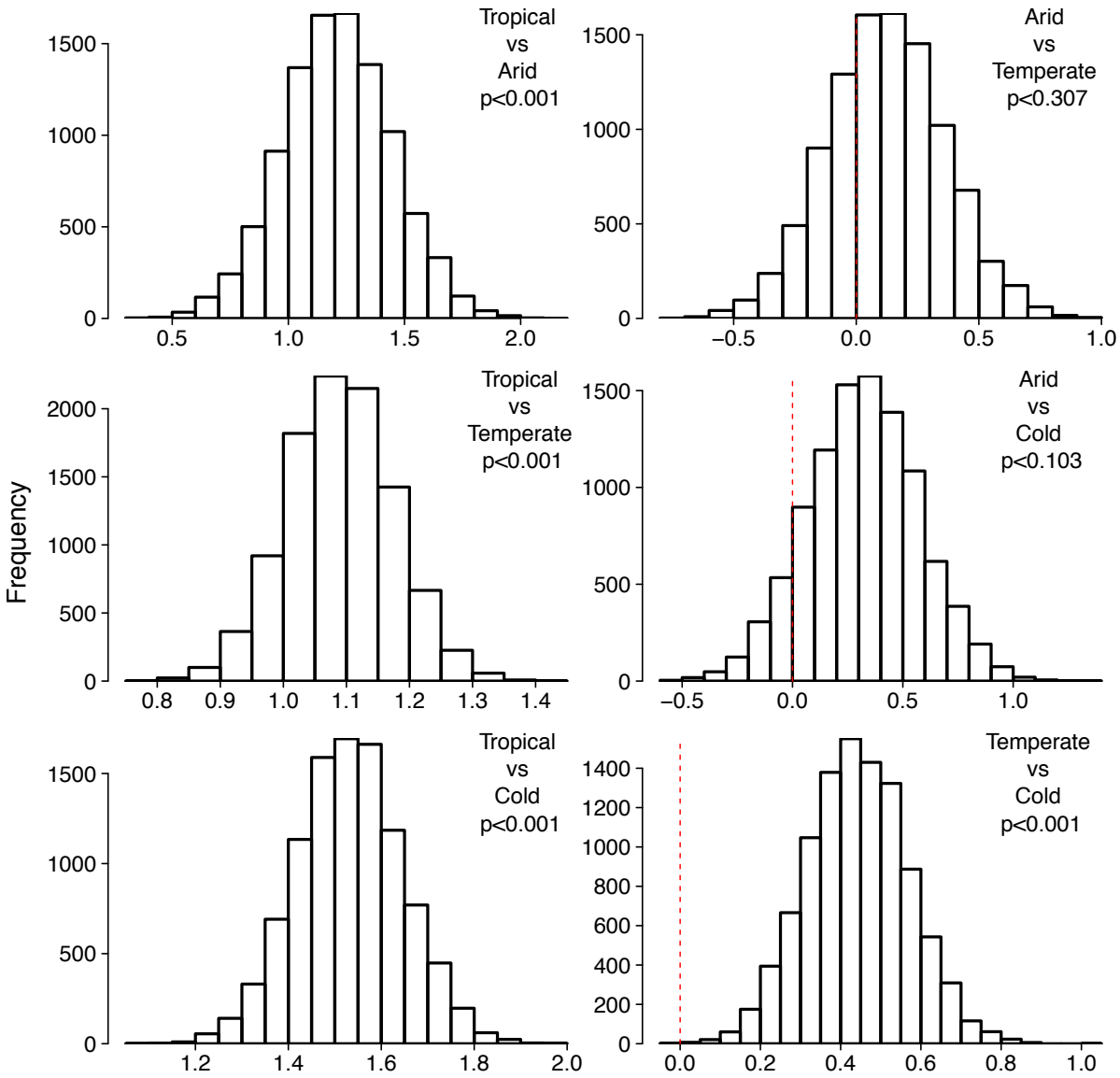

Figure S1 Two−sample Bootstrap Test of Ecological Disparity

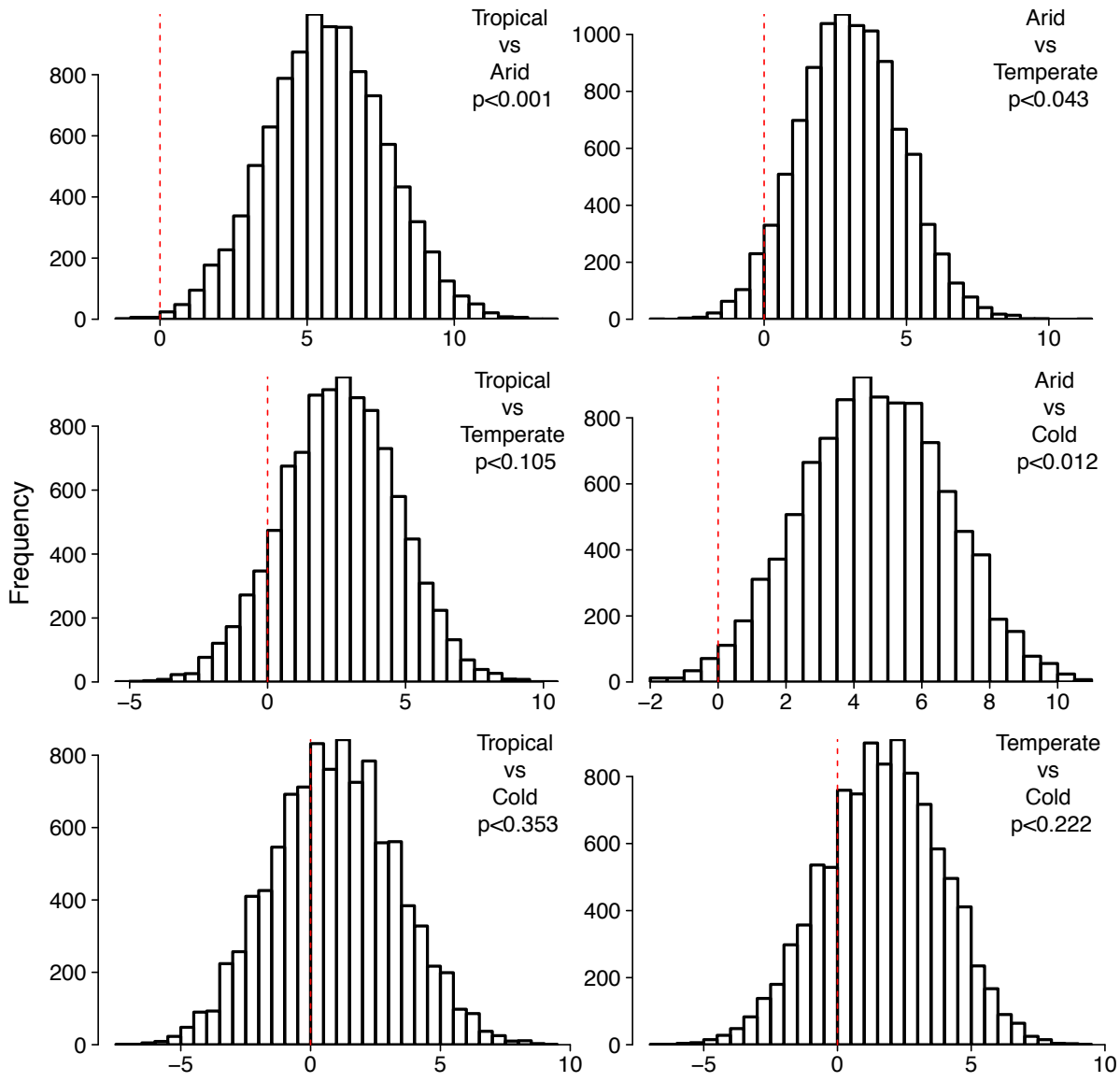

Figure S2 Two−sample Bootstrap Test of Ecological Diversity

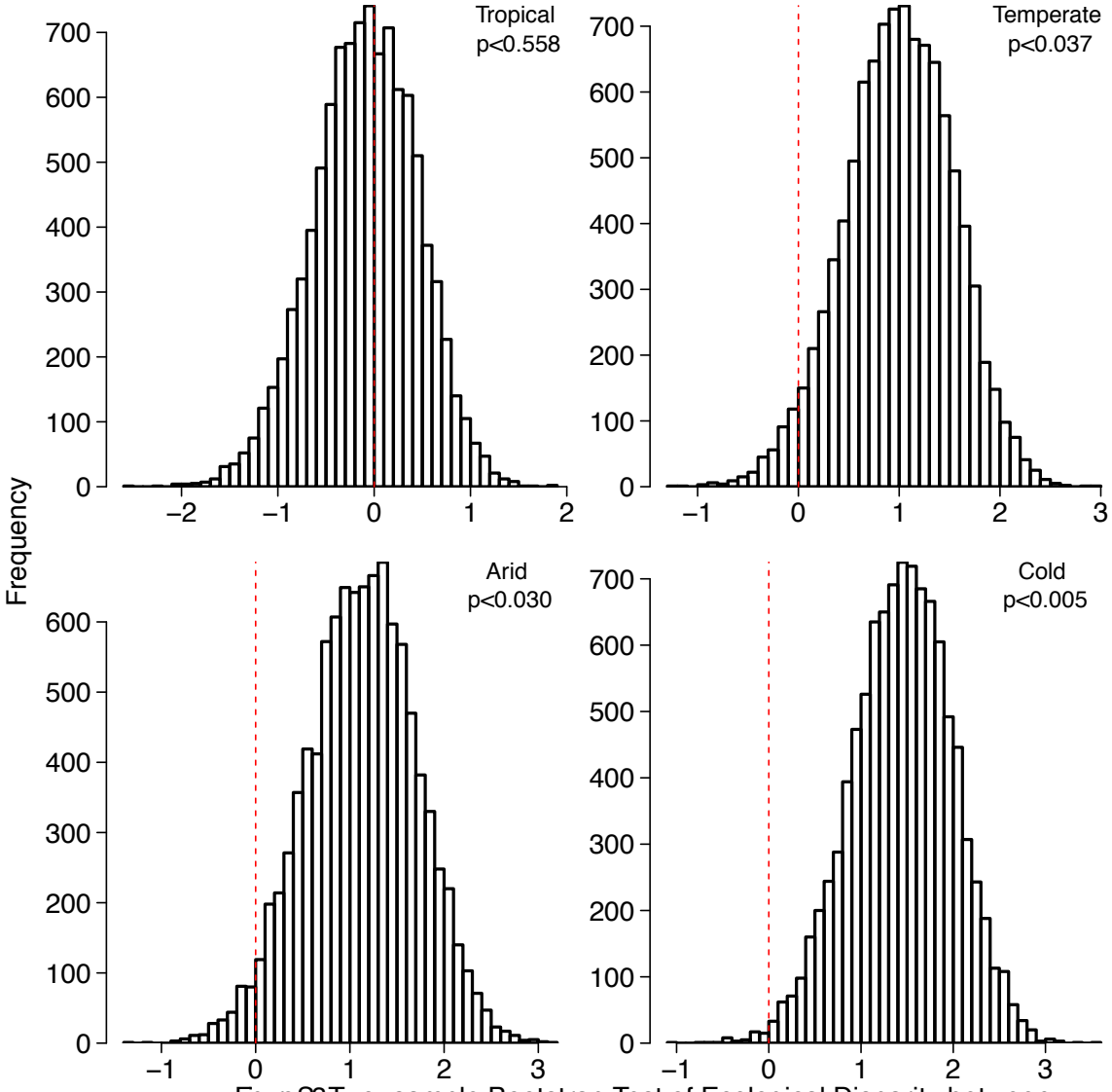

Figure S3 Two−sample Bootstrap Test of Ecological Disparity between Extant and Extinct Mammals (DJ)

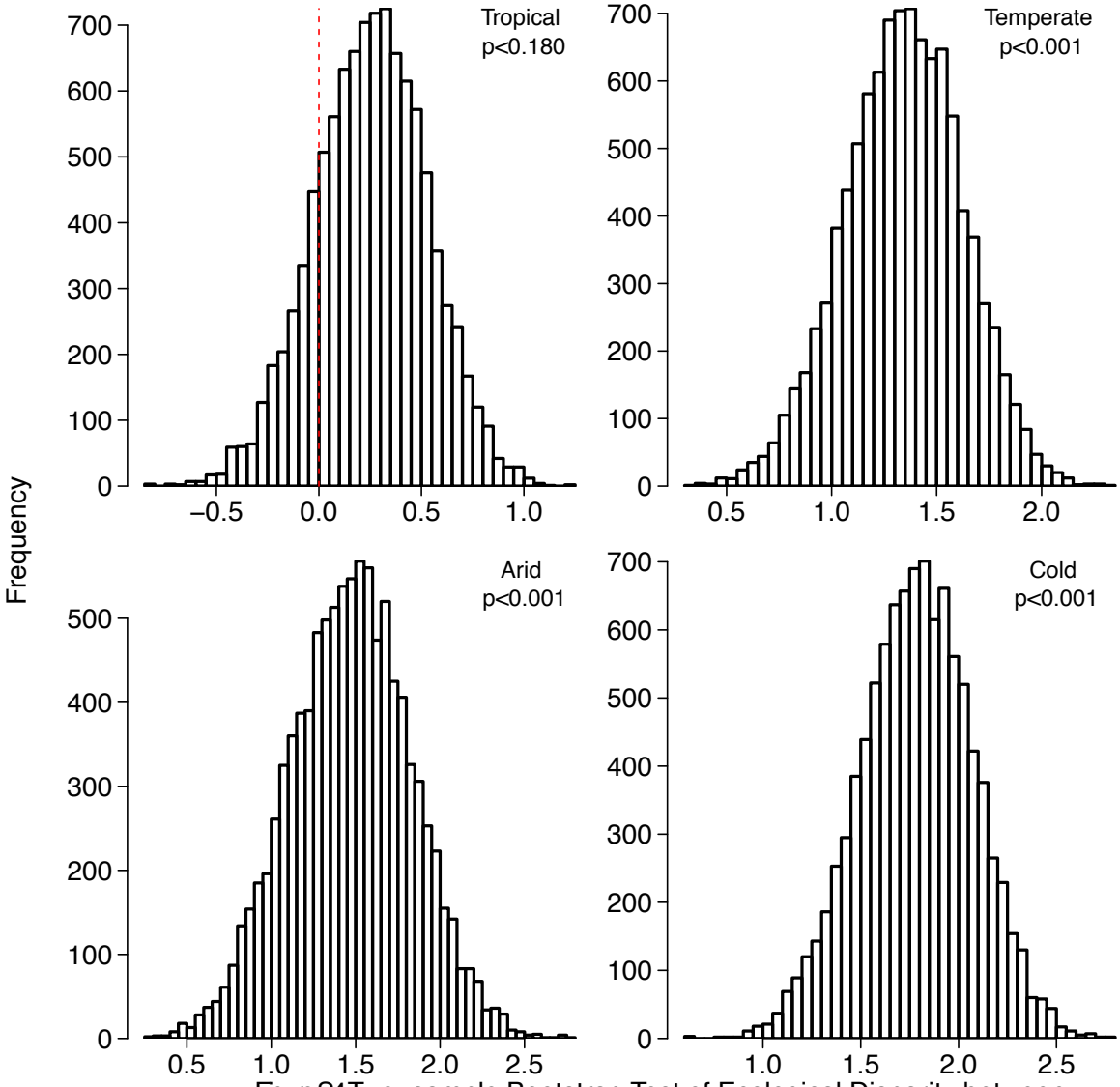

Figure S4 Two–sample Bootstrap Test of Ecological Disparity between Extant and Extinct Mammals (JL)

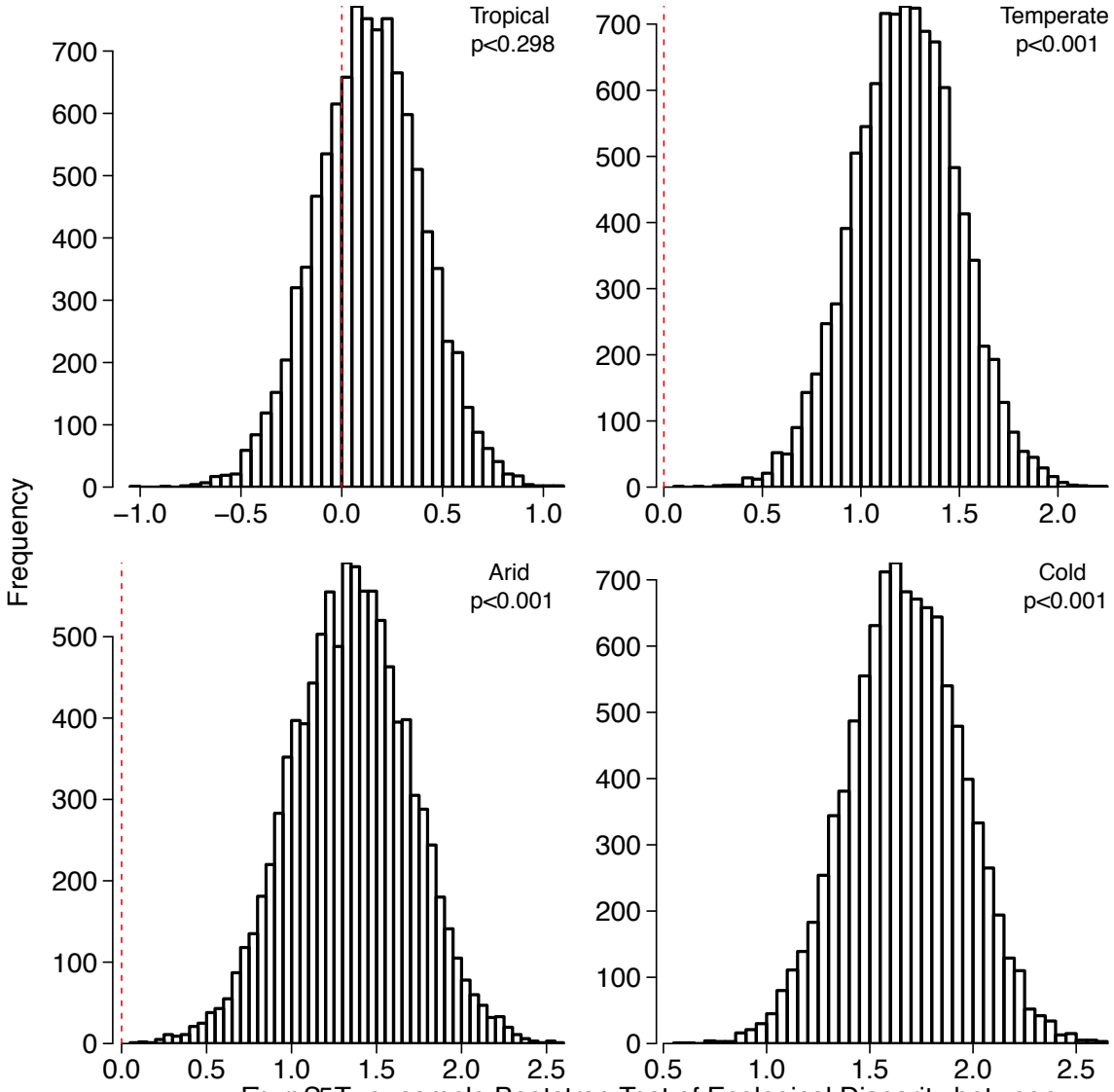

Figure S5 Two−sample Bootstrap Test of Ecological Disparity between Extant and Extinct Mammals

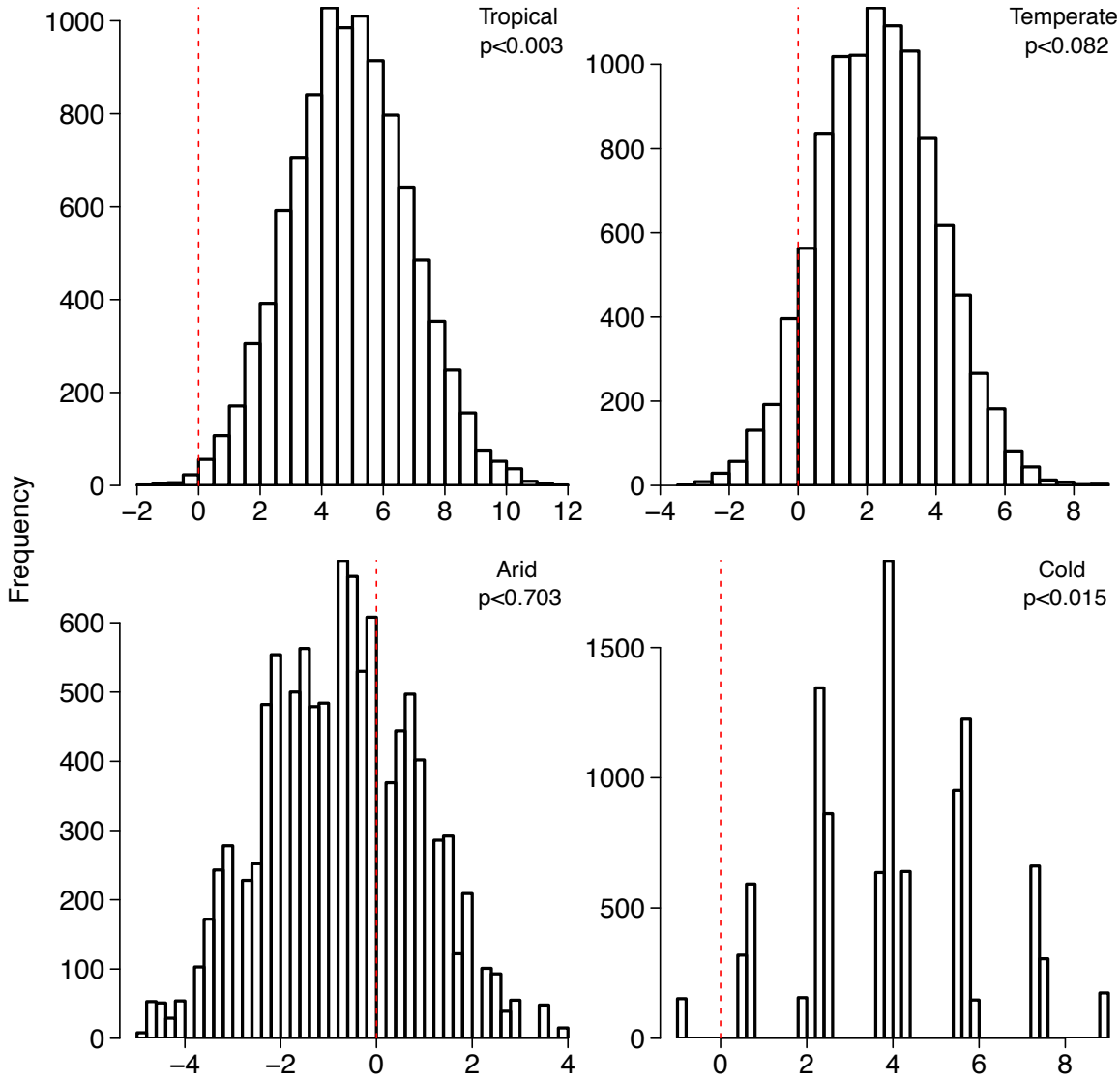

Figure S6 Two−sample Bootstrap Test of Ecological Diveristy between Extant and Extinct Mammals

Table S1 List of small-bodied mammal communities sampled in this study

No.	Community	Longitude	Latitude	MAT (°C)	ATP (mm)	CC	NS	Reference
1	Fairbanks, AK, US	147°42’59.00” W*	64°50’16.00” N*	-5.6	289.7	431	8	13, 17
2	Seward Peninsula, AK, US	165°26’23.9994” W*	64°30’39.599” N*	-5.11^{+} (1948)	500.63^{+} (1948)	433	13	17, 34
3	Olympic Peninsula, WA, US	124°23’40.05” W*	47°57’39.56” N*	9.89^{+} (1988)	2515.4^{+} (1988)	332	14	7
4	Charlevoix County, MI, US	85°15’30.24” W*	45°19’05.03” N*	–	–	432	20	6, 14, 17
5	Ann Arbor or Warren Woods, MI, US	83°48’58.12” W*	42°25’53.26” N*	–	–	432	18	6, 11, 13, 17
6	Wirlwind Valley, NV, US	116°42’53.18” W*	40°49’58.68” N*	6.56^{+} (1982)	472.2^{+} (1982)	222	10	31
7	Herdade da Mitra, Évora, Portugal	7°58’04.71” W*	38°33’32.76” N*			311	3	27
8	Fort A. P. Hill, VA, US	77°16’36.35” W*	38°07’06.04” N*	12.83^{+} (1997)	1060.5^{+} (1997)	331	9	5
9	North slope of Mt Qilian, China	96°31’-103°10’ E	36°45’- 39°30’ N	2.57	309	333	18	23
10	Ningxia, China	105.68 E, 106.19 E, 106.13 E	35.92 N, 35.67 N, 35.93 N	6.50$^{\#}$	332$^{\#}$	312	17	35
11	Great Smoky Mountains, TN, US	83°32’43.02” W*	35°36’43.02” N*	–	–	331	18	17, 21
12	Big black mountain, KY, US	82°18’02.80” W*	35°35’24.93” N*	–	1214.4^{+} (1948)	331	27	3
13	Western Sichun, China	102°12’54.76” E*	31°55’36.68” N*	7.2$^{\#}$	832.9$^{\#}$	323	14	37
14	Khao Nang Rum Research Station, Thailand	99.00’-99.30’ E	15.00’-15.45’ N	24.3$^{\#}$	1500	120	10	38
15	Indira Gandhi Wildlife Sanctuary, India	76°44’-77°48’ E	10°12’-10°54’ N	23$^{\#}$	1800	130	5	10
16	Cristobal, Panama Canal Zone	79°50’02.94” W*	9°16’48.35” N*	26.7	2375$^{\#}$	120	28	15, 16
17	Balboa, Panama Canal Zone	79°29’17.23” W*	8°54’45.10” N*	26.7	2375$^{\#}$	120	30	15, 16
18	Kinabalu National Park, Malaysia	116°33’ E	6°5’ N	20 (30)	2788 (20)	110	19	20, 30, 40
19	Lambir Hills National Park, Malaysia	113°5’ E	4°2’ N	27 (22)	2740 (22)	110	22	22, 29
20	Katavi National Park, Tanzania	30’45’- 31’25’E	6’45’-7”05’S	18 (9)	950	130	12	8, 9
21	Cerrado, Brazil	47°53’ W	15°56’ S	20 (33)	1375$^{\#}$	120	26	24, 33
22	Atherton Tableland, Australia	145°32’ E	17°50’ S	–	2500	110	10	41
23	South-western Kalahari, Botswana	21° 40’ E	24° 04’ S	20$^{\#}$ (36)	359	221	12	36, 39
24	eKundizei Farm, Swaziland	31°16’ E	26°33’ S	17.5$^{\#}$	928	321	8	28
25	Parque Estadual do Turvo, Brazil	53° 40’ W 54°10’ W	27°00’ S 27°20’ S	15$^{\#}$	1900 (4)	331	12	4, 25
26	Namaqua National Park, South Africa	17°47'53" E	30°09'57" S	17$^{\#}$	332.8	222	5	12
27	Parque Nacional Fray Jorge, Coquimbo, Chile	71°40' W	30°38' S	13.9$^{\#}$ (2)	127	212	4	2, 26
28	Fundo San Carlos de Apoquindo, Los Dominicos, Chile	70°31' W	33°23' S	15.9 (18)	376.4 (18)	312	6	18, 19

29	Jehol Biota, northeastern China	110° E*	41.9±6.6° N (1)	10±4 (1); 11.9 (32)	310.6 (32)	15	1, 32

Abbreviation: * Estimated longitudinal and latitudinal coordinates; +, NOAA data; #, calculated based on data presented in paper; CC, climatic code; MAT, mean annual temperature; NS, number of species; ATP, annual total precipitation.

References: 1, Amiot et al. 2011; 2, Barbosa and Marquet 2002; 3, Barbour 1951; 4, Barcellos et al 2008; 5, Bellows et al 2001; 6, Burt 1954; 7, Carey and Johnson 1995; 8, Caro 2002; 9, Celesia et al 2009; 10, Chandrasekar-Rao and Sunquist 1996; 11, Davis 1925; 12, Deventer and Nel 2006; 13, Dice 1920; 14, Dice 1925; 15, Fleming 1970; 16, Fleming 1972; 17, Fleming 1973; 18, Jaksic 2001; 19, Jaksić et al 1981; 20, Kitayama 1992; 21, Komarek and Komarek 1938; 22, Kumagai et al 2005; 23, Li et al 2003; 24, Mares et al 1986; 25, Melo et al 2011; 26, Meserve 1981; 27, Mira and Mathias 2003; 28, Monadjem and Perrrin 1998; 29, Nakagawa et al 2006; 30, Nor 2001; 31, O'Farrell and Clark 1986; 32, Pan and Huang 2013; 33, Pinheiro et al 2002; 34, Quay 1951; 35, Raoul et al 2008; 36, Scholes et al 2002; 37, Vaniscotte et al 2009; 38, Walker and Rabinowitz 1992; 39, Wallgren et al 2008; 40, Wells et al 2004; 41, Williams et al 2005.

Table S2 Ordinal variables of three functional traits of small-bodied mammals

Ordinal variable	Body size (g)	Diet	Locomotor mode
1	0 – 32	Carnivore	Gliding
2	33 –128	Insectivore	Arboreal
3	129 – 512	Omnivore	Scansorial
4	513 – 2048	Fruigvore	Terrestrial
5	2049 – 4096	Granivore	Semiaquatic
6	> 4096	Herbivore	Semifossorial
7	–	–	Fossorial
8	–	–	Saltatorial

Table S3 Functional differences of small-bodied mammal communities among tropical, arid, temperate, and cold climate regions

Functional Group	χ^2	df	*P* value
Body size	94.0389	15	<0.001
Diet	178.7266	15	<0.001
Locomotor mode	192.9836	21	<0.001

Table S4 Descriptive statistics for ecological disparity among different climate regions

CR	N	Mean	SE	Median	SD	Kurtosis	Skewness
Global	3541	4.126405	0.03842	4.00	2.28643	-0.02284	0.37732
Tropical	1762	3.519012	0.04786	3.00	2.00901	1.58918	0.72119
Arid	127	4.732283	0.23141	5.00	2.60783	-0.51715	0.35281
Temperate	1203	4.608479	0.06963	5.00	2.41513	-0.56069	0.01413
Cold	449	5.051225	0.10362	5.00	2.19569	-0.67130	-0.13444

Abbreviation: CR, climate region; N, number of pair-wise ecological disparity; SD, standard deviation; SE, standard error.

Table S5 Pair-wise student test of ecological disparity and ecological diversity across extant and Mesozoic mammal communities

Disparity / Diversity	Extant small-bodied mammal communities				Mesozoic mammal communities	
Climate	Tropical	Arid	Temperate	Cold	JD	JL
Tropical	-	**-5.13, 136.99, <0.01**	**-12.89, 2261.49, <0.01**	**-13.42, 651.99, <0.01**	-0.18, 20.30, 0.86	0.90, 46.65, 0.38
Arid	**2.59, 10.24, 0.03**	-	0.51, 149.72, 0.61	-1.26, 179.56, 0.21	1.85, 27.45, 0.07	**4.05, 108.08, <0.01**
Temperate	1.193, 16.34, 0.25	-1.57, 9.30, 0.15	-	**-3.55, 877.28, <0.01**	1.77, 20.64, 0.09	**4.69, 49.70, <0.01**
Cold	0.36, 7.40, 0.73	-1.94, 5.29, 0.11	-0.69, 6.09, 0.52	-	**2.54, 21.42, 0.02**	**6.02, 56.99, <0.01**
DJ	-	-	-	-	-	0.57, 30.44, 0.57
JL	-	-	-	-	-	-

Three numbers refer to t, df, and p values sequentially. Bold fonts indicates statistical significant.

Table S6 Comparison of different regression models for explanation of ecological disparity of extant small-bodied mammal communities

No	Predictors	AICc	Adjusted r^2	F-test (*p*-value)	Predicted ED
1	Latitude	-13.061	0.651	40.13 (0.000)	3.76
2	Longitude	3.968	0.243	7.728 (0.012)	3.40
3	MAT	-10.030	0.599	32.39 (0.000)	3.91
4	APT	7.521	0.110	3.593 (0.073)	-
5	Latitude + Longitude	-10.459	0.639	19.61 (0.000)	3.72
6	Latitude + MAT	-10.597	0.642	19.79 (0.000)	3.74
7	Latitude + APT	-10.782	0.645	20.04 (0.000)	3.74
8	Longitude + MAT	-11.267	0.652	20.70 (0.000)	3.57
9	Longitude + APT	3.616	0.316	5.853 (0.010)	3.50
10	MAT + APT	-7.691	0.591	16.17 (0.000)	3.66
11	Latitude + Longitude + MAT	-8.561	0.644	13.68 (0.000)	3.64
12	Latitude + Longitude + APT	-7.565	0.630	12.81 (0.000)	3.71
13	Latitude + MAT + APT	-8.343	0.641	13.49 (0.000)	3.72
14	Longitude + MAT + APT	-8.318	0.640	13.46 (0.000)	3.56
15	Latitude + Longitude + MAT + APT	-5.461	0.636	10.17 (0.000)	4.07

AICc: The corrected Δ Akaike Information Criterion; APT, annual precipitation; ED, ecological disparity; MAT, mean annual temperature.

Table S7 Coefficients of regression models used for ecological disparity

No	Latitude	Longitude	MAT	APT	Interception
1*	0.0126*	-	-	-	3.23*
2*	-	-0.00151*	-	-	3.57*
3*	-	-	-0.000116*	-	3.91*
4	-	-	-	-0.0000312	3.72*
5*	0.0118*	-0.000275	-	-	3.25*
6*	0.00936	-	-0.00658	-	3.42*
7*	0.0138*	-	-	0.0000384	3.15*
8*	-	-0.000797	-0.0196*	-	3.86*
9*	-	-0.00138*	-	-0.0000961	3.68*
10*	-	-	-0.0248*	0.0000403	3.90*
11*	0.00495	-0.000552	-0.0120	-	3.61*
12*	0.0130	-0.000186	-	0.0000328	3.18*
13*	0.00977	-	-0.008.66	0.0000481	3.38*
14*	-	-0.000770	-0.0214*	0.0000299	3.85*
15*	-0.000466	0.00598	-0.0129	0.0000388	3.55*

*Statistical significance (P<0.05).

Abbreviations: APT, annual precipitation; MAT, mean annual temperature.

Table S8 Comparison of different regression models for explanation of ecological diversity of 28 extant small-bodied mammal communities

No	Predictors	AICc	Adjusted r^2	F-test (*P*-value)	Predicted ED
1	Latitude	128.634	0.147	4.615 (0.044)	8.31
2	Longitude	133.124	-0.046	0.0716(0.792)	-
3	MAT	129.664	0.106	3.491 (0.076)	-
4	APT	123.566	0.322	10.99 (0.003)	7.32
5	Latitude + Longitude	130.237	0.158	2.971 (0.075)	-
6	Latitude + MAT	131.629	0.103	2.206 (0.138)	-
7	Latitude + APT	126.198	0.299	5.483 (0.013)	7.18
8	Longitude + MAT	132.488	0.067	1.758 (0.199)	-
9	Longitude + APT	126.567	0.287	5.234 (0.015)	7.17
10	MAT + APT	126.552	0.288	5.244 (0.015)	7.33
11	Latitude + Longitude + MAT	132.907	0.140	2.141 (0.131)	-
12	Latitude + Longitude + APT	129.177	0.274	3.645 (0.033)	6.23
13	Latitude + MAT + APT	129.029	0.279	3.710 (0.031)	6.73
14	Longitude + MAT + APT	129.904	0.250	3.331 (0.043)	7.10
15	Latitude + Longitude + MAT + APT	131.631	0.279	3.029 (0.049)	#

AICc: The corrected Δ Akaike Information Criterion; APT, annual precipitation; MAT, mean annual temperature; #, the number is below zero, which is impossible for a real community.

Table S9 Coefficient of regression models for ecological diversity

No	Latitude	Longitude	MAT	APT	Interception
1*	-0.107*	-	-	-	12.80*
2	-	0.00274	-	-	9.85*
3	-	-	0.176	-	7.254*
4*	-	-	-	0.00284*	6.43*
5	-0.146*	-0.0125	-	-	13.73*
6	-0.125	-	-0.0356	-	13.80
7*	-0.0323	-	-	0.00248*	7.76*
8	-	-0.00428	0.192	-	6.99*
9*	-	-0.00107	-	0.00285*	6.41*
10*	-	-	0.0180	0.00272*	6.31*
11	-0.263	-0.0173	-0.207	-	19.96*
12*	-0.0575	-0.00635	-	0.00229	8.63*
13*	-0.10197	-	-0.150	0.00264*	11.69
14*	-	-0.00182	0.0260	0.00270*	6.20*
15*	-0.0120	-0.200	-0.259	0.00241*	16.13

*Statistical significance ($P<0.05$).

Table S10 Early Cretaceous Mammalian Community in Jehol biota, northeastern China

Community	Taxon	Specimen No.	Order	HZ	EBM (g)			Diet	LM
					JL	HL	FL		
DJ Community	*Liaoconodon hui*	IVPP V16051	Eutriconodonta	JFT	140.18	99.16	169.75	I	Sq
	Liaoconodon sp.	BMNH PM001139	Eutriconodonta	JFT	201.56	100.51	225.37	I	Sq
	Yanoconodon allini	NJU-P06001	Eutriconodonta	DWZZ	27.82	8.77	27.66	I	Sq
	Akidolestes cifelli	NIGPAS139381	Symmetrodonta	DWZZ	–	2.69	8.45	I	Sf
	Sinobaatar lingyuanensis	IVPP V12517	Multituberculata	DWZZ	32.15	–	60.98	H	A[4]
	Eomaia scansoria	CAGS01-IG1	Eutheria	DWZZ	36.23	11.34	48.62	I	A
	Sinodelpys szalayi	CAGS00-IG03	Metatheria	DWZZ	28.62	–	–	I	Sc[2]
LJ Community	*Jeholodens jenkinsi*	GMV 2139	Eutriconodonta	JSG	11.34	3.07	15.32	I	A
	Zhangheotherium quinquecuspidens	IVPP V7466	Symmetrodonta	JSG	99.59	55.56	247.74	I	Sc
	Zhangheotherium sp.	DMNH 2847	Symmetrodonta	JSG	–	15.13	119.07	I	Sc
	Maotherium sinensis	NGMC-97-4-15	Symmetrodonta	JSG	61.61	–	113.73	I	T[1, 3]
	Repenomamus giganticus	IVPP V12549	Eutriconodonta	LJT	6145.83	2528.14	6513.76	C	T[5]
	Repenomamus robutus	IVPP V14155	Eutriconodonta	LJT	1578.09	1335.80	2638.19	C	Sf
	Gobiconodon zafiae	IVPP V12585	Eutriconodonta	LJT	151.76	–	–	I	Sc[#]
	Meemannodon lujiatunensis	IVPP V13102	Eutriconodonta	LJT	1958.61	–	–	C	T[#]
	Juchilestes liaoningensis	DMNH 2607	Eutriconodonta	LJT	100.97	–	–	I	Sc[#]
	Maotherium asiaticus	HGM 41H-III-0321	Symmetrodonta	LJT	71.54[$]	28.29[$]	134.59[$]	I	T[1, 3]
	Acristatherium yanensis	IVPP V15004	Eutheria	LJT	25.58	–	–	I	Sc[#]

[#] Assigned locomotion with regard to body size; $ Body size estimation based the measurements in reference.

Abbreviations: A, arboreal; BMNH, Bejing Museum of Natural History, China; CAGS, Chinese Academy of Geological Science, China; DJ, Dawangzhangzi-Jiufotang community; DMNH, Dalian Museum of Natural History, China; DWZZ, Dawangzhangzi bed; EBM, estimated body mass; FL, femoral length; FM, formation; GMV, National Geological Museum of China; HL, humeral length; HZ, horizon; IVPP, Institute of Vertebrate Paleontology and Paleoanthropology, Academy of Science, China; JFT, Jiutotang formation; JL, jaw length; JSG, Jianshangou bed; LM, locomotor mode; LJ, Lujiatun-Jianshangou community; LJT, Lujiatun bed; L., lower; NGMC, National Geological Museum of China; NIGPAS, Nanjing Institute of Geology and Paleontology, Academy of Science, China; Sc, scansorial; Sf, semifossorial; Sq, semiaquatic; T, terrestrial; U., upper.

References: 1, Ji et al 2009; 2, Luo et al 2003; 3, Rougier et al 2003; 4, Hu and Wang 2002; 5, Meng et al 2006.

Table S11 Bray-Curtis distance matrix ecological disparity of 22 small-bodied mammal communities across four climate regions

cm	1	2	3	6	8	9	10	13	14	15	16	17	18	19	20	21	23	24	25	26	27	28
1	0.000	0.524	0.909	0.889	0.765	0.840	0.920	0.926	0.889	0.800	0.941	0.946	0.926	0.933	0.900	0.882	1.000	0.875	0.900	0.846	1.000	1.000
2	0.524	0.000	0.926	0.913	0.818	0.867	0.867	0.813	0.913	0.760	1.000	1.000	0.938	0.886	0.920	0.897	1.000	0.905	1.000	0.889	1.000	1.000
3	0.909	0.926	0.000	0.917	0.739	0.742	0.935	0.758	1.000	0.923	1.000	1.000	1.000	0.833	0.615	0.750	1.000	0.727	0.846	1.000	1.000	1.000
6	0.889	0.913	0.917	0.000	0.789	0.926	0.704	0.862	0.800	0.909	0.889	0.897	0.862	0.938	0.727	0.778	1.000	1.000	0.909	0.867	1.000	0.875
8	0.765	0.818	0.739	0.789	0.000	0.692	0.846	0.714	0.789	0.810	1.000	1.000	1.000	0.935	0.714	0.943	1.000	0.529	0.905	0.857	1.000	1.000
9	0.840	0.867	0.742	0.926	0.692	0.000	0.647	0.833	0.778	0.793	0.907	0.913	0.944	0.846	0.724	0.907	0.929	0.600	0.862	0.909	0.905	0.913
10	0.920	0.867	0.935	0.704	0.846	0.647	0.000	0.667	0.778	0.793	0.860	0.826	0.833	0.949	0.793	0.814	0.929	0.920	0.862	0.909	0.905	0.826
13	0.926	0.813	0.758	0.862	0.714	0.833	0.667	0.000	0.862	0.935	0.956	0.958	0.947	0.854	0.677	0.867	1.000	0.778	0.806	1.000	1.000	0.840
14	0.889	0.913	1.000	0.800	0.789	0.778	0.778	0.862	0.000	0.727	0.778	0.795	0.793	0.813	0.727	0.833	1.000	0.889	0.818	0.867	0.857	0.750
15	0.800	0.760	0.923	0.909	0.810	0.793	0.793	0.935	0.727	0.000	0.842	0.805	0.742	0.706	0.833	0.842	1.000	0.900	0.917	0.882	0.875	0.889
16	0.941	1.000	1.000	0.889	1.000	0.907	0.860	0.956	0.778	0.842	0.000	0.236	0.733	0.792	0.789	0.846	0.892	1.000	0.895	1.000	0.933	0.875
17	0.946	1.000	1.000	0.897	1.000	0.913	0.826	0.958	0.795	0.805	0.236	0.000	0.667	0.843	0.805	0.818	0.850	1.000	0.902	1.000	0.939	0.886
18	0.926	0.938	1.000	0.862	1.000	0.944	0.833	0.947	0.793	0.742	0.733	0.667	0.000	0.659	0.806	0.689	0.933	1.000	0.871	1.000	0.913	0.840
19	0.933	0.886	0.833	0.938	0.935	0.846	0.949	0.854	0.813	0.706	0.792	0.843	0.659	0.000	0.706	0.792	1.000	0.867	0.824	1.000	0.923	0.929
20	0.900	0.920	0.615	0.727	0.714	0.724	0.793	0.677	0.727	0.833	0.789	0.805	0.806	0.706	0.000	0.684	1.000	0.600	0.917	1.000	0.875	0.778
21	0.882	0.897	0.750	0.778	0.943	0.907	0.814	0.867	0.833	0.842	0.846	0.818	0.689	0.792	0.684	0.000	0.892	1.000	0.895	0.806	0.933	0.875
23	1.000	1.000	1.000	1.000	1.000	0.929	0.929	1.000	1.000	1.000	0.892	0.850	0.933	1.000	1.000	0.892	0.000	1.000	1.000	1.000	1.000	1.000
24	0.875	0.905	0.727	1.000	0.529	0.600	0.920	0.778	0.889	0.900	1.000	1.000	1.000	0.867	0.600	1.000	1.000	0.000	0.800	0.846	1.000	1.000
25	0.900	1.000	0.846	0.909	0.905	0.862	0.862	0.806	0.818	0.917	0.895	0.902	0.871	0.824	0.917	0.895	1.000	0.800	0.000	0.882	0.875	1.000
26	0.846	0.889	1.000	0.867	0.857	0.909	0.909	1.000	0.867	0.882	1.000	1.000	1.000	1.000	1.000	0.806	1.000	0.846	0.882	0.000	0.778	0.818
27	1.000	1.000	1.000	1.000	1.000	0.905	0.905	1.000	0.857	0.875	0.933	0.939	0.913	0.923	0.875	0.933	1.000	1.000	0.875	0.778	0.000	0.400
28	1.000	1.000	1.000	0.875	1.000	0.913	0.826	0.840	0.750	0.889	0.875	0.886	0.840	0.929	0.778	0.875	1.000	1.000	1.000	0.818	0.400	0.000

Abbreviation: cm, community.

Table S12 Distance matrix of ecological diversity of 22 small-bodied mammal communities across four climate regions

cm	1	2	3	6	8	9	10	13	14	15	16	17	18	19	20	21	23	24	25	26	27	28
1	0	0	1	0	1	4	4	0	2	3	12	12	5	6	0	5	2	1	2	4	4	2
2	0	0	1	0	1	4	4	0	2	3	12	12	5	6	0	5	2	1	2	4	4	2
3	1	1	0	1	2	3	3	1	1	4	11	11	4	5	1	4	1	2	1	5	5	3
6	0	0	1	0	1	4	4	0	2	3	12	12	5	6	0	5	2	1	2	4	4	2
8	1	1	2	1	0	5	5	1	3	2	13	13	6	7	1	6	3	0	3	3	3	1
9	4	4	3	4	5	0	0	4	2	7	8	8	1	2	4	1	2	5	2	8	8	6
10	4	4	3	4	5	0	0	4	2	7	8	8	1	2	4	1	2	5	2	8	8	6
13	0	0	1	0	1	4	4	0	2	3	12	12	5	6	0	5	2	1	2	4	4	2
14	2	2	1	2	3	2	2	2	0	5	10	10	3	4	2	3	0	3	0	6	6	4
15	3	3	4	3	2	7	7	3	5	0	15	15	8	9	3	8	5	2	5	1	1	1
16	12	12	11	12	13	8	8	12	10	15	0	0	7	6	12	7	10	13	10	16	16	14
17	12	12	11	12	13	8	8	12	10	15	0	0	7	6	12	7	10	13	10	16	16	14
18	5	5	4	5	6	1	1	5	3	8	7	7	0	1	5	0	3	6	3	9	9	7
19	6	6	5	6	7	2	2	6	4	9	6	6	1	0	6	1	4	7	4	10	10	8
20	0	0	1	0	1	4	4	0	2	3	12	12	5	6	0	5	2	1	2	4	4	2
21	5	5	4	5	6	1	1	5	3	8	7	7	0	1	5	0	3	6	3	9	9	7
23	2	2	1	2	3	2	2	2	0	5	10	10	3	4	2	3	0	3	0	6	6	4
24	1	1	2	1	0	5	5	1	3	2	13	13	6	7	1	6	3	0	3	3	3	1
25	2	2	1	2	3	2	2	2	0	5	10	10	3	4	2	3	0	3	0	6	6	4
26	4	4	5	4	3	8	8	4	6	1	16	16	9	10	4	9	6	3	6	0	0	2
27	4	4	5	4	3	8	8	4	6	1	16	16	9	10	4	9	6	3	6	0	0	2
28	2	2	3	2	1	6	6	2	4	1	14	14	7	8	2	7	4	1	4	2	2	0

Abbreviations: cm, community.

Table S13 Distance matrix of climates across 22 small-bodied mammal communities using Euclidean distance

cm	1	2	3	6	8	9	10	13	14	15	16	17	18	19	20	21	23	24	25	26	27	28
1	0	211	2226	183	771	21	44	543	1211	1511	2086	2086	2498	2451	661	1086	74	639	1610	49	164	89
2	211	0	2015	31	560	192	169	333	1000	1300	1875	1875	2288	2240	450	875	144	428	1400	169	374	126
3	2226	2015	0	2043	1455	2206	2183	1683	1016	716	141	141	273	225	1565	1140	2156	1587	615	2183	2388	2139
6	183	31	2043	0	588	163	140	361	1028	1328	1903	1903	2316	2268	478	903	114	456	1428	140	345	96
8	771	560	1455	588	0	752	729	228	440	740	1315	1315	1728	1680	111	315	702	133	840	728	934	684
9	21	192	2206	163	752	0	23	524	1191	1491	2066	2066	2479	2431	641	1066	53	619	1591	28	182	69
10	44	169	2183	140	729	23	0	501	1168	1468	2043	2043	2456	2408	618	1043	30	596	1568	11	205	45
13	543	333	1683	361	228	524	501	0	667	967	1542	1542	1955	1907	118	542	474	96	1067	500	706	457
14	1211	1000	1016	1028	440	1191	1168	667	0	300	875	875	1288	1240	550	125	1141	572	400	1167	1373	1124
15	1511	1300	716	1328	740	1491	1468	967	300	0	575	575	988	940	850	425	1441	872	100	1467	1673	1424
16	2086	1875	141	1903	1315	2066	2043	1542	875	575	0	0	413	365	1425	1000	2016	1447	475	2042	2248	1999
17	2086	1875	141	1903	1315	2066	2043	1542	875	575	0	0	413	365	1425	1000	2016	1447	475	2042	2248	1999
18	2498	2288	273	2316	1728	2479	2456	1955	1288	988	413	413	0	49	1838	1413	2429	1860	888	2455	2661	2412
19	2451	2240	225	2268	1680	2431	2408	1907	1240	940	365	365	49	0	1790	1365	2381	1812	840	2407	2613	2364
20	661	450	1565	478	111	641	618	118	550	850	1425	1425	1838	1790	0	425	591	22	950	617	823	574
21	1086	875	1140	903	315	1066	1043	542	125	425	1000	1000	1413	1365	425	0	1016	447	525	1042	1248	999
23	74	144	2156	114	702	53	30	474	1141	1441	2016	2016	2429	2381	591	1016	0	569	1541	26	232	18
24	639	428	1587	456	133	619	596	96	572	872	1447	1447	1860	1812	22	447	569	0	972	595	801	552
25	1610	1400	615	1428	840	1591	1568	1067	400	100	475	475	888	840	950	525	1541	972	0	1567	1773	1524
26	49	169	2183	140	728	28	11	500	1167	1467	2042	2042	2455	2407	617	1042	26	595	1567	0	206	44
27	164	374	2388	345	934	182	205	706	1373	1673	2248	2248	2661	2613	823	1248	232	801	1773	206	0	249
28	89	126	2139	96	684	69	45	457	1124	1424	1999	1999	2412	2364	574	999	18	552	1524	44	249	0

Abbreviations: APT, annual precipitation; cm, community; MAT, mean annual temperature.

Literature Cited

Amiot, R., X. Wang, Z.-H. Zhou, X.-L. Wang, E. Buffetaut, C. Lécuyer, Z.-L. Ding, F. Fluteau, T. Hibino, N. Kusuhashi, J.-Y. Mo, V. Suteethorn, Y.-Q. Wang, X. Xu, and F.-S. Zhang. 2011. Oxygen isotopes of East Asian dinosaurs reveal exceptionally cold Early Cretaceous climates. Proceedings of the National Academy of Sciences 108:5179–5183.

Barbosa, O., and P. A. Marquet. 2002. Effects of forest fragmentation on the beetle assemblage at the relict forest of Fray Jorge, Chile. Oecologia 132:296–306.

Barbour, R. W. 1951. The mammals of Big Black Mountain, Harlan county, Kentucky. Journal of Mammalogy 32:100–110.

Barcellos, A., L. S. Schmidt, and H. Brailovsky. 2008. Abundance and species richness of Coreoidea (Hemiptera: Heteroptera) from Parque Estadual do Turvo, southern Brazil. Neotropical entomology 37:406–412.

Bellows, A. S., J. F. Pagels, and J. C. Mitchell. 2001. Macrohabitat and microhabitat affinities of small mammals in a fragmented landscape on the upper coastal plain of Virginia. The American Midland Naturalist 146:345–360.

Burt, W. H. 1954. The mammals of Michigan. University of Michigan Press, Ann Arbor. 288p.

Carey, A. B., and M. L. Johnson. 1995. Small mammals in managed, naturally young, and old-growth forests. Ecological applications 5:336–352.

Caro, T. M. 2002. Factors affecting the small mammal community inside and outside Katavi National Park, Tanzania. Biotropica 34:310–318.

Celesia, G. G., A. Townsend Peterson, K. Peterhans, C. Julian, and T. P. Gnoske. 2010. Climate and landscape correlates of African lion (*Panthera leo*) demography. African Journal of Ecology 48:58–71.

Chandrasekar-Rao, A., and M. E. Sunquist. 1996. Ecology of small mammals in tropical forest habitats of southern India. Journal of Tropical Ecology 12:561–571.

Davis, C. M., Jr. 1925. The mammal fauna of a wooded lot in southern Michigan. Paper of Michigan Academy Science 5:425–428.

Van Deventer, M., and J. A. J. Nel. 2006. Habitat, food, and small mammal community structure in Namaqualand. Koedoe 49:99–109.

Dice, L. R. 1920. The land vertebrate associations of interior Alaska. Occasional Papers of University of Michigan Museum of Zoology 86:1–26.

Dice, L. R. 1925. A survey of the mammals of Charlevoix County, Michigan, and vicinity. Occasional Papers of University of Michigan Museum of Zoology 159:1–33.

Fleming, T. H. 1970. Notes on the rodent faunas of two Panamanian forests. Journal of Mammalogy 51:473-490.

Fleming. T. H. 1972. Aspects of the population dynamics of three species of opossums in the Panama Canal Zone. Journal of Mammalogy 53:621–623.

Fleming, T. H. 1973. Numbers of mammal species in North and Central American forest communities. Ecology 54:555–563.

Hu, Y.-M., and Y.-Q. Wang. 2002. *Sinobaatar* gen. nov.: first multituberculate from the Jehol Biota of Liaoning, northeast China. Chinese Science Bulletin 47:933–938.

Jaksic, F. M. 2001. Ecological effects of El Nino in terrestrial ecosystems of western South America. Ecography 24:241–250.

Jaksić, F. M., J. L. Yáñez, and E. R. Fuentes. 1981. Assessing a small mammal community in central Chile. Journal of Mammalogy 62:391–396.

Ji, Q., Z.-X. Luo, X.-L. Zhang, C.-X. Yuan, and L. Xu. 2009. Evolutionary development of the middle ear in Mesozoic therian mammals. Science 326:278–281.

Kitayama, K. 1992. An altitudinal transect study of the vegetation on Mount Kinabalu, Borneo. Vegetatio 102:149–171.

Komarek, E. V., and R. Komarek. 1938. Mammals of the Great Smoky Mountains. Bulletin of Chicago Academy of Science 5:137–162.

Kumagai, T., T. M. Saitoh, Y. Sato, H. Takahashi, O. J. Manfroi, T. Morooka, K. Kuraji, M. Suzuki, T. Yasunari, and H. Komatsu. 2005. Annual water balance and seasonality of evapotranspiration in a Bornean tropical rainforest. Agricultural and Forest Meteorology 128:81–92.

Li, J. S., Y.-L. Song, and Z.-G. Zeng. 2003. Elevational gradients of small mammal diversity on the northern slopes of Mt. Qilian, China. Global Ecology and Biogeography 12:449–460.

Luo, Z.-X., Q. Ji, J. R. Wible, and C.-X. Yuan. 2003. An Early Cretaceous tribosphenic mammal and metatherian evolution. Science 302:1934–1940.

Luo, Z.-X., P. Chen, G. Li, and M. Chen. 2007. A new eutriconodont mammal and evolutionary development in early mammals. Nature 446:288–293.

Mares, M. A., K. A. Ernest, and D. D. Gettinger. 1986. Small mammal community structure and composition in the Cerrado Province of central Brazil. Journal of Tropical Ecology 2:289–300.

Melo, G. L., J. Sponchiado, A. F. Machado, and N. C. Cáceres. 2011. Small-mammal community structure in a South American deciduous Atlantic Forest. Community Ecology 12:58–66.

Meng, J., Y.-M. Hu, C.-K. Li, and Y.-Q. Wang. 2006. The mammal fauna in the Early Cretaceous Jehol Biota: implications for diversity and biology of Mesozoic mammals. Geological Journal 41:439–463.

Meserve, P. L. 1981. Resource Patitioning in a Chilean Semi-Arid Small Mammal Community. The Journal of Animal Ecology 50:745-757.

Pita, R., A. Mira, and M. L. Mathias. 2003. Small mammal community structure in two successional stages of a Mediterranean ecosystem. Galemys 15:67–79.

Monadjem, A., and M. R. Perrin. 1998. Effects of food supplementation and fire on small mammal community structure in a Swaziland grassland. South African journal of science 94:89–93.

Nakagawa, M., H. Miguchi, and T. Nakashizuka. 2006. The effects of various forest uses on small mammal communities in Sarawak, Malaysia. Forest Ecology and Management, 231:55–62.

Nor, S. 2001. Elevational diversity patterns of small mammals on Mount Kinabalu, Sabah, Malaysia. Global Ecology and Biogeography 10:41–62.

O'Farrell, M. J., and W. A. Clark. 1986. Small mammal community structure in northeastern Nevada. The Southwestern Naturalist 31:23–32.

Pan, Y.-Y., and C.-M. Huang. 2013. Quantitative reconstruction of early cretaceous paleoclimate using paleosol carbonates in China. Carbonates and Evaporites 29:327–335.

Pinheiro, F., I. R. Diniz, D. Coelho, and M. P. S. Bandeira. 2002. Seasonal pattern of insect abundance in the Brazilian cerrado. Austral Ecology 27:132–136.

Quay, W. B. 1951. Observations on mammals of the Seward Peninsula, Alaska. Journal of Mammalogy 32:88–99.

Raoul, F., D. Pleydell, J. P. Quere, A. Vaniscotte, D. Rieffel, K. Takahashi, N. Bernard, J.-L. Wang, T. Dobigny, K. E. Galbreath, and P. Giraudoux. 2008. Small-mammal assemblage response to deforestation and afforestation in central China. Mammalia 72:320–332.

Rougier, G., Q. Ji, and M. Novacek. 2003. A new symmetrodont mammal with fur impressions from the Mesozoic of China. Acta Geologica Sinica 77:7–14.

Scholes, R.J., P. R. Dowty, K. K. Caylor, D. A. B. Parsons, and H. H. Shugart. 2002. Spatial patterns of vegetation in southern Africa – relationships across a gradient of rainfall in the Kalahari Desert. Journal of Vegetation Science 13:419–428.

Vaniscotte, A., D. R. Pleydell, F. Raoul, J. P. Quéré, J.-M. Qiu, Q. Wang, T.-Y. Li, N. Bernard, M. Coeurdassier, P. Delattre, K. Takahashi, J.-C. Weidmann, and P. Giraudoux. 2009. Modelling and spatial discrimination of small mammal assemblages: an example from western Sichuan (China). Ecological modelling, 220:1218–1231.

Walker, S., and A. Rabinowitz. 1992. The small-mammal community of a dry-tropical forest in central Thailand. Journal of tropical ecology 8:57–71.

Wallgren, M., C. Skarpe, R. Bergström, K. Danell, L. Granlund, and A. Bergström. 2009. Mammal community structure in relation to disturbance and resource gradients in southern Africa. African Journal of Ecology 47:20–31.

Wells, K., M. Pfeiffer, M. B. Lakim, and K. E. Linsenmair. 2004. Use of arboreal and terrestrial space by a small mammal community in a tropical rain forest in Borneo, Malaysia. Journal of Biogeography 31:641–652.

Williams, S. E., H. Marsh, and J. Winter. 2002. Spatial scale, species diversity, and habitat structure: small mammals in Australian tropical rain forest. Ecology 83:1317–1329.

CHAPTER 5:

CONCLUDING REMARKS

The studies of this dissertation, using both qualitative and quantitative approaches, support previous hypotheses that Mesozoic mammals evolved a diverse array of ecomorphologies that were apparently comparable to those of extant small-bodied mammals. The ecological structure of Mesozoic mammal communities, however, may have been distinct from that of extant small-bodied mammal communities; this suggests that some factors (e.g., species composition and latitude) may shape mammalian communities in different ways at different times. The major conclusions of these studies are as follows:

1. The eutriconodontan *Yanocondon allini* likely had a semi-sprawling posture and primarily adopted terrestrial locomotion, but might have occasionally swum in the water as did some non-mammalian cynodonts. Combined with previous studies of *Jeholodens*, a sister taxa of *Yanoconodon*, it indicates that ecological diversification occurred at the family level within Mesozoic mammals. This is consistent with previous findings for the symmetrodontan family Spalacotheriidae.
2. Postcranial morphological differences of extant small-bodied mammals are subtle but detectable and can be used for distinguishing eight locomotor modes from one another using linear canonical variate analyses. The results of the multivariate analyses indicate a morphofunctional continuum reflecting similarity in biomechanical demands, suggesting that the morphological signatures are gradational across different locomotor modes.
3. The multivariate morphometric analyses based on the model of extant small-bodied mammals indicate that Mesozoic mammals evolved a variety of postcranial morphologies that would have enabled them to adopt a broad range of locomotor modes and to inhabit various niches. It appears that Mesozoic mammals had diversified into seven locomotor

modes (all but the saltatorial mode) by the end of the Jurassic and that eutriconodonts and multituberculates had the most pronounced locomotor diversification.

4. Ecological structure, which was approximated using three ecological traits, of extant small-bodied mammal communities from tropical, arid, temperate, and cold regions show clear differences in ecological diversity and disparity. These differences are likely due to differences in environmental parameters, suggesting that the environment may shape the ecological structure of extant small-bodied mammal communities.
5. Two Early Cretaceous mammal communities from the Jehol Group have distinctive ecological structures relative to extant small-bodied mammal communities. This suggests that there may have been fundamental differences in the factors that shaped Early Cretaceous mammal communities versus those that shaped extant small-bodied mammal communities.
6. The differences between the extant small-bodied and Early Cretaceous mammal communities may result from sampling artifacts of the fossil record, non-analog paleoenvironments, and/or evolutionary ecological transitions that only occurred after the extinction of non-avian dinosaurs.